Aspects of the Neuroanatomy and Physiology of Sleep in African Mole Rats.

Adhil BHAGWANDIN

This thesis is submitted in fulfillment of the requirements for the degree of Doctor of Philosophy

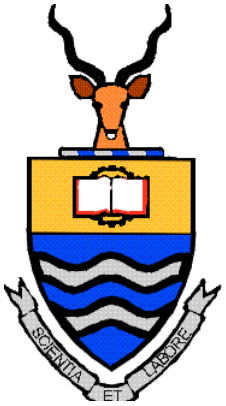

SCHOOL OF ANATOMICAL SCIENCES
UNIVERSITY OF THE WITWATERSRAND
JOHANNESBURG

May, 2011

Declaration

I declare that this thesis is my own, unaided work. It is being submitted for the Degree of Doctor of Philosophy in the University of the Witwatersrand, Johannesburg. It has not been submitted before for any degree or examination in any other University.

_____

Adhil Bhagwandin

5th day of January 2011

Abstract

Mole rats are a unique family of the rodent order and are known for a subterranean lifestyle, reduced eye size, regressed visual system and unusual patterns of circadian rhythmicity (co-existence of rhythmic and arrhythmic chronotypes within a species has been documented). Such dramatic changes especially that of phenotype, may lead to the prediction of significant differences in organisation of the brain and physiology, therefore these unusual phenotypic features form the core rationale providing the impetus for the present series of studies. Neuroanatomical examination of the mole rat brain for immunohistochemical markers of the cholinergic, catecholaminergic, serotonergic, orexinergic, and histaminergic systems revealed neuronal organisation that was remarkably similar to those previously reported in other rodents and mammals, despite the notable differences in lifestyle and phenotype. These results indicate a strong phylogenetic constraint acting at the systems level of neuronal organisation. The study of sleep and wake in rhythmic and arrhythmic chronotypes of a species of mole rat indicated the arrhythmic chronotype spent more time awake with a longer average duration of a waking episode and less time in sleep with a shorter average duration of a SWS episode. While remaining somewhat similar between mole rat chronotypes, total sleep time in the mole rats was significantly reduced in comparison to other rodents. These results also indicate independence of circadian rhythmicity and sleep homeostasis and possible alteration of specific genes involved in the sleep-wake cycle of the mole rats examined. Stereological assessment of absolute numbers of orexinergic neurons revealed that the arrrhythmic chronotype tends to have more orexinergic neurons per gram of body mass that the rhythmic chronotype, leading to the conclusion that enhanced vigilance and

peripheral metabolism of the arrhythmic chronotype may underlie this difference. Immunohistochemical identification of nuclei involved with the sleep-wake cycle, showed no difference in the distribution of these nuclei between circadian chronotypes and no major differences when compared to other rodents. Some interesting and potentially functionally important homogeneities were observed in the distribution of GABAergic interneurons within the pontine region. Furthermore differential orexinergic terminal network densities were observed between chronotypes within the arcuate nucleus and the intergeniculate leaflet. Therefore despite unusual features in lifestyle and phenotype, the organisation of the mole rat brain remains remarkably similar to other rodents; however, distinctions of circadian chronotype consistently produced subtle differences in both the anatomy and physiology of these rodents.

In memory of

Brijnarayan Brijbal

1930 – 2010

Dedication

To Mum and Dad, my brother Bivash, sister Rahistha, Jason and Natasha

Your patience and faith in me has been truly astounding

I am forever grateful

Acknowledgements

There a many people I would like to thank. First and foremost a huge thank you to my supervisor Prof. P. Manger!!!! Paul, your passion for science and yearning for knowledge is inspirational. Thanks for making what is generally considered a daunting experience, the most exciting and enjoyable educational excursion. Your guidance has taught me a great number of invaluable lessons.

I would like to thank Prof. Nigel Bennett and Dr. Marietjie Oosthuizen for the generous supply the mole rats and consults on the behaviour of these critters. I'm also grateful to Prof. Kjell Fuxe whose eternal optimism is a lesson for us all. Thanks for the many consultations and guidance in understanding neuronal organisation. Many thanks to Dr. Oleg Lyamin for passing down his sleep scoring skills and for his assistance with the analysis and interpretation of sleep scoring. Furthermore, I would like to express my gratitude to Prof. Jerry Siegel for the opportunity to briefly work in his lab and for advice on hypocretin.

To all my friends Nix, Kavir, Dustin, Subhash, Kershen and Kamesh, thanks for being patient with me, it is greatly appreciated. I guess we have proved that high school friendships don't have an expiry date. Special thanks to Nadine...thanks for keeping me sane!

I would like to thank the National Research Foundation (NRF) and the Scholarships Office (University of the Witwatersrand) for funding my postgraduate studies from 2005. Finally I would like to thank the dark horses of the School of Anatomical Sciences that being the technical staff, the likes of Alison, Jacob, Philip and Benny. Thanks for all the help.

Abbreviations

III – oculomotor nucleus

IV – trochlear nucleus

Vmot – motor nucleus of trigeminal nerve

VI – abducens nucleus

VIId – facial nerve nucleus, dorsal

VIIv – facial nerve nucleus, ventral

Vmes – fifth mesencephalic nucleus

X – dorsal motor vagus nucleus

XII – hypoglossal nucleus

3V – third ventricle

4V – fourth ventricle

5n – trigeminal nerve

7n – facial nerve

A1 – caudal ventrolateral medullary tegmental nucleus

A2 – caudal dorsomedial medullary nucleus

A4 – dorsal medial division of locus coeruleus

A5 – fifth arcuate nucleus

A6d – diffuse portion of locus coeruleus

A7d – nucleus subcoeruleus, diffuse portion

A7sc – nucleus subcoeruleus, compact portion

A8 – retrorubral nucleus

A9l – substantia nigra, lateral

A9m – substantia nigra, medial

A9pc – substantia nigra, pars compacta

A9v – substantia nigra, ventral, pars reticulata

A10 – ventral tegmental area

A10c – ventral tegmental area, central

A10d – ventral tegmental area, dorsal

A10dc – ventral tegmental area, dorsal caudal

A11 – caudal diencephalic group

A12 – tuberal cell group

A13 – zona incerta

A14 – rostral periventricular nucleus

A15d – anterior hypothalamic group, dorsal division

A15v – anterior hypothalamic group, ventral division

A16 – catecholaminergic neurons of the olfactory bulb

ac – anterior commissure

Amyg – amygdala

AP – area postrema

B9 – supralemniscal serotonergic nucleus

bic – brachium of the inferior colliculus

C – caudate nucleus

C1 – rostral ventrolateral medullary tegmental group

C2 – rostral dorsomedial medullary nucleus

C3 – rostral dorsal midline medullary nucleus

ca – cerebral aqueduct

cc – corpus callosum

cc – central canal

cic – commissure of the inferior colliculus

Cing ctx – cingulate cortex

cl – claustrum

CLi - caudal linear nucleus

CN – cerebellar nuclei

CVL – caudal ventrolateral serotonergic group

Diag. B – diagonal band of Broca

DC – dorsal cochlear nucleus

DLG – dorsal lateral geniculate nucleus

DMSp5d – dorsomedial spinal trigeminal nucleus, dorsal part

DMTg – dorsomedial tegmental area

DpMe – deep mesencephalic nucleus

DR – dorsal raphe

DRc – dorsal raphe nucleus, caudal division

DRd – dorsal raphe nucleus, dorsal division

DRif – dorsal raphe nucleus, interfascicular division

DRl – dorsal raphe nucleus, lateral division

DRv – dorsal raphe nucleus, ventral division

DRp – dorsal raphe nucleus, peripheral division

DT – dorsal thalamus

DTg – dorsal tegmental nucleus

EW – Edinger-Westphal nucleus

f – fornix

fr – fasciculus retroflexus

GC – central periaqueductal grey matter

GP – globus pallidus

GrC – granular cell layer of cochlear nucleus

Hbl – habenular nucleus, lateral

Hbm – habenular nucleus, medial

HIP – hippocampus

Hyp – hypothalamus

Hyp.d – dorsal hypothalamic cholinergic nucleus

Hyp.l – lateral hypothalamic cholinergic nucleus

Hyp.v – ventral hypothalamic cholinergic nucleus

IC – inferior colliculus

ic – internal capsule

icp – inferior cerebellar peduncle

io – inferior olive

IGL – intergeniculate leaflet

ILL – intermediate nucleus of the lateral lemniscus

IP – interpeduncular nucleus

IPC – interpeduncular nucleus, caudal subnucleus

Is.Call/TOL – islands of Calleja and olfactory tubercule

LDT - laterodorsal tegmental nucleus

lfp – longitudinal fasciculus of pons

LHA – lateral hypothalamic area

LL – lateral lemniscus

LVHA – lateral ventral hypothalamic area

LSO – lateral superior olive

LV – lateral ventricle

LVe – lateral vestibular nucleus

LVPO – lateroventral periolivary nucleus

Mc – main orexinergic cluster

mcp – middle cerebellar peduncle

MD – mediodorsal thalamic nucleus

MGD – medial geniculate nucleus, dorsal part

MGP - medial geniculate nucleus, posterior part

MGV – medial geniculate nucleus, ventral part

ML – medial lemniscus

ml – medial mammillary nucleus, lateral part

mlf – medial longitudinal fasciculus

mm – medial mammillary nucleus, medial part

MnR – median raphe nucleus

mt – mammillothalamic tract

mtf – cholinergic medullary tegmental field

MVPO – medioventral periolivary nucleus

N.Acc – nucleus accumbens

N.Arc – arcuate nucleus of the hypothalamus

N.Amb – nucleus ambiguus

N.Bas – nucleus basalis

NEO – neocortex

OB – olfactory bulb

ot – optic tract

OTc – optic tract orexinergic cluster

pVII – preganglionic motor neurons of the superior salivatory nucleus or facial nerve

pIX – preganglionic motor neurons of the inferior salivatory nucleus

P – putamen nucleus

PBg – parabigeminal nucleus

PC – cerebral peduncle

pc – posterior commissure

PDTg – posterior dorsal tegmental nucleus

PFR – perifornical area

Pg – pineal gland

PIL – posterior intralaminar thalamic nucleus

PIR – piriform cortex

PLi – posterior limitans thalamic nucleus

PnO – pontine reticular nucleus, oral part

PnV – pontine reticular nucleus, ventral part

POA – preoptic area

PoT – posterior thalamic nucleus, triangular

PP – peripeduncular nucleus

PPT – pedunculopontine tegmental nucleus

Pr5DM – principal sensory trigeminal nucleus, dorsomedial part

Pr5VL – principal sensory trigeminal nucleus, ventrolateral part

Pta – pretectal area

PV – thalamic paraventricular nuclei

py – pyramidal tract

R – reticular nucleus of the dorsal thalamus

RCh – retrochiasmatic area

Rmc – red nucleus, magnocellular part

RMg – raphe magnus nucleus

ROb – raphe obscurus nucleus

RPa – raphe pallidus nucleus

RVL – rostral ventrolateral serotonergic group

SC – superior colliculus

sco – subcommissural organ

scp – superior cerebellar peduncle

Sep – septum

Sep.L – lateral septal nucleus

Sep.M – medial septal nucleus

SNR – substantia nigra, reticular part

Sp5 – spinal trigeminal tract

Sp5I – spinal trigeminal nucleus, interpolar part

Spo – superior paraolivary nucleus

SO – supraoptic nucleus

TOL – olfactory tubercle

Tz – nucleus of the trapezoid body

tz – trapezoid body

VCP – ventral cochlear nucleus, posterior part

vh – ventral horn

VLG – ventral lateral geniculate nucleus

VLL – ventral nucleus of the lateral lemniscus

VLTg – ventrolateral tegmental area

VMPO – ventromedial preoptic nucleus

VTg – ventral tegmental nucleus

VPO – ventral pons

VPO – ventral pons

vtgx – ventral tegmental decussation

xscp – decussation of the superior cerebellar peduncle

ZI – zona incerta

ZIc – zona incerta orexinergic cluster

TABLE OF CONTENTS **PAGE**

Chapter 4 – Sleep and wake in rhythmic *vs* arrhythmic chronotypes of a microphthalmic species of African mole rat (*Cryptomys mechowi*).

LIST OF FIGURES **Page**

LIST OF TABLES

APPENDICES

Chapter 1

1.1 Introduction

Knowledge of sleep in rodents is mainly limited to studies of the standard laboratory rat and mouse; however, when examining the evolution of sleep in mammals, generally mammals of different sizes from different orders are compared and some rough trends have been found, for example, the total duration of sleep is dependent on the body size of an animal and the amount of rapid eye movement (REM) sleep in an organism decreases gradually from birth (Siegel, 2003). These trends fail to explain what exactly changes when features such body size, brain size or phenotype are compared to measurable sleep parameters. Alternatively, examining representative species of the same order may shed light on the important issue of the evolutionary changes surrounding specific mammalian sleep phenomenology. This series of studies focuses on the neuroanatomy and physiology of sleep of a family of microphthalmic rodents, the African mole rats. Mole rats are well known for their significantly regressed visual system (Cooper et al, 1993; Hart et al, 2004; McMullen et al, 2010) as well as unusual patterns of circadian rhythmicity (Oosthuizen et al., 2003 Lovegrove and Papenfus, 1995; Lovegrove and Muir 1996). From earlier studies (reviewed by Manger, 2005) it has been shown that the anatomical complexity of certain neural systems involved in the sleep-wake cycle are consistent within a mammalian order, but vary across orders. Thus selecting species of the same order controls for changes in the complexity of sleep controlling systems. In an attempt to clarify the understanding of the evolution of sleep phenomenology in rodents, this series of studies, focusing on microphthalmic rodents, aims to examine several unanswered questions about sleep evolution, such as: (1) Does dramatic phenotypic change, such as the significantly reduced visual system of the of the molerats, affect quantifiable sleep parameters; (2) Do features of sleep, such as these listed above, vary with the neuronal number of the sleep controlling neural mechanisms of the brain?; (3) Do

variables such as total sleep time, REM sleep time, and SWS time vary predictably with individuals that possess rhythmic circadian patterns as opposed to individuals that are distinguishably arrhythmic? It will be interesting to investigate whether factors, such as a regressed visual system and an unusual circadian rhythm, have a significant effect on sleep parameters in this microphthalamic species of rodent.

1.2 Background

1.2.1 Mole rats

The rodent family Bathyergidae, comprising five genera of mole rats, is separated into two sub-families, namely Bathyerginae (containing the single genus *Bathyergus*) and Georychinae (comprised of the remaining four genera; *Heterocephalus*, *Heliophobius*, *Georychus* and *Cryptomys*) (Roberts, 1951; De Graaf, 1981). In comparison to other families of mole rats, Bathyergidae exhibits the greatest variation of social organisation that ranges from strictly solitary to cooperative breeding and eusociality. It has been reported that the social Bathyergids characteristically share a burrow system, live together throughout the year and limit reproduction to a single breeding female and a few males (Bennett and Faulkes, 2000). It has been shown that the Bathyergids have a dispersed pattern of activity during a 24 hour cycle and that these patterns are not necessarily influenced by changes in burrow temperature or photoperiod but rather influenced by the risk of hyperthermia in foraging tunnels (Bennett, 1992; Lovegrove, 1988). It appears that most mole rats spend the majority of time within the nest chambers either resting or sleeping; however, the Bathyergid family reports an indistinct sleeping period. Interestingly though, the breeding female (queen) is the most active member of social Bathyergids despite the presence of behavioural division of labour. The concept of behavioural division of labour is based on the frequency of burrow maintenance (these include nest building, digging, transporting food and soil) and is

performed by individuals belonging to three castes within the colony namely; the 'frequent workers', the 'infrequent workers' and the 'non-workers' (Jarvis, 1981). In addition it has been previously shown that species of the Bathyergidae family demonstrate a seasonal breeding pattern (Jarvis, 1969; Bennett and Jarvis, 1988; Van der Horst, 1972).

1.2.2 Evolution of mammalian Sleep

Currently, studies aimed at understanding the evolution of mammalian sleep comprise isolated studies of distantly related species. As an example, it was thought that the monotremes, the earliest distinct extant branch of mammals, lacked REM sleep (Allison and Van Twyver, 1970) and it was concluded that REM sleep evolved after the divergence of monotremes from the remainder of mammals and thus existed as an evolutionary novelty in therian (marsupial and placental) mammals. More recent studies (Siegel et al., 1996, 1998, 1999) however, show that the monotremes actually have more REM sleep than any other mammal, but the cerebral cortex exhibits slow wave activity during REM periods. Studies focusing specifically on phenotypical bihemispheric sleep in mammals are less frequent. The available studies examining bihemispheric sleepers focus upon sleep parameters such as total sleep time, amount of REM sleep, and their relationship to variables such as body size, brain size and immaturity at birth. It has been shown that increases in REM sleep time are related to safe sleeping conditions and immaturity at birth (Siegel, 1995). It was also demonstrated that the total sleep time is roughly correlated with body size (Siegel, 2003). From these studies, which do not specifically address the patterns of sleep evolution in mammals in general, a great deal of speculation has risen regarding the evolution of mammalian sleep phenomenology and the potential reasons for its existence (for example: Nicolau et al., 2000; Taylor et al., 2000; Staedt and Stoppe, 2001; Kavanau, 2002; Gamundi et al., 2003). Most of these studies support evolutionary adaptation, citing specific selection pressures, as the

reason behind the appearance of mammalian sleep phenomenology. All these studies have examined sleep evolution at the phylogenetic level of the class and none have examined more specific phylogenetic levels.

Another line of investigation has been those studies that have examined phenotypically unusual (in the mammalian sense) sleep patterns, such as those of the unihemispheric slow wave sleep (USWS) in dolphins and whales, eared seals and manatees (reviewed in Rattenborg et al., 2000). The first electroencephalographic (EEG) evidence for USWS, studied in the pilot whale (*Globicephala scammoni*), showed that interhemispheric EEG asymmetry tended to alternate between hemispheres and was subsequently identified as a state of "relaxed wakefulness" (Shurley et al., 1969; Serafetinides et al., 1972), but Mukhametov et al (1977) were the first to classify interhemispheric asymmetry in cetaceans as USWS. The function of cetacean USWS has been isolated to the maintenance of the necessary motor activity required for breathing (Mukhametov et al., 1988). It has been argued that the physical movements and reflexes required for cetacean respiration are incompatible with bilateral slow wave sleep (BSWS) since the muscle atonia during REM may adversely affect cetacean respiratory mechanisms, henceforth propagating a potential explanation for the nearly absent nature of cetacean REM sleep (Mukhammetov, 1984; 1988; 1995). In somewhat contrast to the cetaceans, eared seals have reported distinguishable USWS, BSWS and REM whereas only BSWS and REM were identified in the true seals (Rattenborg et al., 2000). In the case of the seals, USWS in the eared seals facilitated sleep and breathing at the surface of the water but the true seals had to hold their breath under water while both hemispheres sleep simultaneously. On the other hand, in the manatee, USWS has been reported to play a role in predator detection rather than facilitate motor activities controlling respiration. The case of the manatee casts inconsistency with the hypothesis that USWS evolved in aquatic mammals only as a response to facilitate respiration during sleep

(Rattenborg et al., 2000). These studies show the variability not only in constitution of sleep but also in its functionality.

Many regard sleep as a physiological and behavioural state, measured by physiological parameters such as EEG, EKG, EOG, EMG, specific single unit neuronal measures, behavioural in-activity, and non-responsiveness; however, sleep is controlled by an anatomically distinct set of nuclei lying within the ventral portion of the brain (hypnogenic system) (Siegel, 2004). Manger (2005) suggested that there is a potential predictability of the anatomy of the neural systems that control sleep and other functions. Earlier studies (Manger et al 2002a, b, c, 2003, 2004) have shown that a distinct evolutionary trend in the nuclear complexity of neural systems is present. Changes in the complexity (in terms of the number of homologous nuclei) of the neural systems implicated in sleep-wake control is consistent within a mammalian order, but may change between mammalian orders. Therefore any evolutionary changes in the anatomy of the hypnogenic system should result in evolutionary changes in both physiological and behavioural parameters associated with sleep. It can be argued that at the phylogenetic level of the class there is predictability, in that all mammals exhibit some form of REM and SWS as a constraining feature of being a mammal, while birds and reptiles also show a class phenotypic type of sleep physiology. While this is true, and is the level of understanding that previous studies have taken us to, it doesn't examine sleep physiology and behaviour in a more specific manner. Sleep studies targeting the phylogenetic level of the order have been ignored. The current series of studies attempts to provide data relevant to this, by examining a species of rodent that has undergone a major reduction in the visual system and show an unusual circadian pattern. Most terrestrial mammals exhibit a lifestyle above the ground however the mole rats of the present series of studies are exclusively subterranean. It is also known that circadian patterns are regulated by exposure to cycles of light and dark therefore the unique features (i.e. regressed visual system and unusual

patterns of circadian rhythmicity) of the species of rodent studied herein provide interesting material to determine whether this species of mole rat conforms to "typical" rodent sleep, or is there a level of adaptive flexibility apparent?

1.3 Specific Aims

With regard to the present series of studies, there are four specific aims: (1) To examine the nuclear complexity of the various hypnogenic neural systems in various species of mole rat; (2) To record sleep parameters such as EEG and EMG in a species of mole rat where distinct circadian rhythmicity patterns vary between individuals; (3) To determine if distinct patterns of circadian rhythmicity lead to predictable and observable differences in sleep phenomenology compared to other rodents; and (4) To determine if the somnogenic system anatomy can provide clues to any predictability or variance in the recordable sleep parameters.

1.4 Individual Chapters

1.4.1 Chapter 2: Nuclear organisation and morphology of cholinergic, putative catecholaminergic and serotonergic neurons in the brains of two African mole rats

The distribution, morphology and nuclear subdivisions of the cholinergic, putative catechlolaminergic and serotonergic systems within the brains of two species of African mole rat (Cape dune mole rat – *Bathyergus suillus*; highveld mole rat – *Cryptomys hottentotus pretoriae*) were identified following immunohistochemistry for cholineacetyltransferase, tyrosine hydroxylase and serotonin. The aim of the study was to investigate possible differences in the complement of nuclear subdivisions of these systems by comparing those

of the mole rats to published studies of other rodents. The mole rats used exhibit a major reduction of the visual system, unusual circadian rhythms and live a subterranean lifestyle. These wild caught animals also have differing social systems, the Cape dune mole rat is strictly solitary whereas the highveld mole rat occurs in social familial units. While these differences, especially that of the phenotype, may lead to the prediction of significant differences in the nuclear complement of these systems, it was observed that all nuclei identified in all three systems in the laboratory rat and other rodents had direct homologues in the brains of the mole rats studied. There were no additional nuclei in the brains of the mole rats that are not found in laboratory rat or other rodents and *vice versa*. The mole rats are phylogenetically distant from the laboratory rat, but still part of the order Rodentia. It appears that despite the unique lifestyle and phenotype of the mole rats examined, changes in nuclear organisation of the systems studied appear to demonstrate a form of constraint related to the phylogenetic level of the order (see appendix A).

1.4.2 Chapter 3: Distribution of orexinergic neurons and terminal networks in the brains of two African mole rats

The distribution of orexinergic cell bodies and terminal networks within the brains of two species of African mole rat (Cape-dune mole rat – *Bathyergus suillus* and highveld mole rat – *Cryptomys hottentotus*) were identified using immunohistochemistry for orexin-A. The aim of the study was to investigate possible differences in the nuclear complement and terminal distribution of this system by comparing those of the mole rats to published studies of other rodents and mammals. The wild-caught mole rats used in this study live a subterranean lifestyle and are well known for their regressed visual system, which may lead to the prediction of differences in the distribution of the cell bodies and the terminal networks; however, we found that both species of mole rat displayed orexinergic nuclei

limited to the hypothalamus in regions similar to those previously reported for other rodent and mammalian species. No immunoreactive neurons could be identified, in either species of mole rat, within the anterior hypothalamic paraventricular organ as was reported for Murid rodents. The terminal networks, while remaining similar between the species, are more overtly expressed in the Cape-dune mole rat than in the highveld mole rat, however, a few intra-order and interspecific exceptions were noted within the intergeniculate nucleus, superior colliculus and area postrema (see appendix B).

1.4.3 Chapter 4: Sleep and wake in rhythmic *vs* arrhythmic chronotypes of a microphthalmic species of African mole rat (*Cryptomys mechowi*).

The giant Zambian molerat (*Cryptomys mechowi*) is a subterranean African rodent noted for its regressed visual system and unusual patterns of circadian rhythmicity – within this species some individuals exhibit distinct regular circadian patterns while others have arrhythmic circadian patterns. The current study was aimed at understanding whether differences in circadian chronotypes in this species affects the patterns and proportions of the different phases of the sleep-wake cycle. Physiological parameters of sleep (EEG and EMG) and behaviour (video recording) were recorded continuously for 72 hours each from six mole rats (three rhythmic and three arrhythmic) using a telemetric system and a low light CCTV camera connected to a DVD recorder. The telemetric data was scored (in both 5 s and 1 min intervals) as wake, sleep (SWS) and rapid eye movement (REM) stages subject to the correlation between EEG, EMG and behaviour. Spectral power was calculated for EEG in each implanted individual, which assisted in understanding the sleep phases and the intensity of slow wave sleep (SWS) between the chronotypes. In addition REM periodicity was calculated from which sleep cycle length was inferred. The results indicate that the arrhythmic individuals spend more time in waking with a longer average duration of a

waking episode, less time in SWS with a shorter average duration of a SWS episode though a greater slow wave sleep intensity, and similar sleep cycle lengths. The time spent in REM and the average duration of a REM episode remained similar between the chronotypes.

1.4.4 Chapter 5: Orexinergic neuron numbers in three species of African mole rats with rhythmic and arrhythmic chronotypes

In this chapter orexinergic cell bodies within the brains of rhythmic and arrhythmic circadian chronotypes from three species of African mole rat (Highveld mole rat - *Cryptomys hottentotus pretoriae*, Ansel's mole rat – *Fukomys anselli* and the Damaraland mole rat – *Fukomys damarensis*) were identified using immunohistochemistry for orexin-A. Immunopositive orexinergic (Orx+) cell bodies were stereologically assessed and absolute numbers of orexinergic cell bodies were determined for the distinct circadian chronotypes of each species of mole rat examined. The aim of the study was to investigate whether the absolute numbers of identified orexinergic neurons differs between distinct circadian chronotypes with the hypothesis of elevated hypothalamic orexinergic neurons in the arrhythmic chronotypes compared to the rhythmic chronotypes. We found statistically significant differences between the circadian chronotypes of *F. anselli*, where the arrhythmic group had higher mean numbers of hypothalamic orexin neurons compared to the rhythmic group. These differences were observed when the raw data was compared and when the raw data was corrected for body mass (M_b) and brain mass (M_{br}). *C. hottentotus pretoriae* showed tendencies toward the hypothesis though the data was not significantly different. *F. damarensis* showed data that was opposite to the hypothesis though this data was not significantly different. A statistically significant difference was noted between all rhythmic and arrhythmic individuals of the current study when the counts of orexin neurons were corrected for M_b, with arrhythmic individuals having larger numbers of orexin cells.

1.4.5 Chapter 6: The interrelations of the distribution and terminal networks of sleep associated nuclei in the brain of an African species of mole rat

In an attempt to broaden the understanding of the sleep-wake cycle, the distribution and interrelations of sleep associated nuclei needs to be determined. The sleep-associated nuclei include the cholinergic lateral dorsal tegmental (LDT) and pedunculopontine (PPT) nuclei, the putative catecholaminergic locus coeruleus (A6) nucleus, the serotonergic raphe nuclear group, nuclei within the preoptic hypothalamic-basal forebrain region, nucleus of the solitary tract, and nucleus reticularis (Siegel, 1990). In terms of the generalised stages of the sleep wake cycle, the LDT and PPT have been implicated in the arousal of waking, whereas the raphe nuclei reportedly have some influence on wakefulness that induces non-REM (NREM) sleep but the posterior hypothalamus has been identified as the 'centre of waking'. The NREM stage appears to be controlled by the nucleus of the solitary tract, nucleus reticularis and mainly the preopotic hypothalamic-basal forebrain region (which encompasses the nucleus of the diagonal band, the substantia innominata, and the lateral preoptic area). REM sleep on the other hand, appears under control of nuclei located caudal to the midbrain and rostral to the spinal cord, though the inactivity of locus coeruleus during this phase may result in the loss of muscle tone (Siegel, 1990; Lyamin et al., 2008). In this chapter, brains, from distinct cicardian chronotypes in which sleep was recorded (discussed in Chapter 4), were collected and later sectioned (50µm) and stained in a one in ten series for nissl, myelin, choline acetyltransferase (ChAT), tyrosine hydroxylase (TH), serotonin (5-HT), orexin (OrxA), histamine (Hst) calbindin (CB), calretonin (CR) and parvalbumin (PV). The antibodies for PV, CB and CR stain specifically for cell bodies and terminal networks associated with the GABAergic system. The aim of the study was to determine the nuclear distribution (of each of the aforementioned systems) and extent of their interrelations, for

example, do the GABA-ergic terminal networks represent a high, medium or low density around the LDT and so forth.

Chapter 2 - Nuclear organisation and morphology of cholinergic, putative catecholaminergic and serotonergic neurons in the brains of two African mole rats

2.1 Introduction

Nearly half of all known mammalian species, over 2300, belong within the order Rodentia (Jansa and Weksler, 2004). Of these, the laboratory rat and mouse are the most commonly used animal models in modern neuroscience (Manger et al., 2008); however, the extent to which the brains of these two species are representative of rodents, mammals, or indeed humans remains unclear. While there are many similarities, the differences are also quite significant, and knowledge of these similarities and differences in the structure of the brain within rodents is essential in aiding interpretation of the often-extrapolated findings based on studies of neural systems of laboratory rat and mouse to humans and other mammals. The question that might be posed here is: are the laboratory rodents always the best model animal to use when attempting to understand aspects of human brain function or dysfunction?

A recent study detailing the occurrence of cholinergic neurons in the cerebral cortex of various species of rodent revealed that these neurons were present in the cortex of members of the sub-family Muridae, but absent in the cortex of other species of rodent including the highveld mole-rat (Bhagwandin et al., 2006). However, a number of studies of two immunohistochemically identifiable neural systems (the catecholaminergic and serotonergic systems) within the subcortical regions of the brain of various rodents, such as the laboratory rat (Dahlström and Fuxe, 1964; Fuxe et al., 1969, 1970; Lindvall and Bjorklund, 1974; Bjorklund and Lindvall, 1984; Steinbusch, 1981; Hökfelt et al., 1976, 1984; Törk, 1990), laboratory mouse (Ruggerio et al., 1984; Daszuta and Portalier, 1985; Ishimura

et al., 1988; Léger et al., 1998; Satoh et al., 1991; D'Este et al., 2007), highveld mole-rat (Da Silva et al., 2006), grass rat (Mahoney et al., 2007), guinea pig (Mulders and Robertson, 2005), hamster (Vincent, 1988), Mongolian gerbil (Janusonis et al., 1999, 2003; Janusonis and Fite, 2001), Chilean degus (Fite and Janusonis, 2001), highveld gerbil (Moon et al., 2007) and greater canerat (Dwarika et al., 2008), have all demonstrated that the nuclear organization of these systems are the same despite differences in phenotype, life history and many millions of years since the occurrence of the most recent common ancestor.

It has been hypothesised that irrespective of brain size, phenotype or life history, those species of the same mammalian order will exhibit the same complement of homologous nuclei, at the systems level of organization, for the imunohistochemically identifiable neuronal systems (Manger, 2005). Recent studies in rodents have shown that despite major increases in brain size (Dwarika et al., 2008), large phylogenetic distances (Da Silva et al., 2006; Moon et al., 2007; Dwarika et al., 2008), and substantive differences in phenotype (Da Silva et al., 2006; Moon et al., 2007; Dwarika et al., 2008), the nuclear organization of the catecholaminergic and serotonergic systems was identical. The cholinergic system has yet to be examined fully in this comparative sense, apart from the cortical cholinergic neurons (Bhagwandin et al., 2006); however, it may be predicted that all rodent species will show the same complement of homologous nuclei for the cholinergic system, as seen thus far for the catecholaminergic and serotonergic systems.

The current study extends the earlier work of Da Silva et al. (2006) by using two species of mole-rat, the highveld mole-rat (*Cryptomys hottentottus pretoriae*) and the Cape dune mole-rat (*Bathyergus suillus*) (Fig. 2.1), and examining the entire brain of each using immunohistochemistry for choline acetyltransferase, tyrosine hydroxylase and serotonin. This allows us to describe the nuclear organization and neuronal morphology of the cholinergic, putative catecholaminergic and serotonergic systems. Both species studied have a greatly

reduced visual system (Oelschlager et al., 2000; Cernuda-Cernuda et al., 2003; Nemec et al., 2004), are subterranean and rarely exposed to light, and appear to have a free-running circadian activity oscillator (Lovegrove and Papenfus, 1995; Lovegrove and Muir, 1996; Negroni et al., 2003; Oosthuizen et al., 2003; Gutjahr et al., 2004). These unusual phenotypic and physiological features, combined with the phylogenetic distance of both species to the laboratory rat (Adkins et al., 2003; Faulkes et al., 2004), will provide a strong phenotypic and phylogenetic test of the hypothesis proposed by Manger (2005). If the prediction of Manger (2005) is supported, the nuclear organization of the systems under study will be identical to that seen in the laboratory rat; however, the phenotypic differences may be reflected in changes such as a reduction in total neuronal numbers within specific nuclei as demonstrated previously for the highveld mole-rat (Da Silva et al., 2006).

2.2 Materials and Methods

The brains of six adult male highveld mole-rats (*Cryptomys hottentotus pretoriae*) (Fig. 2.1A) and six adult male Cape dune mole-rats (*Bathyergus suillus*) (Fig. 2.1B) were used in the current study. All animals were treated and used according to the guidelines of the University of the Witwatersrand Animal Ethics Committee, which parallel those of the NIH for the care and use of animals in scientific experimentation. The highveld mole-rats were captured within the north-eastern portion of Gauteng Province, South Africa, while the Cape dune mole-rats were caught in the metropolitan region of Cape Town, South Africa, both under the permission of the relevant Nature Conservation Directorates. Both species of mole rat display a seasonal breeding pattern. The mole-rats were placed under deep barbiturate anaesthesia (Euthanaze, 200mg sodium pentobarbital/kg, i.p.), and then perfused intracardially upon cessation of respiration. The perfusion was initially done with a rinse of 0.9% saline solution at 4°C, followed by a solution of 4% paraformaldehyde in 0.1M

phosphate buffer (PB, pH: 7.4) (approximately 1 l for each kilogram of body mass of each solution). Brains were then removed from the skull and post-fixed overnight (24 h) in 4% paraformaldehyde in 0.1M PB, and then allowed to equilibrate in 30% sucrose in 0.1 M PB. The brains were then frozen and sectioned into serial coronal and sagittal sections of 50µm thickness. A one in five series of stains was made for Nissl, myelin, choline-acetyltransferase (ChAT), tyrosine hydroxylase (TH), and serotonin (5HT). Sections kept for the Nissl series were mounted on 0.5% gelatine coated glass slides, cleared in a solution of 1:1 chloroform and absolute alcohol, then stained with 1% cresyl violet to reveal cell bodies. Myelin sections were stored in 5% formalin for a period of two weeks and were then mounted on 1% gelatine coated glass slides and subsequently stained with silver solution to reveal myelin sheaths (Gallyas, 1979).

For immunohistochemical staining the sections were first treated for 30 min with an endogenous peroxidase inhibitor (49.2% methanol: 49.2% of 0.1PB: 1.6% of 30% H_2O_2) followed by three 10 min rinses in 0.1M PB. This was followed by a 2 hour pre-incubation, at room temperature, in a solution (blocking buffer) containing 3% normal goat serum (NGS) for serotonin and TH but 3% normal rabbit serum (NRS) for ChAT sections, 2% bovine serum albumin (BSA, Sigma), and 0.25% Triton X-100 (Merck) in 0.1M PB. The sections were then placed in a primary antibody solution containing the appropriately diluted antibody in blocking buffer (as described above) for 48 hours at 4°C under constant gentle shaking. To reveal cholinergic neurons we used anti-cholineacetyltransferase (AB144P, Chemicon, raised in goat) at a dilution of 1:1500. To reveal putative catecholaminergic neurons we used anti-tyrosine hydroxylase (TH) (AB151, Chemicon, raised in rabbit) at a dilution of 1:6000. To reveal serotonergic neurons we used anti-serotonin (AB938, Chemicon, raised in rabbit) at a dilution of 1:7500. This step was followed by three 10 min rinses in 0.1M PB, after which the sections were incubated in a secondary antibody for two hours (room temperature, 22-24°C).

The secondary antibody solution contained a 1:500 dilution of biotinylated anti-rabbit IgG (BA-1000, Vector Labs) in 3% NGS (or anti-goat IgG, BA-5000 in 3% NRS for the ChAT sections), and 2% BSA in 0.1M PB. After three 10 min rinses in 0.1M PB, the sections were incubated for 1 hour in AB solution (Vector Labs), and again rinsed. The sections were then treated in a solution of 0.05% diaminobenzidine (DAB) in 0.1M PB for 5 minutes, following which 3µl of 30% H_2O_2 was added to each 1 ml of solution in which each section was immersed. Staining development was monitored visually and checked under a low power stereomicroscope. This was allowed to continue until the background staining was at a level at which it could assist reconstruction without obscuring the immunopositive neurons. Development was then arrested by placing the sections in 0.1M PB, and then rinsed twice more in the same solution. Sections were mounted on glass slides coated with 0.5% gelatine and left to dry overnight. They were then dehydrated in a graded series of alcohols, cleared in xylene, and coverslipped with Depex. Two controls were employed in the immunohistochemistry, including the omission of the primary antibody, and omission of the secondary antibody in selected sections from which no staining was evident.

The sections were observed with a low power stereomicroscope, and the architectonic borders of the sections traced according to the Nissl and myelin stained sections using a camera lucida. The immuno-stained sections were then matched to the drawings and the immuno-positive neurons marked. The drawings were then scanned and redrawn using the Canvas 8 drawing program. The nomenclature used for the cholinergic system was adopted from Woolf, (1991), Manger et al. (2002a), Maseko and Manger (2007), and Maseko et al. (2007), the putative catecholaminergic system from Dahlström and Fuxe (1964), Hökfelt et al. (1984), Smeets and Gonzalez (2000), Manger et al. (2002b), Maseko and Manger (2007), Maseko et al. (2007), Moon et al. (2007), and Dwarika et al. (2008) and for the serotonergic system from Törk, (1990), Bjarkam et al. (1997), Manger et al. (2002c), Maseko and Manger

(2007), Maseko et al. (2007), Moon et al. (2007), and Dwarika et al. (2008). While we use the standard nomenclature for the catecholaminergic system in this paper, we realise that the neuronal groups we revealed with tyrosine hydroxylase immunohistochemistry may not correspond directly with these nuclei as has been described in previous studies by Dahlström and Fuxe (1964),Hökfelt et al. (1976), Meister et al. (1988), Kitahama et al. (1990, 1996), and Ruggerio et al. (1992). However, given the striking similarity of the results of the tyrosine hydroxylase immunohistochemistry to that seen in other mammals we feel this terminology is appropriate. Clearly further studies in the mole-rat species used with a wider range of antibodies, such as those to phenylethanolamine-*N*-methyltransferase (PNMT), dopamine-β-hydroxylase (DBH) and aromatic L-amino acid decarboxylase (AADC) would be required to fully determine the implied homologies ascribed in this study. We address this potential problem with the caveat of putative catecholaminergic neurons where appropriate in the text.

2.3 Results

In the current study the cholinergic, putative catecholaminergic, and serotonergic systems of two species of mole-rat were visualised using immunohistochemical techniques. The two species of mole-rat used, the highveld mole-rat (*Cryptomys hottentotus pretoriae*) and the Cape dune mole-rat (*Bathyergus suillus*) (Fig. 2.1), while being closely related (Bennett and Faulkes, 2000), differ substantially in both body and brain mass, where the Cape dune mole-rats had an average body mass of 965 g and an average brain mass of 3.4 g, while the highveld mole-rats had an average body mass of 86.5 g and an average brain mass of 1.5 g. Our analysis of these systems indicated extreme similarity in terms of both nuclear organization and neuronal morphology, thus the following description applies to both species unless otherwise specified. Moreover, the cohort of nuclei described in the present study for

the two species of mole-rat does not differ from observations previously provided for these systems in other rodent species (e.g. Da Silva et al., 2006; Moon et al., 2007; Dwarika et al., 2008).

2.3.1. Cholinergic Neurons

The cholinergic system of mammals is most often divided into striatal, basal forebrain, diencephalic, and pontomesencephalic groups, as well as the motor cranial nerve nuclei (Woolf, 1991; Manger et al., 2002a; Maseko et al., 2007). Each of these groups contains a cluster of distinct nuclei that are found throughout the brain from the level of the anterior horn of the lateral ventricle through to the spino-medullary junction. The mole-rats investigated showed no specific differences to this general mammalian organizational plan.

2.3.1.1 Striatal cholinergic interneurons

2.3.1.1.1 Nucleus Accumbens

A cluster of choline acetyltransferase immunopositive (ChAT+) neurons located ventral to the dorsal striatopallidal complex (caudate, putamen, globus pallidus, see below) was designated as the nucleus accumbens. The anterior border of this nucleus was coincident with the anterior border of the lateral ventricle and the posterior border was located at the level of the anterior commissure (Figs. 2.2D-F, 2.3C-E). The location of the nucleus accumbens in the mole-rat species studied is typical of all mammals (Woolf, 1991; Manger et al., 2002a; Maseko et al., 2007). There was a moderate density of ChAT+ neurons throughout this nucleus and the cell bodies were ovoid in shape. These neurons evinced a varying mixture of bipolar and tripolar types and showed no specific dendritic orientation (Fig. 2.4A).

2.3.1.1.2 Dorsal Striatopallidal Complex - Caudate/Putamen and Globus Pallidus

This nuclear complex was located between the level of the anterior border of the lateral ventricle (anteriorly) and at the level of the habenular nuclei (posteriorly) within the cerebral hemisphere (Figs. 2.2D-I, 3C-H). It is not until the level of the globus pallidus that the caudate and putamen form distinct nuclei that are clearly split by the internal capsule. A moderate density of ChAT+ interneurons were observed throughout the caudate and putamen. Within the ventral portion of the globus pallidus, at its borders with the putamen and nucleus basalis (see below), a small number of ChAT+ neurons were observed. The ChAT+ neurons were ovoid in shape, mostly bipolar, but with some multipolar forms, and showed no specific dendritic orientation (Fig. 2.4A).

2.3.1.1.3 Islands of Calleja and Olfactory Tubercle

These nuclei were found in the ventral most portion of the anterior part of the telencephalon deep to the nucleus accumbens from the level of the anterior pole of the lateral ventricle to the level of the globus pallidus (Figs. 2.2D-F, 2.3C-E). A moderate density of ChAT+ neurons was observed throughout the olfactory tubercle with some clustering of neurons in the ventral most portion representing the islands of Calleja. The cell bodies were ovoid in shape, a varying mixture of bi- and multipolar types and exhibited a weak mediolateral dendritic orientation.

2.3.1.2 Cholinergic nuclei of the Basal Forebrain

2.3.1.2.1 Medial Septal Nucleus

This nucleus was located in the rostral half of the medial wall of the cerebral hemispheres within the septal nuclear complex below the rostrum of the corpus callosum in a position dorsal to the diagonal band of Broca (see below) (Figs. 2.2E, 2.3E-F). A moderate to

high density of ChAT+ neurons was found throughout this nucleus. The ChAT+ neurons were ovoid in shape, a varying mixture of bi- and multipolar types, and had a rough dorsoventral orientation of the dendrites.

2.3.1.2.2 Diagonal band of Broca

The diagonal band of Broca was located in the ventromedial corner of the cerebral hemispheres in a position anterior to the hypothalamus (Figs. 2.2D-E, 2.3D-F). A moderate to high density of ChAT+ neurons was found throughout this nucleus. The neuronal cells of this nucleus were slightly larger than those of adjacent cholinergic groups but they maintained an ovoid shape and were a mixture of bi- and multipolar types (Fig. 2.4A). The dendrites were oriented parallel to the ventromedial edge of the cerebral hemisphere. It was possible to divide this nucleus into both horizontal and vertical limbs, but this was not deemed necessary since it would not add any value to the description.

2.3.1.2.3 Nucleus Basalis

ChAT+ neurons located ventral to the anterior pole of globus pallidus at the level of the anterior commissure as well as in a position ventral to globus pallidus and caudal to the olfactory tubercle were assigned to the nucleus basalis (Figs. 2.2F-I, 2.3F-H). A varying density, from low to high, of ChAT+ neurons was seen throughout this region. At the caudal region of this nucleus the neurons appear to be continuous with those of the ventral portion of the globus pallidus (see above). These ChAT+ neurons were a mixture of ovoid and fusiform shapes, showed a varying combination of bi- and multipolar types, and evinced no specific dendritic orientation.

2.3.1.3 Diencephalic Cholinergic nuclei

2.3.1.3.1 Medial Habenular Nucleus

The medial habenular nucleus, which contained a dense aggregation of ChAT+ neurons, formed part of the epithalamus and was located in the dorsomedial aspect of the diencephalon adjacent to the third ventricle (Figs. 2.2I, 2.3H-I). The ChAT+ neurons in this nucleus were round and small in shape, and due to the dense packing it was impossible to determine if there was any specific dendritic orientation (Fig. 2.4B). The axons emanating from these neurons formed the distinct fasciculus retroflexus that was visible with ChAT immunoreactivity along its entire trajectory to the interpeduncular nucleus.

2.3.1.3.2 Dorsal Hypothalamic Group

Located within the dorsomedial aspect of the hypothalamus between the third ventricle and the fornix, a cluster of ChAT+ neurons, intermingled with those of the A15D nucleus (see below) was designated as the dorsal hypothalamic cholinergic group (Figs. 2.2G-I, 2.3I-K). The ChAT+ neurons were sparsely populated within this nucleus and they were also not intensely ChAT immunoreactive (in comparison to other immunoreactive neurons). These ChAT+ neurons were round to fusiform in shape and showed no specific dendritic orientation.

2.3.1.3.3 Lateral Hypothalamic Group

This nucleus was located within the dorsolateral portion of the hypothalamus, lateral to the fornix, and contained palely stained ChAT+ neurons, in a low to moderate density (Figs. 2.2H-I, 2.3J). The neurons forming this nucleus were intermingled with those of A13 nucleus (see below). The cell bodies of the ChAT+ neurons were ovoid in shape, bipolar in type and exhibited no specific dendritic orientation.

2.3.1.3.4 Ventral Hypothalamic Group

The ChAT+ neurons representing this nucleus were located in the ventral portion of the hypothalamus and were intermingled with neurons of the A12 and A15v nuclei (see below) respectively (Figs. 2.2H-I, 2.3J). At the midline a moderate density of ChAT+ neurons were found, but the density decreased steadily with distance from the midline. The neuronal bodies were round, bipolar in type, and exhibited a rough mediolateral dendritic orientation.

2.3.1.4 Pontomesencephalic Cholinergic nuclei

2.3.1.4.1 Parabigeminal Nucleus

Located at the very lateral aspect of the pontine tegmentum, ventral to the inferior colliculus, was a small cluster of ChAT+ neurons that were assigned to the parabigeminal nucleus (Fig. 2.3N). As previously reported (Da Silva et al., 2006) there were less than10 neurons in this nucleus in the highveld mole-rat, but up to approximately 50 neurons could be observed in this nucleus in the larger-brained Cape dune mole-rat. The neurons were palely stained as reported previously for rodents (Woolf, 1991) and specifically the highveld mole-rat (Da Silva et al., 2006), were found in a very low density, appeared ovoid in shape, were bipolar and showed no specific dendritic orientation.

2.3.1.4.2 Pedunculo-Pontine Tegmental (PPT) Nucleus

The ChAT+ neurons comprising the PPT nucleus were located within the dorsal aspect of the pontine tegementum immediately inferior to the superior cerebellar peduncle, from the level of the oculomotor nucleus to the trigeminal motor nucleus, a position that is typical of all mammals (Figs. 2.2N-O, 2.3M-O) (Woolf, 1991; Manger et al., 2002a; Maseko

et al., 2007). A moderate to high density of intensely reactive ChAT+ neurons were found throughout the region. The cell bodies of the ChAT+ neurons were of a mixture of varying shapes, and the neurons themselves expressed a mixture of bi- and multipolar types, with no specific dendritic orientation irrespective of polarity (Fig. 2.4C).

2.3.1.4.3 Laterodorsal Tegemental (LDT) Nucleus

A cluster of ChAT+ neurons located within the ventrolateral portion of the peri-aqueductal and periventricular grey matter, immediately caudal to the oculomotor nucleus were classified as belonging to the LDT nucleus (Figs. 2.2N-O, 2.3N-O). These neurons were seen to intermingle with the caudal-most neurons of the diffuse division of the locus coeruleus (A6d) neurons (see below). A moderate to high density of ChAT+ neurons were found throughout this region. The cell bodies were a mixture of ovoid and other shapes, mostly multipolar in type, with a predominant dorsomedial to ventrolateral dendritic orientation (Fig. 2.4C).

2.3.1.5 Cholinergic Cranial Nerve Motor Nuclei

These nuclei were found in positions typical of all mammals and all contained large multipolar motor neurons (Woolf, 1991; Manger et al., 2002a; Maseko et al., 2007). The ChAT+ nuclei identified in both mole-rat species include: a fused oculomotor (III) and trochlear (IV) nucleus (Fig. 2.4D), motor division of the trigeminal (Vmot), adbucens (VI), dorsal and ventral subdivisions of the facial (VIId and VIIv), nucleus ambiguus, dorsal motor vagus (X), hypoglossal (XII), Edinger-Westphal (EW), medullary tegemental field (mtf) and the preganglionic motor neurons of the salivatory (pVII) and the glossopharyngeal (pIX) nerves (Figs. 2.2M-V, 2.3L-U). The few, small, round, palely stained ChAT+ neurons of the Edinger-Westphal nucleus, a primarily visual structure, were located in the midline between

the fused oculomotor and trochlear nuclei and this nucleus was generally very reduced in size compared to other mammals. ChAT+ neurons found belonging to the pVII and pIX nerves were located in a region dorsal to the dorsal division of the facial nucleus and ventral to the abducens and dorsal motor vagus nuclei in the medullary tegmentum and evince a similar morphology to all other motor neurons. Caudal to these, cholinergic neurons of a similar morphology were assigned to the medullary tegmental field.

2.3.2 Putative Catecholaminergic Nuclei

Tyrosine hydroxylase immunoreactive neurons (TH+), classified in this study as putative catecholaminergic neurons (see above), formed a number of identifiable nuclear complexes and nuclei that were found throughout the brains of the mole-rats studied extending from the olfactory bulbs to the spinomedullary junction. The locations of these nuclear complexes and nuclei were identical to those seen in other rodents and other mammals, and divisible into distinct regional clusters including the olfactory bulb, diencephalic, midbrain, pontine and medullary nuclei. For simplicity, the nuclei are referred to using the nomenclature of Dahlström and Fuxe (1964) and Hökfelt et al (1984). No putative catecholaminergic nuclei outside the bounds of the classically defined nuclei (e.g. Smeets and González, 2000) were found.

2.3.2.1 Olfactory Bulb (A16)

A high density of TH+ neurons, probably representing periglomerular dopaminergic interneurons were found within the stratum granulosum of the olfactory bulb (Figs. 2.2A, 2.3A). The cell bodies were ovoid to triangular in shape, small in size, multipolar and were found surrounding the glomeruli, especially so the deeper aspect. A dense dendritic network emanating from these neurons was seen to surround the glomeruli.

2.3.2.2 Diencephalic Nuclei

Six clusters of TH+ neurons, forming distinct nuclei, were observed within the hypothalamus, these being: the anterior hypothalamic group, dorsal division (A15d); the anterior hypothalamic group, ventral division (A15v); the rostral periventricular cell group (A14); the zona incerta (A13); the tuberal cell group (A12); and the caudal diencephalic group (A11) (Figs. 2.2G-K, 2.3H-K). Within the dorsal anterior portion of the hypothalamus, between the third ventricle and the fornix intermingled with cholinergic neurons of the dorsal hypothalamic group (see above), a moderate density of TH+ neurons representing the A15d nucleus was found. These neurons were ovoid in shape, bipolar and showed a mostly mediolateral dendritic orientation. The A15v nucleus was located in the ventrolateral portion of the hypothalamus close to the floor of the brain. A low to moderate density of TH+ neurons was found in this region and the cell bodies of these were ovoid in shape, bipolar, with a dendritic orientation running parallel to the floor of the hypothalamus (Fig. 2.5D). TH+ neurons assigned to the A14 nucleus were found in bilateral low to moderately densely packed columns adjacent to the lateral edges of the third ventricle. The cell bodies were ovoid in shape, predominantly bipolar but there were some multipolar neurons, and exhibited a dendritic orientation, for the most part, parallel to the lateral wall of the third ventricle (Fig. 2.5C). Within the dorsolateral aspect of the hypothalamus, lateral to the fornix and intermingling with the zona incerta of the ventral thalamus and the cholinergic neurons of the lateral hypothalamic group (see above) was a small number of TH+ neurons that were assigned to the A13 nucleus. These neurons appeared to form a lateral continuation of the A15d neurons and showed a similar ovoid, bipolar morphology with a mediolateral dendritic orientation. TH+ neurons assigned to the A12 nucleus were found in the ventral medial portion of the hypothalamus, surrounding and below the floor of the third ventricle in the

vicinity of the arcuate nucleus. These neurons were ovoid, bipolar and showed a dendritic orientation either parallel to the floor of the hypothalamus or the wall of the third ventricle (Fig. 2.5D). Within the hypothalamic grey matter adjacent to the posterior pole of the third ventricle, a moderate density of TH+ neurons were located and these formed the A11 nucleus. For the most part, these neurons were ovoid and bipolar with a dorsoventral dendritic orientation (Figs. 2.5A,B).

2.3.2.3 Midbrain Nuclei

2.3.2.3.1 Ventral Tegmental Area Nuclei (VTA, A10 complex)

In the medial portion of the tegmentum of the midbrain at the level of the oculomotor nucleus, a nuclear complex containing four nuclei (A10 – ventral tegmental area, A10c – ventral tegmental area central, A10d – ventral tegmental area dorsal, A10dc – ventral tegmental area dorsal caudal) was found. These nuclei extended from within the periaqueductal grey matter around the base of the aqueduct, into the tegmentum below the periaqueductal grey matter around the midline, through to and around the interpeduncular nucleus (Figs. 2.2K-M, 2.3K-M). A high density of TH+ neurons, found dorsal and dorsolateral to the interpeduncular nucleus, between this nucleus and the root of the oculomotor nerve (IIIn), was assigned to the A10 nucleus. These neurons were ovoid in shape, bipolar in type and the dendrites were oriented parallel to the edge of the interpeduncular nucleus (Figs. 2.5E, 2.6). Immediately dorsal to the interpeduncular nucleus intermingled with neurons of the CLi (see below), in a location just anterior to the decussation of the superior cerebellar peduncle, was a dense cluster of ovoid, bipolar TH+ neurons forming the A10c nucleus (Figs. 2.5E, 2.6). The dendrites of these neurons were oriented parallel to the dorsal margin of the interpeduncular nucleus. Immediately dorsal to A10c, between it and the oculomotor nucleus, was a dense bilateral parasagittal cluster of

ovoid, bipolar TH+ neurons, with a dorsoventral dendritic orientation, that formed the A10d subdivision (Figs. 2.5B,E, 2.6). The TH+ neurons assigned to the A10dc nuclear complex were found within the periaqueductal grey matter adjacent to and surrounding the ventral half of the cerebral aqueduct. A moderate density of small neurons was seen in this region and the cell bodies were ovoid in shape, a mixture of bi- multipolar types with a dendritic orientation running parallel to the edge of the cerebral aqueduct (Figs. 2.5B, 2.6). The number of neurons in the A10dc nucleus appear to be far more numerous and widespread in the Cape dune mole-rat when compared with the highveld mole-rat (Fig. 2.7).

2.3.2.3.2 Substantia Nigra (A9)

The substantia nigra nuclear complex was located in the ventral and lateral portions of the midbrain tegmentum, lying just dorsal to the cerebral peduncles. Evidence for four distinct nuclei namely, the substantia nigra, pars compacta (A9pc), substantia nigra, ventral or pars reticulata (A9v), substantia nigra, pars lateralis (A9l) and substantia nigra, pars medialis (A9m), were found within the A9 complex (Figs. 2.2J-M, 2.3J-L). A9pc was seen to be a dense band of TH+ neurons that ran from medial to lateral immediately dorsal to the cerebral peduncle. The neurons were ovoid in shape, bipolar in type and showed a dendritic orientation parallel to the mediolateral orientation of the band (Figs. 2.5E, 2.6). Within the dorsal portion of the cerebral peduncle ventral to A9pc, occasional TH+ neurons that were ovoid in shape, bipolar in type, with no specific dendritic orientation, were assigned to the A9v nucleus (Fig. 2.6). Not many neurons were evident in this nucleus in either species. At the lateral edge of A9pc, a loose aggregation of ovoid, bipolar TH+ neurons formed the A9l nucleus (Figs. 2.5E, 2.6). Within this nucleus the neurons were moderate in density and showed no specific dendritic orientation. Medial to A9pc and lateral to the root of the

oculomotor nerve (IIIn), a dense cluster of ovoid, bipolar TH+ neurons with no specific dendritic orientation, formed the A9m subdivision (Figs. 2.5E, 2.6).

2.3.2.3.3 Retrorubal Nucleus (A8)

Scattered throughout the midbrain tegmentum, in a position caudal to the magnocellular division of the red nucleus and dorsal to the A9 complex, was a sparsely packed but relatively numerous, cluster of TH+ neurons that formed the A8 nucleus (Figs. 2.2M, 2.3L-M). The cells of this region were ovoid in shape, a mixture of bipolar and multipolar types and showed no specific dendritic orientation.

2.3.2.3.4 The Locus Coeruleus (LC) Nuclear Complex

Within the pontine region a large number of TH+ neurons forming the locus coeruleus complex were readily identified in both species. In each mole-rat investigated the locus coeruleus complex could be readily subdivided into five nuclei, these being: the subcoeruleus compact portion (A7sc), subcoeruleus diffuse portion (A7d), locus coeruleus diffuse portion (A6d), fifth arcuate nucleu (A5), and the dorsal medial division of locus coeruleus (A4) (Figs. 2.2N-P, 2.3O). Within the dorsal portion of the pontine tegmentum adjacent to the ventrolateral region of the periaqueductal grey matter, a tightly packed cluster of TH+ neurons represented the A7 compact portion of the LC. This division is the same as what was previously described as the subcoeruleus (Dahlström and Fuxe, 1964; Olson and Fuxe, 1972). The cells were ovoid in shape, bipolar in type and showed no specific orientation of the dendrites (Fig. 2.5F). Ventral and lateral to the A7sc, a diffusely organised aggregation of TH+ neurons formed the A7d nuclear complex. These neurons are located both medially and laterally around the trigeminal motor nucleus (Vmot). They are more numerous in the cape dune mole-rat but this appears to be related to the larger brain size rather than a specific

increase in number that may be interpreted as an adaptive increase in neuronal number. The TH+ neurons of this region were ovoid in shape, bipolar in appearance and showed no specific dendritic orientation (Fig. 2.5F). Within the ventrolateral portion of the periventricular grey matter a loose to moderate density of TH+ neurons were assigned to the A6d nucleus. The neurons of this group were not found adjacent to the wall of the fourth ventricle as seen in the laboratory rat (Dahlström and Fuxe, 1964) but were located in the ventrolateral half of the periventricular grey matter as seen in other rodent species (Moon et al., 2007; Dwarika et al., 2007). The neuronal morphology was again similar to that of other nuclei in this complex; however there was a predominant dendritic orientation in the dorsomedial to ventrolateral plane, although many other dendrites were oriented in various other directions (Fig. 2.5F).

In the ventrolateral pontine tegmentum lateral to the superior olivary nucleus and lateral to Vmot and A7d, a small cluster of TH+ neurons formed the A5 nucleus. These neurons showed irregular somal shapes, were mostly multipolar and formed a rough mesh-like dendritic network around the ascending fascicles located within the ventrolateral pontine tegmentum. Immediately adjacent to the wall of the fourth ventricle, in the dorsolateral portion of the periaqueductal grey matter, a very few TH+ neurons represent the A4 nucleus, which showed a similar morphology to the neurons of the A6d nucleus.

2.3.2.3.5 Medullary Nuclei

Within the medulla of both species we found evidence for six putative catecholaminergic nuclei these being: rostral ventrolateral tegmental group (C1), rostral dorsomedial group (C2), rostral dorsal midline group (C3), caudal ventrolateral tegmental group (A1), caudal dorsomedial group (A2) and area postrema (AP) (Figs. 2.2Q-U, 2.3Q-T). The TH+ neurons forming the C1 nucleus were found in the ventrolateral medulla from the

level of the facial nerve nucleus to the mid-level of nucleus ambiguus. The neurons were found at a low density throughout the region and the neuronal morphology was similar to those found in the A5 group. Continuing in the ventrolateral medulla, a column of TH+ neurons located laterally to the posterior most part of the C1 nucleus and extending to the spinomedullary junction, was designated as forming the A1 nucleus. The somata were irregular in shape, multipolar and formed a mesh-like dendritic network around the ascending fascicles. The A1 column was distinguished from the ventrolateral C1 column by occupying a position lateral to the lateral reticular nucleus and nucleus ambiguus, whereas C1 was located medial to these structures.

In the dorsal part of the medulla, in the region of the anterior part of the dorsal and medial border of the nucleus tractus solitarius, a distinct cluster of numerous TH+ neurons was designated as the C2 nucleus. Within this nucleus there was a clear region close to the floor of the fourth ventricle termed the dorsal strip and a continuation of this cluster into the region of the tractus solitarius termed the rostral subdivision of the C2 nucleus. Within the dorsal strip of C2 the neurons were ovoid in shape, bipolar in appearance and showed a dendritic orientation parallel to the floor of the fourth ventricle. In the rostral region the cells were ovoid in shape, a varying mixture of bi- and multi- polar types and there was no specific orientation of the dendrites. Within the dorsal medial medullary tegmentum at the midline, dorsal to the raphe obscurus and close to the floor of the fourth ventricle, a small number of TH+ neurons representing the C3 nucleus were found. These neurons were ovoid in shape, bipolar in appearance and showed a dorsoventral dendritic orientation. Between the caudal portions of the dorsal motor vagus and hypoglossal cranial nerve nuclei, a small number of TH+ neurons represented the A2 nucleus. The cells bodies were ovoid in shape, with the neurons being mostly bipolar, but there were a few multipolar neurons in this cluster. These neurons showed a mediolateral orientation of the dendrites. Some of these A2 neurons were

located a small distance into the dorsal caudal medullary tegmentum. Straddling the midline, dorsal to the central canal and the dorsal motor vagus nucleus, and between the most caudal region of the bilateral C2 nucleus, was a single large cluster of intensely stained TH+ neurons, the area postrema. These small round TH+ neurons were very densely packed within this region and no particular dendritic orientation could be identified.

2.3.3. Serotonergic Nuclei

The serotonergic (5HT+) nuclei identified in the current study of the mole-rats were the same as those previously identified in all rodents and other eutherian mammals studied to date (Maseko et al., 2007). The serotonergic nuclei were all located within the brainstem and can be divided into a rostral and a caudal cluster. Both of these clusters contained a number of distinct nuclei that are found throughout the brainstem from the level of the decussation of the superior cerebellar peduncle through to the spinomedullary junction.

2.3.3.1 Rostral Cluster

2.3.3.1.1 Caudal Linear Nucleus (CLi)

This nucleus was the most rostral of the serotonergic nuclei found in the brains of both species of mole-rat studied. The 5HT+ neurons formed a cluster around the midline immediately dorsal to the interpeduncular nucleus in a location just anterior to the decussation of the superior cerebellar peduncle (Figs. 2.2M, 2.3M). A moderate density of 5HT+ neurons was seen throughout this region and the cell bodies were ovoid in shape, bipolar and show a dorsoventral orientation of the dendrites in the more dorsal parts of the nucleus but a mediolateral orientation in the remainder of the nucleus.

2.3.3.1.2 Supralemniscal (B9) Nucleus

The neurons forming this nucleus appeared to be a lateral extension of the neuronal cluster comprising the most ventral portion of CLi (see above). The 5HT+ B9 neurons were found immediately caudal to the A9pc (see above) above the cerebral peduncle and extended as an arc of neurons into the lateral and ventrolateral portion of the midbrain tegmentum (Figs. 2.2N, 2.3M-N). The 5HT+ neurons exhibited a low to moderate density throughout this nucleus and the cell bodies were ovoid in shape, bipolar in type and exhibit a rough mediolateral dendritic orientation parallel to the upper border of the cerebral peduncle.

2.3.3.1.3 Median Raphe (MnR)

The median raphe nucleus was characterised by two distinct, densely packed 5HT+ neuronal columns on either side of the midline in a para-raphe position (Figs. 2.2N-P, 2.3M-O). The rostral border of this nucleus was coincident with the level of the decussation of the superior cerebellar peduncle and the caudal border of this nucleus was found at the level of the trigeminal motor nucleus (Vmot, see above). The 5HT+ neurons in this nucleus exhibited cell bodies that were ovoid in shape, bipolar, and had a mostly dorsoventral dendritic orientation (Fig. 2.8C,D).

2.3.3.1.4 Dorsal Raphe (DR) Nuclear Complex

Within the 5HT+ neuronal region designated as the dorsal raphe nuclear complex there were six distinct nuclei, these being: the dorsal raphe interfascicular (DRif) nucleus, dorsal raphe ventral (DRv) nucleus, dorsal raphe dorsal (DRd) nucleus, dorsal raphe lateral (DRl) nucleus, dorsal raphe peripheral (DRp) nucleus and the dorsal raphe caudal (DRc) nucleus (Figs. 2.2L-P, 2.3L-O). These six nuclei were found, for the most part, within the periaqueductal and periventricular grey matter from the level of the oculomotor nucleus to

the trigeminal motor nucleus. The DRif was located between the two medial longitudinal fasciculi and exhibited a high density of 5HT+ neurons that were ovoid in shape, bipolar and had a dorsoventral dendritic orientation. The DRv was found immediately dorsal to the DRif between and just caudal to the oculomotor nuclei. The DRv exhibited a high density of 5HT+ neurons that had a similar neuronal morphology to the DRif but exhibited a range of dendritic orientations. Immediately dorsal to DRv and ventral to the inferior border of the cerebral aqueduct a cluster of 5HT+ neurons with a similar neuronal morphology to DRif and DRv, but with a mediolateral dendritic orientation, was designated as the DRd nucleus (Fig. 2.8A). 5HT+ neurons representing the DRp, were located in the ventrolateral portion of the periaqueductal grey matter lateral to the DRd and DRv. Some neurons were found in the adjacent tegmentum and are the only ones found outside the periaqueductal grey matter. There was a moderate density of these neurons within the periaqueductal grey matter and a lower density of more scattered neurons in the tegmental region. The 5HT+ neurons of the DRp were ovoid in shape and marginally larger than those of DRd, DRv and DRif. They were bipolar and showed no specific dendritic orientation. The 5HT+ neurons of the DRl were located dorsolateral to the DRd and adjacent to the ventrolateral edges of the cerebral aqueduct. The neurons of this nucleus were readily distinguishable from the remainder of the dorsal raphe nuclei since they were larger and showed a mixture of bipolar and multipolar neurons (Fig. 2.8A). These neurons showed dendrites orientated parallel to the wall of the aqueduct, and were found in a low to moderate density within the nucleus. The neurons of this serotonergic nucleus were intermingled with putative catecholaminergic neurons of the A10dc (see above). As we followed the DRl caudally, where the cerebral aqueduct opened into the fourth ventricle and the DRd, DRv and DRif dissappeared, the neurons of the DRl formed an arc across the midline of the dorsal portion of the periventricular grey matter. This caudal arc of the DRl was classified as the DRc nucleus (Fig. 2.8C,D). The neuronal

morphology of the 5HT+ neurons in the DRc was identical to that of the DRl, but we classified this as an independent nucleus due to the lack of 5HT+ neurons in this region in the brain of monotremes (Manger et al., 2002c; Maseko et al., 2007).

2.3.3.2 Caudal Cluster

2.3.3.2.1 Raphe Magnus (RMg)

This nucleus was seen to be two columns of loosely aggregated moderate to large 5HT+ neurons located either side of the midline from the level of the caudal pole of the trigeminal motor nucleus to the anterior pole of nucleus ambiguus (Figs. 2.2Q-R, 2.3O-R). The 5HT+ neurons within this nucleus were ovoid in shape, bipolar and exhibited a dorsoventral dendritic orientation (Figs. 2.8D, 2.9A,C).

2.3.3.2.2 Rostral and Caudal Ventrolateral Nuclei (RVL and CVL)

Within the left and right ventrolateral medullary tegmentum a distinct anteroposterior column of 5HT+ neurons extending from the level of the facial nucleus to the spinomedullary junction were observed (Figs. 2.2Q-T, 2.3O-S). These have previously been termed the rostral and caudal ventrolateral serotonergic columns (e.g. Maseko et al., 2007; Moon et al., 2007; Dwarika et al., 2008). The RVL began as a lateroventral continuation of 5HT+ neurons from the lower portion of the RMg extending over the pyramidal tracts and consolidating as a distinct column lateral to the inferior olives. This column was characterised by moderate density of 5HT+ neurons that exhibit a cellular morphology identical to those of the RMg except for a mediolateral dendritic orientation (Fig. 2.9A,C). The appearance of the inferior olive distinguishes left and right RVL and at the level of nucleus ambiguus the RVL becomes the CVL. The CVL continues in the caudal ventrolateral medullary tegmentum until the spinomedullary junction is reached. The neuronal morphology did not change. The

number of neurons within this column steadily decreases from rostral to caudal. Although the RVL and CVL are continuous in the mole-rats studied, and indeed several other eutherian mammals previously studied (e.g. Maseko et al., 2007; Moon et al., 2007; Dwarika et al., 2008), we make the distinction of two components of these ventrolateral columns, as the caudal portions have not been reported in the opossum or the monotremes (Crutcher and Humbertson, 1978; Manger et al., 2002c).

2.3.3.2.3 Raphe Pallidus (RPa)

The 5HT+ neurons forming this nucleus were found in the ventral midline of the medulla associated with the pyramidal tracts (Figs. 2.2Q-T, 2.3P-S). These neurons were for the most part located between the two pyramidal tracts, but some neurons belonging to this nucleus (based on neuronal morphology) were identified dorsal to the pyramidal tract, between it and the inferior olive. The fusiform shaped 5HT+ neurons of the raphe pallidus were smaller than those of RMg, RVL and CVL, bipolar and exhibited a dendritic orientation parallel to the edges of the pyramidal tract (Figs. 2.8B, 2.9B,C).

2.3.3.2.4 Raphe Obscurus (ROb)

Two loosely arranged bilateral columns of 5HT+ neurons located either side of the midline from the level of nucleus ambiguus to the spinomedullary junction were classified as the raphe obscurus (Figs. 2.2S-T, 2.3R-T). These 5HT+ neurons were marginally smaller than those within the RMg but larger than those forming the RPa. The neurons were ovoid in shape, a mix of bi- multipolar types and show a dorsoventral dendritic orientation irrespective of polarity (Figs. 2.8B, 2.9D,E). Occasional 5HT+ neurons associated with this nucleus were identified within a short distance (less than 200 μm) lateral to the central

columns and were generally multipolar with some lateral dendritic orientation, but others showed a dorsoventral dendritic orientation.

Figure 2.1: Photographs of the two mole-rat species investigated. A – highveld mole-rat (*Cryptomys hottentotus*) (Mean head and body length: 133 mm for males and 129 mm for females; Chimimba and Bennett, 2005). B – Cape dune mole-rat (*Bathyergus suilius*) (Mean head and body length: 335 mm for males and 300 mm for females; Chimimba and Bennett, 2005). Note the unusual phenotype associated with a subterranean lifestyle and the greatly reduced, though still present, eyes.

Figure 2.2: Serial drawings of coronal sections A to U through the left half of the Cape dune mole-rat brain, from the olfactory bulbs through to the medulla. The outlines of the architectonic regions were drawn using nissl and myelin stains and immunoreactive cells marked on the drawings. Solid black circles depict cholinergic neurons, solid triangles depict catecholaminergic neurons (those immunoreactive for tyrosine hydroxylase) and open squares depict serotonergic neurons. Each circle, triangle or square represents an individual neuron. The figures are approximately 1500 μm apart. See list for abbreviations.

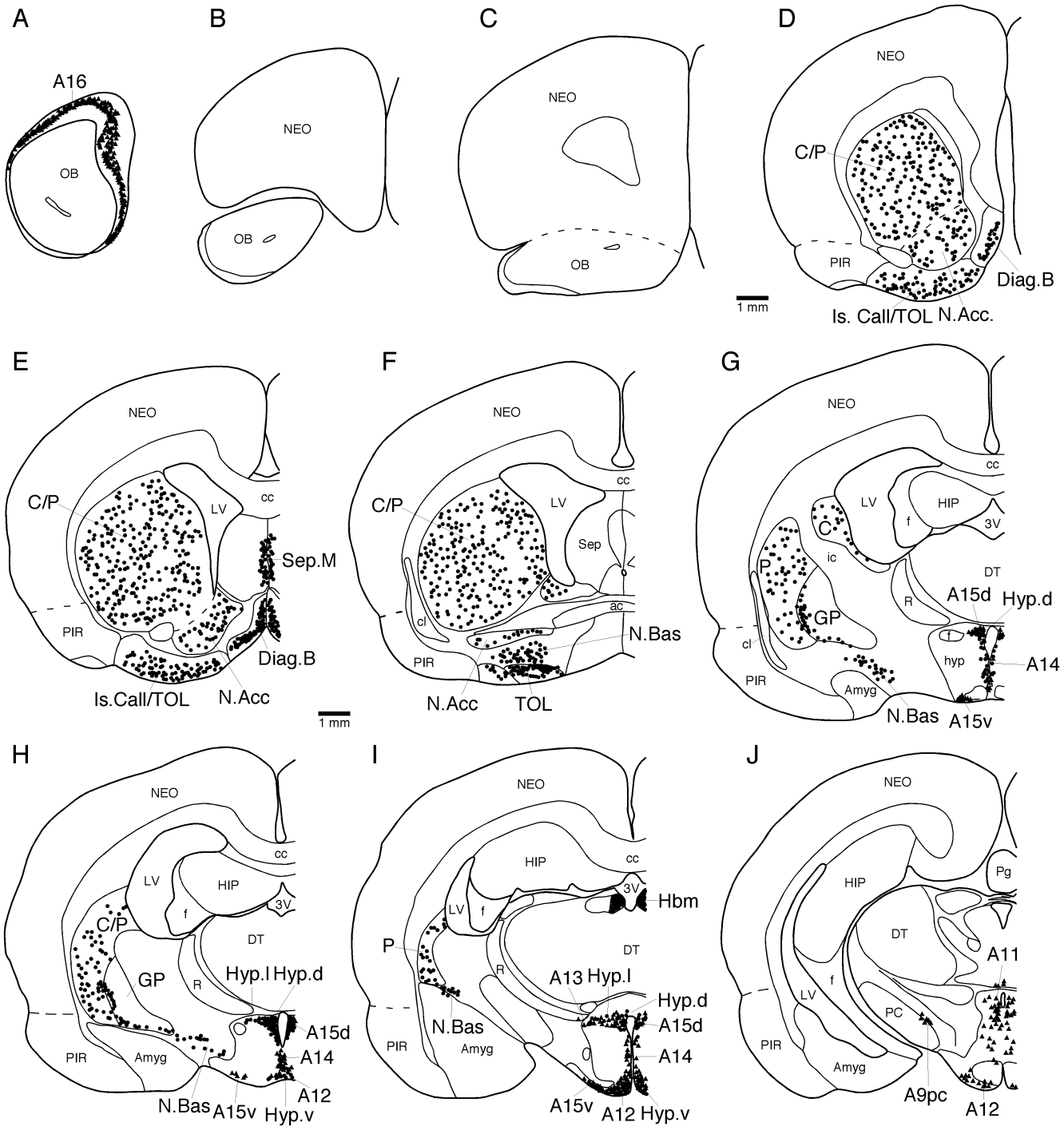
A
A16
OB
B
NEO
OB
C
NEO
OB
D
NEO
C/P
PIR
Diag.B
1 mm
Is. Call/TOL
N.Acc.
E
NEO
C/P
LV
cc
Sep.M
PIR
Diag.B
Is.Call/TOL
N.Acc
1 mm
F
NEO
C/P
LV
cc
Sep
ac
cl
N.Bas
PIR
N.Acc
TOL
G
NEO
cc
LV
HIP
f
3V
C
P
ic
DT
R
A15d
Hyp.d
GP
cl
hyp
A14
PIR
Amyg
N.Bas
A15v
H
NEO
cc
LV
HIP
f
3V
C/P
DT
GP
R
Hyp.l
Hyp.d
A15d
A14
PIR
Amyg
A12
N.Bas
A15v
Hyp.v
I
NEO
HIP
cc
3V
Hbm
LV
f
P
DT
R
A13
Hyp.l
Hyp.d
A15d
N.Bas
PIR
Amyg
A14
A15v
A12
Hyp.v
J
NEO
Pg
HIP
DT
A11
f
LV
PC
PIR
Amyg
A9pc
A12

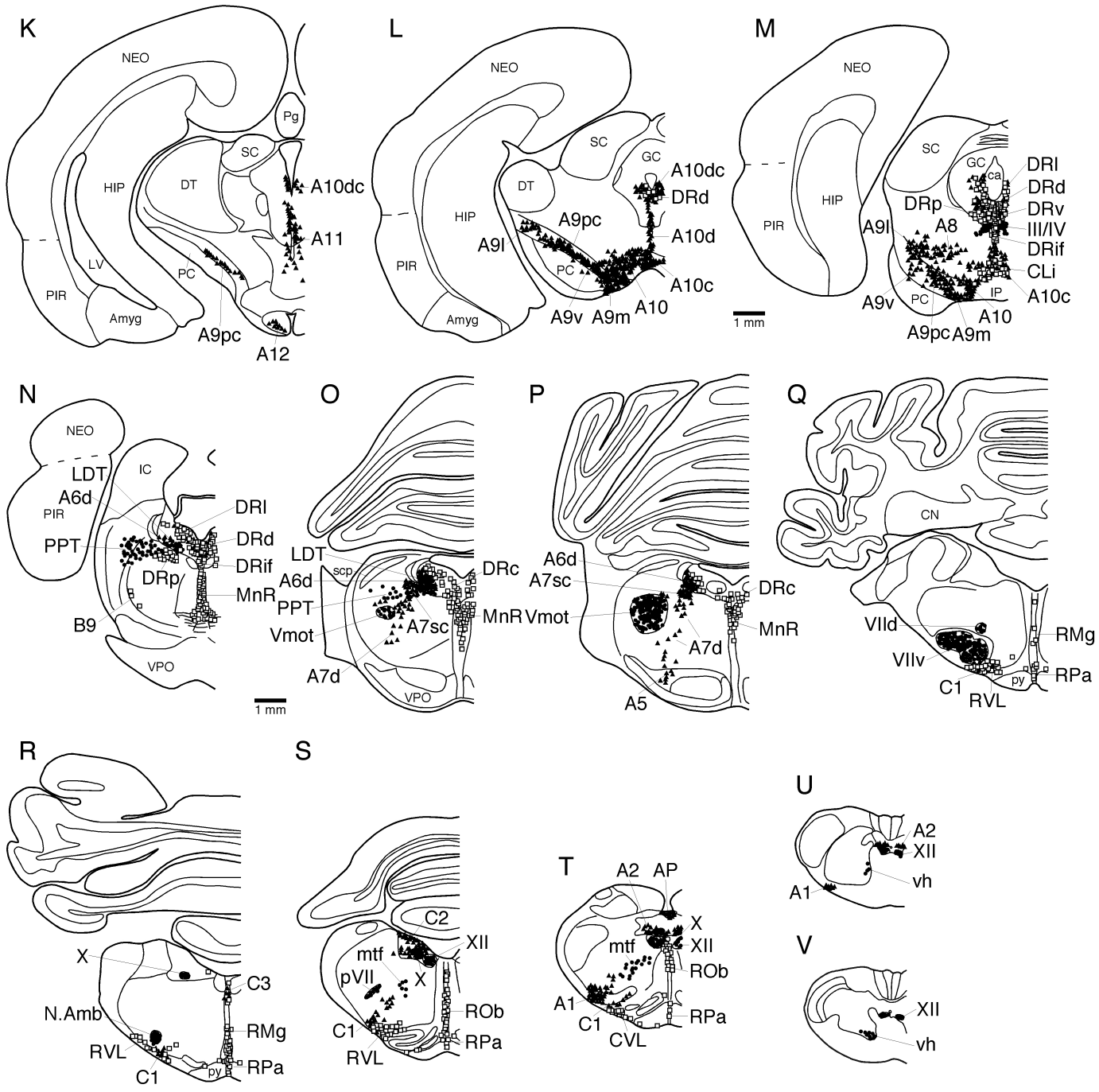
K
NEO
Pg
SC
HIP
DT
A10dc
A11
LV
PC
PIR
Amyg
A9pc
A12
L
NEO
SC
GC
A10dc
DRd
DT
HIP
A9pc
A10d
A9l
PC
A10c
PIR
Amyg
A9v
A9m
A10
M
NEO
SC
GC
ca
DRl
DRd
DRv
III/IV
DRif
CLi
A10c
HIP
DRp
A8
A9l
PIR
A9v
PC
IP
A10
A9pc
A9m
1 mm
N
NEO
LDT
IC
A6d
DRl
PIR
DRd
PPT
DRif
DRp
MnR
B9
VPO
1 mm
O
LDT
scp
DRc
A6d
A6d
PPT
MnR
Vmot
A7sc
Vmot
A7d
VPO
P
A6d
A7sc
DRc
MnR
Vmot
A7d
A5
Q
CN
VIId
RMg
VIIv
RPa
py
C1
RVL
R
X
C3
N.Amb
RMg
RVL
RPa
py
C1
S
C2
XII
mtf
pVII
X
ROb
C1
RPa
RVL
T
A2
AP
X
mtf
XII
ROb
A1
RPa
C1
CVL
U
A2
XII
vh
A1
V
XII
vh

Figure 2.3: Serial drawings of coronal sections A to U through the right half of the highveld mole-rat brain, from the olfactory bulbs through to the medulla. Conventions as in Fig. 2.2. The figures are approximately 750 μm apart. See list for abbreviations.

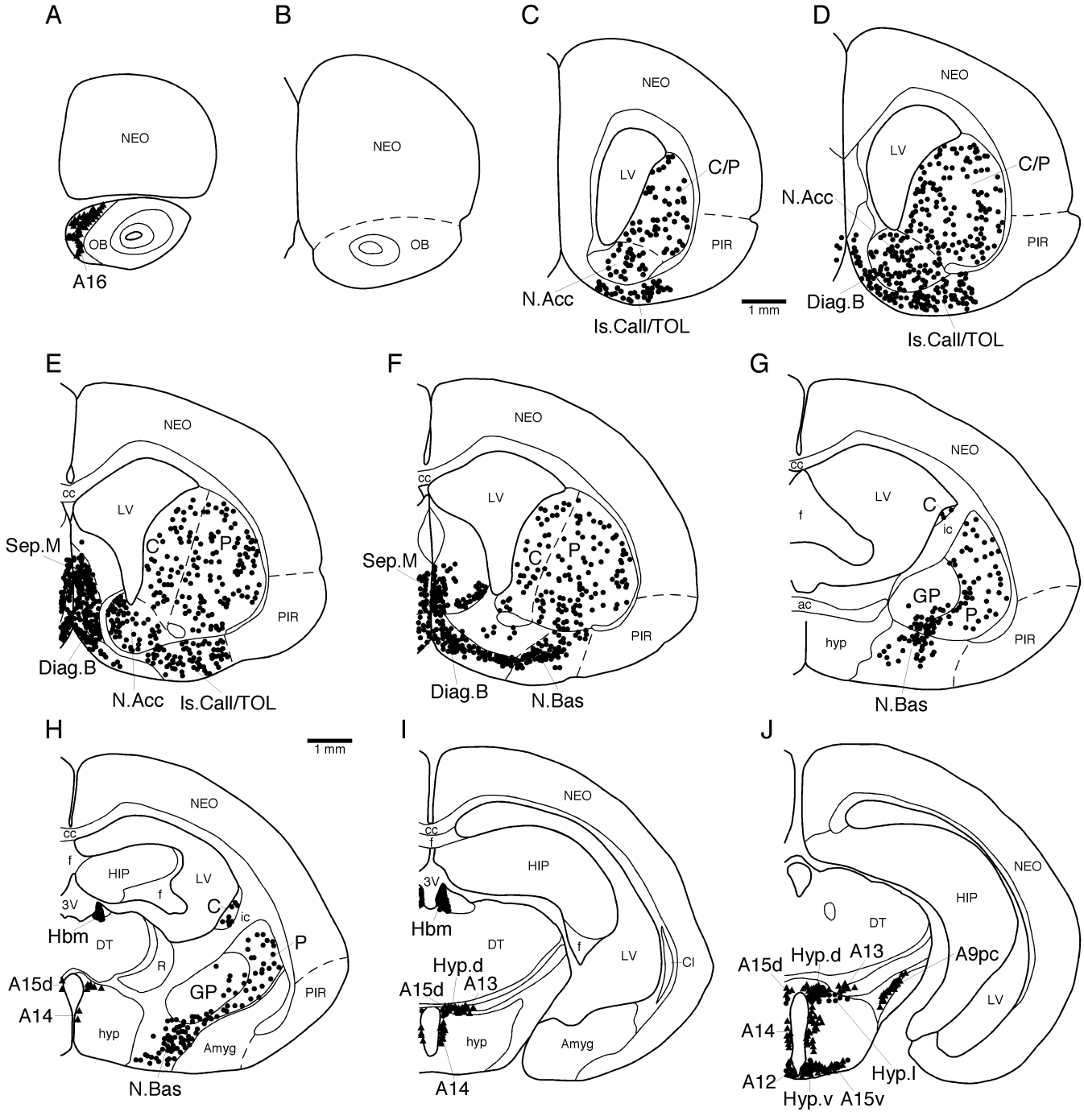
A
NEO
OB
A16
B
NEO
OB
C
NEO
LV
C/P
PIR
N.Acc
Is.Call/TOL
1 mm
D
NEO
LV
C/P
N.Acc
PIR
Diag.B
Is.Call/TOL
E
NEO
cc
LV
Sep.M
C
P
PIR
Diag.B
N.Acc
Is.Call/TOL
F
NEO
cc
LV
Sep.M
C
P
PIR
Diag.B
N.Bas
G
NEO
cc
LV
C
ic
f
GP
ac
P
hyp
PIR
N.Bas
H
1 mm
NEO
cc
f
HIP
LV
f
3V
C
ic
Hbm
DT
P
R
A15d
GP
PIR
A14
hyp
Amyg
N.Bas
I
NEO
cc
f
HIP
3V
Hbm
DT
f
LV
Cl
Hyp.d
A15d
A13
hyp
Amyg
A14
J
NEO
HIP
DT
A15d
Hyp.d
A13
A9pc
LV
A14
A12
Hyp.l
Hyp.v
A15v

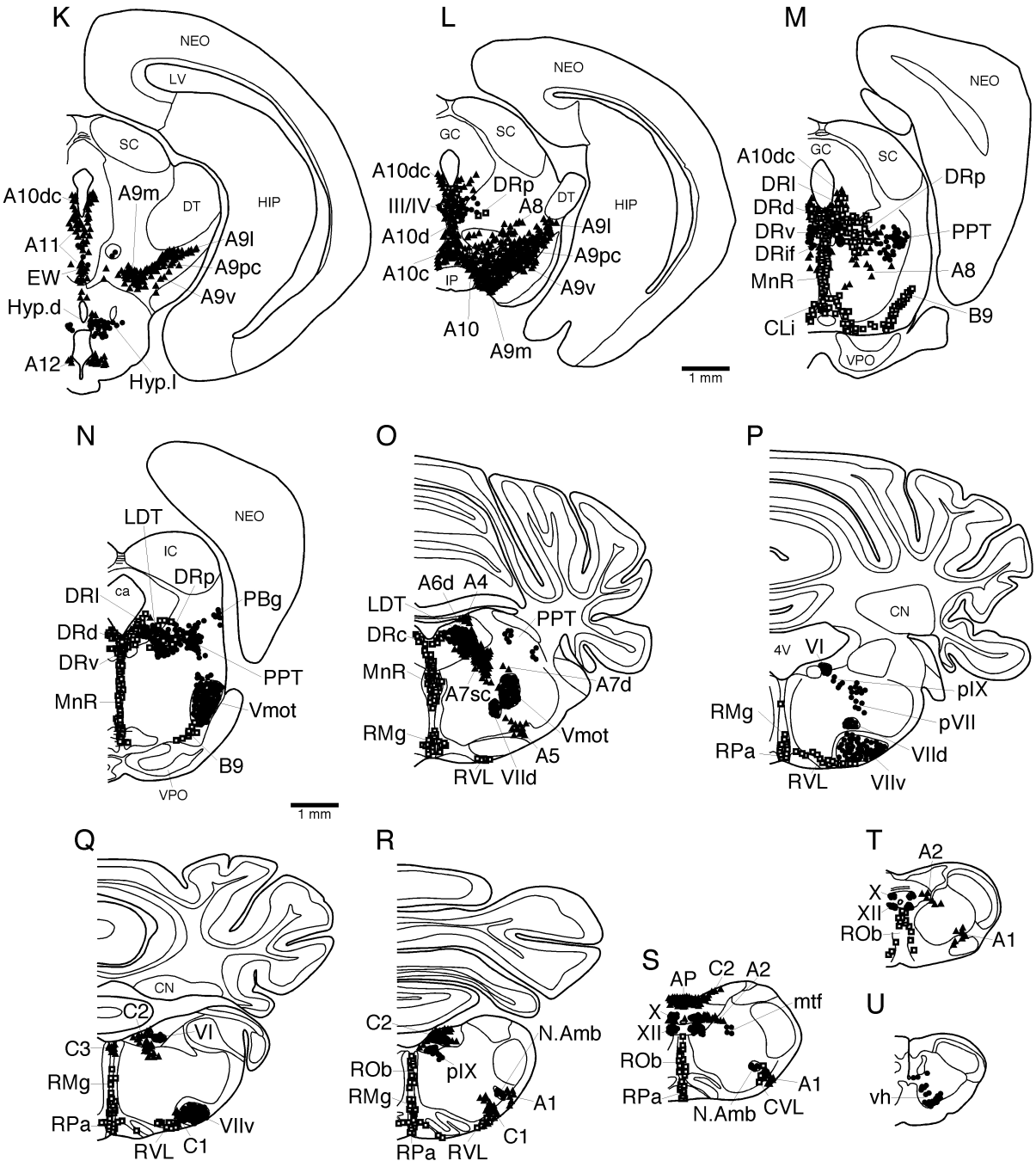
K
NEO
LV
SC
A10dc
A9m
DT
HIP
A11
A9l
EW
A9pc
A9v
Hyp.d
A12
Hyp.l
L
NEO
GC
SC
A10dc
DRp
III/IV
A8
DT
HIP
A10d
A9l
A10c
IP
A9pc
A9v
A10
A9m
1 mm
M
NEO
A10dc
GC
SC
DRp
DRl
DRd
DRv
PPT
DRif
A8
MnR
B9
CLi
VPO
N
LDT
NEO
IC
DRp
DRl
ca
PBg
DRd
DRv
PPT
MnR
Vmot
B9
VPO
1 mm
O
A6d A4
LDT
PPT
DRc
MnR
A7d
A7sc
RMg
Vmot
A5
RVL VIId
P
CN
4V VI
pIX
RMg
pVII
RPa
VIId
RVL
VIIv
Q
CN
C2
VI
C3
RMg
RPa
VIIv
RVL C1
R
C2
N.Amb
ROb
pIX
RMg
A1
C1
RPa RVL
S
AP C2 A2
mtf
X
XII
ROb
A1
RPa
N.Amb CVL
T
A2
X
XII
ROb
A1
U
vh

Figure 2.4: Photomicrographs showing neuronal groups that are immunoreactive for choline acetyltrasnferase in the brain of the highveld mole-rat. (A) Basal forebrain showing the Diag.B. located below the Sep and medial to the N.Acc., LV and head of the C. (B) The densely populated Hbm located between the 3V and the Hbl in the dorsal diencephalon. (C) The LDT and PPT nuclei in the dorsal pontine region ventral to the 4V. (D) The merged III and IV nuclei located in the midbrain. Scale bar in B = 500 µm. Scale bar in D = 1 mm and applies to A, C and D.

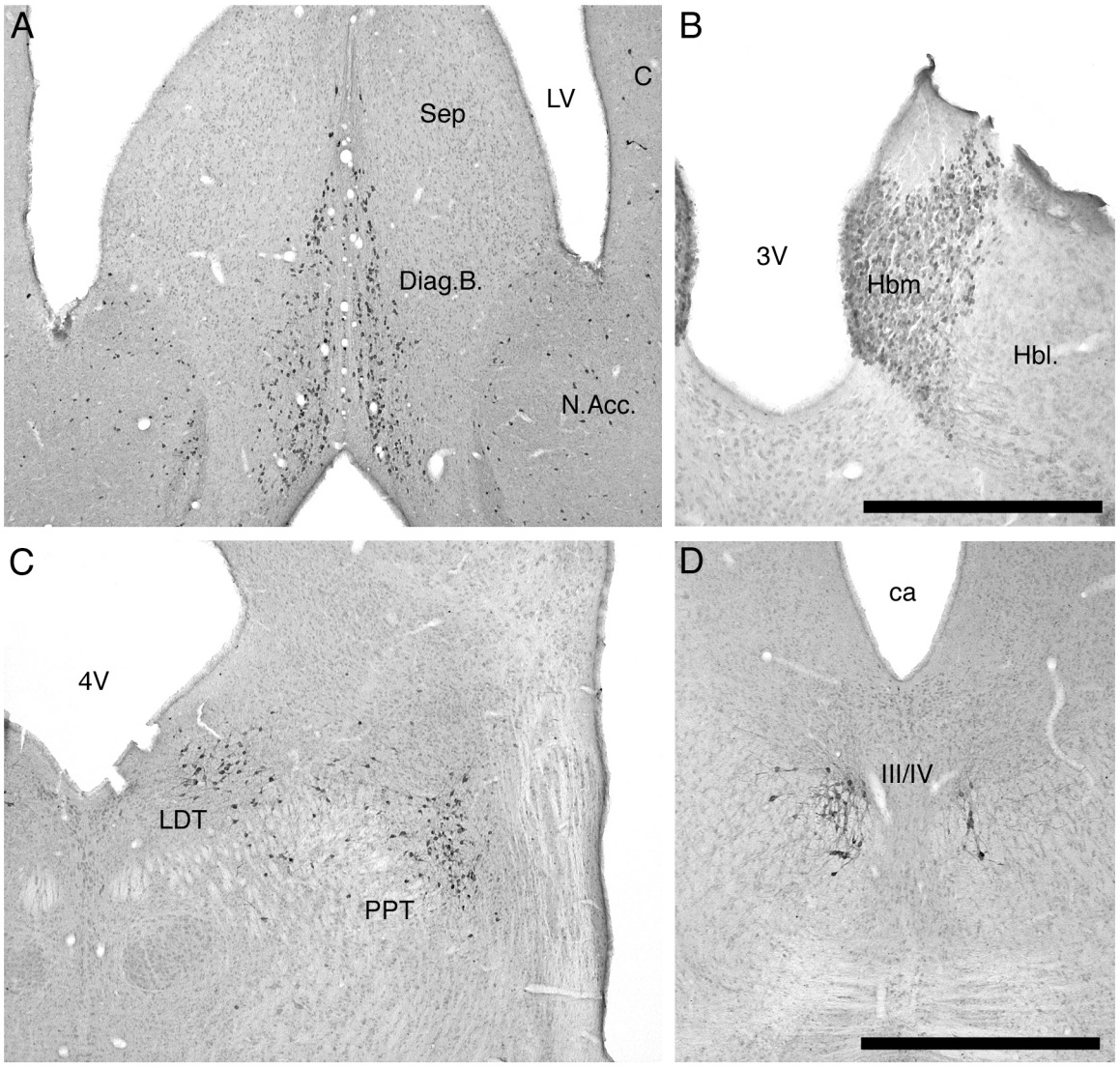
A
Sep
LV
C
Diag.B.
N.Acc.
B
3V
Hbm
Hbl.
C
4V
LDT
PPT
D
ca
III/IV

Figure 2.5: Photomicrographs showing neuronal groups that are immunopositive for tyrosine hydroxylase in the diencephalon, midbrain and pons of the mole-rat brain. Images A, C and D are from the brain of the Cape dune mole-rat, and B, E and F are from the highveld mole-rat. (A) The A11 in the Cape dune mole-rat. (B) A11, A10dc and A10d in the highveld mole-rat. (C) The A14 in the Cape dune mole-rat. (D) The A15v and A12 in the Cape dune mole-rat. Scale bar in D = 500 μm and applies to A–D. (E) Some nuclei of the ventral tegmental area (A10, A10c, A10d) and substantia nigra (A9m, A9pc, A9l) in the highveld mole-rat. (F) Some nuclei of the locus coeruleus complex (A6d, A7sc, A7d) in the highveld mole-rat. Scale bar in F = 1 mm and applies to E and F.

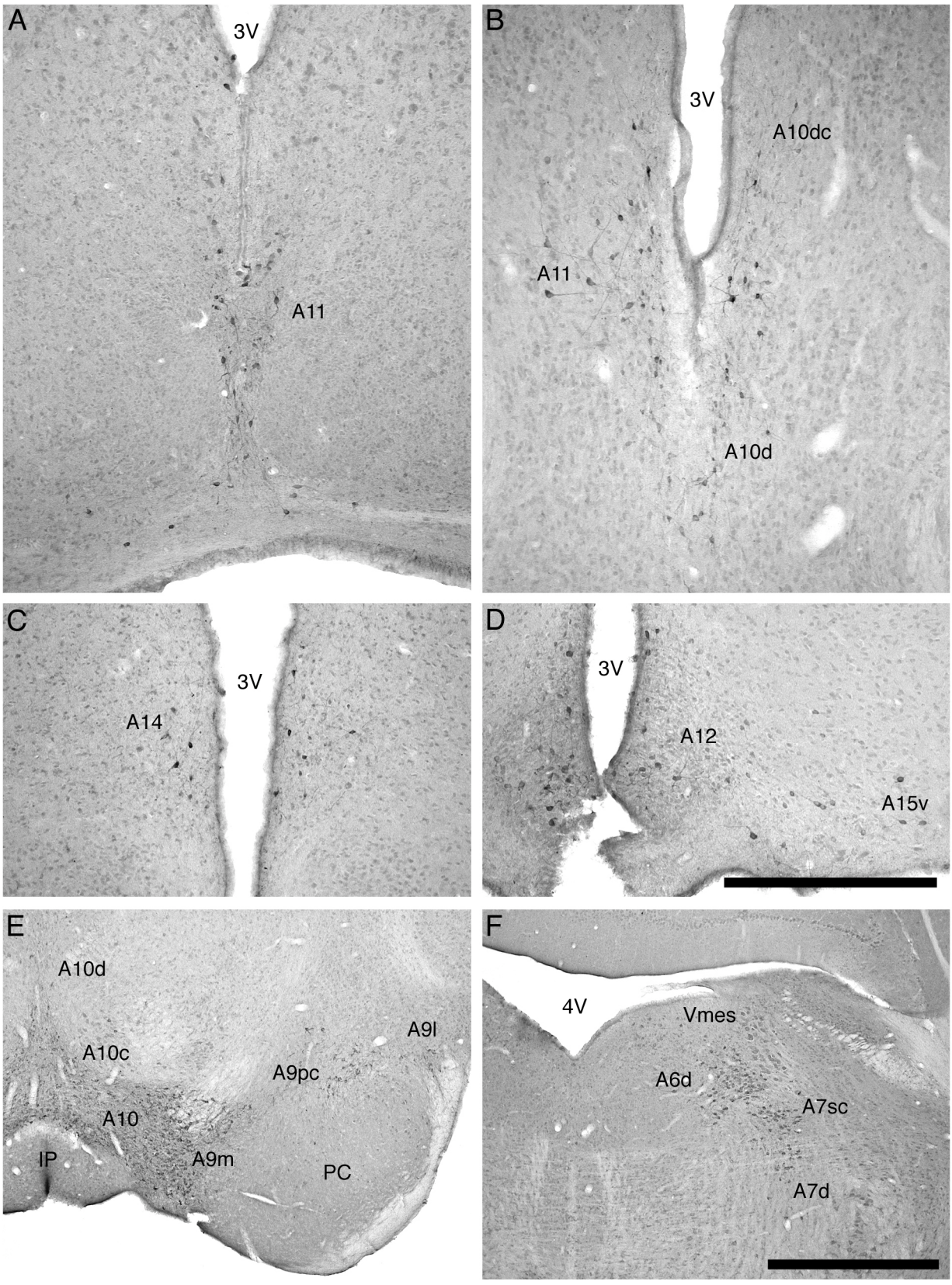
A
3V
A11
B
3V
A10dc
A11
A10d
C
3V
A14
D
3V
A12
A15v
E
A10d
A9l
A10c
A9pc
A10
IP
A9m
PC
F
4V
Vmes
A6d
A7sc
A7d

Figure 2.6: Photomontage of the nuclear organization of the ventral tegmental area (A10, A10c, A10d, A10dc) and the substantia nigra (A9m, A9pc, A9l, A9v) in the Cape dune mole-rat as revealed using tyrosine hydroxylase immunohistochemistry. Scale bar = 1 mm.

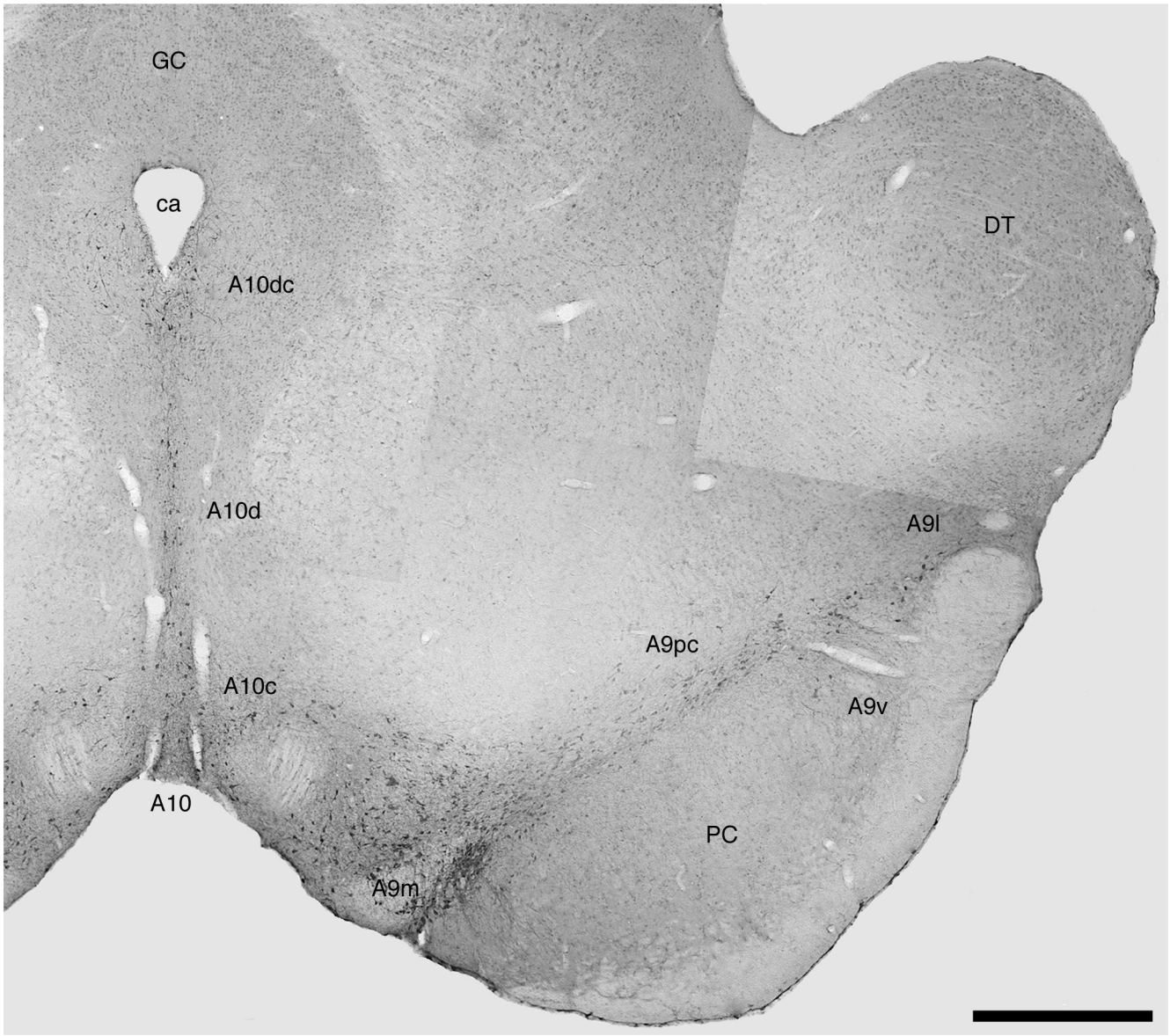
GC
ca
A10dc
DT
A10d
A9l
A9pc
A10c
A9v
A10
PC
A9m

Figure 2.7: Photomicrographs of the A10dc in the (A) Cape dune mole-rat and (B) highveld mole-rat. Note the significant expression of this nucleus in the Cape dune mole-rat compared with the highveld mole-rat that has an A10dc nucleus similar to that seen in other rodents. Scale bar in B = 500 μm and applies to both A and B.

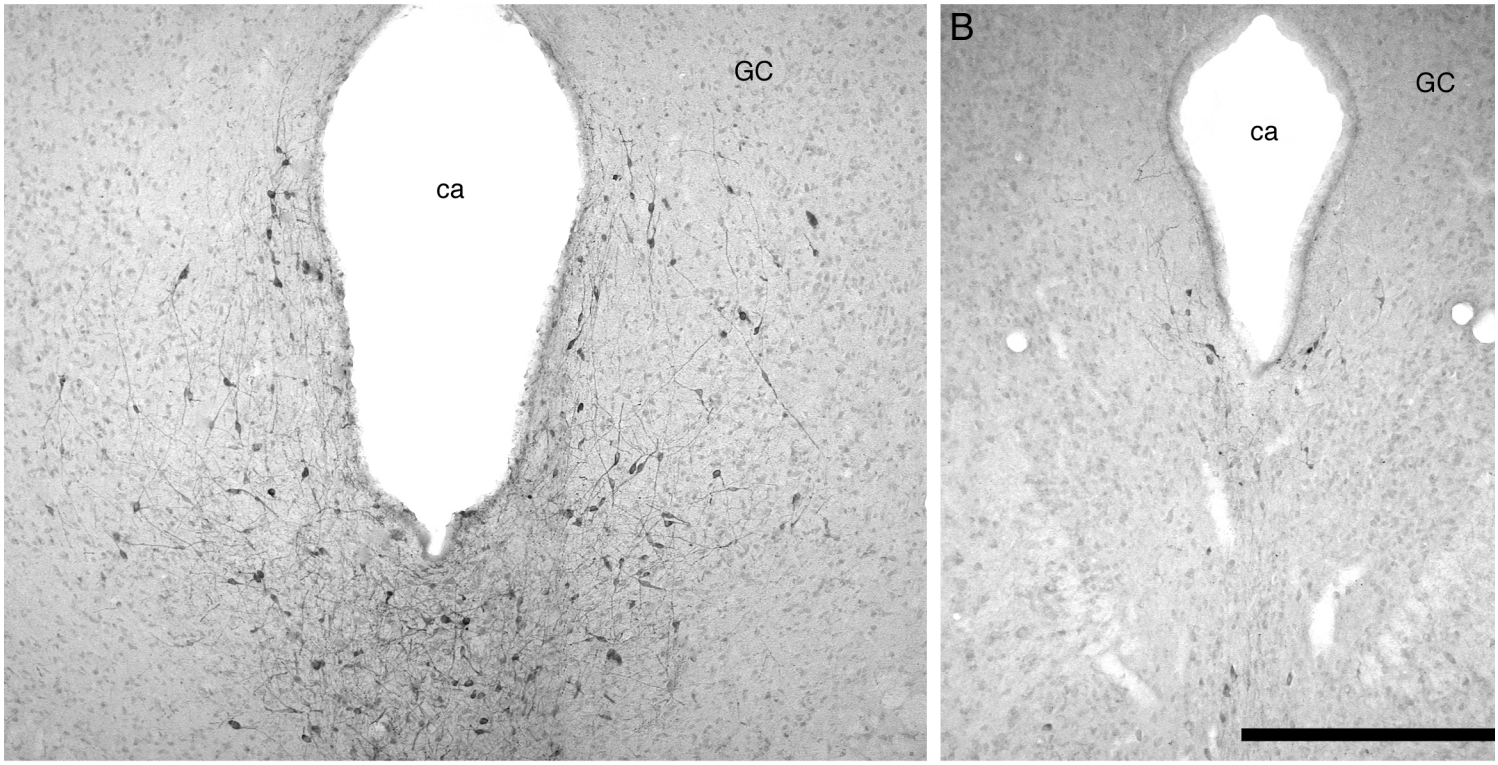
B
GC
ca
GC
ca

Figure 2.8: Photomicrographs showing neuronal groups that are immunopositive for serotonin in the pons and medulla of the Cape dune mole-rat (A, B, C) and highveld mole-rat (D) brain. (A) The distinction between the morphology of the neurons comprising the DRl and DRd nuclei of the dorsal raphe. (B) The ROb and RPa nuclei of the Cape dune mole-rat. (C) The DRc and MnR of the Cape dune mole-rat. (D) A similar image to C showing the DRc, MnR and RMg of the highveld mole-rat. Scale bar in A = 500 μm. Scale bar in C = 1 mm and applies to B, C and D.

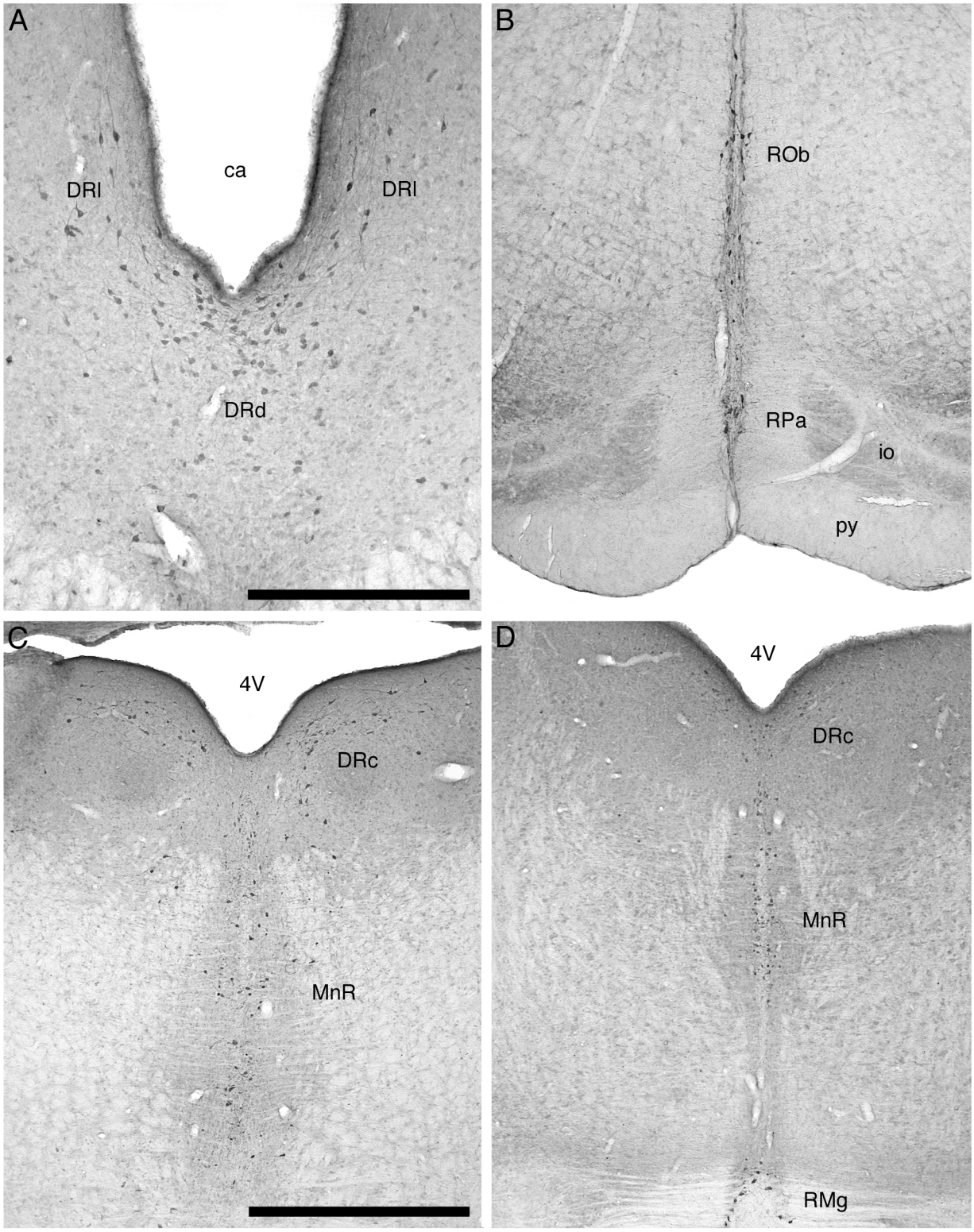
A
ca
DRl
DRl
DRd
B
ROb
RPa
io
py
C
4V
DRc
MnR
D
4V
DRc
MnR
RMg

Figure 2.9: Photomicrographs showing neuronal groups that are immunopositive for serotonin in the medulla of the Cape dune mole-rat (A,E) and highveld mole-rat (B,C,D) brain. (A) This photomicrograph depicts the lateral continuation of RMg as it forms the most anterior portion of the RVL in the Cape dune mole-rat. (B) The RPa nucleus of the highveld mole-rat is intimately associated with the py. (C) The topography of the RMg, RPa and RVL in the highveld mole-rat. (D) The pararaphe position of the ROb of the highveld mole-rat. (E) A higher power view of the neuronal morphology of the ROb in the Cape dune mole-rat. Scale bar in B = 500 μm and applies to B and E. Scale bar in C = 1 mm and applies to A, C and D.

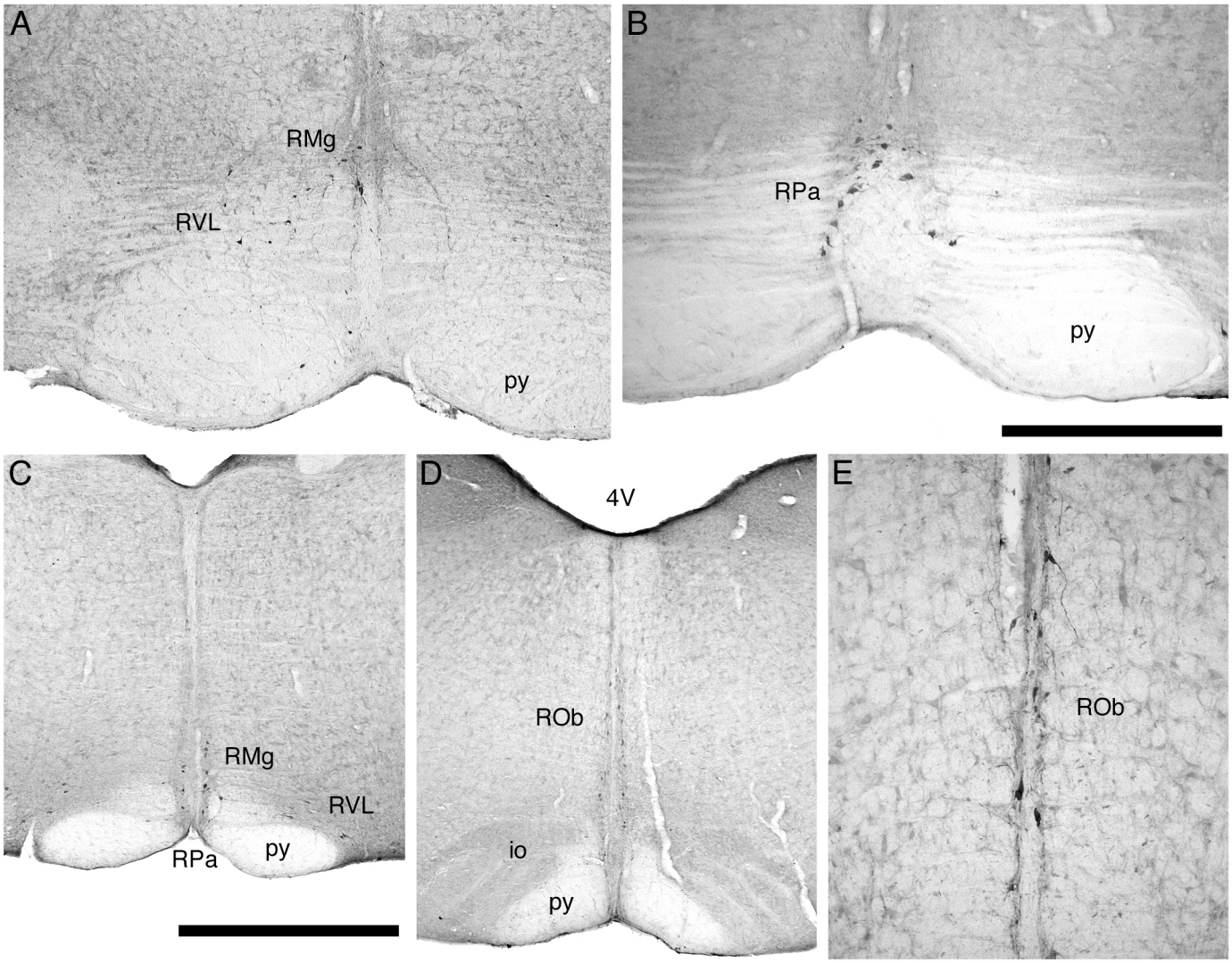
A
RMg
RVL
py
B
RPa
py
C
RMg
RVL
RPa
py
D
4V
ROb
io
py
E
ROb

2.4 Discussion

The central aim of the current study was to assess the nuclear organization of the cholinergic, putative catecholaminergic and serotonergic systems of two species of subterranean rodents that both have an extensively reduced visual system. The central finding was that there exists no difference in the nuclear complexity of these systems in both species of mole-rat studied compared with that of the laboratory rat. This lack of differences is in spite of several factors that may lead to the prediction of differences including the unusual phenotype and life history of the mole-rats and the time since the existence of the last common ancestor of these species and those of other rodents. All nuclei identified for the cholinergic, putative catecholaminergic and serotonergic systems appear to be homologous to those previously described for the laboratory rat (Dahlström and Fuxe, 1964; Fuxe et al., 1969, 1970; Lindvall and Bjorklund, 1974; Steinbusch, 1981; Bjorklund and Lindvall, 1984; Hökfelt et al., 1984; Meredith et al., 1989; Törk, 1990; Oh et al., 1992; Ichikawa et al., 1997) and other species of rodent (Ruggerio et al., 1984; Daszuta and Portalier, 1985; Ishimura et al., 1988; Mufson and Cunningham, 1988; Vincent, 1988; Léger et al., 1998; Satoh et al., 1991; Janusonis et al., 1999, 2003; Janusonis and Fite, 2001; Fite and Janusonis, 2001; Mulders and Robertson, 2005; Da Silva et al., 2006; D'Este et al., 2007; Mahoney et al., 2007; Moon et al., 2007; Dwarika et al., 2008). Moreover, there were not any nuclei that have been reported in laboratory rat that were not present in both the highveld and Cape dune mole-rats, or *vice versa*. This finding indicates the potential for the existence of a phylogenetic constraint in the evolution of the nuclear parcellation (*sensu* Ebbeson, 1980) of these systems acting at the level of the order (see tabulated data in Maseko et al., 2007). These findings support an earlier proposal indicating this to be the case for the nuclear organization of systems within the central nervous system (Manger, 2005).

2.4.1 Cholinergic System

Prior descriptions of the nuclear organization of the cholinergic system in rodents are limited to the laboratory rat (Meredith et al., 1989; Oh et al., 1992; Ichikawa et al., 1997) and the CD-1 strain of laboratory mouse (Mufson and Cunningham, 1988). The current study extends the basis for comparison in providing a full mapping study of the nuclear organization of this system in two species of mole-rat. The cholinergic nuclei of the dorsal striatopallidal complex and the basal forebrain of the mole-rats studied are similar to that seen in the rat (Oh et al., 1992) and mouse (Mufson and Cunningham, 1988). This result is perhaps not surprising, as all other mammals previously studied appear to demonstrate the same nuclear organization within these regions of the cholinergic system (Woolf, 1991; Manger et al., 2002a; Maseko and Manger, 2007; Maseko et al., 2007). Within the diencephalon of the mole-rats studied, four cholinergic nuclei were found, the lateral, ventral and dorsal hypothalamic cholinergic nuclei, as well as the medial habenular nucleus of the epithalamus. These three hypothalamic groups have been reported for rats, laboratory shrews, cats, primates, microbat and the megabat (Satoh et al., 1983; Tago et al., 1989; Vincent and Reiner, 1987; Tinner et al., 1989; Karasawa et al., 2003; Maseko and Manger, 2007; Maseko et al., 2007); however no hypothalamic cholinergic neuronal groups have been reported for the monotremes (Manger et al., 2002a). Within the pontine region of the mole-rats, the laterodorsal tegmental (LDT), pedunculopontine (PPT) and parabigeminal (Pbg) cholinergic nuclei were observed. The LDT and PPT have been identified in all mammals studied to date (Woolf, 1991; Maseko et al., 2007); however the PBg has only been reported in rats, CD-1 mouse, highveld mole-rat, cat, ferret, tree shrew, megabat and primates (Kimura et al., 1981; Mufson and Cunningham, 1988; Murray et al., 1982; Vincent and Reiner, 1987; Henderson, 1987; Mesulam et al., 1989; Da Silva et al., 2006; Maseko et al., 2007). The parabigeminal nucleus in the mole-rats was weakly represented, in terms of number of neurons as observed

previously in the mole-rat (Da Silva et al., 2006), and in terms of the strength of the immunoreactivity of the neurons, as described previously for the rat and mouse (Mufson and Cunningham, 1988; Woolf, 1991; Oh et al., 1992). This low neuronal number within the parabigeminal nucleus of the mole-rats appears to be consistent with the reduced visual system of these rodents as previously suggested (Da Silva, 2006), despite the visually observed difference in the number of neurons between the two species of mole rat studied herein. The parabigeminal nucleus has not been observed in the monotremes (Manger et al., 2002a), laboratory shrew (Karasawa et al., 2003) or the microbat (Maseko and Manger, 2007). A basic similarity in location and identity of the cranial nerve nuclei were found in both species of mole-rat as with all other mammals studied to date (Woolf, 1991; Maseko et al., 2007). Both species of mole rat showed a small number of ChAT immunoreactive neurons in the Edinger-Westphal nucleus; however, this nucleus appeared to have fewer neurons than that seen in rat, cat, ferret, megabat and primates (Kimura et al., 1981; Armstrong et al., 1983; Satoh et al., 1983; Mizukawa et al., 1986; Henderson, 1987; Vincent and Reiner, 1987; Mesulam et al., 1989; Lavoie and Parent, 1994; Maseko et al., 2007). We also found ChAT immunoreactive neurons that represent the preganglionic motor neurons of the superior and inferior salivatory nuclei in both species of mole-rat, as reported for the rat, cat, ferret, megabat, and primates (Armstrong et al., 1983; Mesulam et al., 1989; Satoh and Fibiger, 1985; Mizukawa et al., 1986; Henderson, 1987; Shiromani et al., 1988; Maseko et al., 2007).

2.4.2 Putative catecholaminergic system

Putative catecholaminergic nuclei were found throughout the brain of both species of mole-rats, extending from the olfactory bulbs to the spinomedullary junction. Within the stratum granulosum of the olfactory bulbs, periglomerular TH+ neurons appear to be

homologous to the dopaminergic neurons previously reported in other rodent and other mammalian species (Lichtensteiger, 1966; Lidbrink et al., 1974; Lindvall and Bjorklund, 1974; Hökfelt et al., 1976; Bjorklund and Lindvall, 1984; Smeets and Gonzalez, 2000; Maseko et al., 2007, Moon et al., 2007; Dwarika et al., 2008). All nuclei previously reported for the putative catecholaminergic system within the diencephalon, midbrain, pons and medulla in the laboratory rat (Dahlström and Fuxe, 1964; Fuxe et al., 1969; Lindvall and Bjorklund, 1974; Bjorklund and Lindvall, 1984; Hökfelt et al., 1976, 1984), hamster (Vincent, 1988), grass rat (Mahoney et al., 2007), guinea pig (Mulders and Roberston, 2005), laboratory mouse (Ruggerio et al., 1984, Satoh et al., 1991; D'Este et al., 2007), highveld mole-rat (De Silva et al., 2006), highveld gerbil (Moon et al, 2007) and greater canerat (Dwarika et al., 2008) were found in both species of mole-rat examined in this study.

Despite the lack of difference in nuclear organization there were two differences of note. The first difference is that the number and density of tyrosine hydroxylase immunoreactive neurons in the dorsal caudal nucleus of the ventral tegmental complex (A10dc) of the cape dune mole-rat appeared to be far greater than that seen in the highveld mole-rat, or indeed any other rodent species previously examined (see references given above and Fig. 2.7). It is difficult to interpret what this difference might actually mean in terms of function, as even in the laboratory rat the connections and detailed neurochemistry of these neurons are unknown.

The second difference centres on the location and packing density of the diffuse nucleus of the locus coeruleus (A6d). In the laboratory rat the A6d nucleus, sometimes referred to just as the locus coeruleus, is found within the pontine periventricular grey matter but in a medial location adjacent to the ventricular wall. The catecholaminergic neurons within this region are densely packed and appear to be continuous dorso-caudally with the A4 nucleus (Dahlström and Fuxe, 1964; Fuxe et al., 1969; Lindvall and Bjorklund, 1974;

Bjorklund and Lindvall, 1984; Hökfelt et al., 1976, 1984). This location, packing density and continuity with the A4 nucleus is different to that reported here for both species of mole-rat, and in comparison to that reported for other rodent species such as the laboratory mouse (Ginovart et al., 1996; Von Coelln et al., 2004), hamster (Vincent, 1988), guinea pig (Mulders and Robertson, 2005), highveld gerbil (Moon et al., 2007) and greater canerat (Dwarika et al., 2008). In these other rodents species studied, the locus coeruleus nucleus is located in the ventrolateral corner of the pontine periventricular grey matter and no neurons are found near the ventricular wall. In these other rodent species, only the neurons of the A4 nucleus are found adjacent to the ventricular wall and the packing density of the A6d neurons are much lower than that of the laboratory rat. It is unclear what the factors underlying the rat *vs* other rodents difference may be; however, it is possible that this is a feature of the genus *Rattus*, or it may be the result of selected inbreeding of laboratory strains. Further studies of wild caught *Rattus* species may confirm or eliminate at least one of these possibilities (as previously demonstrated for the cortical cholinergic system, Bhagwandin et al., 2006).

2.4.3 Serotonergic system

The nuclei observed with immunohistochemistry for serotonin in the present study are identical in both species of mole-rat examined and to those previously described for the laboratory rat (Dahlström and Fuxe, 1964; Fuxe et al., 1969; Steinbusch, 1981; Lidov and Molliver, 1982; Waterhouse et al., 1993), mouse (Daszuta and Portalier, 1985), the Mongolian gerbil (Janusonis et al., 1999, 2003; Janusonis and Fite, 2001) greater canerat (Dwarika et al., 2007), highveld gerbil (Moon et al., 2007), and the portion of the brain studied in the Chilean degus (Fite and Janusonis, 2001). The nuclear organization of the serotonergic system across all eutherian mammals studied to date is identical (Bjarkam et al.,

1997; Maseko et al., 2007); in nonplacental mammals, however, other patterns are seen. There are serotonergic neurons in the hypothalamus of monotremes (Manger et al., 2002c), there is a lack of serotonergic neurons in the region of the CVL column in the monotremes and the opossum (Manger et al., 2002; Crutcher and Humbertson, 1978), and there is a lack of a caudal division of the dorsal raphe in the monotremes (Manger et al., 2002c).

2.4.4 Evolutionary considerations

The current investigation of three immunohistochemically identifiable neuronal systems in the brain of two species of wild caught mole-rat, demonstrates that despite major differences in phenotype (regressed visual system; Oelschlager et al., 2000; Cernuda-Cernuda et al., 2003; Nemec et al., 2004), life-history (unusual circadian rhythms, subterranean lifestyle, range of social systems; Lovegrove and Papenfus, 1995; Lovegrove and Muir, 1996; Negroni et al., 2003; Oosthuizen et al., 2003; Gutjahr et al., 2004) and time since evolutionary divergence (Adkins et al., 2003; Faulkes et al., 2004), no change in the complexity of the nuclear organization of the neural systems has occurred. It appears likely that a constraint, acting at the phylogenetic level of the order is limiting parcellation (*sensu* Ebbesson, 1980) of these systems, such that all species belonging to the same mammalian order demonstrate the same complement of homologous nuclei of these systems (Manger, 2005; Maseko et al., 2007). The complexity of nuclear organization, in terms of the number of nuclei, appears to be able to change between, but not within, orders (see tables provided in Maseko et al., 2007). The current study is aligned with previous studies in rodents that have shown that neither the time since evolutionary divergence (Da Silva et al., 2006; Dwarika et al., 2008), changes in phenotype (Moon et al., 2007), nor an increase in brain size (Dwarika et al., 2008) initiate any major differences in the nuclear complexity of the systems under study within the same mammalian order. Thus, it is possible to reasonably conclude at the

moment that for the order Rodentia, varying phenotype, varying life history, evolutionary divergence and brain size do not lead to changes in nuclear complexity of the cholinergic, putative catecholaminergic and serotonergic systems. Further studies examining species that show greater changes in brain size, both large and small, and changes in relative brain size are required to fully test the proposed phylogenetic constraint that appears to be emerging as an explanation surrounding the observations made to date on various rodent, and other, species.

Chapter 3 - Distribution of orexinergic neurons and terminal networks in the brains of two African mole rats

3.1 Introduction

Orexin (also known as hypocretin) is a neuropeptide that has been reported to play a role in the regulation of feeding, drinking, body temperature, general activity (Lubkin and Stricker-Krongrad, 1998; Edwards et al., 1999; Hagan et al., 1999; Kunii et al., 1999; Mondal et al., 1999; Piper et al., 2000; Estabrooke et al., 2001; Hungs et al., 2001; Yoshimichi et al., 2001; Kotz et al., 2002; Berthoud et al., 2005), energy homeostasis (Mintz et al., 2001), stimulation of gastric secretion in rats (Takahashi et al., 1999), increasing metabolic rate in rats (Lubkin and Stricker-Krongard, 1998), altering luteinising hormone release in rats (Pu et al., 1998) and in the regulation of the sleep-wake cycle specifically associated with increased wakefulness and inhibition of REM sleep (Sakurai et al., 1998; Chemelli et al., 1999; Siegel, 1999; Bourgin et al., 2000; Kilduff and Peyron, 2000; Thannickal et al., 2000; van den Pol, 2000).

The distribution of orexin-immunopositive (Orx +) cell bodies and terminal networks within the brain has been reported in a range of mammals including: humans (*Homo sapiens*, Moore et al., 2001); domestic cat (*Felis catus*, Zhang et al., 2001, 2002); domestic sheep (*Ovis aries*, Iqbal et al., 2001); six species of rodent (laboratory rat, *Rattus norvegicus* – Broberger et al., 1998; Peyron et al., 1998; Chen et al., 1999; Cutler et al., 1999; Date et al., 1999; Hagan et al., 1999; Nambu et al., 1999, Risold et al., 1999; Baldo et al., 2003; Chou et al., 2004; Espana et al., 2005; Kirouac et al., 2005; Nixon and Smale, 2007; Nile grass rat, *Arvicanthus niloticus* – Novak and Albers, 2002; Nixon and Smale, 2007; golden or Syrian hamster, *Mesocricetus auratus* – McGranaghan and Piggens, 2001; Mintz et al., 2001; Vidal et al., 2005; Nixon and Smale, 2007; laboratory mouse, *Mus musculus*, C57B1 strain,

Broberger et al., 1998; Siberian or Djungarian hamster, *Phodopus sungorus* – McGranaghan and Piggins, 2001; Khorooshi and Klingenspor, 2005; degu, *Octodon degus* – Nixon and Smale, 2007); five microchiropteran species (Kruger et al., 2010); and the Eastern grey kangaroo (*Macropus giganteus*, Yamamoto et al., 2006). The Orx + neuronal cell bodies were invariably localized within the hypothalamus and while for most mammals they were represented as a rather homogenous loosely packed large cluster of neurons located in the perifornical and lateral hypothalamus (see above references), in certain rodents there may be up to four clusters, or nuclei, of orexinergic neurons – the two described above, plus one cluster located in the anterior hypothalamic paraventricular subnucleus and one in the lateral ventral hypothalamic supraoptic area (LVHA) (Nixon and Smale, 2007).

Orexin immunoreactive terminal networks have been found in differential relative densities throughout the varying brain regions previously examined (see references cited above). A high relative density of Orx+ terminals have been consistently observed within the paraventricular nucleus of the epithalamus, the noradrenergic locus coeruleus complex and the serotonergic dorsal raphe nuclear complex. The majority of the nuclei of the hypothalamus as well as the septal region, cholinergic nuclei of the pons, the ventral tegmental area, the nuclei of the solitary tract, the remaining serotonergic nuclei and both limbs of the diagonal band of Broca were consistently described as having a medium relative density of Orx+ terminals. A low to absent density of Orx+ terminals have been recorded in regions such as the cerebral cortex, major nuclei of the dorsal thalamus and other regions of the central nervous system (see references above).

Recent studies have demonstrated that in rodents and other species, the complexity of the nuclear organization of the diffusely projecting cholinergic, catecholaminergic and serotonergic systems remains consistent within an order despite differences in brain size, phenotype, lifestyle or evolutionary distance (e.g. Manger, 2005; Maseko et al., 2007;

Bhagwandin et al., 2008; Dwarika et al., 2008; Limacher et al., 2008, Gravett et al., 2009, Pieters et al., 2010; Bux et al., 2010). In terms of the orexinergic system this appears to hold true for most mammals; however, the observations of variance in the number of potential orexinergic nuclei in rodents (Nixon and Smale, 2007) may indicate greater organizational variance within an order for this diffusely projecting system than other systems previously studied.

In contrast to this order level consistency in nuclear organization, the pattern of terminal networks of these diffusely projecting neurotransmitter systems appears to be more variable within the order. For example, when the innervation patterns of the serotonergic (Raghanti et al., 2008a) and cholinergic (Raghanti et al., 2008b) terminal networks within the cerebral cortex of humans, chimpanzees and macaque monkeys were compared, there were no species differences in the primary motor cortex (Brodmann's area 4), but significant quantitative and qualitative differences were observed between macaques on the one hand and chimpanzees and humans on the other (which were similar) in two pre-motor cortical areas (Brodmann's areas 9 and 32). These studies are suggestive of family level consistencies and inter-family differences in the terminal networks of the diffusely projecting neural systems. Comparative studies of the orexinergic projections in rodents are also suggestive of certain qualitative differences in terminal network densities within and between families despite many overall similarities (McGranaghan and Piggins, 2001; Nixon and Smale, 2007).

In the current study, whole brains of two species of African mole rat, the highveld mole rat (*Cryptomys hottentotus*) and the Cape dune mole rat (*Bathyergus suillus*) were examined immunohistochemically for orexin-A. Both species studied have a greatly reduced visual system (Oelschlager et al., 2000; Cernuda-Cernuda et al., 2003; Nemec et al., 2004), are subterranean, and appear to have a free-running circadian activity oscillator (Lovegrove

and Papenfus, 1995; Lovegrove and Muir, 1996; Negroni et al., 2003; Oosthuizen et al., 2003; Gutjahr et al., 2004). These atypical rodent features combined with the distant (but familial) relation to each other and to the non-familial laboratory rat (Adkins et al., 2003), provide an interesting model to examine changes in nuclear organization and terminal network patterns that may be related to phenotype, life history and behaviour.

3.2 Materials and Methods

The brains of three adult highveld mole rats (*Cryptomys hottentotus*) (average body weight: 86.5 g; average brain weight: 1.5 g) and three adult Cape dune mole rats (*Bathyergus suillus*) (average body weight: 965 g; average brain weight: 3.4 g) were used in the current study. All animals were treated and used according to the guidelines of the University of the Witwatersrand Animal Ethics Committee, which parallel those of the NIH for the care and use of animals in scientific experimentation. Both species of mole rat display a seasonal breeding pattern. The mole rats were placed under deep barbiturate anaesthesia (Euthanaze, 200mg sodium pentobarbital/ kg, i.p.), and then perfused intracardially upon cessation of respiration. The perfusion was initially done with a rinse of 0.9% saline solution at 4°C, followed by a solution of 4% paraformaldehyde in 0.1M phosphate buffer (PB, pH: 7.4) (approximately 1l/kg of each solution). Brains were then removed from the skull and post-fixed overnight (24 h) in 4% paraformaldehyde in 0.1M PB, and then allowed to equilibrate in 30% sucrose in PB. The brains were then frozen and sectioned into serial coronal and sagittal sections of 50 μm thickness. A one in three series of stains was made for Nissl, myelin and orexin A. Sections kept for the Nissl series were mounted on 0.5% gelatine coated glass slides, cleared in a solution of 1:1 chloroform and absolute alcohol, then stained with 1% cresyl violet. Myelin sections were stored in 5% formalin at 4°C for a period of two weeks and were then mounted on 1% gelatine coated glass slides and subsequently stained

with a modified silver stain (Gallyas, 1979).

For immunohistochemical staining the sections were first treated for 30 min with an endogenous peroxidase inhibitor (49.2% methanol: 49.2% of 0.1PB: 1.6% of 30% H_2O_2) followed by three 10 min rinses in 0.1M PB. This was followed by a 2 hour pre-incubation, at room temperature, in a solution (blocking buffer) containing 3% normal goat serum (NGS, Chemicon), 2% bovine serum albumin (BSA, Sigma), and 0.25% Triton X-100 (Merck) in 0.1M PB. The sections were then placed in a primary antibody solution containing the appropriately diluted antibody in blocking buffer, for 48 hours at 4°C. To reveal orexinergic neurons we used the anti-orexin A antibody (AB 3704, Millipore, raised in rabbit) at a dilution of 1:1500. This step was followed by three 10 min rinses in 0.1M PB, after which the sections were incubated in a secondary antibody for two hours (room temperature, 22-24°C). The secondary antibody solution contained a 1:1000 dilution of biotinylated anti-rabbit IgG (BA-1000, Vector Labs) in 3% NGS, and 2% BSA in 0.1M PB. After three 10 min rinses in 0.1M PB, the sections were incubated for 1 hour in AB solution (Vector Labs), and again rinsed. The sections were then treated in a solution of 0.05% diaminobenzidine in 0.1M PB for 5 minutes, following which 3µl of 30% H_2O_2 was added to the 1ml of solution in which each section was immersed. Staining development was monitored visually and checked under a low power stereomicroscope until the background staining was at a level at which it could assist reconstruction without obscuring the immunopositive neuronal structures. Development was arrested by placing the sections in 0.1M PB, and then rinsed twice more in the same solution. Sections were mounted on glass slides coated with 0.5% gelatine and left to dry overnight. They were then dehydrated in a graded series of alcohols, cleared in xylene, and coverslipped with Depex. Two controls were employed in the immunohistochemistry, including the omission of the primary antibody and the omission of the secondary antibody in selected sections. The sections were observed with a low power stereomicroscope, and the

architectonic borders of the sections traced according to the Nissl stained sections using a camera lucida. The immunostained sections were then matched to the drawings and the immunopositive neurons marked, in addition the density of axon terminal staining was graded from low to high for each immunostained section and medium and high marked on the drawings. The drawings were then scanned and redrawn using the Canvas 8 drawing program. The location of Orx+ neuronal structures and the corresponding orexinergic terminal network distribution were described in relation to the general neuroanatomy of the brain and the cholinergic, catecholaminergic and serotonergic systems described previously for these two speceis of mole rat (Bhagwandin et al., 2008).

3.3 Results

In both species of mole rat examined, immunohistochemically identifiable, morphologically homogenous, orexinergic (Orx+) cell bodies were limited to the hypothalamus, as previously reported in all other mammals studied to date. The terminal networks, while remaining similar in distribution between both species, are more strongly expressed in the Cape dune mole rat than in the highveld mole rat. The following descriptions of the Orx+ cell bodies and terminal networks, for both species of mole rat (unless otherwise specified), are provided in relation to the general anatomy of the brain, or to the neuronal groups of the cholinergic, catecholaminergic and serotonergic systems (as described for these particular species in Bhagwandin et al., 2008) where overlap occurs.

3.3.1 Orexinergic Cell Body Distribution

Both species of mole rat expressed Orx+ neurons only within the hypothalamus and were observed as sharing a common neuronal locality within the lateral hypothalamic area (LHA), perifornical region (PFR) and the lateral ventral hypothalamic supraoptic area

(LVHA) (Figs. 3.1G-I, 3.2I-J). Within the LHA of both species a moderate density of Orx+ cells bodies were found to intermingle with the lateral hypothalamic cholinergic nucleus and the dopaminergic neurons of the A13 (zona incerta) nucleus. The Orx+ neurons of the PFR were observed to show a moderate density and did not overlap with any previously described cholinergic or dopaminergic neurons. In both species, the LVHA Orx+ neurons were found in the same region as the dopaminergic A15v (ventral division of the anterior hypothalamic group) nucleus, in the lateral and ventral portions of the hypothalamus, immediately dorsal to the greatly reduced optic tract (Fig. 3.3). No Orx+ neurons could be identified in the anterior hypothalamic paraventricular subnucleus in either mole rat species. Thus, there appears to be three distinct clusters of Orx+ neurons in the hypothalamus of the mole rats studied, a large homogeneous cluster spanning the lateral and perifornical regions, a distinct cluster extending into the region of the zona incerta, and a final cluster in the ventral lateral hypothalamus adjacent to the optic tracts. Both mole rats exhibited neuronal cell bodies that were morphologically homogenous in all three clusters, and that were ovoid in shape, and a varying mixture of bi- and multi- polar types that showed no specific dendritic orientation (Fig. 3.3).

3.3.2. Orexinergic Terminal Networks

3.3.2.1 Telencephalon

Throughout the telencephalon of both species there was only one region of high-density Orx+ terminal networks, this being within the very anterior portion of the septal nuclear complex of the highveld mole rat (Fig. 3.2D). In both species a medium relative density of Orx + terminals were observed within the shell of the nucleus accumbens, the entire septal nuclear complex (overlapping with the cholinergic medial septal nucleus), the cholinergic diagonal band of Broca, and in small portions of the nucleus basalis and the

olfactory tubercule (Figs. 3.1C-F, 3.2C-F). All remaining regions of the telencephalon (cerebral cortex, the dorsal striatopallidal complex, hippocampal complex, amygdalar complex) were observed to have a low-density terminal network in both species of mole rat.

3.3.2.2 Diencephalon

A medium density Orx+ terminal network characterized the entire hypothalamus in both species examined; however, high terminal network densities were noted in a region adjacent to the dorsal aspect of the third ventricle within the hypothalamus of both species of mole rat in the region where the dopaminergic neurons of the A15d (dorsal division of the anterior hypothalamic group) nucleus were located (Figs. 3.1H-J, 3.2H-I). A second region of high-density Orx+ terminals was found in the premammillary nuclei of both species; however, the mammillary nuclei themselves only exhibited a low density of Orx+ terminals. A low-density terminal network was observed through both the dorsal and ventral thalamus, except for the intralaminar central median nucleus of the dorsal thalamus where a medium-density network of Orx+ terminals was observed. In contrast to this, the epithalamus evinced a high-density terminal network in the dorsal aspects of the paraventricular nuclei and a medium density terminal network in the the ventral midline part of the paraventricular thalamic nuclei and in the regions surrounding the habenular nuclei, especially the lateral habenular nucleus and dorsal most portions of the fasciculus retroflexus (Figs. 3.1H-I, 3.2H-I, 3.5).

3.3.2.3 Midbrain (Mesencephalon)

Within the midbrain of both species a high-density Orx+ terminal network was observed throughout the serotonergic dorsal raphe nuclear complex and the serotonergic median raphe nucleus (Figs. 3.1M-N, 3.2M-O, 3.6A). A second region of high-density Orx+

terminals was observed in the dorsomedial periaqueductal gray matter (DMPAG) in both species. The remainder of the periaqueductal gray matter was observed to contain a medium density Orx+ terminal network, which was also observed within the superior colliculus, parts of the ventral tegmental nuclear complex, specifically the A10dc, A10c and A10d nuclei, and in the serotonergic caudal linear nucleus (CLi) and supralemniscal serotonergic group (B9). The medium-density Orx+ terminal network within the midbrain of the highveld mole rat was more extensive than that seen in the cape dune mole rat and was observed in the A10 nucleus, the inferior colliculus, upper midbrain tegmentum and interpeduncular nucleus, whereas in the cape dune mole rat these regions only contained a low-density Orx+ terminal network, or in the case of the superior colliculus and interpeduncular nucleus appeared to be limited to a specific portion of these nuclei (Figs. 3.1J-N, 3.2K-N). All other regions of the midbrain evinced a low-density Orx+ terminal network in both species of mole rat.

3.3.2.4 Pontine region (Metencephalon)

Within the pons of both species, high-density Orx+ terminal networks were observed in the cholinergic laterodorsal tegmental nucleus (LDT), the noradrenergic diffuse nucleus of the locus coeruleus (A6d) and compact nucleus of the subcoeruleus (A7sc), and the serotonergic caudal nucleus of the dorsal raphe complex (DRc) (Figs. 3.1N-P, 3.2N-O, 3.4A, 3.6A). In the dorsal pontine tegmentum of both species, a medium-density Orx+ terminal network was seen to overlap with the regions where the neurons of the cholinergic pedunculopontine tegmental nucleus (PPT) and noradrenergic diffuse nucleus of the subcoeruleus (A7d) were found. Other medium density Orx+ terminal networks were observed to overlap with the distribution of the noradrenergic neurons of the fifth arcuate nucleus (A5) and the pontine portion of the serotonergic median raphe nucleus (MnR) (Fig. 3.6B). All other portions of the pontine region were observed to contain a relatively low-density Orx+ terminal network.

3.3.2.5 Medulla oblongata (Myelencephalon) and Cerebellum

Within the medulla there was only one region that contained a high-density Orx+ terminal network and this was the area postrema (AP) of the Cape dune mole rat (Fig. 3.1T). Interestingly, in the highveld mole rat there was only a low-density Orx+ terminal network in this structure. Medium-density Orx+ terminal networks were observed in all the regions where serotonergic neurons were located, which include the raphe magnus nucleus (RMg) and its continuation in the rostral and caudal ventrolateral serotonergic columns (RVL and CVL), the raphe pallidus nucleus (RPa) and the raphe obscurus nucleus (ROb) (Fig. 3.6C). The remaining regions of the medulla that showed medium-density Orx+ terminal networks were coincident with the catecholaminergic nuclei previously reported, including the rostral ventrolateral medullary tegmental group (C1) (Fig. 3.4C), rostral dorsomedial medullary nucleus (C2), caudal ventrolateral medullary tegmental group (A1) and the caudal dorsomedial medullary nucleus (A2). The extent of this medium-density network around the C2 and A2 nuclei was quite expansive and appeared to include the majority of the nuclei of the solitary tract. A global low-density Orx+ terminal network was observed throughout the remaining regions of the medulla oblongata. No specific species differences were observed in the medulla. A low-density Orx+ terminal network was observed throughout all regions of the cerebellum, both cortical and nuclear, for both species.

Figure 3.1: Drawings of coronal sections A to V through the left half of the brain of the Cape-dune mole rat (*Bathyergus suillus*) depicting the distribution of orexinergic terminal network densities (an absence of shading represents low density, grey shaded areas represents medium density and black shaded areas represents high density) and Orx immunoreactive neurons (each black dot represents a single neuron) relative to the nuclear organization of the cholinergic system, catecholiminergic system and serotonergic system [previously described in Bhagwandin et al. (2008) for this species]. Absence of shading indicates either a minor terminal network or no terminal network (see text for details). See list for abbreviations.

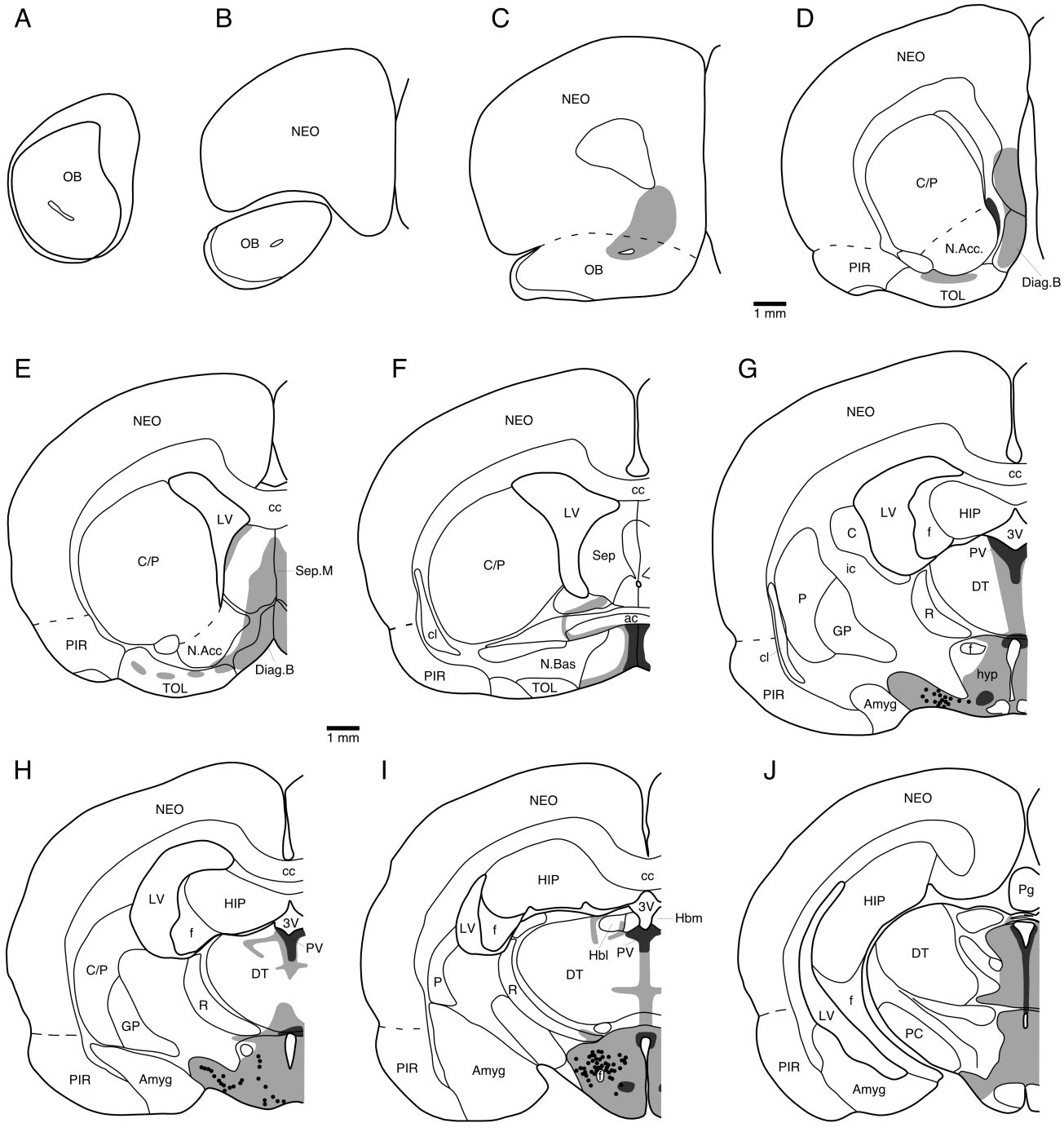
A
OB
B
NEO
OB
C
NEO
OB
D
NEO
C/P
N.Acc.
PIR
TOL
Diag.B
1 mm
E
NEO
cc
LV
C/P
Sep.M
PIR
N.Acc
TOL
Diag.B
F
NEO
cc
LV
C/P
Sep
cl
ac
PIR
N.Bas
TOL
G
NEO
cc
LV
HIP
C
f
3V
PV
ic
DT
P
R
GP
cl
f
hyp
PIR
Amyg
1 mm
H
NEO
cc
LV
HIP
f
3V
PV
C/P
DT
R
GP
PIR
Amyg
I
NEO
HIP
cc
3V
Hbm
LV
f
Hbl
PV
DT
P
R
PIR
Amyg
J
NEO
Pg
HIP
DT
f
LV
PC
PIR
Amyg

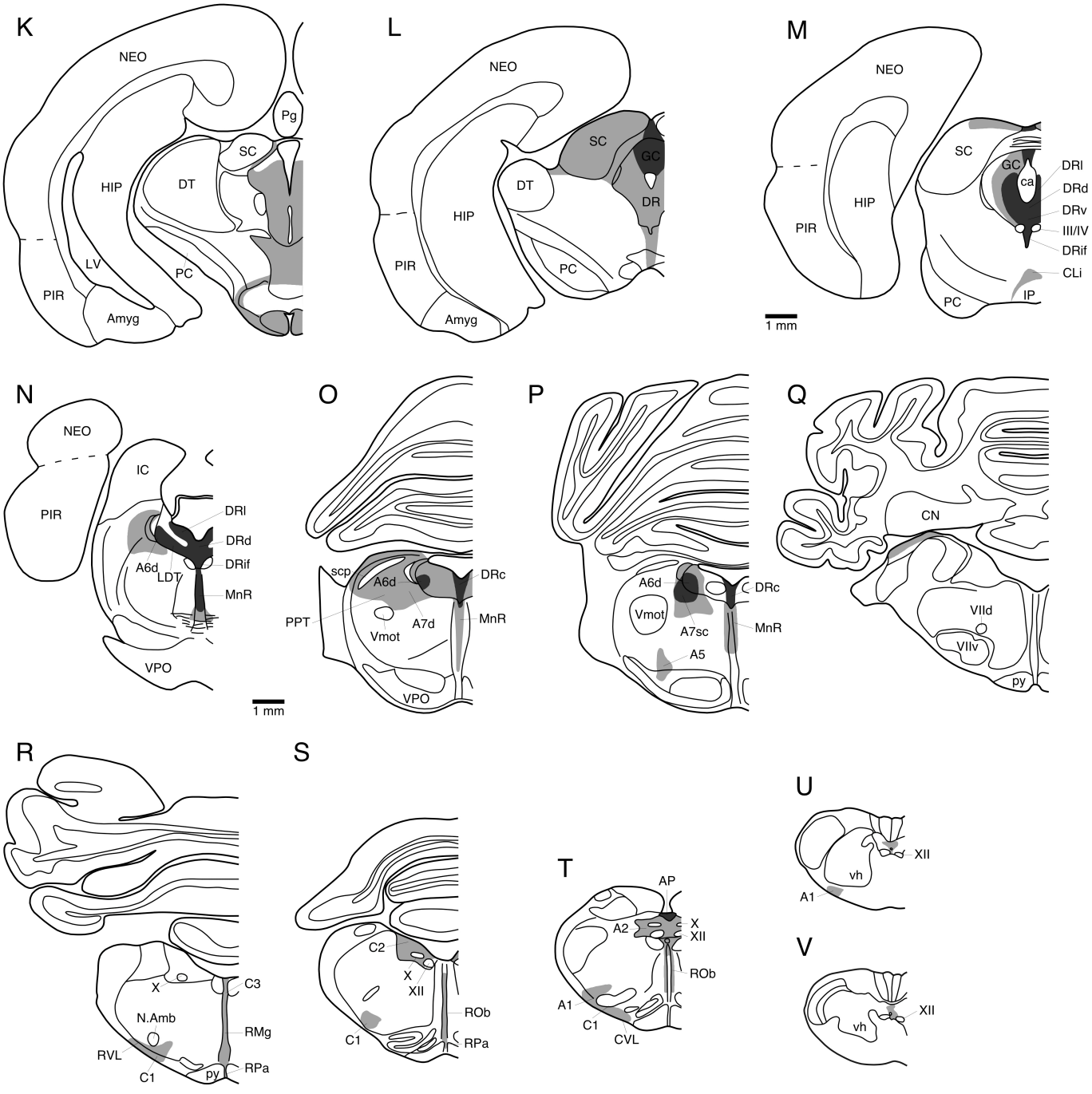
K
NEO
Pg
SC
HIP
DT
LV
PC
PIR
Amyg
L
NEO
SC
GC
DR
HIP
DT
PIR
PC
Amyg
M
NEO
SC
GC
ca
DRl
DRd
DRv
III/IV
DRif
CLi
HIP
PIR
PC
IP
1 mm
N
NEO
IC
PIR
DRl
DRd
DRif
A6d
LDT
MnR
VPO
1 mm
O
scp
A6d
DRc
PPT
A7d
MnR
Vmot
VPO
P
A6d
DRc
Vmot
A7sc
MnR
A5
Q
CN
VIId
VIIv
py
R
X
C3
N.Amb
RMg
RVL
py
RPa
C1
S
C2
X
XII
ROb
C1
RPa
T
AP
A2
X
XII
ROb
A1
C1
CVL
U
XII
vh
A1
V
XII
vh

Figure 3.2: Drawings of coronal sections A to U through the right half of the brain of the Highveld mole rat (*Cryptomys hottentotus*) depicting the distribution of orexinergic terminal network densities (an absence of shading represents low density, grey shaded areas represents medium density and black shaded areas represents high density) and Orx immunoreactive neurons (each black dot represents a single neuron) relative to the nuclear organization of the cholinergic system, catecholaminergic system and serotonergic system [previously described in Bhagwandin et al. (2008) for this species]. Absence of shading indicates either a minor terminal network or no terminal network (see text for details).See list for abbreviations.

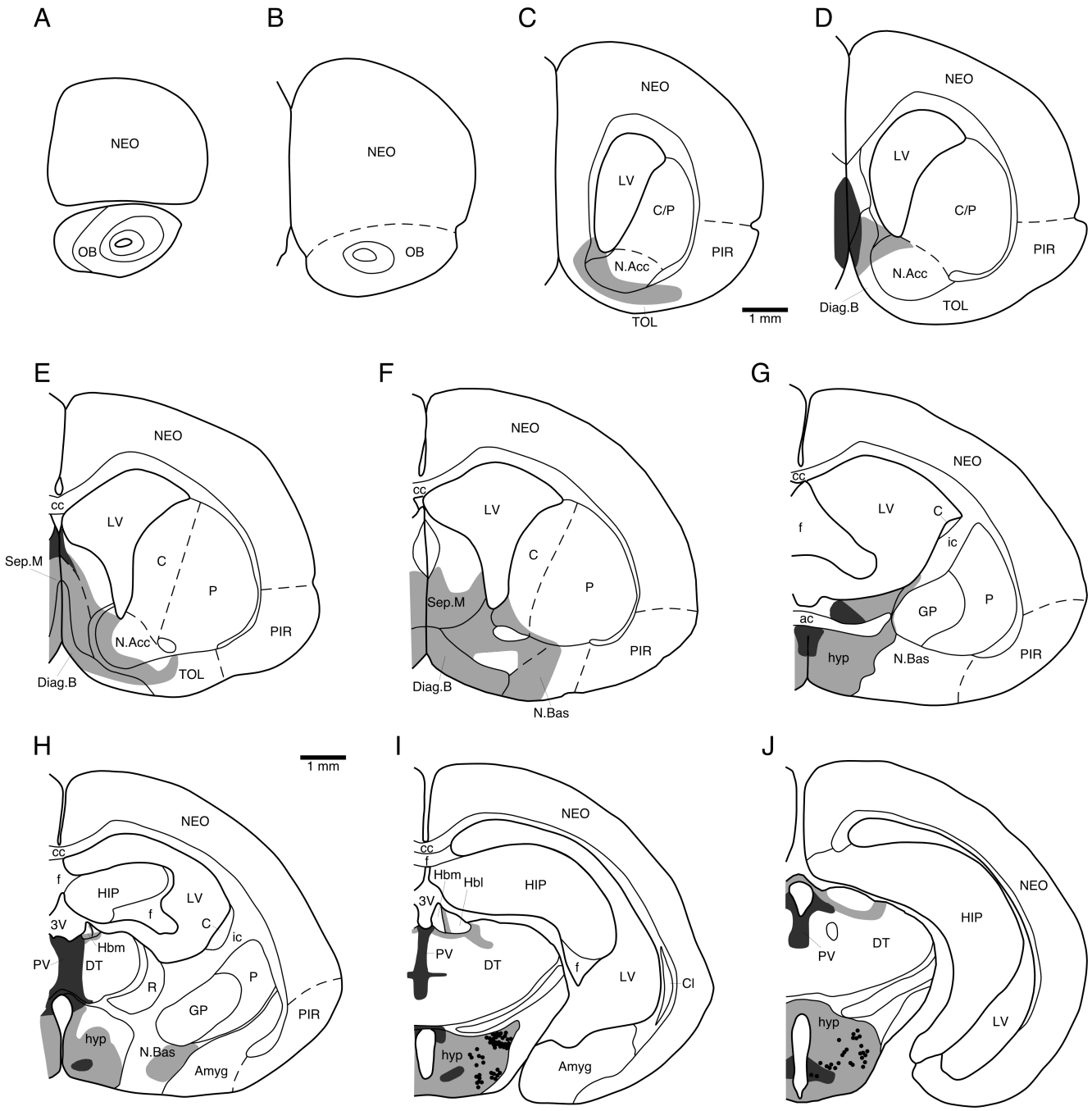
A
NEO
OB
B
NEO
OB
C
NEO
LV
C/P
PIR
N.Acc
TOL
1 mm
D
NEO
LV
C/P
PIR
N.Acc
Diag.B
TOL
E
NEO
cc
LV
Sep.M
C
P
PIR
N.Acc
TOL
Diag.B
F
NEO
cc
LV
C
P
Sep.M
PIR
Diag.B
N.Bas
G
NEO
cc
LV
C
f
ic
P
GP
ac
hyp
N.Bas
PIR
H
1 mm
NEO
cc
f
HIP
LV
f
C
3V
ic
Hbm
PV
DT
R
P
GP
PIR
hyp
N.Bas
Amyg
I
NEO
cc
f
Hbm
Hbl
HIP
3V
PV
DT
f
LV
Cl
hyp
Amyg
J
NEO
HIP
DT
PV
hyp
LV

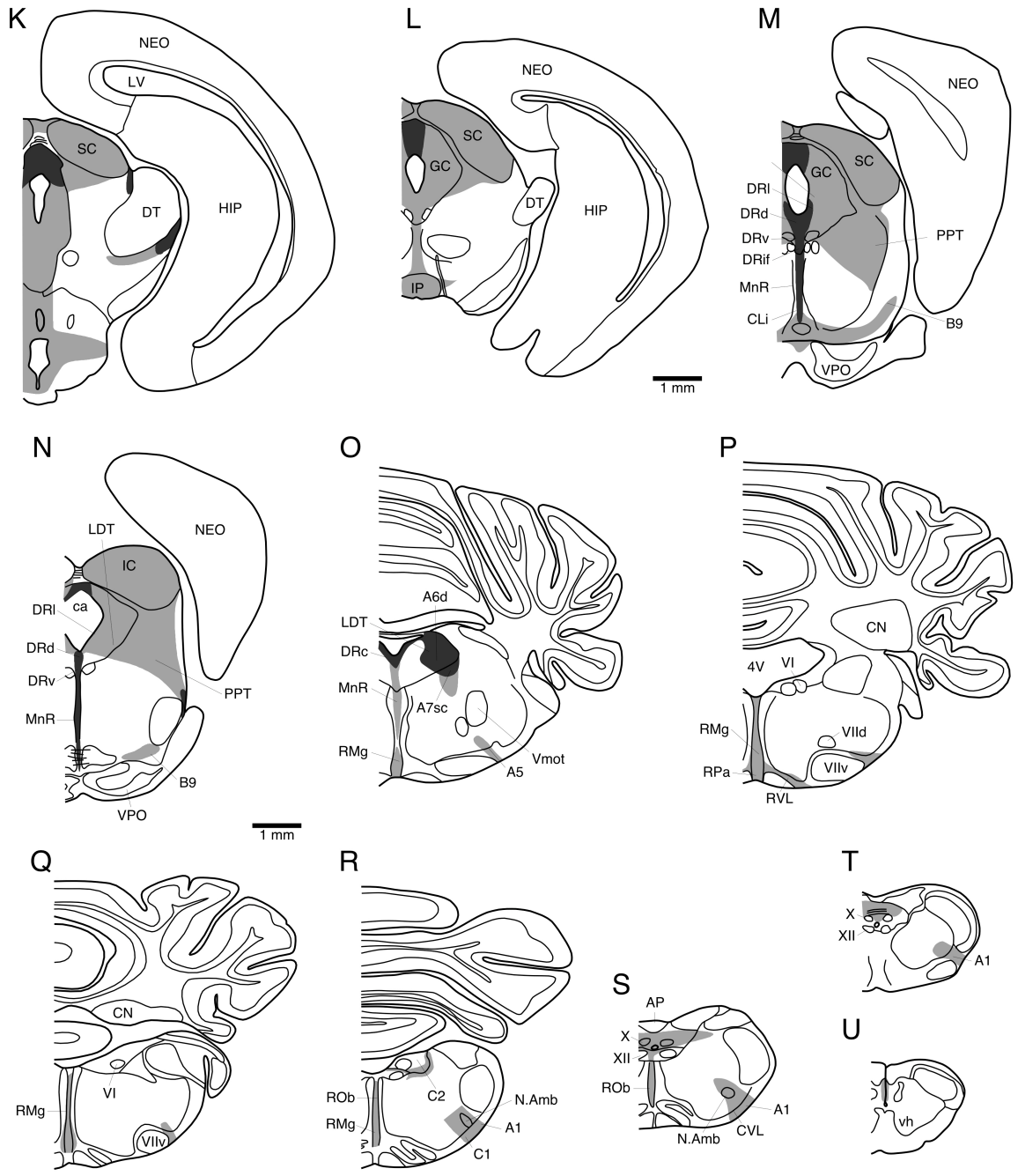
K
NEO
LV
SC
DT
HIP
L
NEO
SC
GC
DT
HIP
IP
1 mm
M
NEO
SC
GC
DRl
DRd
DRv
DRif
MnR
CLi
PPT
B9
VPO
N
LDT
NEO
IC
DRl
ca
DRd
DRv
MnR
PPT
B9
VPO
1 mm
O
A6d
LDT
DRc
MnR
A7sc
RMg
Vmot
A5
P
CN
4V
VI
RMg
VIId
VIIv
RPa
RVL
Q
CN
VI
RMg
VIIv
R
ROb
C2
N.Amb
RMg
A1
C1
S
AP
X
XII
ROb
A1
N.Amb
CVL
T
X
XII
A1
U
vh

Figure 3.3: A. Photomicrographic montage showing the Orx immunoreactive neurons within the hypothalamus of *Bathyergus suillus*. Scale = 500um. **B**. and **C**. High power photomicrographs showing the morphology of Orx immunoreactive neurons within the hypothalamus of *Bathyergus suillus*. Scale = 50um.

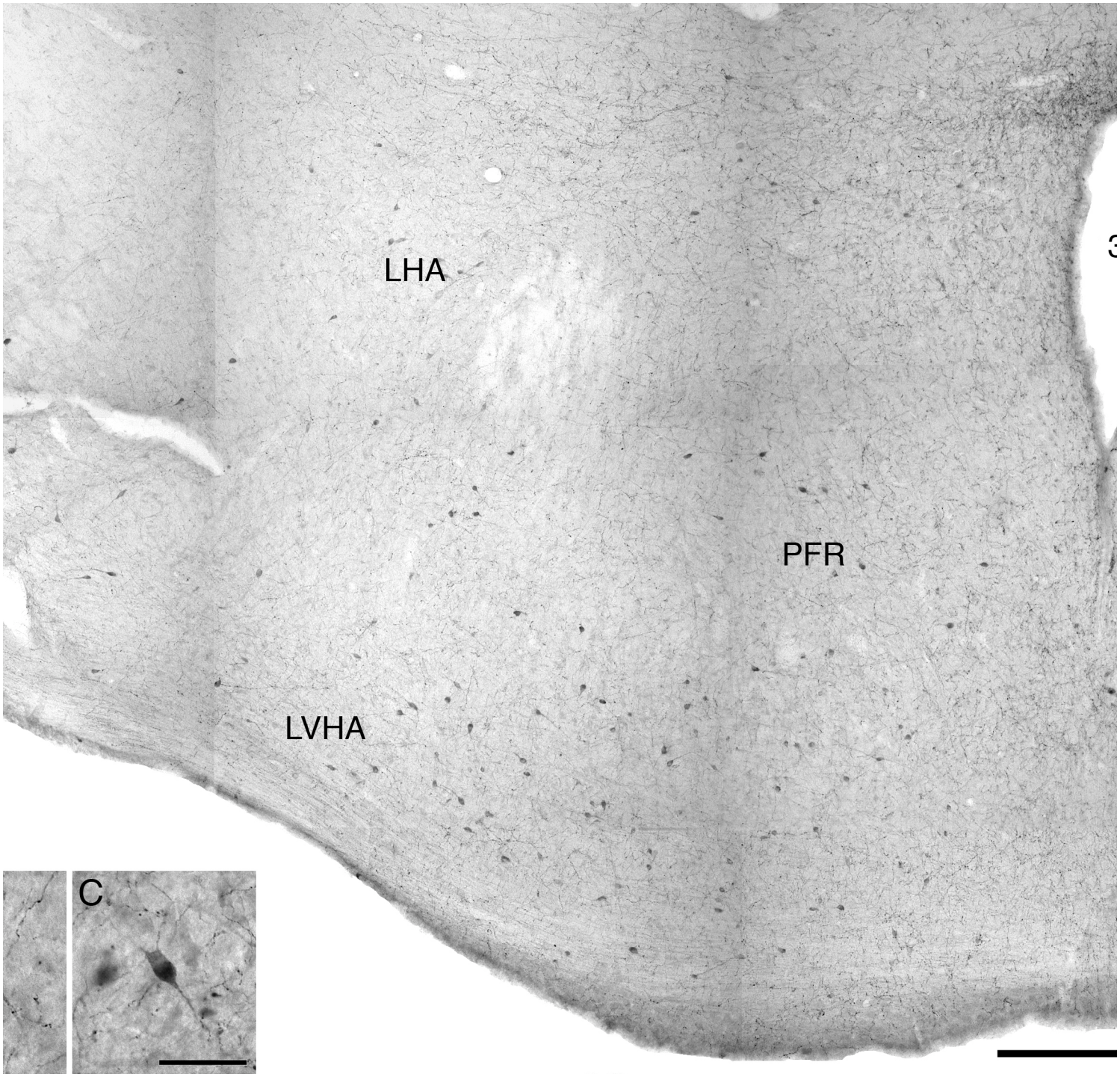
LHA
PFR
LVHA
C

Figure 3.4: High power photomicrographs showing varying orexinergic terminal network densities in the brains of *Cryptomys hottentotus* (**A**-**D**) and *Bathyergus suillus* (**E**). **A**. High density terminal network within the A6d neuronal group. **B**. Low density terminal network within the cingulate cortex. **C**. Medium density terminal network in the region of the C1 nucleus. **D**. Medium density terminal network within the cholinergic medial septal nucleus. **E**. Medium density terminal networks surrounding the central canal. Scale = 100 μm and applies to all. See list for abbreviations.

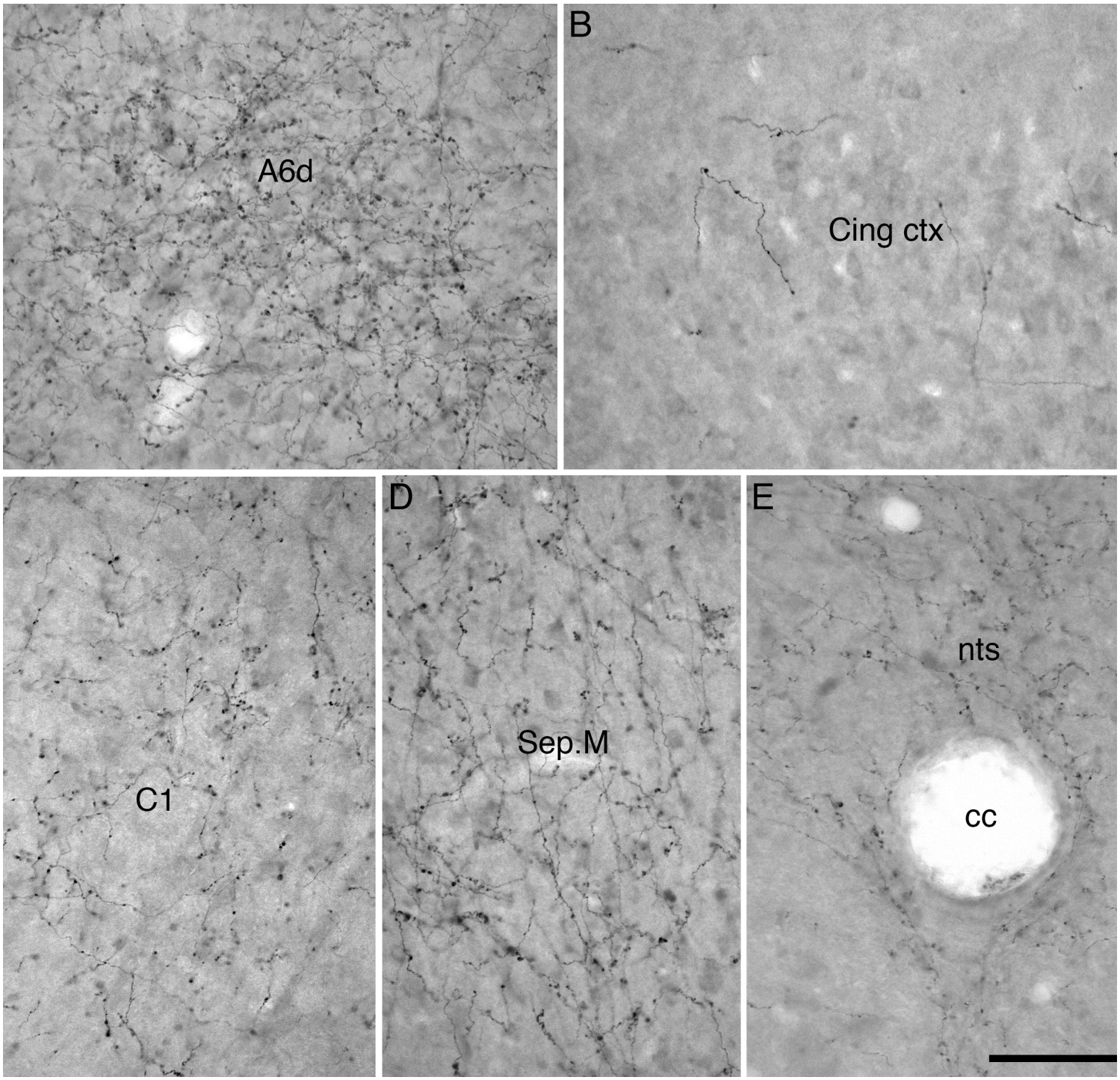
A6d
B
Cing ctx
C1
D
Sep.M
E
nts
cc

Figure 3.5: Photomicrographs illustrating the difference in expression of high density orexinergic terminal networks within the paraventricular nucleus of: **A**. *Bathyergus suillus*, **B**. *Cryptomys hottentotus*. Scale = 500um and applies to both. See list for abbreviations.

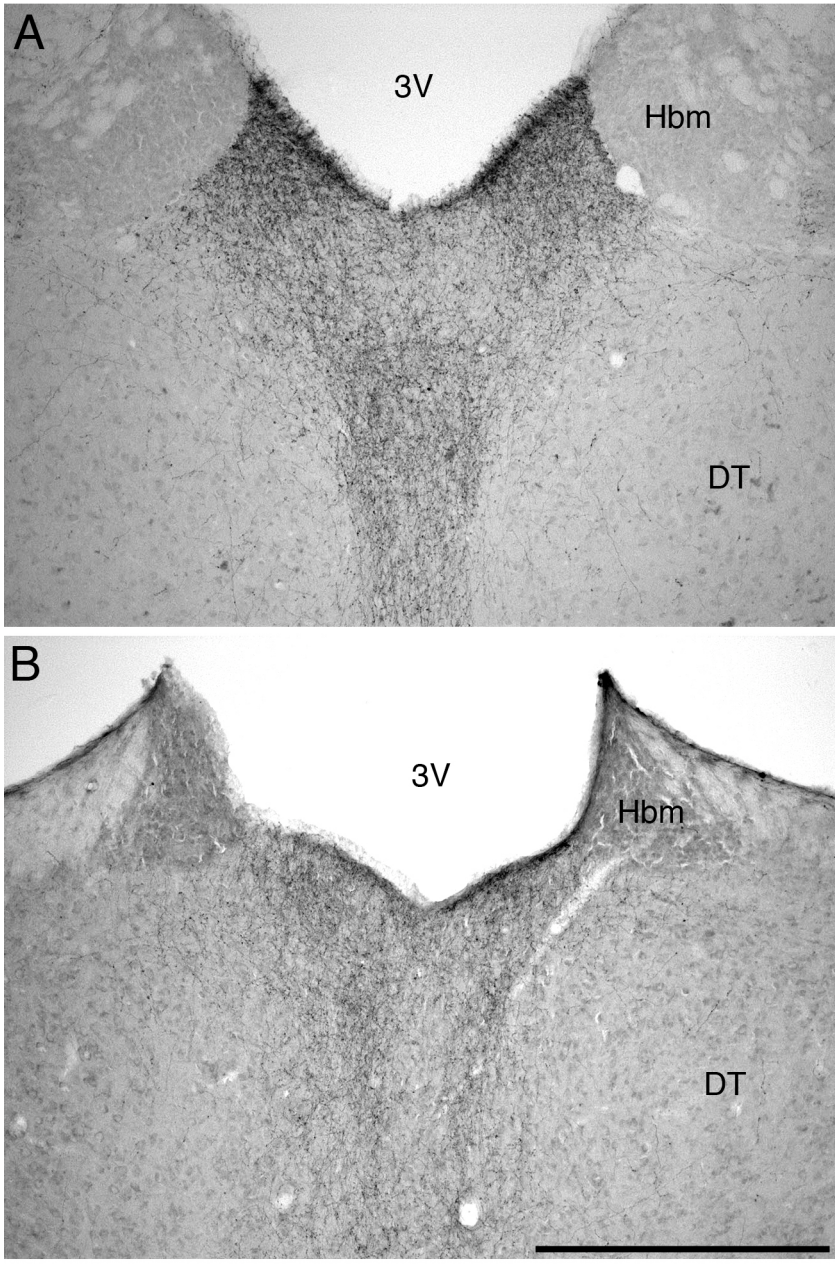
A
3V
Hbm
DT
B
3V
Hbm
DT

Figure 3.6: High power photomicrograph showing varying terminal network densities within the brain of *Cryptomys hottentotus*. **A**. high density orexinergic terminal networks within the serotonergic **DR** nuclear complex. **B**. high density orexinergic terminal networks in the region of the serotonergic **MnR**. **C**. medium density oerxinergic terminal networks within the serotonergic **ROb** nucleus, Scale = 50um and appiles to all. See list for abbreviations.

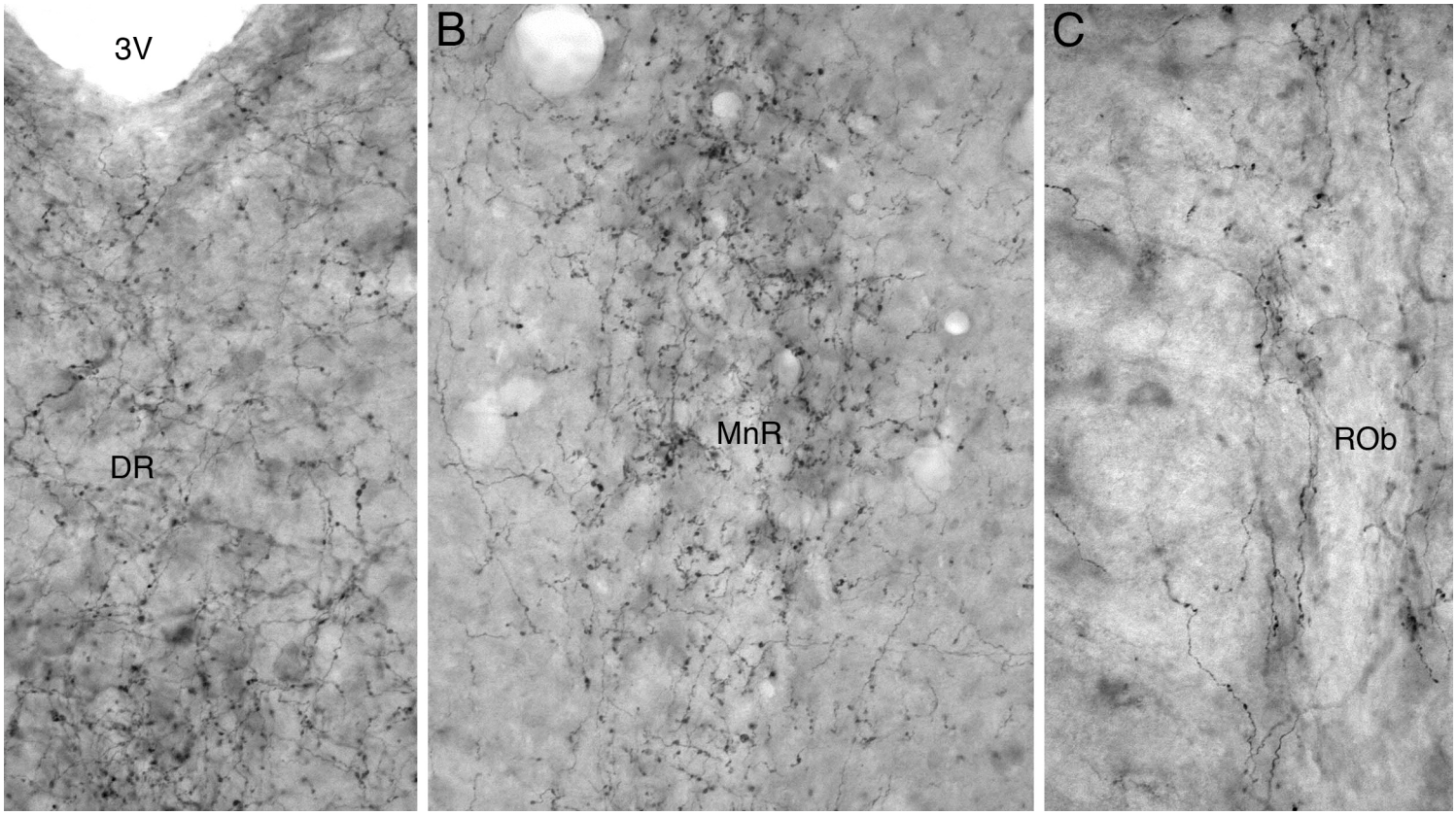
3V
DR
B
MnR
C
ROb

3.4 Discussion

In the current study, it was observed that both species of mole rat displayed three clusters of orexinergic immunoreactive neurons within the hypothalamus, thereby maintaining significant congruency with previous studies in other mammals (see references listed in Introduction). In addition, it was noted that no immunoreactive orexinergic (Orx+) cell bodies, in either species of mole rat, could be identified within the anterior hypothalamic paraventricular organ as was previously reported in some Murid rodents (Nixon and Smale, 2007). In both species of mole rat the orexinergic terminal network distribution, for the most part, maintained similarity to that observed in other mammals; however, a few differences were identified between both species of mole rat and collectively in all other mammals studied to date.

3.4.1 Comparison to other rodents and other mammals

3.4.1.1 Distribution of orexinergic cell bodies

The distribution of Orx+ cell bodies, in both species of mole rat, was both similar and different to those previously reported in other rodents. Both species of mole rat expressed Orx+ neurons within the perifornical region (PFR) and the lateral hypothalamic area (LHA), comprising the main cluster of orexinergic neurons, which is a common feature of the orexinergic system shared by all rodents studied to date; however, neither species of mole rat, as with the Syrian hamster and degu, displayed Orx+ neurons within the anterior hypothalamic paraventricular subnucleus as seen in the Long-Evans rat and grass rat (Nixon and Smale, 2007; but see Novak and Albers, 2002 who do not report these neurons in the Nile grass rat but they used an Orexin B antibody). In this case we appear to have a difference in the nuclear organization of the orexinergic system within the rodents, with the two Murid rodents studied (Long-Evans rat and Nile grass rat, both closely related) showing

a difference to the closely related Syrian hamster (a member of the Cricetidae) and the more distantly related Ctenohystrica (Octodon and the bathyergid mole rats) (Nixon and Smale, 2007; Blanga-Kanfi et al., 2009). This is not the first time such Murid *vs* non-Murid differences have been observed for such systems in the rodents (Bhagwandin et al., 2006). In the mole rats, as with all other rodents, two additional, but smaller, clusters of orexinergic neurons were located, one in the dorsolateral region of the hypothalamus intermingling with the region of the zona incerta, and a second cluster in the ventrolateral region of the hypothalamus near the optic tract (that is immunoreactive for both orexin-A and orexin-B, Nixon and Smale, 2007), although the optic tract is greatly reduced in the mole rats. Thus, within the rodents, while many similarities in neural systems occur across all species, there are at least two differences reported to date (orexinergic anterior hypothalamic paraventricular neurons, Nixon and Smale, 2007; and cortical cholinergic neurons, Bhagwandin et al., 2006). These differences would be of interest to study further and delineate potential phylogenetic boundaries for these features and the possible behavioural correlates of these differences.

An important aspect of the parcellation of the orexinergic system needs to be highlighted at this point. In the current study we have lumped the orexinergic neurons of the PFR and LHA into a single cluster that we have termed the main cluster (in this study and in a previous study on microchiropterans, Kruger et al., 2010). This was done as there appears to be no anatomical distinction in the aggregation of the orexinergic neurons across this large cluster, being organized in what can be loosely termed a diffuse nucleus; however, a previous study of the connectivity of these regions of the main cluster (PFR and LHA) would suggest that these two regions likely represent distinct nuclei (Yoshida et al., 2006). Yoshida et al. (2006) showed that, while the PFR and LHA orexinergic neurons project to many of the same regions, the intensity of the projection differs substantially between several of these terminal

territories. In addition, they showed that the medial, or PFR, portion of what we term the main orexinergic cluster innervates the anterior and ventromedial hypothalamus plus the suprachiasmatic nucleus, whereas the LHA orexinergic neurons do not. They also showed that the LHA orexinergic neurons innervate the dorsal raphe, whereas the PFR orexinergic neurons do not (Yoshida et al., 2006). These differences in projection fields appear to warrant a distinction of what we term the main orexinergic cluster into medial or PFR and LHA orexinergic nuclei. It would be of importance to study such differences across species to determine whether such differential projection territories exist in other mammals and warrant cross species parcellation of the orexinergic system in a similar manner.

In the mole rats and other rodents the location of the main cluster of orexinergic (Orx+) cell bodies (PFR and LHA), is similar to that seen in all other mammals studied to date (Iqbal et al., 2001; Moore et al., 2001; Zhang et al., 2001, 2002; Yamamoto et al., 2006; Kruger et al., 2010). Interestingly, all mammalian species appear to have orexinergic neurons overlapping with the medial most portion of the zona incerta. Of less similarity is the appearance of orexinergic neurons in the ventrolateral hypothalamus, near the optic tract, which while present in most mammals (and appears greatly expanded in the kangaroo, Yamamoto et al., 2006), are lacking in the microchiropterans (Kruger et al., 2010) and the two species of hamster studied to date (McGranaghan and Piggens, 2001; Mintz et al., 2001; Khorooshi and Klingenspor, 2005; Vidal et al., 2005; Nixon and Smale, 2007). Further contrasts in the location of orexinergic neurons amongst mammals include: (1) the presence of Orx+ neurons in the dorsomedial hypothalamic region in the sheep, minipig and kangaroo (Iqbal et al., 2001; Yamamoto et al., 2006; Ettrup et al., 2010); and (2) Orx+ neurons in the supraoptic and paraventricular magnocellular nucleus of the minipig (Ettrup et al., 2010). Thus, while for the most part the nuclear organization of the orexinergic system appears to quite conserved across mammalian species, there are definitely some points of departure that

may be interesting in both a functional and phylogenetic aspect, and warrants the investigation of orexinergic cellular location in a broader range of mammalian species.

3.4.1.2 Distribution of orexinergic terminal networks

Previous studies of the terminal networks of the orexinergic neurons have demonstrated that in mammals the majority of the brain is either in receipt of very minor, or no, orexinergic innervation. In this sense the mole rats studied herein are no exception. These regions of minor to no orexinergic innervation include the cerebral neocortex, the dorsal striatopallidal complex, the dorsal thalamus, cerebellum and most of the brainstem.

Despite this, there are areas of the brain that consistently show medium to dense orexinergic innervation across many of the mammalian species studied to date. Within the telencephalon of the mole rats studied, medium to high-density orexinergic terminal networks were observed in the septal nuclei, the shell of the nucleus accumbens and the cholinergic basal forebrain. This telencephalic distribution is similar across all rodents and all mammals for which these projections have been described to date. Similarly, in the mole rats and all mammals studied, the paraventricular nuclei of the epithalamus exhibited a high-density orexinergic terminal network in the dorsal division. This specific network extended around the habenular nuclear complex in the mole rats, again being similar to that seen in other mammals. A medium density network was observed throughout the mole rat hypothalamus as seen in all other mammals. Interestingly, in several mammals studied, a clear medium-density orexinergic terminal network is observed in the intergeniculate leaflet, but this was not observed in the mole rats. This is likely due to the major reduction in size of the visual system in these species (Nemec et al., 2004). Previously, Vidal et al. (2005) demonstrated that the orexinergic projection to the intergeniculate leaflet arises from the orexinergic neurons located near the zona incerta. The mole rats possess these zona incerta orexinergic

neurons, but not the projection to the intergeniculate leaflet. This indicates that these Orx+ zona incerta neurons mostly likely have projections to other structures in addition to the intergeniculate leaflet, and the existence of these additional, but currently unknown projections, are the possible reason for the maintenance of this cell group in the mole rats.

As in all species where the orexinergic terminal networks have been described, the mole rats studied herein have high to moderate density projections to all the serotonergic nuclei, the pontine cholinergic nuclei, and the locus coeruleus complex (Bhagwandin et al., 2008). In addition, both mole rats expressed a high to medium-density Orx+ terminal network within the periaqueductal grey matter and the ventral tegmental area (VTA), similar to that previously reported for other rodents and other mammals. Interestingly though, while a low to absent density of Orx+ terminal networks has been reported for the superior colliculus in other rodent species, a medium-density Orx+ terminal network was observed in this study despite the reduced size of the superior colliculus previously noted for mole rats (Nemec et al., 2004; Da Silva, 2006). Variations in terminal densities within the inferior colliculus (IC) and interperduncular (IP) nulei, amongst rodent species, were similarly noted in both species of mole rat. The highveld mole rat expressed a medium-density Orx+ terminal network in both the IC and IP, similar to the hamster, grass rat, degu and wistar rat; whereas the Cape dune mole rat demonstrated a low-density Orx+ terminal network within the IC and IP, consistent with the Long-Evans and Wistar rats; however, these terminal networks also appear to vary significantly across the IP and IC of other mammals studied to date. Interestingly no other rodent species, except for the Cape dune mole rat of the current study, exhibited a high-density Orx+ terminal network within area postrema (AP) with medium-density Orx+ terminal networks reported within AP for the degu and wistar rat, whereas the highveld mole rat demonstrates a low-density Orx+ terminal network for this homologous region. The catecholaminergic medullary nuclei (C1, C2, A1 and A2) expressed a medium-

density Orx+ terminal network in both species of mole rat and this is congruent with previous rodent species however it must be noted that there is no clarity with regard to the distribution of Orx+ terminal networks within C2 amongst other rodent and mammalian species studied to date.

Chapter 4 - Sleep and wake in rhythmic *vs* arrhythmic chronotypes of a microphthalmic species of African mole rat (*Cryptomys mechowi*).

4.1 Introduction

The reversible, homeostatically controlled state of reduced responsiveness, reduced motor ability and reduced metabolism, commonly defines the physiological phenomenon of sleep (Siegel, 2008). In mammals, this state is often separated into rapid eye movement (REM) and non-REM stages that are differentiated by changes in the electroencephalogram (EEG) and electromyogram (EMG) amongst other features (Siegel, 2009). Within mammals, sleep has been studied by visual observation or physiological recording in 17 orders, 47 families and 178 species (McNamara et al., 2008), but the exact function of sleep remains unclear.

Most mammals studied meet the standard criteria for sleep in that they have clearly distinguishable SWS and REM states (the marine mammals being unusual in this sense, Lyamin et al., 2008). Tobler (1995) proposed that sleep is not fundamentally different in mammalian species, but Siegel (2004) suggests that adaptive mechanisms rather than phylogenetic relationships provide a better explanation of the variation in sleep time and other parameters across species. In contrast to this, Capellini et al (2008) indicate that they have detected a 'phylogenetic signal' in mammalian sleep, perhaps indicating some predictability of this state across species. Detailed sleep studies in rodents have examined the rat (Alfoldi et al., 1990), mouse (Richardson et al., 1985; Ayala-Guerrero et al., 1998; Tang and Sanford, 2002), Djungarian hamster (Deboer et al., 1994), Syrian hamster (Tobler and Jaggi, 1987), chipmunk (Dijk and Daan, 1989; Estep et al., 1978), gerbil (Kastaniotis and Kaplan, 1976; Susic and Masirevic, 1986; Ambrosini et al., 1994), guinea pig (Tobler et al.,

1993; Tobler and Franken, 1994), squirrel (Folk, 1963; Chepkasov, 1980), Octodon degu (Kas and Edgar, 1998) and the blind mole rat (Tobler and Deboer, 2001).

In the current study sleep was physiologically and behaviourally recorded in the giant Zambian mole rat (*Cryptomys mechowi*) which is well known for its subterranean lifestyle, regressed visual system (Cooper et al., 1993; Hart et al., 2004; Nemec et al., 2004; McMullen et al., 2010) and unusual patterns of circadian rhythmicity (Lovegrove and Papenfus, 1995; Lovegrove and Muir, 1996; Oosthuizen et al., 2003). It has been shown that the two main retinorecipient structures of the circadian system, the suprachiasmatic nucleus and the intergeniculate nucleus/leaflet, have different neuropeptide populations and afferents and are reduced in size in mole rats compared to other rodents (Negroni et al., 2003; Bhagwandin et al., 2011). Other approaches directed at understanding the unusual circadian rhythmicity in mole rats have shown that these subterranean rodents possess an endogenous melatonin rhythm that has a circadian pattern (Gutjah et al., 2004) and that body temperature is not a reliable indicator of endogenous circadian activity in mole rats (Lovegrove and Muir, 1996). Furthermore, locomotor activity studies have shown that within a species of mole rat there are individuals that have a rhythmic chronotype and others that have a distinctly arrhythmic chronotype, and this is seen in both social and solitary species of mole rat (Oosthuizen et al., 2003).

The giant Zambian mole rat leads a solitary lifestyle, inhabiting diverse soil types in the tropical woodland and savannah regions of northern Zambia, southern Democratic Republic of Congo and central Angola (De Graaf, 1971). This species is typically pale brown in colour with a maximum body weight of 600g for males and 350g for females (Burda and Kawalika, 1993). The current study was aimed at determining: (1) whether measurable sleep parameters vary predictably with individuals that possess rhythmic chronotypes as opposed to

individuals that are distinguishably arrhythmic; and (2) if dramatic changes in phenotype, such as the regressed visual system, affect sleep parameters in comparison to other rodents.

4.2 Materials and Methods

In the present study, physiological measures of EEG and EMG were telemetrically recorded from six individual wild caught adult male giant Zambian mole rats (*Cryptomys mechowi*) (Table 1). At the Mammal Research Institute, University of Pretoria the circadian activity these animals were recorded and the mole rats were identified as either rhythmic or arrhythmic (Fig. 4.1) (see section 4.2.1). Prior to the commencement of sleep recording, the animals were brought to the University of the Witwatersrand and were allowed a month of acclimatisation in an isolated (to minimise noise and other disturbances) and environmentally controlled room (12h light/dark cycle with a constant ambient temperature of 25°C). A single mole rat was housed in an enclosure (60 x 50 cm) in which a transparent perspex tube (20 cm long with a diameter of 6.5 cm) was secured to the floor of the enclosure. Wood shavings were used to line the floor, but not enough was placed to hinder visual observation of the animals. Each animal was fed a mixture of sweet-potatoes, apples and carrots once a day. All animals were treated and used according to the guidelines of the University of the Witwatersrand Animal Ethics Committee, which parallel those of the NIH for the care and use of animals in scientific experimentation.

4.2.1 Determination of Rhythmicity patterns

A system using infrared detectors was used to detect activity patterns in the mole rats. The mole rats were exposed to differing light conditions that included, light (L) and dark (D) cycles, DD cycles and LL cycles. Initially the experimental protocol started with a 12L:12D cycle (stage 1) and once entrainment was achieved the light cycle was switched to constant

darkness for 1 month (stage 2) to determine the expression of endogenous rhythms. Once this was completed the light cycle was reversed to 12L:12D (stage 3). To determine rhythmicity patterns, patterns of activity were determined under the various light and dark cycles and a mole rat was considered rhythmic when it exhibited the same preference for phase activity during stage 3 as it did in stage 1. Conversely a mole rat was deemed arrhythmic when no discernable preference for phase of activity could be ascertained between stage 3 and stage 1. For the purposes of the current project a total of 12 mole rats were recorded for circadian rhythmicity and the three that exhibited the strongest patterns of rhythmicity or arrhythmicity were used for sleep recordings. For details regarding the specifics of circadian rhythm determination see Oosthuizen et al. (2003).

4.2.2 Surgery

Once the animals were acclimatised, they were administered a weight dependant mixture of ketamine and xylazine (2:1, 0.01ml/100g, Bayer HealthCare). Throughout surgery, anaesthesia was maintained using Isoflurane (at a concentration of 1% - 2.5% in an oxygen/70% nitrous oxide mixture, Safe Line Pharmaceuticals) fed from a mask placed directly over the nostrils that was supplied by a respirator. After shaving the scalp and left abdomen, a chemical disinfectant (CHX Chlorhexidine, 0.5% chlorhexidine in 75% alcohol, Kyron Laboratories) was applied to the skin using sterile swabs. Two incisions were made for implantation of the transmitter and electrodes, one over the midline of the skull and one over the left abdomen. At the abdominal incision a subcutaneous pocket was created to house the transmitter. The lead wires of the transmitter (two for EEG and one for EMG) were then fed subcutaneously from the abdominal incision to the cranial incision. Once the skin had been reflected at the cranial incision, the temporalis muscle over the left hemisphere was retracted to reveal the dorsal cranial surface. Cotton swabs immersed in H_2O_2 were used to clean the

surface of the cranial vault and a small dental drill was used to bore two holes over the motor cortex of the left hemisphere without penetrating the dura mater. Thirty six hours prior to surgical implantation, the transmitter and electrode wires were sterilised for 18 h using Cidex (a non-irritant chemical sterilant, Johnson & Johnson) and then placed in sterile normal saline for a further 18 h. Using a surgical microscope, the EEG electrodes (the leads of which were made out of stainless steel, have an outer diameter of 0.3 mm and a lead diameter of 0.2 mm) were placed into each hole to rest above the dura mater and secured in place using dental acrylic (Profdent). The EMG electrodes were then sutured into the nuchal musculature. Once the electrodes were secure, the transmitter was carefully inserted into the subcutaneous pocket and both incisions sutured. Anaesthesia was reversed by switching off the flow of Isoflurane and the analgesic Temgesic (0.3mg/100g i.m., Reckitt Benckisser Healthcare) was administered. The animals were then returned to the enclosure and monitored for seven days prior to recording.

4.2.3 Recording

EEG and EMG were recorded using a Data Sciences International (DSI) telemetric system that included a transmitter (PhysioTel Telemeric Systems, TL11 M2 F40-EET-Implant, the leads of which were made out of stainless steel, have an outer diameter of 0.3 mm and a lead diameter of 0.2 mm; weight: 7 g; volume: 4.5 cc; height: 13.8 mm) and a receiver (placed directly under the enclosure) connected to a DEM matrix that was connected to a computer. EEG and EMG were recorded continuously for 72-h in each animal and stored as a DSI file. Once recording was completed, the DSI files were converted to text files (containing information for the frequency bands 1-4, 4-8, 8-12 and 12-16 Hz; as well as information relating to muscle movements) that were subsequently converted into Spike files using the Spike 2 software (version 4.2, Cambridge Electronic Design). The Spike files

generated presented the EEG and EMG data in a fashion that facilitated visual scoring of defined physiological states. Spectral power for the EEG was also calculated for each individual.

In addition to EEG and EMG, behaviour was recorded using the output of a low light CCTV camera connected to the hard disk drive of a commercially available DVD recorder. At the cessation of recording, this information was copied to DVD-R discs and analysed in conjunction with the physiological data. Red dark room lights were used to illuminate the enclosure throughout the 72 h period.

4.2.4 Analysis

EEG and EMG allowed the scoring of 3 states: waking (W) which was characterised by low amplitude, high frequency EEG activity and irregular high amplitude EMG activity; SWS which was defined by high amplitude, low frequency EEG activity and stable low amplitude EMG activity; and REM/paradoxical (R) which was defined by low amplitude, high frequency EEG activity (similar to that of waking) and low amplitude EMG activity that displayed large, high amplitude infrequent spikes that were correlated with observed behavioural muscle twitches and jerks. EEG and EMG were scored in 5 s epochs (where a state was recorded only if it persisted for 50% or more of the scoring interval) and the results entered into a Microsoft Excel generated template. Subsequently, this data was rescored at 1 min intervals (where a state was recorded only if it persisted for 50% or more of the scoring intyerval) by employing a mode formula (using Microsoft Excel) on the 5 s scored data, whereby the modal state for each minute was recorded.

Behavioural data was scored at 1 min intervals (where a state was recorded only if it persisted for 50% or more of the scoring interval) as eating (1), active wake (2), grooming (3), repositioning (4), immobile (5) and sleep posture (6), the latter of which was assigned

when the animal assumed a curled 'ball-like' position where the head was noticeably tucked underneath the body. The time spent in wake and sleep states (represented as a % of 24 h) and distribution of wake and sleep states between light and dark periods (% of 12 h) for both physiological and behavioural data were calculated in each individual.

The average number of episodes (where an episode is the period of time occupied by a particular physiological state from distinguishable initiation to termination of that state) of wake and sleep states and the average duration of an episode of wake and sleep states were calculated for a 24 h cycle and for light and dark periods. In four individuals the average spectral power of slow wave activity (SWA, 1.2 – 4.0 Hz) during SWS for consecutive 2 h periods was plotted for the 72 h recording. Total spectral power of SWA during SWS was calculated in rhythmic and arrhythmic groups and compared between light and dark periods. The length of a sleep cycle was calculated as the difference in time between the onsets of consecutive REM episodes. This calculation eliminated episodes of waking with an uninterrupted duration that was greater than 10 min for example, if between consecutive onsets of REM there was a period of only active wake (as determined by both physiology and behaviour) that was longer than 10 min in duration, then this episode was eliminated.

Data collected for the circadian chronotypes of the current study was analysed for statistically significant differences in the time spent in wake and sleep states, the average number of episodes of wake and sleep states and average duration of an episode of wake and sleep states, within and between chronotypes and within and between days and light and dark periods. Statistical tests used in the current study employed the PAleontological STatistics (PAST, version 2.02) software program (Hammer et al., 2001). A normality test was employed on each dataset and if the dataset was normally distributed ($p>0.05$), a one-way ANOVA was employed; but if the dataset was not normal in its distribution ($p<0.05$), a Mann-Whitney test was performed. Statistical significance was noted when the $p<0.05$ for

both ANOVA and Mann-Whitney tests. To determine the root of the statistical significance, univariate analyses were carried out for the datasets in question.

4.3 Results

In the present study, electroencephalographic waking, SWS and REM, through the recording of EEG and EMG, were telemetrically recorded continuously over a period of 72 hours, in conjunction with behavioural recordings, from six individual giant Zambian mole rats (*Cryptomys mechowi*). Three of the mole rats displayed a rhythmic chronotype, while three displayed an arrhythmic chronotype (Fig. 4.1). Behaviourally scored waking involved the animal moving around the enclosure, eating, grooming and re-posturing (Fig. 4.2). These behavioural states were identified physiologically by low amplitude, high frequency EEG activity and irregular high amplitude EMG activity. SWS was behaviourally identified when the animal presented itself in either a curled 'ball-like' position, where the head was noticeably tucked under the body, or a state of immobility with the head resting on the floor of the enclosure. SWS was characterised by high amplitude, low frequency EEG activity and stable low amplitude EMG activity. REM sleep was behaviourally scored when body twitches or muscle jerks were observed while the animal was in a curled 'ball-like' posture or other immobile postures such as lying prone. This state was physiologically identified by low amplitude, high frequency EEG waves (similar to that seen in waking) and when the EMG had a very low muscle tone (lower than waking and SWS) and when the EMG displayed large, high amplitude infrequent spikes (that correlated with behavioural twitches and jerks upon *post hoc* analysis) (Figs. 4.3, 4.4). The results of the present study showed that the rhythmic chronotype spent more time in a state of SWS and had a longer average duration of an episode of SWS, while the arrhythmic chronotype spent more time in a state of waking and had a longer average episode of waking. The time spent in REM sleep, the average

number of episodes of REM sleep and the average duration of an episode of REM was similar between the rhythmic and arrhythmic groups.

4.3.1 Behavioural analysis

Behaviour was recorded continuously over 72 h in each animal (n=6) and in 1 min epochs as: eating, active wake, grooming, repositioning, immobility and sleep posture (curled 'ball-like' position). Behavioural analysis showed that, on average per 24 h, the rhythmic mole rats spent 1.3 h eating, 4.1 h in a state of active wake, 1.3 h grooming, 0.4 h repositioning, 1.6 h immobile and, 15.6 h in sleep postures. The arrhythmic animals spent 1 h eating, 1.9 h in a state of active wake, 1.6 h grooming, 0.5 h repositioning, 0.3 h immobile and, 18.5 h in sleep postures (Fig. 4.2) (also see attached video files 1 – 8 showing the behavioural states). When the distribution of the various behavioural states between light and dark periods were compared it was observed that both rhythmic and arrhythmic animals spent, on average, similar times during both light and dark periods in the various behavioural states. The rhythmic animals were in a state of active wake 1.5 times more during the light than the dark periods, whereas the arrhythmic individuals were actively awake almost twice the time in light compared to dark periods (Fig. 4.2). A comparison of the total times spent in various behavioural states between the rhythmic and arrhythmic groups yielded no significant statistical differences across the 24 h periods or between the 12 h light and dark periods.

4.3.2 Physiological Analysis

4.3.2.1 State Definitions

The state of wake was determined by low amplitude, high frequency EEG activity and irregular high amplitude EMG activity and this was behaviourally correlated with activities that included moving around the enclosure (often in a clockwise direction), attempted

burrowing which was identified in one of two ways: (1) when the animal was observed gnawing the inside of the perspex tube using their incisors; and (2) when the animal would flick the wood shavings backwards using their hind legs while moving in a backward direction), eating, grooming and repositioning (see video files 1 - 4, 8). The state of SWS was identified by high amplitude, low frequency EEG activity and stable low amplitude EMG activity and this was behaviourally associated with either the curled 'ball-like' position defined when the head was tucked beneath the abdomen of the animal (behaviourally scored as sleep posture), or when the head was rested on the floor of the enclosure (behaviourally scored as immobile) (see video files 5, 6). Paradoxical (REM) sleep was identified by low amplitude, high frequency EEG waves (similar to that seen in waking) and when the EMG displayed large, high amplitude infrequent spikes and this was behaviourally identified as varying combinations of neck jerks, leg jerks and body jerks that correlated with the large, high amplitude spikes observed in the EMG during sleep posture or immobility (Figs. 4.2, 4.3) (see video file 7). The peak amplitude for spectral power calculated within the rhythmic group during the 72 h recording was: $0.4 \times 10^{-4} V^2$ during waking, $1.4 \times 10^{-4} V^2$ during SWS and $0.9 \times 10^{-4} V^2$ during REM sleep. The peak amplitude for spectral power calculated within the arrhythmic group during the 72 h recording was: $0.35 \times 10^{-4} V^2$ during waking, $1.4 \times 10^{-4} V^2$ during SWS and $0.6 \times 10^{-4} V^2$ during REM sleep. It was observed that the frequency range for spectral power in the rhythmic group was 0 – 7 Hz for the physiologically defined wake and sleep states but the peak amplitude of spectral power occurred at: 4.5 Hz during waking, 4 Hz during SWS and 4.4 Hz during REM sleep. The arrhythmic group also displayed the 0 – 7 Hz range for spectral power, but it was noticed that the peak amplitude of spectral power occurred at: 4.5 Hz during waking, 3.9 Hz for SWS and 4.6 Hz during REM sleep in this group (Fig. 4.5).

4.3.2.2 Time spent in wake and sleep states

Upon analysis of the five second (5 s) epoch scored physiological data, it was observed that the rhythmic animals, on average for a 24 h cycle, spent 16.6 h (69%) in a state of wake (the distribution of which was numerically higher during the light period than the dark period), 5.9 h (26%) in SWS (the distribution of which was numerically higher during the dark period than the light period) and 1.2 h (5.0 %) in REM sleep (where the distribution was numerically higher during the dark period than the light period). Total sleep time (TST) per 24 h measured 29 % (~7.0 h) and the percentage of REM of TST was 16 % (~1.2 h) (Tables 4.1, 4.3). The arrhythmic individuals generally spent 18.2 h (76%) in a state of wake (the distribution of which was numerically higher during the light period than the dark period), 4.2 h (19%) in SWS (the distribution of which was numerically higher during the dark period than the light period) and 1.2 h (5.0 %) in REM sleep (where the distribution remained similar between light and dark times) (Figs. 4.6, 4.7, 4.8). Total sleep time (TST) per 24 h measured 22 % (~5.3 h) and the percentage of REM of TST was 21 % (~1.1 h) (Tables 4.1, 4.3)

When the physiological data was scored at 1 min intervals, the results revealed that the rhythmic group, on average for a 24 h cycle, spent 17.8 h (74%) in a state of wake (the distribution of which was numerically higher during the light period compared to the dark period), 5.1 h (21%) in SWS (the distribution of which was numerically higher during the dark period compared to the light period) and 1.2 h (5.0 %) in REM sleep (where the distribution was numerically higher during the dark period compared to the light period). Total sleep time (TST) per 24 h measured 26 % (~6.2 h) and the percentage of REM of TST was 19 % (~1.2 h) (Tables 2, 3). Similarly, the arrhythmic individuals spent 19.6 h (82%) in a state of wake (the distribution of which was numerically higher during the light period compared to the dark period), 3.4 h (14%) in SWS (the distribution of which was numerically

higher during the dark period compared to the light period) and 1 h (4.0 %) in REM sleep (where the distribution was numerically higher during the dark period than the light period) (Fig. 4.6, 4.7, 4.8). Total sleep time (TST) per 24 h measured 18 % (~4.3 h) and the percentage of REM of TST was 23 % (~1 h) (Tables 4.2, 4.3).

The time spent in waking, SWS and REM were then statistically compared (using both scoring techniques) between the groups for the 72 h recording and the light and dark periods. With regard to the 5 s epoch scored data, statistical significance was noted between the groups in: (1) the time spent in waking (One-way Anova, p-value: 2.99E-06; where the arrhythmic group showed a numerically higher mean amount of time spent awake); (2) the time spent in waking during the light period (One-way Anova, p-value: 1.50E-02, ; where the arrhythmic group showed a numerically higher mean amount of time spent awake); (3) the time spent in waking during the dark (One-way Anova, p-value: 1.81E-05; where the arrhythmic group showed a numerically higher mean amount of time spent awake); (4) the time spent in SWS (One-way Anova, p-value: 5.32E-09; where the rhythmic group showed a numerically higher mean amount of time spent in SWS); (5) the time spent in SWS during the light period between days (One-way Anova, p-value: 3.92E-02; where the rhythmic group showed a numerically higher mean amount of time spent in SWS); and (6) the time spent in SWS during the dark period between days (One-way Anova, p-value: 2.76E-03; where the rhythmic group showed a numerically higher mean amount of time spent in SWS). No statistically significant differences were noted for REM sleep times in the 5 s epoch data. When the 1 min epoch data was compared no statistically significant differences between the groups were observed.

4.3.2.3 Number of episodes of wake and sleep states

The number of episodes of waking, SWS and REM sleep were calculated for both 5 s epoch data and 1 min epoch data, in both rhythmic and arrhythmic groups. The results of the 5 s epoch data indicates that within the rhythmic group, the average number of episodes in 24 h was: 940 for waking (the number of which was numerically higher during the dark period than in the light period), 779 for SWS (the number of which was numerically higher during the dark period compared to the light period) and 28 for REM sleep (where the number was numerically higher during the dark period than in the light period). The average number of episodes for the arrhythmic group for 24 h was: 966 for the waking state (the number of which was numerically higher during the dark period compared to the light period), 669 for SWS (the number of which was numerically higher during the dark period than the light period) and 28 for REM sleep (where the number was numerically higher during the dark period compared to the light period) (Figs. 4.6, 4.7, 4.8). Analysis of the 1 min epoch data showed that the average number of episodes during a 24 h cycle within the rhythmic group was: 136 for waking (the number of which was numerically higher during the dark period compared to the light period), 127 for SWS (the number of which was numerically higher during the dark period compared to the light period) and 23 for REM sleep (where the number was numerically higher during the dark period compared to the light). The arrhythmic average episodic composition for the 1 min epoch data was: 115 for waking (the number of which was numerically higher in the dark period than the light period), 103 for SWS (the number of which was numerically higher during the dark period compared to the light period) and 18 for REM (where the number was numerically higher during the dark period compared to the light period) (Figs. 4.6, 4.7, 4.8).

The number of episodes for waking, SWS and REM were statistically compared (using both scoring techniques) between the groups for the 72 h recording and the light and

dark periods. With regard to the 5 s epoch data, statistical significance was noted between the groups in: (1) the number of SWS episodes (One-way Anova, p-value: 2.62E-03; where the rhythmic group showed a numerically higher mean number of episodes); and (2) the number of SWS episodes during the light period (One-way Anova, p-value: 5.89E-03; where the rhythmic group showed a numerically higher mean number of episodes). No statistically significant differences between the groups were observed when the 1 min epoch data was compared.

4.3.2.4 Duration of wake and sleep states

The average duration of an episode of waking, SWS and REM sleep were calculated for both 5 s epoch and 1 min epoch data in both rhythmic and arrhythmic groups. The results of the 5 s epoch data indicates that within the rhythmic group, the average duration of an episode was 64 s for waking (the duration of which was longer during the light period than the dark period), 27 s for SWS (where the duration was longer in the dark period than the light period) and 150 s for REM sleep (where the duration was longer in the light period than in the dark period). The arrhythmic group revealed an average duration of an episode of 68 s for waking (where the duration was longer in the light period than the dark period), 23 s for SWS (where the duration was similar between light and dark period) and 146 s for REM sleep (where the duration was longer in the dark period than the light period) (Figs. 4.6, 4.7, 4.8). Analysis of the 1 min epoch data showed that the average duration of an episode of waking was 453 s (where the duration was longer in the dark period than in the light period), 147 s for SWS (where the duration was longer in the dark period than in the light period) and 189 s for REM sleep (where the duration was longer in the dark period than in the light period). The arrhythmic group revealed an average duration for an episode of waking of 609 s (where the duration was longer in the light period than the dark period), 119 s for SWS

(where the duration was longer in the light period than in the dark period) and 195 s for REM sleep (where the distribution was longer in the light period than the dark period) (Figs. 4.6, 4.7, 4.8).

The average duration of an episode of waking, SWS and REM were then statistically compared (using both scoring techniques) between the groups for the 72 h recording and the light and dark periods. With regard to the 5 s epoch data, statistical significance was noted between the groups in: (1) the average duration of a waking episode (One-way Anova, p-value: 1.56E-02; where the arrhythmic group showed a numerically higher mean average duration); (2) the average duration of a waking episode during the dark period (One-way Anova, p-value: 1.64E-02; where the arrhythmic group showed a numerically higher mean average duration); (3) the average duration of a SWS episode (One-way Anova, p-value: 1.99E-04; where the rhythmic group showed a numerically higher mean average duration); and (4) the average duration of a SWS episode during the light period (One-way Anova, p-value: 5.98E-03; where the rhythmic group showed a numerically higher mean average duration). No statistically significant differences between the groups were observed when 1 min epoch data was compared.

4.3.2.5 Slow wave activity (SWA) and spectral power

Spectral power (from the frequency band 1.4 – 4 Hz) is used to indicate the intensity of the SWA. The distribution of spectral power was calculated as an average of 2 h intervals. In the present study, SWA (calculated as a measure of spectral power) was compared between the groups during waking, SWS and REM sleep. It was observed that SWA was highest during SWS sleep and lowest during REM sleep in both groups of mole rats. The arrhythmic group showed a numerically higher SWA during SWS sleep compared to the rhythmic group. When SWA was analysed between the groups during the light and dark

period, it was observed that the arrhythmic group showed a numerically higher SWA during SWS in both light and dark period compared to the rhythmic group (Fig. 4.9).

4.3.2.6 State transitions and REM periodicity

Transitions between the physiologically identified states were counted in both groups for both the 5 s and 1 min scored data. The 5 s data showed that from the waking state the rhythmic individuals transitioned with greater frequency to SWS (99.5%) and only 0.5% into REM, whilst the arrhythmic group transitioned 99.6% and 0.4% respectively. From a state of SWS the rhythmic group transitioned significantly more often to waking (98.5%) than to REM (1.5%) while the arrhythmic group transitioned 98.4% and 1.6% respectively. In both groups, the state of REM transitioned only to waking (Figs. 4.10, 4.11). The 1 min scored data showed that from the state of waking the rhythmic group transitioned with greater frequency to SWS (90.7%) than into REM (9.3%) while the arrhythmic group transitioned 96.1% and 3.9% respectively. From a state of SWS the rhythmic group transitioned significantly more often to waking (86.6%) than to REM (13.4%) while the arrhythmic group transitioned into these states 87% and 13% respectively. Transitions from a state of REM were limited to waking only in both groups (Figs. 4.10, 4.11).

REM periodicity was calculated as the difference in time (1 min data only) between the onsets of consecutive REM episodes, and also when episodes of waking with duration greater than 10 min were eliminated in alignment with standard protocol (Fig. 4.12). The results revealed that the rhythmic group exhibited a higher frequency of REM onset within an hour period indicating that the peak sleep cycle duration was 25-30 min in length. A similar scenario was noted when waking episodes greater than 10 min were eliminated but peak cycle lengths were observed in the range of 15 -25 min. The arrhythmic group showed a relative variation in the frequency of REM onsets within an hour bracket with a peak cycle

length that occurred in the range of 10-15 min and 20-25 min, suggesting a more a variable cycle duration in this group (Fig. 4.12). REM periodicity was also calculated with episodes of waking with duration greater than 10 min. The results revealed a peak cycle length in the range of 20-25 min for the rhythmic chronotype whereas the arrhythmic chronotype revealed a peak cycle length 10-15 min and 20-30 min.

Figure 4.1: Actigrams illustrating circadian patterns of locomotor activity for one week in a rhythmic and arrhythmic giant Zambian mole rat (*Cryptomys mechowi*). The first period between 00:00 to 00:00 (the left half of the figure) is a repeat of the previous days' activity. Therefore the figure shows activity patterns for the respective chronotypes for one week only. These actigrams indicate that the rhythmic mole rats have a predictable period of activity during the light period whereas locomotor activity in the arrhythmic animals is irregular.

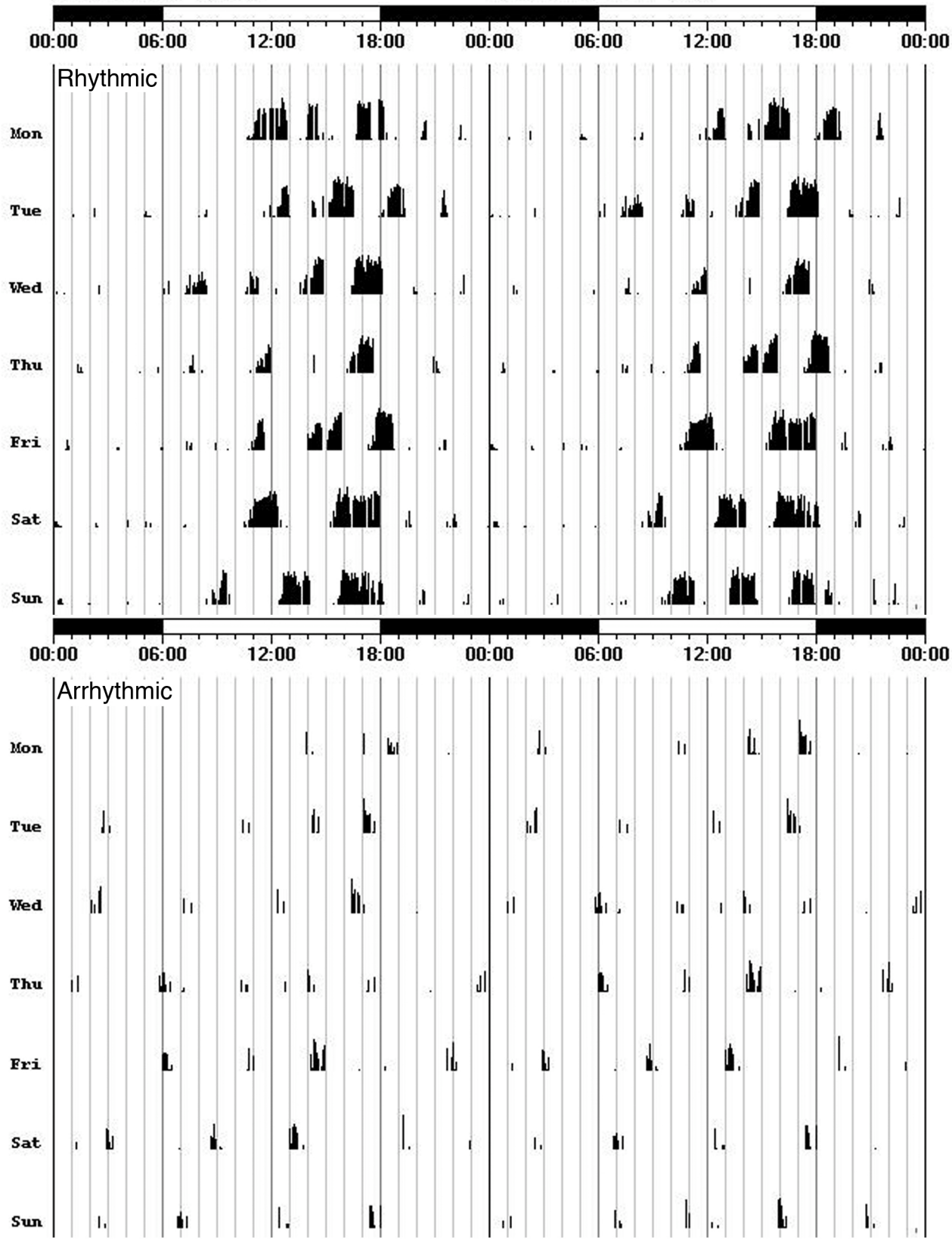
00:00
06:00
12:00
18:00
00:00
06:00
12:00
18:00
00:00
Rhythmic
Mon
Tue
Wed
Thu
Fri
Sat
Sun
00:00
06:00
12:00
18:00
00:00
06:00
12:00
18:00
00:00
Arrhythmic
Mon
Tue
Wed
Thu
Fri
Sat
Sun

Figure 4.2: Graphs showing data for the various behavioural states in rhythmic and arrhythmic individuals (grey bars, same individuals from left to right in each graph and in all subsequent similar graphs) and the respective weighted means (black bars). The graphs represent the percentage and average amount of time spent in the various behavioural states for a 24h cycle (from 72 h of recording) and for the 12 h light and dark period periods (from 36 h of recording).

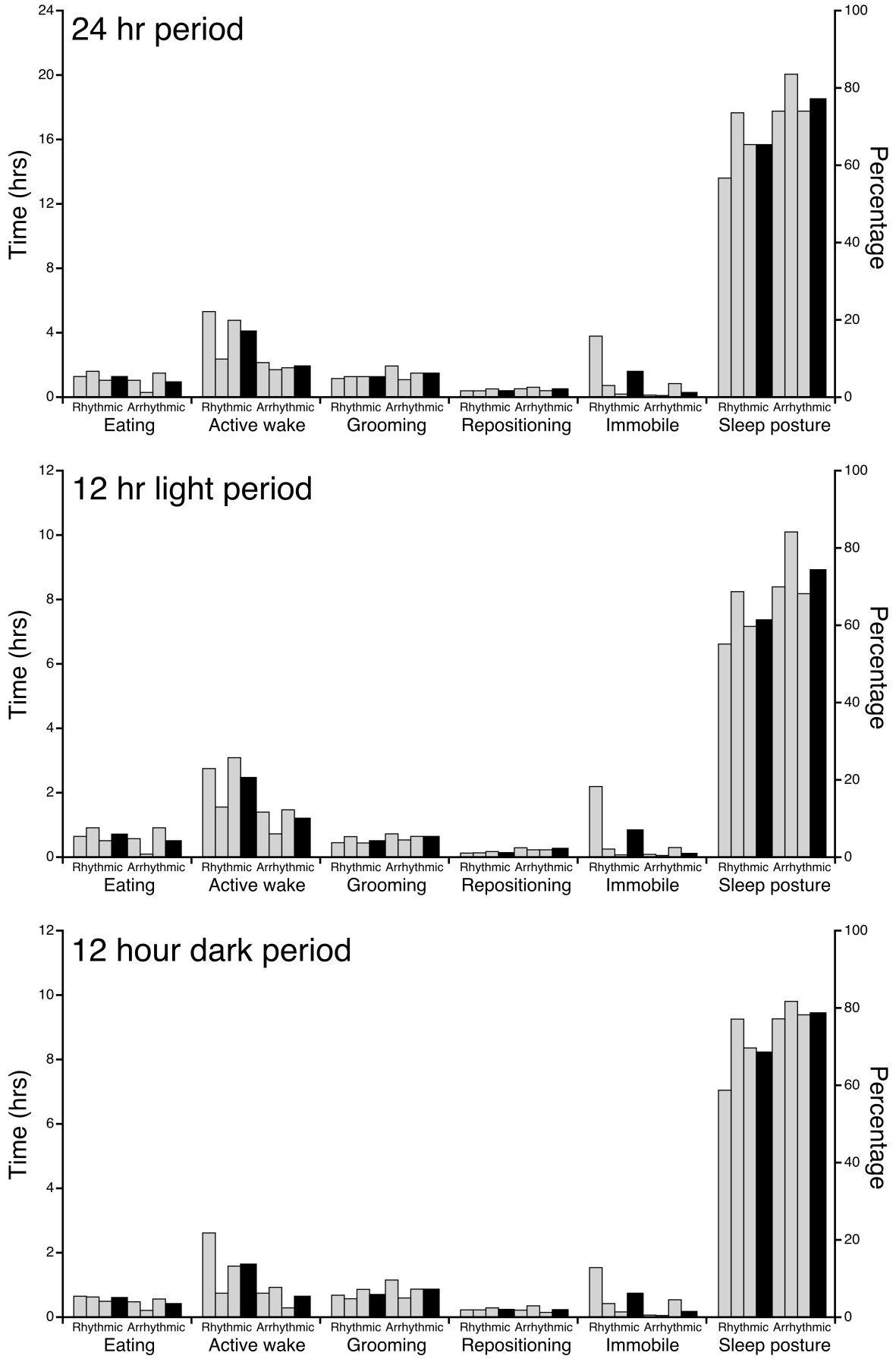
24 hr period
12 hr light period
12 hour dark period
Time (hrs)
Percentage
Rhythmic Arrhythmic
Eating
Active wake
Grooming
Repositioning
Immobile
Sleep posture

Figure 4.3: Polygraphic traces illustrating examples of the EEG and EMG recorded during sleep and wake states in the giant Zambian mole rat (*Cryptomys mechowi*). Active wake was characterised by low amplitude, high frequency EEG and high amplitude EMG. SWS was characterised by high amplitude, low frequency EEG and low amplitude EMG. Paradoxical (REM) sleep was characterised by low amplitude, high frequency EEG (similar to that seen in waking) and low amplitude EMG that contained large, high amplitude infrequent spikes (indicative of muscle twitches and jerks).

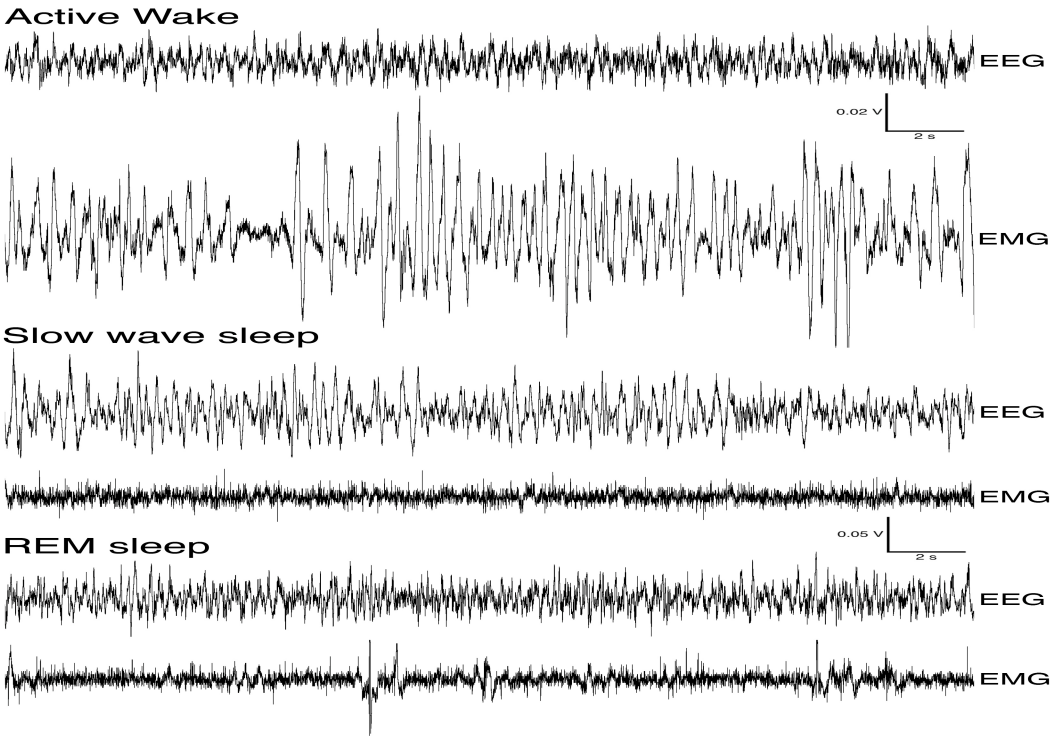
Active Wake
EEG
0.02 V
2 s
EMG
Slow wave sleep
EEG
EMG
0.05 V
2 s
REM sleep
EEG
EMG

Figure 4.4: Polygraphic traces illustrating examples of the EEG and EMG during transitions from wake to SWS to REM to wake between wake and SWS.

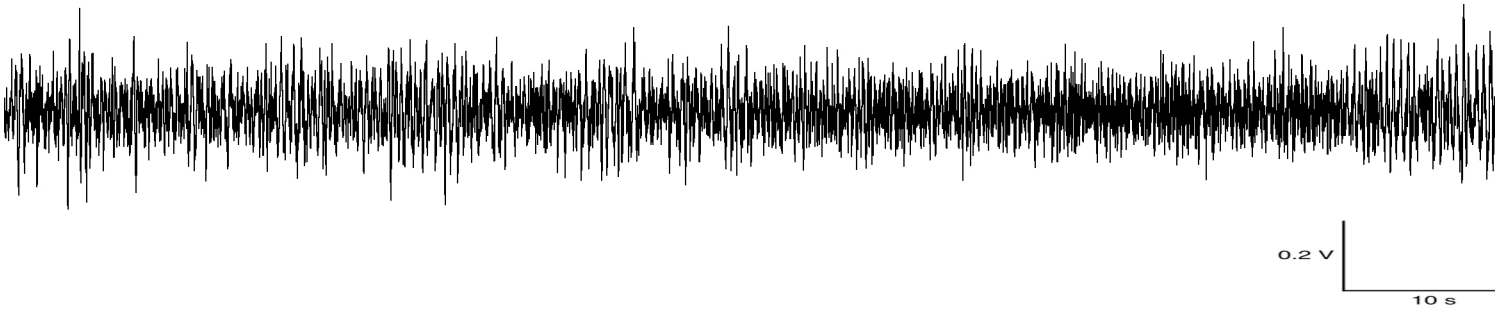
0.2 V
10 s

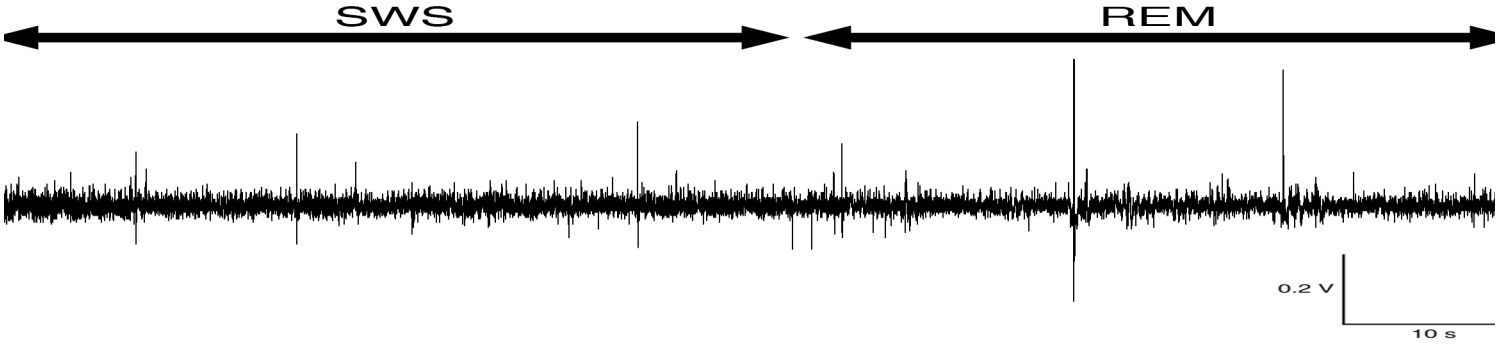
SWS
REM
0.2 V
10 s

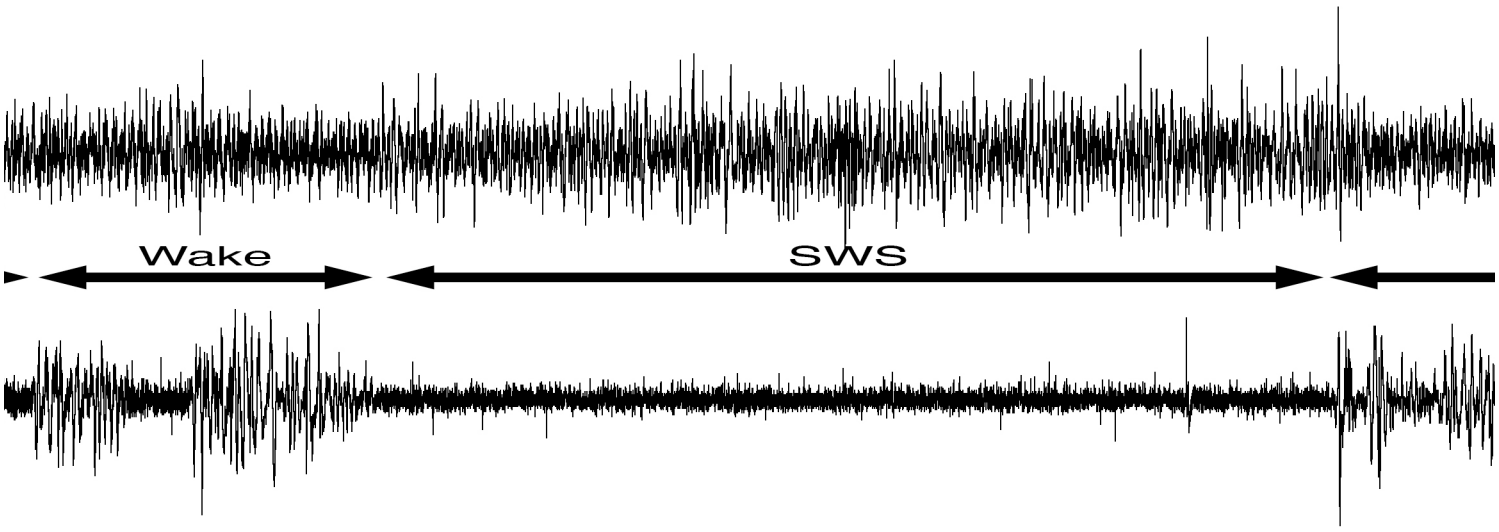
Wake
SWS

Figure 4.5: Graphs indicating the spectral power range during wake and sleep states for rhythmic and arrhythmic mole rats.

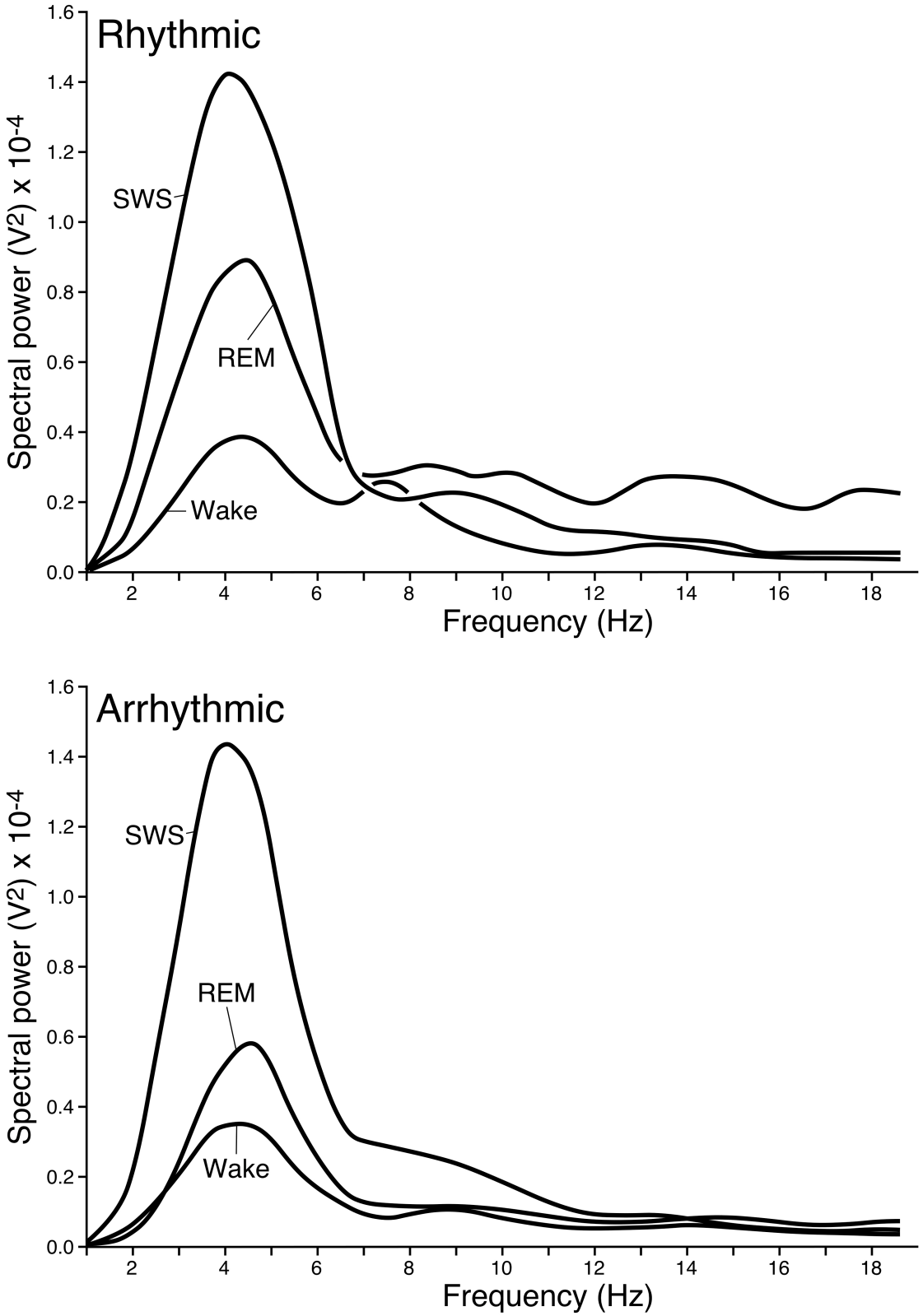
Rhythmic
Spectral power (V2) x 10-4
SWS
REM
Wake
Frequency (Hz)
Arrhythmic
Spectral power (V2) x 10-4
SWS
REM
Wake
Frequency (Hz)

Figure 4.6: Graphs illustrating physiological data (5 s epoch scoring, left column of graphs, and 1 min epoch scoring, right column of graphs) for sleep and wake states during a 24 h cycle in rhythmic and arrhythmic individuals (grey bars) and the respective weighted means (black bars). The graphs indicate percentage and the average amount of time spent in wake and sleep states, the average number of episodes for wake and sleep states and the average duration of an episode in wake and sleep states.

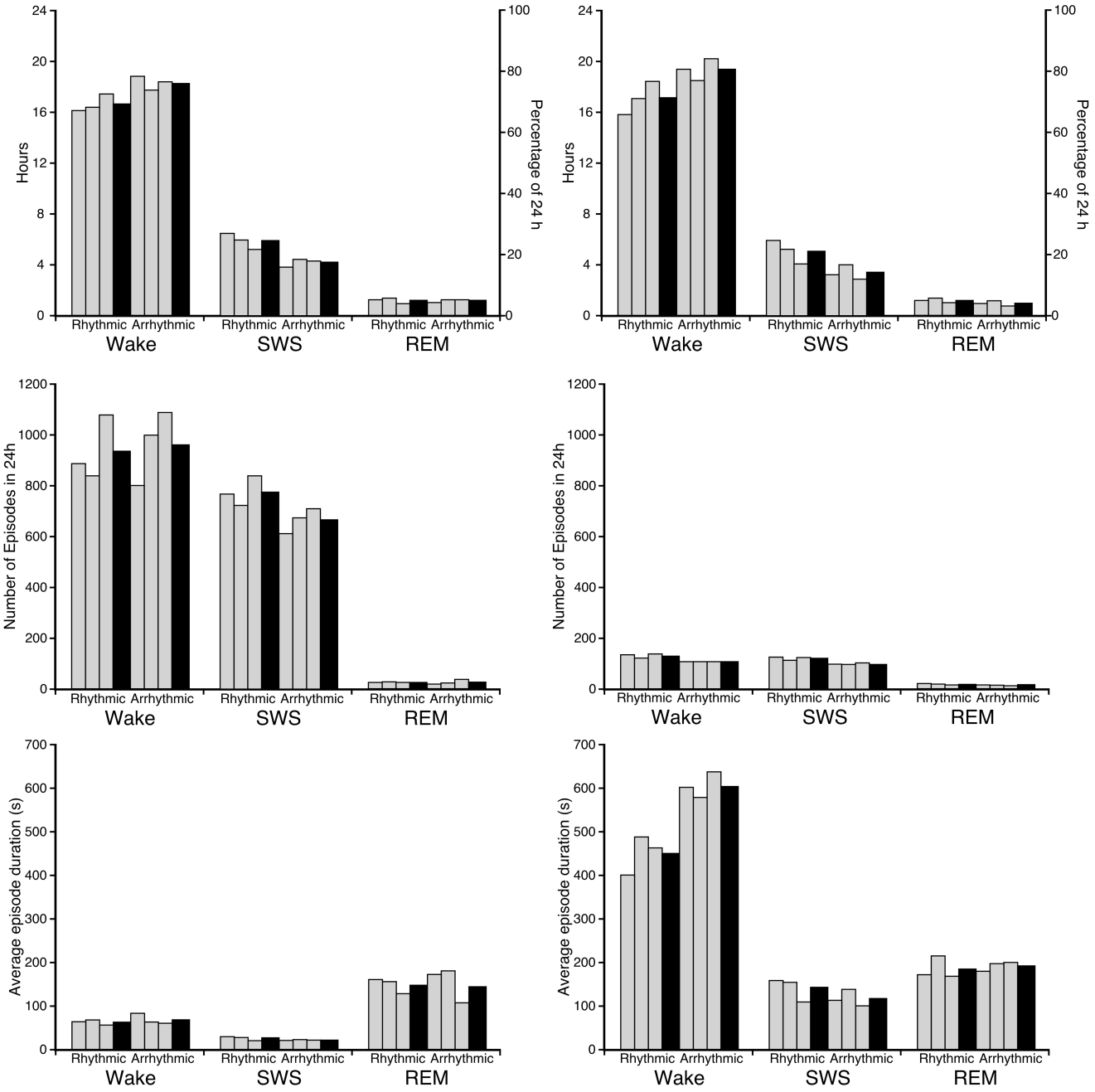
Hours
Percentage of 24 h
Number of Episodes in 24h
Average episode duration (s)
Rhythmic Arrhythmic
Wake
SWS
REM

Figure 4.7: Graphs illustrating physiological data (5 s epoch scoring, left column of graphs, and 1 min epoch scoring, right column of graphs) for sleep and wake states during the 12 h light period in rhythmic and arrhythmic individuals (grey bars) and the respective weighted means (black bars). The graphs indicate percentage and the average amount of time spent in wake and sleep states, the average number of episodes for wake and sleep states and the average duration of an episode in wake and sleep states.

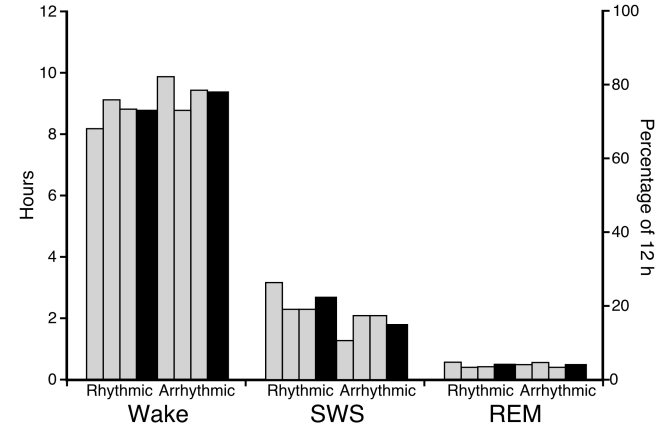
Hours
Percentage of 12 h
Rhythmic Arrhythmic
Wake
SWS
REM

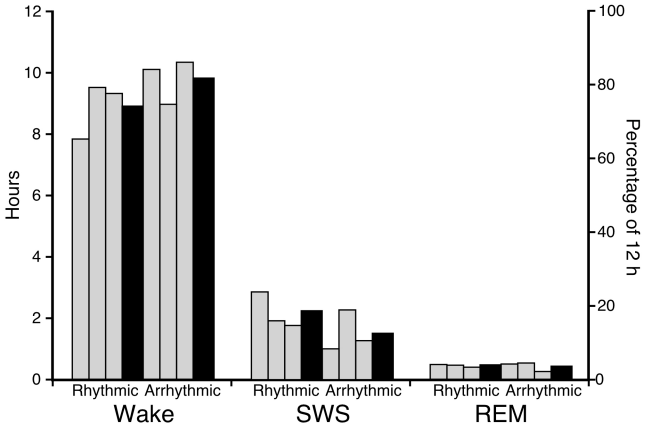
Hours
Percentage of 12 h
Rhythmic Arrhythmic
Wake
SWS
REM

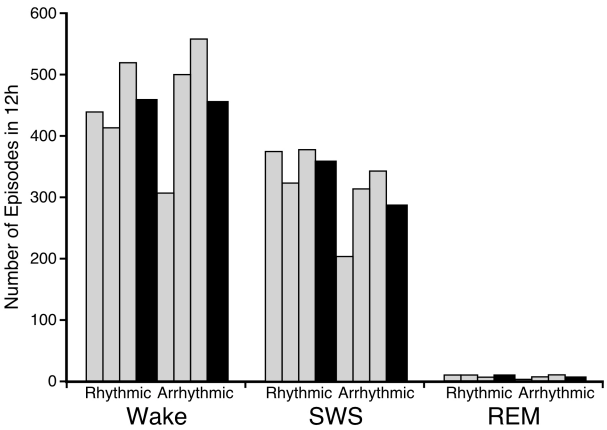
Number of Episodes in 12h
Rhythmic Arrhythmic
Wake
SWS
REM

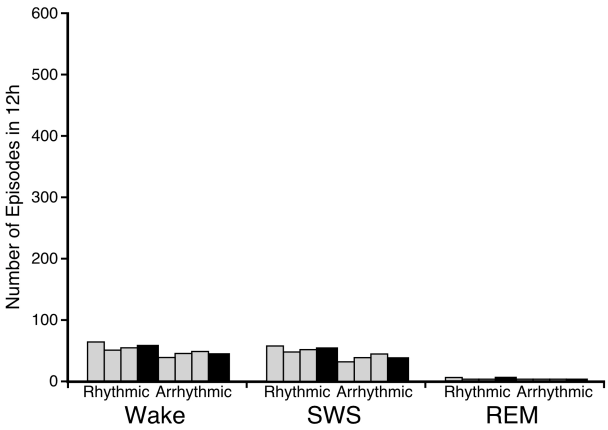
Number of Episodes in 12h
Rhythmic Arrhythmic
Wake
SWS
REM

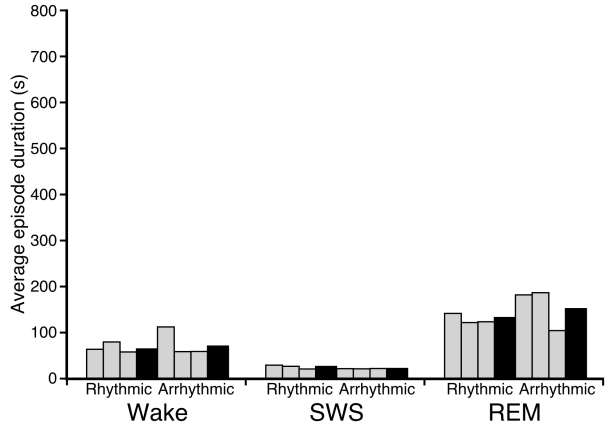
Average episode duration (s)
Rhythmic Arrhythmic
Wake
SWS
REM

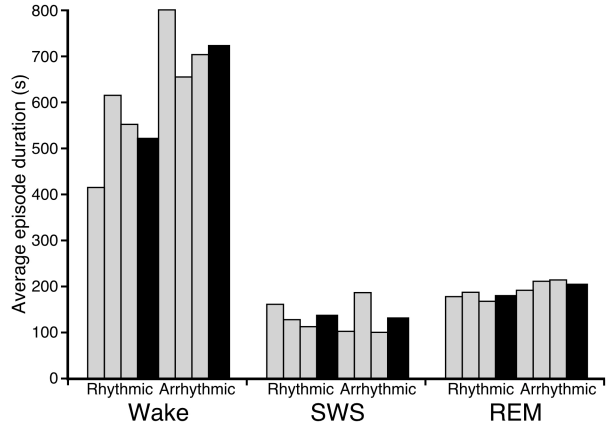
Average episode duration (s)
Rhythmic Arrhythmic
Wake
SWS
REM

Figure 4.8: Graphs illustrating physiological data (5 s epoch scoring, left column of graphs, and 1 min epoch scoring, right column of graphs) for sleep and wake states during the 12 h dark period in rhythmic and arrhythmic individuals (grey bars) and the respective weighted means (black bars). The graphs indicate percentage and the average amount of time spent in wake and sleep states, the average number of episodes for wake and sleep states and the average duration of an episode in wake and sleep states.

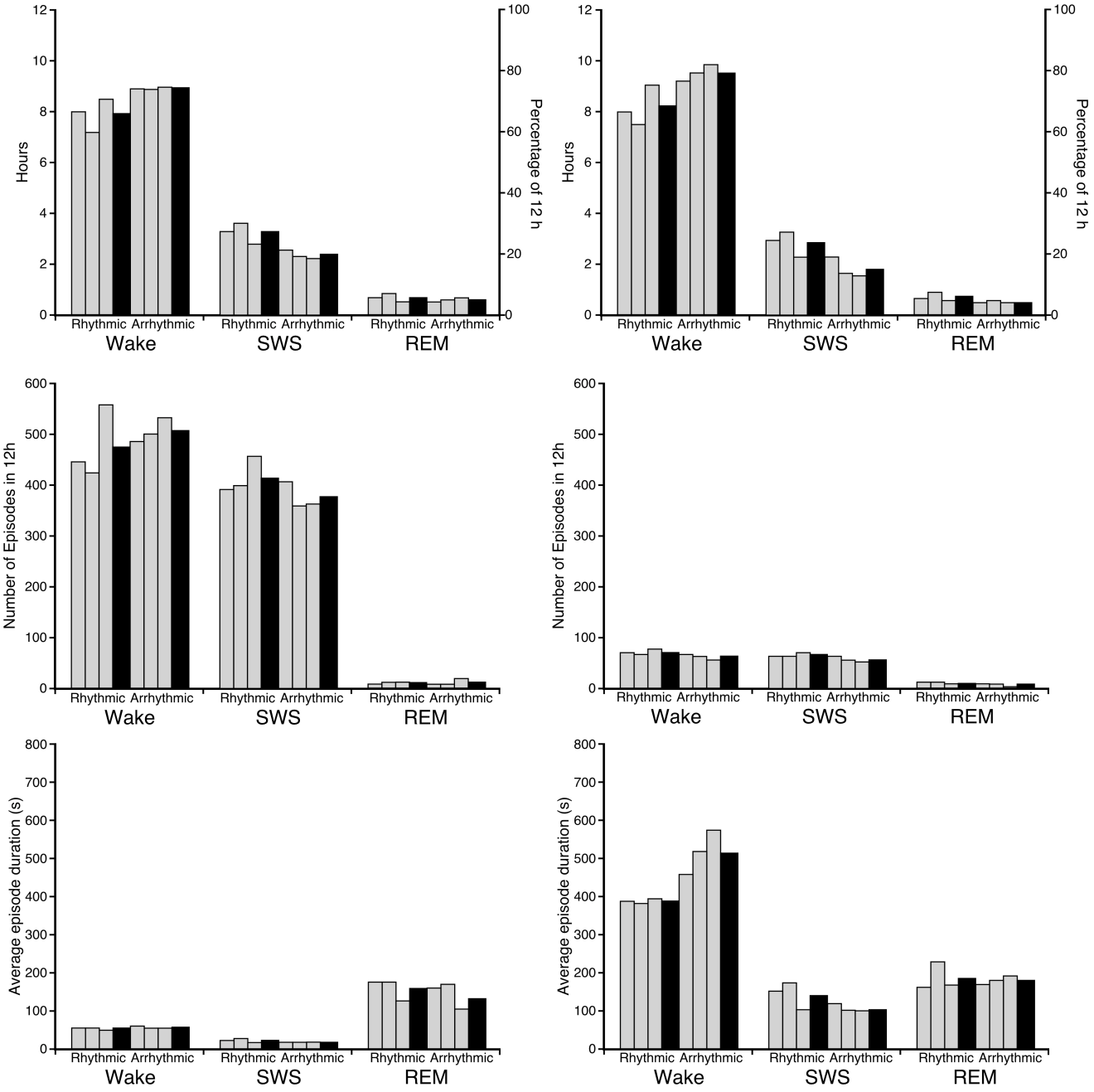
Hours
Percentage of 12 h
Number of Episodes in 12h
Average episode duration (s)
Rhythmic Arrhythmic
Wake
SWS
REM

Figure 4.9: (A) Graphs representing the variations of spectral power of slow wave activity (SWA) in SWS for 72 h from two individuals of the rhythmic and arrhythmic groups respectively; (B) the total spectral power of SWA in SWS for 72 h during the light and dark phases between rhythmic and arrhythmic groups; and (C) the total spectral power in SWA during sleep and wake states for 72 h between rhythmic and arrhythmic groups for each day.

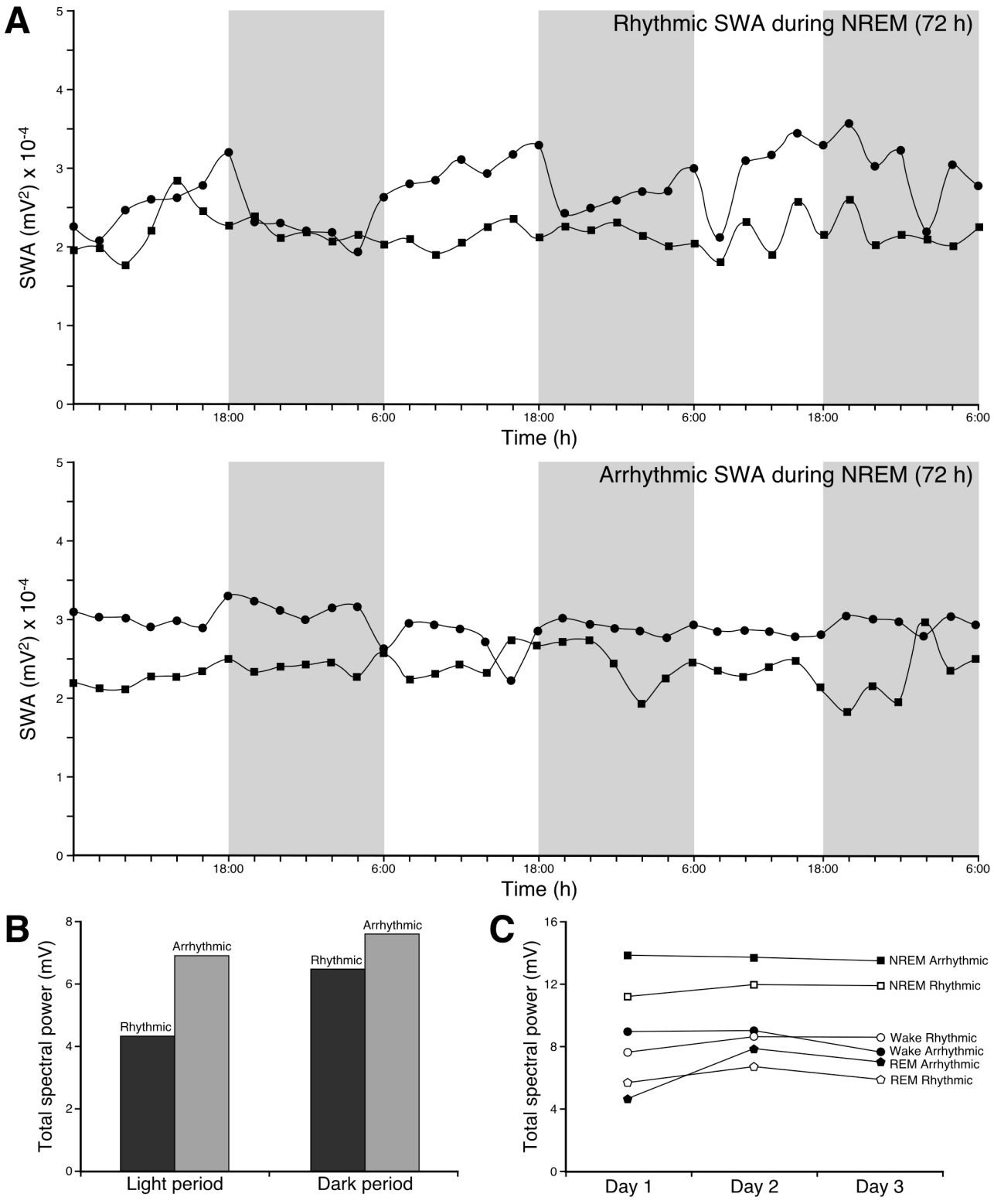
A
Rhythmic SWA during NREM (72 h)
SWA (mV²) x 10⁻⁴
Time (h)
18:00
6:00
Arrhythmic SWA during NREM (72 h)
B
Total spectral power (mV)
Rhythmic
Arrhythmic
Light period
Dark period
C
NREM Arrhythmic
NREM Rhythmic
Wake Rhythmic
Wake Arrhythmic
REM Arrhythmic
REM Rhythmic
Day 1
Day 2
Day 3

Figure 4.10: Hypnograms depicting physiological (5 s epoch scoring and 1 min epoch scoring) and behavioural data (1 min epoch scoring) in 24 h from a rhythmic and an arrhythmic individual. Grey shaded areas indicate the dark period of a 24 h cycle.

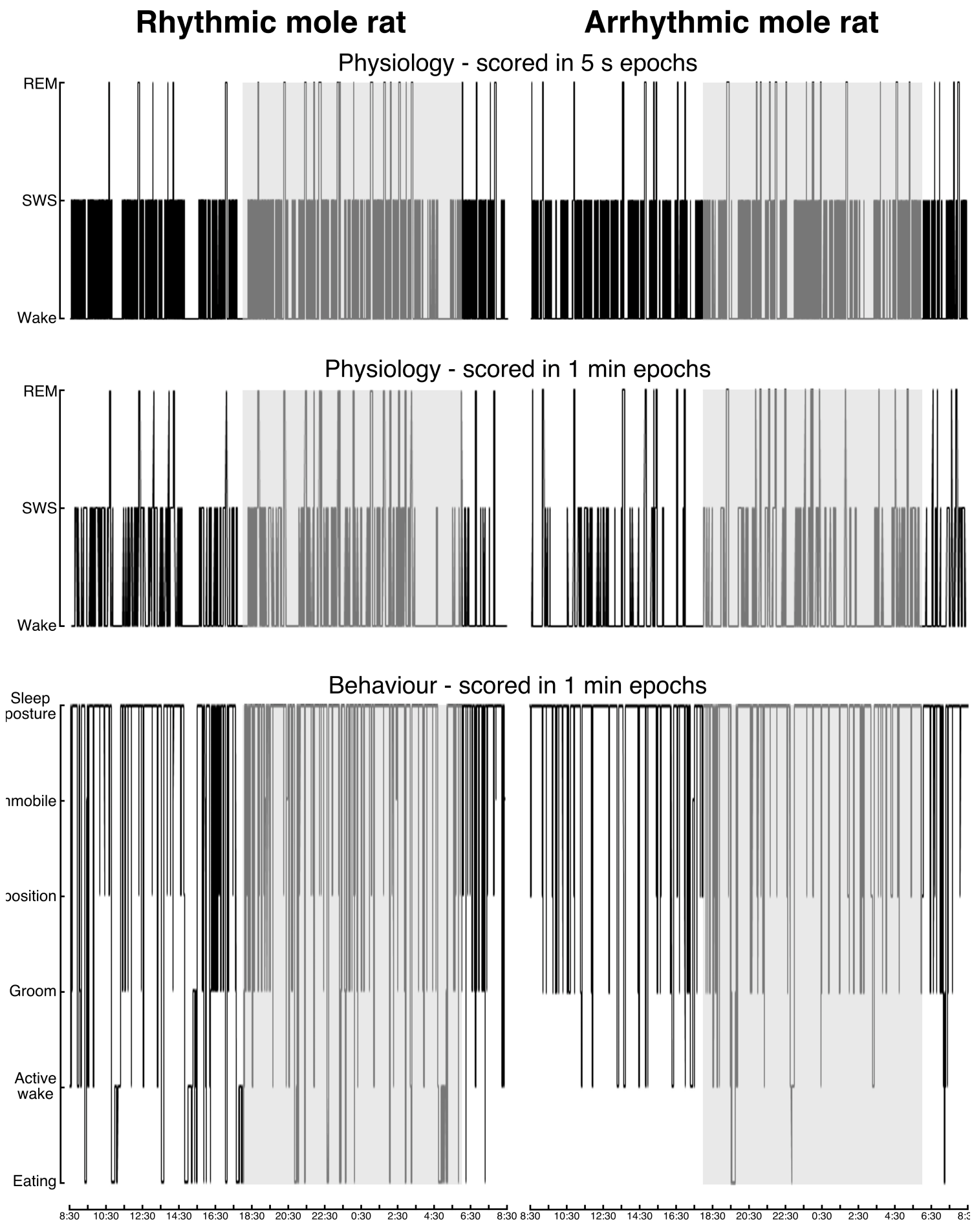
Rhythmic mole rat
Arrhythmic mole rat
Physiology - scored in 5 s epochs
REM
SWS
Wake
Physiology - scored in 1 min epochs
REM
SWS
Wake
Behaviour - scored in 1 min epochs
Sleep posture
ımobile
ɔosition
Groom
Active wake
Eating
8:30
10:30
12:30
14:30
16:30
18:30
20:30
22:30
0:30
2:30
4:30
6:30
8:30

Figure 4.11: Flow diagrams illustrating transitions (represented as a percentage) between physiological wake and sleep states in 24 h for 5 s epoch scoring and 1 min epoch scoring data from rhythmic and arrhythmic individuals.

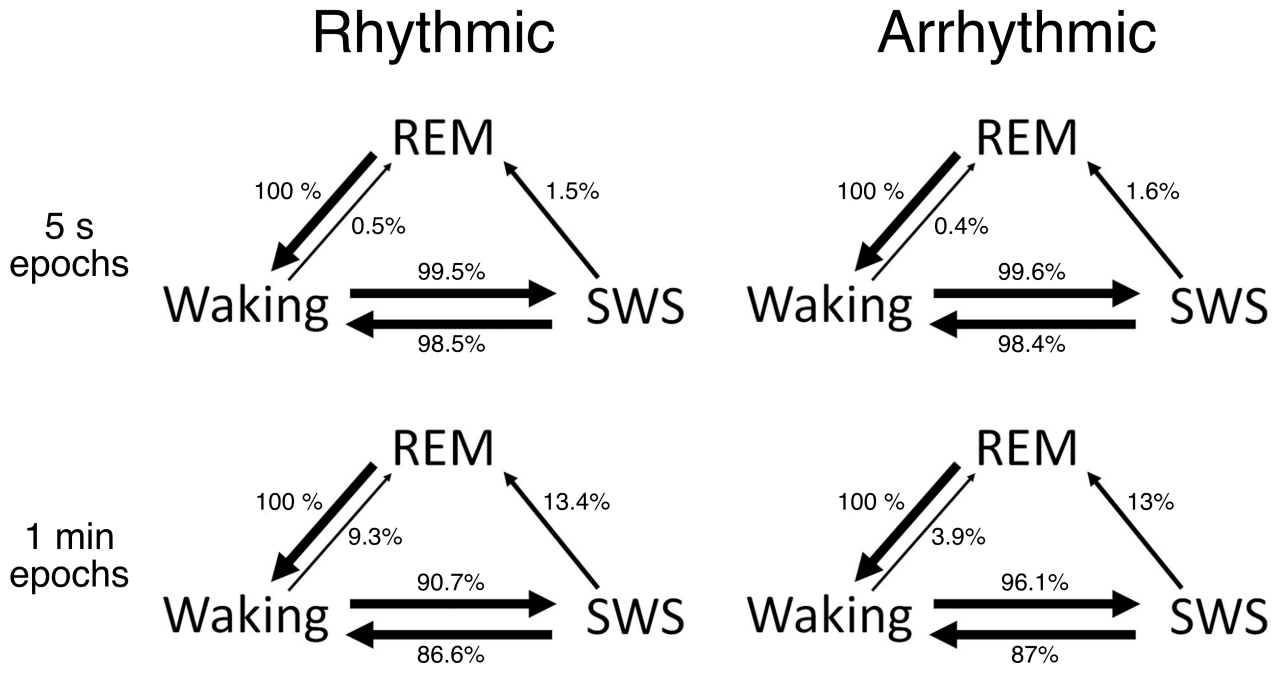
Rhythmic
Arrhythmic
5 s epochs
1 min epochs
REM
Waking
SWS
100 %
0.5%
1.5%
99.5%
98.5%
100 %
0.4%
1.6%
99.6%
98.4%
100 %
9.3%
13.4%
90.7%
86.6%
100 %
3.9%
13%
96.1%
87%

Figure 4.12: Graphs representing the time lapse (5 min periods) frequency between onsets of consecutive physiologically identified REM episodes (REM periodicity) for 1 min epoch scoring data from rhythmic and arrhythmic individuals for data that excluded episodes of waking greater than 10 min.

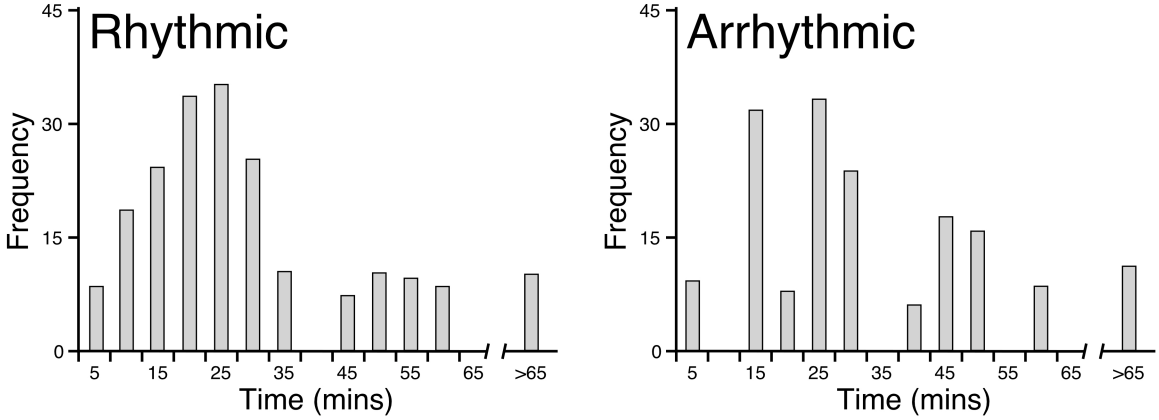
Rhythmic
Frequency
45
30
15
0
5
15
25
35
45
55
65
>65
Time (mins)
Arrhythmic
Frequency
45
30
15
0
5
15
25
35
45
55
65
>65
Time (mins)

Table 4.1: Table presenting 5 s epoch scored data for rhythmic and arrhythmic mole rats for parameters measured in the current study. TWT – Total waking time; TST – Total sleep time; TSWS – Total slow wave sleep; TREM – Total REM. (*) indicates statistical significance between rhythmic and arrhythmic chronotypes using One-way Anova where $p<0.05$ and the post hoc Turkey's pairwise comparison test where $p<0.05$. The location of the asterisks indicates the chronotype with the higher mean.

Animal ID	M3	M8	M9	Weighted mean rhythmic	M1	M5	M6	Weighted mean arrhythmic
Circadian chronotype	Rhythmic	Rhythmic	Rhythmic		Arrhythmic	Arrhythmic	Arrhythmic	
Body mass (g)	389	254	350	**331**	208	220	310	**246**
Brain Mass (g)	2.2	2.2	2.4	**2.3**	2.2	2.2	2.2	**2.2**
Sex	Male	Male	Male		Male	Male	Male	
TWT (% 24 h)	68	68	72	**69**	78	74	77	**76***
TST (% 24 h)	32	30	26	**29**	20	23	23	**22**
TSWS (% 24 h)	27	25	22	**25***	16	18	18	**17**
TREM (% 24 h)	5	5	4	**5**	4	5	5	**5**
TWT-Light period (% 12 h)	68	77	74	**73**	82	74	79	**78***
TST-Light period (% 12 h)	31	23	23	**26**	15	22	21	**19**
TSWS-Light period (% 12 h)	27	20	19	**22**	11	17	17	**15**
TREM-Light period (% 12 h)	5	4	3	**4**	4	5	4	**4**
TWT-Dark period (% 12 h)	67	60	71	**66**	74	75	75	**75***
TST- Dark period (% 12 h)	33	37	28	**33**	26	25	25	**25**
TSWS-Dark period (% 12 h)	28	30	24	**27**	21	19	19	**20**
TREM-Dark period(% 12	6	7	5	**6**	4	5	6	**5**

Table 4.2: Table presenting 1 min epoch scored data for rhythmic and arrhythmic mole rats for parameters measured in the current study. TWT – Total waking time; TST – Total sleep time; TSWS – Total slow wave sleep; TREM – Total REM.

Animal ID	M3	M8	M9	Weighted mean rhythmic	M1	M5	M6	Weighted mean arrhythmic
Circadian chronotype	Rhythmic	Rhythmic	Rhythmic		Arrhythmic	Arrhythmic	Arrhythmic	
Body mass (g)	389	254	350	**331**	208	220	310	**246**
Brain Mass (g)	2.2	2.2	2.4	**2.3**	2.2	2.2	2.2	**2.2**
Sex	Male	Male	Male		Male	Male	Male	
TWT (% 24 h)	66	71	77	**72**	72	81	78	**80**
TST (% 24 h)	30	28	21	**26**	18	22	15	**18**
TSWS (% 24 h)	25	22	17	**21**	14	17	12	**14**
TREM (% 24 h)	5	6	4	**5**	4	5	3	**4**
TWT-Light period (% 12 h)	66	80	78	**75**	85	75	87	**82**
TST-Light period (% 12 h)	29	20	19	**23**	12	24	13	**16**
TSWS-Light period (% 12 h)	24	16	15	**19**	8	19	11	**13**
TREM-Light period (% 12 h)	4	4	4	**4**	4	5	3	**4**
TWT-Dark period (% 12 h)	67	63	76	**68**	77	80	82	**80**
TST- Dark period (% 12 h)	31	35	24	**30**	23	19	17	**20**
TSWS-Dark period (% 12 h)	25	28	19	**24**	19	14	13	**15**
TREM-Dark period(% 12	6	8	5	**6**	4	5	4	**5**

Table 4.3: Table presenting results from rhythmic and arrhythmic mole rats of the current study for: Total sleep time (TST), percentage REM sleep of TST, average duration of an episode of SWS, and average duration of episode of REM; compared to other rodents. Source references: (1) Mistlberger et al., 1983; (2) Van Twyver, 1969; (3) Valtax and Bugat, 1974; (4) Kastaniotis and Kaplan, 1976; (5) Tobler and Deboer, 2001; (6) Borbély and Neuhaus, 1979; (7) Franken et al., 1992; (8) Deboer et al., 1994; (9) Huber et al., 2000.

	TST (h)	% REM of TST	Duration SWS episode (min)	Duration REM episode (min)	TSWS (h)	TREM (h)	Source
C. mechowi Rhythmic 5s epoch scored data	7	16	0.5	2.5	5.9	1.1	Current study
C. mechowi Arrhythmic 5s epoch scored data	5.3	21	0.4	2.4	4.2	1.1	Current study
C. mechowi Rhythmic 1 min epoch scored data	6.2	19	2.5	3.2	5.1	1.2	Current study
C. mechowi Arrhythmic 1 min epoch scored data	4.3	23	2.0	3.3	3.3	1	Current study
(*R.norwegicus*) Long-Evans rat	13.2	18	5.2	1.7	10.8	2.4	1, 2, 6, 7
(*R.norwegicus*) Sprague Dawley rat	13.7				11.2	2.5	
(*M.musculus*) Laboratory mouse	12.8	13 - 20	4.7 – 7.1	0.7 – 0.9	10.2 – 11.1	1.7 – 2.6	3, 9
(*M.auratus*) Golden hamster	14.4	-	-	-			2
(*M. unguiculatus*) Mongolian gerbil	15.3	-	-	-			4
(*C. laniger*) Chinchilla	12.5	-	-	-			2
(*S. ehrenbergi*) Blind mole rat	12.4	15.1	9.7	2.5	10.5	1.9	5
Djungarian hamster	-	15	7	1.8			8

4.4 Discussion

The present study was undertaken to examine whether differences in wake and sleep states were readily observable in a species of mole rat from which individuals with a rhythmic or arrhythmic chronotype were identified and if a regressed visual system affected these parameters in comparison to other rodents. The current study used standard techniques for identifying the chronotype of the individual molerats (Oosthuizen et al., 2003) and then employed telemetric recording of physiological EEG and EMG combined with behavioural recording. In assigning physiological states the EEG and EMG enabled identification of between wake, SWS and REM sleep in this species and these assignations correlated closely with behavioural recordings. We used both a 5 s epoch scoring method and a 1 min epoch scoring method to probe for potential differences, both methods having advantages and disadvantages in revealing similarities and differences, of which several were noted. The results indicate that the arrhythmic individuals spend more time in waking with a longer average duration of a waking episode, and less time in SWS with a shorter average duration of a SWS episode though with a greater slow wave sleep intensity. Total time spent in sleep (TST) for both chronotypes of this rodent species was shorter than that seen in other rodents. This was a result of the species studied spending less time in SWS compared to other rodents (see Table 4.3), as the amount of time spent in REM sleep was within the range, though at the upper end of the range, reported previously for other rodents.

4.4.1 State definitions

In the present study wake and sleep states were telemetrically recorded and subsequently scored for both the 5 s epoch scoring and the 1 min epoch scoring. The state of wake was polygraphically identified by low amplitude, high frequency cortical EEG activity and irregular high amplitude nuchal EMG activity and these correlated with the behavioural

states of eating, moving around, grooming and repositioning. The state of SWS was polygraphically identified by high amplitude, low frequency cortical EEG activity and stable low amplitude nuchal EMG activity and was always associated with the behavioural states of either immobility or sleep posture (identified when the animal presented itself in a curled 'ball-like' position). REM sleep was polygraphically identified by low amplitude, high frequency cortical EEG waves (similar to that seen in waking) and when the nuchal EMG was lower in amplitude compared to waking and SWS and displayed large, high amplitude infrequent spikes (that correlated with behavioural twitches and jerks only when the animal was in either a state of immobility or in a curled 'ball-like' position). These criteria used for the polygraphic identification of wake and sleep states in the mole rats of the current study are congruent with those previously utilised in the physiological identification of wake and sleep states in a different species of mole rat (Tobler and Deboer, 2001) and in other rodents and terrestrial mammals (see review by Campbell and Tobler, 1984; Tobler, 1995; McNamara et al., 2010).

4.4.2 5 s epoch scoring *vs* 1 min epoch scoring

The scoring techniques employed in the current study yielded some similarities and differences in the results. It was observed that between the rhythmic and arrhythmic mole rats for both methods of scoring (5 s and 1 min epochs) the time spent in waking (rhythmic comparison; One-way Anova, p-value: 0.574 and arrhythmic comparison; One-way Anova, p-value: 0.1298), SWS (rhythmic comparison; One-way Anova, p-value: 0.2884 and arrhythmic comparison; One-way Anova, p-value: 0.1004) and REM sleep (rhythmic comparison; One-way Anova, p-value: 0.7759 and arrhythmic comparison; One-way Anova, p-value: 0.3777) remained similar. This is of importance as it reveals that the determination of the time spent in the various wake and sleep states is not affected by which scoring method

is utilised. The 5 s epoch scored data produced more statistically significant differences for the average number of episodes of wake and sleep states and average duration of an episode of wake and sleep states, within and between chronotypes and within and between days and light and dark periods when compared to the 1 min epoch scored data (see description of statistically significant differences in sections 4.3.2.2 to 4.3.2.4). The average duration of an episode of waking and SWS generated by the 5 s epoch scoring data seem unusually short, but if the average number of episodes is factored into this equation then the results indicate that both the rhythmic and arrhythmic individuals may exhibit a form of sleep fragmentation, as determined by the occurrence in brief arousals during SWS (Franken et al., 1991). The differences between the methods of scoring are a direct result of a decrease in sampling size from the 5 s epoch scoring to the 1 min epoch scoring, but the 1 min epoch scoring data generates a more believable biological scenario for waking and SWS without significantly changing the times spent in these physiological states. Interestingly, despite the differences between the two methods for waking and SWS, the average number of episodes (rhythmic comparison; One-way Anova, p-value: 0.0862 and arrhythmic comparison; One-way Anova, p-value: 0.1964) and average duration of an episode of REM sleep (rhythmic comparison; One-way Anova, p-value: 0.09602 and arrhythmic comparison; One-way Anova, p-value: 0.1624) remained similar for both scoring methods. In light of the above, both the 5 s and 1 min scoring data appear to be a reasonable methods to draw conclusions regarding the total time spent in wake and sleep states, while the 1 min scoring data provides a more biologically relevant, as it correlated more closely with the behaviour, method to determine the average number of episodes of wake and sleep states and the average duration of an episode of wake and sleep states. In the text that follows the values generated from the 1 min scoring data are used for comparisons and discussion.

4.4.3 Rhythmic vs Arrhythmic mole rats

The results of the present study indicated that the arrhythmic mole rats spent more time in a state of wake (19.4 h *vs* 17.1 h, with a peak during the dark period), and had a longer average duration for a waking episode (609 s *vs* 453 s) than the rhythmic group. In contrast, the rhythmic mole rats spent more time in SWS (5.1 h *vs* 3.4 h, especially during the light period), had a higher average number of SWS episodes (122 *vs* 103) and had a longer average duration of a SWS episode (147 s *vs* 119 s) than the arrhythmic mole rats. Both groups spent a similar amount of time in REM sleep (1.2 h for rhythmic *vs* 1 h for arrhythmic), had a similar average number of REM sleep episodes (23 for rhythmic *vs* 18 for arrhythmic) and had a similar average duration of a REM episode (189 s for rhythmic *vs* 194 s for arrhythmic). The homeostatic nature of sleep dictates that sleep propensity is related to the history of prior waking i.e. the longer the vigilance state of wake is maintained, the greater the drive for sleep becomes (Tucci and Nolan, 2010). Given that the arrhythmic group spends more time awake than the rhythmic group, it is tempting to suggest that sleep propensity in the arrhythmic group should be higher. Interestingly, in potential mitigation of this apparent paradox, it was observed that SWA during SWS was consistently higher in the arrhythmic group compared with the rhythmic group, indicating that the arrhythmic individuals display a greater intensity of SWS compared to the rhythmic individuals. As SWA in SWS can be used as an indicator of SWS intensity, it is possible that the decrease in SWS observed in the arrhythmic mole rats is compensated for by increasing SWA in SWS rather than by lengthening the duration of SWS. The SWA activity during SWS of the arrhythmic mole rats of the current study is congruent with previous studies of sleep deprivation in different mammals that have consistently shown an increase in SWA during SWS following sleep deprivation (Tobler, 1995).

Furthermore, it was observed that both chronotypes of mole rat spend a large percentage of time in behavioural sleep posture yet they are mostly in a physiological state of wake while in this position. An explanation for this presents as an adaptative feature to a subterranean lifestyle with a regressed visual system. These animals are known to have extensive tunnel systems and spend a large percentage of the day in these tunnels. Therefore the mole rats observed in the current study devote a large percentage of their daily activity in this posture.

4.4.4 Comparison to other rodents

In the present study it was found that the total sleep time (TST) in the rhythmic individuals was 6.5 h whereas that of the arrhythmic group was 4.3 h. These values are lower than those noted (under similar recording conditions) for other rodents (Table 4.3). The amount of time spent in REM sleep in both groups of mole rats is lower than the range that has been observed in other rodents (1.7 – 2.6 h, Table 4.3); however, the proportion of REM sleep relative to the total sleep time in the rhythmic group is 19 % while that of the arrhythmic group is 23 %, which while within the range seen for other rodents are on the higher end of the range (Table 4.3). The average duration of an episode of SWS in the rhythmic and arrhythmic mole rats (147 s and 119 s respectively) are shorter than that seen in other rodents (Table 4.3), but the average duration of a REM episode in the rhythmic and arrhythmic mole rats (189 s and 195 s respectively) are longer than those reported in other rodents (Table 4.3).

The consistency in the average duration of an episode of REM sleep between rhythmic and arrhythmic groups suggests a crucial baseline function for REM sleep in the mole rats. It has been previously noted that subterranean mole rats have a lower body temperature than surface dwelling mammals (Bennett and Faulkes, 2000) though it is

unknown whether body temperature differences exist between different circadian chronotypes. It is has been shown that REM sleep reaches maximal activity when body temperature is at its lowest (Dijk and Franken, 2005), therefore it could be possible that REM sleep is specifically regulated in these mole rats irrespective of their chronotype in relation to their body temperature, and this may explain the slightly higher duration of REM in the mole rats of the current study compared to other rodents (Table 4.3). A possible explanation for the discrepancy observed between the mole rats of the current study and other rodents could lie in the genetic variation of these rodents, as some of the classic sleep disorders have been associated with single gene mutations (Kimura and Winkelmann, 2007) and several studies have identified genomic regions that contain allelic variations affecting quantifiable sleep parameters commonly referred to as quantitative trait loci (QLT) (Tafti et al., 1997; Tafti, 2007). It is known in humans and mice that genetics are responsible for the phenomenological architecture of sleep (Lindowski et al., 1991; Franken et al., 1998, 1999; Tafti et al., 1997). It would appear that a series of loci on chromosomes 5, 7, 12 and 17 are associated with the vigilance phenotype in mice (Tafti et al., 1997), and this was further assessed by characterising differences in EEG parameters in inbred mice strains where a number of differences between sleep states but also significant genotype-specific variations were reported, thereby indicating that EEG parameters are under genetic control (Franken et al., 1998).

4.4.5 Circadian rhythmicity and sleep

One of the aims of the current study was to determine whether baseline physiological sleep parameters would differ in individuals of the same species with distinct circadian chronotypes. The results of the present study indicate that while there were some differences between the rhythmic and arrhythmic groups, for the most part the measured sleep parameters

were not significantly different. It is known that circadian rhythmicity and sleep homeostasis both contribute to the sleep-wake cycle and the structure of sleep in animals, yet it is apparent that sleep homeostasis is driven by sleep-wake behaviour, whilst the circadian clock is influenced by light and might be affected by the feedback of the sleep-wake cycle (Dijk and Franken, 2005). Several studies have shown that the phase relationship between the sleep-wake cycle and circadian rhythms may change and that the duration and structure of sleep may depend on the circadian phase at which sleep occurs (e.g. Czeisler et al., 1980; Zulley et al., 1981). Furthermore, sleep deprivation studies in species with an ablated SCN demonstrated an increase in SWA and sleep duration that suggests a neuroanatomical separation of the circadian and homeostatic regulation of sleep (Dijk and Franken, 2005). The results of the present study support the notion of elevated SWA as it was observed that SWA in SWS of the arrhythmic group was consistently higher when compared to the rhythmic group and this was seen in both light and dark periods; however, the results disagree with notion of an increase in sleep duration as it was observed that the average duration of an episode of SWS in the arrhythmic group was significantly lower when compared to the rhythmic group.

Circadian rhythms can be altered through genetic mutation of clock genes. Studies have shown that ablation of the clock genes *per1* and *per2*, which results in the absence of circadian rhythms in mice, do not affect sleep homeostasis and are not associated with a major change in the sleep deprivation induced increase in SWA (Kopp et al., 2002; Shiromani et al., 2004)., Wisor et al (2002) showed that mice lacking the cryptochrome genes, *cry1* and *cry2*, also had an absence of circadian rhythmicity. This study concluded that the cryptochrome genes affect sleep homeostasis, where SWS sleep time is increased and SWA is higher compared to wild types and sleep deprivation produces no change to SWS sleep time yet attenuates SWA compared to wild types. These genetic mutation studies

indicate that the separation of circadian rhythmicity and sleep homeostasis does not extend to all components of circadian rhythm generation (Dijk and Franken, 2005). In the present study, the results are congruent with the theory postulating independence of circadian rhythmicity and sleep homeostasis, since no statistical significance could be identified between the rhythmic and arrhythmic groups in the amount of waking, amount of SWS sleep, percentage of total sleep time, amount of REM sleep and the percentage of REM sleep relative to the total sleep time; however, changes in the clock genes within the arrhythmic group may explain the statistically longer duration of waking and shorter duration of SWS sleep compared to the rhythmic group.

Chapter 5 - Orexinergic neuron numbers in three species of African mole rats with rhythmic and arrhythmic chronotypes

5.1 Introduction

It is well known that mole rats, subterranean, visually regressed rodents, have unusual patterns of circadian rhythmicity (Lovegrove and Papenfus, 1995; Lovegrove and Muir, 1996; Oosthuizen et al., 2003). Locomotor activity studies have shown that within a species of mole rat there are individuals that have a rhythmic chronotype, and others that are distinctly arrhythmic and this is seen in both social and solitary species of mole rat (Oosthuizen et al., 2003). A study of sleep patterns in the giant Zambian mole rat (*Cryptomys mechowi*) showed some differences in sleep patterns between rhythmic and arrhythmic chronotypes of this species (Chapter 4).

The neurotransmitter orexin is known to promote wakefulness, particularly during motor activities (Estabrooke et al., 2001; Mileykovskiy et al., 2005; Lee et al., 2005; Saper et al., 2005). Orexinergic neurons, which are restricted to the hypothalamus, have ascending projections to the cerebral cortex and descending projections to the cholinergic (basal forebrain, lateral dorsal tegmental nucleus, pedunculopontine nucleus) and monoaminergic (locus coeruleus, ventral tegmental area, raphe) nuclear groups of the arousal systems (Peyron et al., 1998; Chemelli et al., 1999; Baumann and Bassetti, 2005). Orexinergic neurons further reinforce the arousal system by mutual communication with the sleep promoting ventral lateral preoptic nucleus, though they may not directly inhibit the neurons of this nucleus (Chou et al., 2000; Sakurai et al., 2005; Saper et al., 2005; Yoshida et al., 2006). Loss of orexinergic neurons has been associated with narcolepsy (Chemelli et al., 1999; Lin et al., 1999; Siegel, 1999), narcolepsy with cataplexy in humans (Peyron et al.,

2000; Thannickal et al., 2000), narcolepsy without cataplexy in humans (Thannickal et al., 2009) and the narcoleptic like symptoms in patients with Parkinson's disease (Thannickal et al., 2007).

It is also known that orexins are involved in appetite regulation through activation of the leptin sensitive neurons of the arcuate nucleus and its subsequent feeding associated signalling to orexinergic neurons of the lateral hypothalamus (LH) and henceforth interaction between LH and the hypothalamic ventro-medial nucleus (VMH) (Stellar, 1954; Rodgers et al., 2002; Sakurai, 2003; Sakurai, 2005). Several studies have demonstrated increased orexinergic activity during states of vigilance and foraging and as a result have paired waking with hunger sensations and optimal feeding (Sakurai et al., 1998; Edwards et al., 1999; Haynes et al., 1999; Van Itallie 2006). Conversely anorexinergic activity has been associated with sleep states, thereby pairing satiety with sleep (Rodgers et al., 2002; Nicolaidis, 2006, Van Itallie, 2006). These studies are indicative of a coordinated orexinergic control of appetite regulation with the sleep-wake cycle that is responsive to the SCN circadian clock and nutritional status (Sakurai, 2005; VanItallie, 2006), plus, it has been suggested that disruption of the circadian cycle and sleep deprivation can affect energy balance resulting in changes in body composition (Taheri et al., 2004; Van Itallie, 2006).

Given this scenario on the action of the orexinergic neurons, and the clearly distinct circadian chronotypes of the African mole rats, along with differences in the neuropeptide population of the suprachiasmatic nucleus of the mole rats (Negroni et al., 2003), it was thought that an investigation of orexinergic neuronal numbers may yield results of interest in relation to function, especially so in the mole rats. In the current study, orexinergic neuronal numbers of three species of African mole rat, the Highveld mole rat (*Cryptomys hottenttotus pretoriae*), Ansel's mole rat (*Fukomys anselli*) and the Damaraland mole rat (*Fukomys*

damarensis) were quantified. All three species of mole rat have a reduced visual system, live a subterranean lifestyle and have unusual patterns of circadian rhythmicity (Lovegrove and Papenfus, 1995; Lovegrove and Muir, 1996; Oelschlager et al., 2000; Cernuda-Cernuda et al., 2003; Negroni et al., 2003; Oosthuizen et al., 2003; Gutjahr et al., 2004; Nemec et al., 2004). Brains from circadian distinct rhythmic and arrhythmic individuals of each species were examined. The unusual circadian patterns of individuals within a species provide interesting models to examine whether the absolute numbers of identified orexinergic neurons differs between circadian chronotypes amongst the species examined.

5.2 Materials and Methods

A total of 18 brains (15 males and 3 females – see table 5.1) from three species of wild caught African mole rat, the Highveld mole rat (*Cryptomys hottentotus pretoriae*) (CHP) (average body mass: 127.9g; average brain mass: 1.5g), Ansel's mole rat (*Fukomys anselli*) (FA) (average body mass: 84.5g; average brain mass: 1.2g), and the Damaraland mole rat (*Fukomys damarensis*) (FD) (average body mass: 107.8g; average brain mass: 1.8g) were utilised in this study. For the purposes of the current study, three rhythmic and three arrhythmic individuals per species were used.

5.2.1 Determination of Rhythmicity patterns

A system using, infrared detectors was used to detect activity patterns in the mole rats see Oosthuizen et al. (2003). The mole rats were exposed to differing light conditions that included, light (L) and dark (D) cycles, DD cycles and LL cycles. Initially the experimental protocol started with a 12L:12D cycle (stage 1) and once entrainment was achieved the light cycle was switched to constant darkness for 1 month (stage 2) to determine the expression of endogenous rhythms. Once this was completed the light cycle was reversed to 12L:12D

(stage 3). To determine rhythmicity patterns, patterns of activity were determined under the various light and dark cycles and a mole rat was considered rhythmic when it exhibited the same preference for phase activity during stage 3 as it did in stage 1. Conversely a mole rat was deemed arrhythmic when no discernable preference for phase of activity could be ascertained between stage 3 and stage 1. For details regarding the specifics of circadian rhythm determination see Oosthuizen et al. (2003).

5.2.2 Orexin Immunohistochemistry

The mole rats were euthanazed (Euthanaze, 200mg sodium pentobarbital/kg, i.p.) and then perfused intracardially. The perfusion was initially done with a rinse of 0.9% saline solution at 4°C, followed by a solution of 4% paraformaldehyde in 0.1M phosphate buffer (PB, pH: 7.4) (approximately 1 l/kg of each solution). Brains were removed from the skull and post-fixed overnight (24 h) in 4% paraformaldehyde in 0.1M PB, and then allowed to equilibrate in 30% sucrose in PB. The brains were blocked and the diencephalon frozen and sectioned coronally (50 μm section thickness). A one in two series of stains was made for Nissl and orexin-A immunohistochemistry. Sections used for the Nissl series were mounted on 0.5% gelatine coated glass slides, cleared in a solution of 1:1 chloroform and absolute alcohol, then stained with 1% cresyl violet.

For immunohistochemical staining the sections were first treated for 30 min with an endogenous peroxidase inhibitor (49.2% methanol: 49.2% of 0.1PB: 1.6% of 30% H_2O_2) followed by three 10 min rinses in 0.1M PB. This was followed by a 2 h pre-incubation, at room temperature, in a solution (blocking buffer) containing 3% normal goat serum (NGS, Chemicon), 2% bovine serum albumin (BSA, Sigma), and 0.25% Triton X-100 (Merck) in 0.1M PB. The sections were then incubated in a primary antibody solution containing the appropriately diluted antibody in blocking buffer for 48 h at 4°C under gentle agitation. To

reveal orexinergic neurons, we used the anti-orexin-A antibody AB 3704 (Chemicon, raised in rabbit) at a dilution of 1:1500. This step was followed by three 10 min rinses in 0.1M PB, after which the sections were incubated in a secondary antibody solution for 2 h (room temperature, 22-24°C). The secondary antibody solution contained a 1:1000 dilution of biotinylated anti-rabbit IgG (BA-1000, Vector Labs) in 3% NGS and 2% BSA in 0.1M PB. After three 10 min rinses in 0.1M PB, the sections were incubated for 1 h in AB solution (Vector Labs) and again rinsed three times. The sections were then treated in a solution of 0.05% diaminobenzidine in 0.1M PB for 5 min, following which 3µl of 30% H_2O_2 was added to the 1 ml of solution in which each section was immersed. Staining development was monitored visually and checked under a low power stereomicroscope. Development was allowed to continue until the immunopositive neurons became readily identifiable from the background stain. Development was arrested by placing the sections in 0.1M PB, and then rinsed twice more in the same solution. Sections were mounted on glass slides coated with 0.5% gelatine and left to dry overnight. They were then dehydrated in a graded series of alcohols, cleared in xylene, and coverslipped with Depex. Two controls were employed in the immunohistochemistry, including the omission of the primary antibody and the omission of the secondary antibody in selected sections, which eliminated staining.

5.2.3 Quantitative analysis

The number of orexinergic (Orx+) positive cells was determined with stereological techniques on a one in two series of sections through the complete hypothalamus in all 18 brains. All analyses were done blind to the rhythmicity status of the individual. A Nikon E600 microscope with three axis motorized stage, video camera, Neurolucida interface and Stereo-Investigator software (MicroBrightfield Corp., Colchester, Vermont) was used for the stereological counts. In an attempt to achieve the most accurate estimation of Orx+ neurons, a

pilot study was first conducted in an individual of each species. The pilot study determined the best counting frame size and grid size and these parameters were then used for all individuals of each species investigated. A 275 x 185 μm counting frame and a 300 x 400 μm sampling grid were employed in each individual. Only orexinergic neurons with clearly visible nuclei were marked in the sampling grids. The 'optical fractionator probe' function of the software computationally determined the total number of Orx+ cell in the hypothalamus of each individual using the following formula:

$$\mathbf{N = Q / (SSF \times ASF \times TSF)}$$

Where: N – was the total estimated neuronal number, Q – was the number of neurons counted, SSF – was the section sampling fraction (in the current study this was 0.5), ASF – is the area sub fraction (this was the ratio of the size of the counting frame to the size of the sampling grid), and TSF – was the thickness sub fraction (this was the ratio of the dissector height relative to 50 μm).

A function in the stereology programme called the "nucleator probe" facilitated the estimation of the mean cross-sectional area, volume and length of the orexinergic positive cells. Only neurons with a distinct nucleus were chosen for analysis. The "nucleator probe" was employed in conjunction with the optical fractionator and stereology procedures for systematic random sampling to identify cells (Gunderson, 1988).

5.2.4 Statistical analysis

In addition the quantitative values generated using stereological techniques; data for body mass (M_b), brain mass (M_{br}) and encephalisation quotient (EQ) were compiled for analysis. EQ in each individual was determined using the formula (from Manger, 2006):

$$\mathbf{EQ = M_{br} / (0.069\ M_b^{0.718})}$$

Comparisons were conducted between species (CHP vs FA, CHP vs FD and FA vs FD) and within species (CHP rhythmic vs CHP arrhythmic, FA rhythmic vs FA arrhythmic, and FD rhythmic vs FD arrhythmic). These comparisons were made for M_b, M_{br}, EQ, number of Orx+ cell bodies (counts), estimated volume of an Orx+ cell body, estimated cross-sectional area of an Orx+ cell body and estimated length of an Orx+ cell body. The values obtained for the counts, volume, area and length of Orx+ cell bodies in each mole rat were divided by the *Mb* of each individual and the M_{br} of each individual thereby creating an index that corrected for M_b and M_{br}. These indices were statistically analysed between species and within species for the counts, volume, area and length. The indices also facilitated comparisons between all rhythmic individuals and all arrhythmic individuals. The Kruskal-Wallis test(PAST, PAleontological Statistics, version 2.02; Hammer et al., 2001) was used for the aforementioned comparisons and statistically significant differences were noted when $p<0.05$.When using the PAST Kruskal-Wallis test, an automated Mann-Whitney U p-value, adjusted using Bonferroni correction factor, is generated and henceforth statistically significant differences were noted when $p<0.05$. In the text that follows, statistically significant differences have only been noted for the Mann-Whitney U test using the Bonferroni correction factor. To determine the root of the statistically significant differences, univariate analyses (PAST) were performed and the groups with the higher means were noted. Furthermore weighted means were calculated for body mass, brain mass, *EQ*, estimated cell counts, estimated cell volume, estimated cell area and estimated cell length. To calculate a weighted mean, the total of a parameter was divided by the number of individuals constituting that parameter e.g. to calculate the weighted mean for the estimated cell counts

of the rhythmic chronotype of *Cryptomys hottentotus pretoriae*, the individual rhythmic cell counts of this species (i.e. 4875, 12344 and 9922) were totalled to give 27141. This total was then divided by the total number of individuals (i.e. three) to give a weighted mean of 9047. This formula was applied in all instances were weighted means were calculated.

5.3 Results

In all three species of mole rat, orexinergic immunopositive (Orx+) cell bodies were located within the hypothalamus, as previously reported in all mammals studied to date, including mole rats (Bhagwandin et al., 2011). Stereological counts of Orx+ cell bodies were found to be statistically significantly different only between the distinct circadian chronotypes of Ansel's mole rat (*Fukomys anselli*) and between all rhythmic and arrhythmic individuals of the current study when the counts of Orx+ cell bodies were corrected for body mass (M_b). Estimation of cell volume, cross-sectional area and length showed statistically significant differences between species without correction for M_b and brain mass (M_{br}) and statistically significant differences between species when these variables were corrected for M_b and M_{br} though no statistically significant differences were reached for these parameters within species when similar comparisons were made.

5.3.1 Orexinergic cell body distribution

All three species of mole rat expressed Orx+ neurons only within the hypothalamus and were observed as sharing common neuronal locality within the lateral hypothalamic area (LHA), perifornical region (PFR) and the lateral ventral hypothalamic supraoptic area (LVHA), similar to those reported in two other species of mole rat (Bhagwandin et al., 2011). Thus, there appears to be three distinct clusters of Orx+ neurons in the hypothalamus of the mole rats studied, a large homogeneous cluster spanning the lateral and perifornical regions

(the main cluster), a distinct cluster extending into the region of the zona incerta (the zona incerta cluster), and a final cluster in the ventral lateral hypothalamus adjacent to the diminutive optic tracts (the optic tract cluster). The mole rats, from both chronotypes and all three species, exhibited neuronal cell bodies that were morphologically homogenous in all three clusters, that were ovoid in shape, a varying mixture of bi- and multi- polar types and that showed no specific dendritic orientation (Figs. 5.2, 5.3).

5.3.2 Comparisons of body mass (M_b), brain mass (M_{br}) and encephalisation quotient (EQ)

Mean M_b in *C. hottentotus pretoriae* was 132.8 g for the rhythmic group and 123 g for the arrhythmic group. *F. anselli* had a mean M_b of 90.6 g for the rhythmic group and 78.5 g for the arrhythmic group (Table 5.1). *F. damarensis* had a mean M_b measurement of 121.5 g for the rhythmic group and 93.7 g for the arrhythmic group. M_b comparisons between species were only statistically significant (p-value: 0.008) between *C. hottentotus pretoriae* and *F. anselli* where it was observed that *C. hottentotus pretoriae* had a higher mean M_b. When M_b was compared between all rhythmic and all arrhythmic individuals, no statistically significant differences were observed though univariate analysis of this data did reveal a higher mean in the rhythmic chronotypes compared to the arrhythmic chronotype.

Mean M_{br} in *C. hottentotus pretoriae* measured 1.4 g for the rhythmic group and 1.5 g for the arrhythmic group. *F. anselli* had a mean M_{br} measurement of 1.2 g for the rhythmic group and 1.2 g for the arrhythmic group. *F. damarensis* had a mean M_{br} measurement of 1.8 g for the rhythmic group and 1.8 g for the arrhythmic group (Table 5.1). Statistically significant differences were noted between the *C. hottentotus pretoriae* and *F. anselli* (where the *C. hottentotus pretoriae* had a higher mean M_{br}, p-value: 0.004) and *F. anselli* and *F. damarensis* (where *F. damarensis* had a higher mean M_{br}, p-value: 0.004).

Mean *EQ* in *C. hottentotus pretoriae* was calculated as 0.67 for the rhythmic group and 0.70 for the arrhythmic group. *F. anselli* had a mean *EQ* calculation of 0.67 for the rhythmic group and 0.77 for the arrhythmic group. *F. damarensis* had a mean *EQ* calculation of 0.83 for the rhythmic group and 1 for the arrhythmic group (Table 5.1). Statistically significant differences were obtained when *F. damarensis* was compared to *C. hottentotus pretoriae* (where *F. damarensis* had a higher mean *EQ*, p-value: 0.02) and when *F. damarensis* was compared to *F. anselli* (where the *F. damarensis* showed a higher mean *EQ*, p-value: 0.02) (Table 5.2).

5.3.3 Stereological counts of Orx+ cell bodies

Stereological counts of Orx+ cell bodies in the *C. hottentotus pretoriae* revealed a mean of 9047 for the rhythmic group and 11547 for the arrhythmic group. Counts from *F. anselli* revealed a mean of 5785 for the rhythmic group and 9299 for the arrhythymic group. *F. damarensis* revealed a mean of 9850 for the rhythmic group and 9274 for the arrhythmic group (Fig. 5.4) (Table 5.1).

Comparisons of Orx+ cell body counts between rhythmic and arrhythmic groups in each species revealed a statistically significant difference only between the circadian chronotypes of *F. anselli* (where the mean number of Orx+ neurons in the hypothalamus of the arrhythmic group was higher than the rhythmic group, p-value: 0.009). Even though statistical significance was not reached in the other two species investigated, the mean number of Orx+ neurons in the hypothalamus of *C. hottentotus pretoriae* was higher for the arrhythmic group than the rhythmic group. For *F. damarensis* stereological counts of Orx+ cell bodies yielded similar totals for both the rhythmic and arrhythmic groups. When the counts of Orx+ cell bodies were corrected for M_b and M_{br}, statistically significant differences were noted only between the circadian chronotypes of *F. anselli*. In both cases the arrhythmic

groups had a higher mean numbers of Orx+ neurons in the hypothalamus than the rhythmic groups (p-value: 0.003). Additionally, when all rhythmic individuals of all species studied here were compared to all arrhythmic individuals, a statistically significant difference was only reached in counts that had been corrected for M_b (where the arrhythmic group had a higher mean number of Orx+ neurons in the hypothalamus than the rhythmic group, p-value: 0.03) (Table 5.2).

5.3.4 Stereological estimation of volume, area and length of Orx+ cell bodies

Stereological estimation of the volume of an Orx+ cell body in *C. hottentotus pretoriae* presented a weighted mean of 2068 μm^3 for the rhythmic group and 2281.2 μm^3 for the arrhythmic group. *F. anselli* presented a weighted mean of 3228.6 μm^3 for the rhythmic group and 3337.3 μm^3 for the arrhythmic group. *F. damarensis* presented a weighted mean of 2429.5 μm^3 for the rhythmic group and 2163.2 μm^3 for the arrhythmic group (Fig. 5.4) (Table 5.1). Statistically significant differences were noted: (1) between species (where *F. anselli* showed a higher mean volume of an Orx+ cell body than the other two species, p-value: 0.0005); (2) when volume was corrected for M_b between species (where *F. anselli* had a higher mean volume of an Orx+ cell body than *C. hottentotus pretoriae*, p-value: 0.0008), and where *F. anselli* had a higher mean volume of an Orx+ cell body *F. damarensis*, p-value: 0.008); and (3) when volume was corrected for M_{br} between species (where *F. anselli* had a higher mean volume of an Orx+ cell body than the other two species, p-value: 0.005, and where *C. hottentotus pretoriae* had a higher mean volume of an Orx+ cell body than *F. damarensis*, p-value: 0.03) (Table 5.2).

Stereological estimation of the cross-sectional area of an Orx+ cell body in the *C. hottentotus pretoriae* revealed a weighted mean of 180.9 μm^2 for the rhythmic group and 193.3 μm^2 for the arrhythmic group. *F. anselli* revealed a weighted mean of 247.7 μm^2 for

the rhythmic group and 250.7 μm^2 for the arrhythmic group. *F. damarensis* revealed a weighted mean of 202.4 μm^2 for the rhythmic group and 189.3 μm^2 for the arrhythmic group (Fig.5.4) (Table 5.1). Statistically significant differences were noted: (1) between species (where *F. anselli* showed a higher cross-sectional area of an Orx+ cell body than the other two species, p-value: 0.005); (2) when cross-sectional area was corrected for M_b between species (where *F. anselli* had a higher cross-sectional area of an Orx+ cell body than *C. hottentotus pretoriae*, p-value: 0.005, and where *F. anselli* had a higher cross-sectional area of an Orx+ cell body than *F. damarensis*, p-value: 0.01); and (3) when area was corrected for M_{br} between species (where *F. anselli* had a higher cross-sectional area of an Orx+ cell body than the other two species, p-value: 0.005, and where *C. hottentotus pretoriae* had a higher cross-sectional area of an Orx+ cell body than *F. damarensis*, p-value: 0.03) (Table 5.2).

Stereological estimation of the length of an Orx+ cell body in *C. hottentotus pretoriae* revealed a weighted mean of 7.3 μm for the rhythmic group and 7.5 μm for the arrhythmic group. *F. anselli* revealed a weighted mean of 8.6 μm for both rhythmic and arrhythmic groups. *F. damarensis* revealed a weighted mean of 7.8 μm for the rhythmic group and 7.5 μm for the arrhythmic group (Fig. 5.4) (Table 5.1). Statistically significant differences were noted: (1) between species (where *F. anselli* showed a longer length of an Orx+ cell body than the other two species p-value: 0.005); (2) when length was corrected for M_b between species (where *F. anselli* had a longer length of an Orx+ cell body than *C. hottentotus pretoriae*, p-value: 0.005); and (3) when volume was corrected for M_{br} between species (where *F. anselli* had longer length of an Orx+ cell body than the other two species, p-value: 0.005, and where *C. hottentotus pretoriae* had a longer length of an Orx+ cell body *F. damarensis,* p-value: 0.03) (Table 5.2).

Figure 5.1: Actigrams illustrating circadian patterns of locomotor activity in rhythmic and arrhythmic individuals from *C. hottentotus pretoriae*, *F. anselli* and *F. damarensis*. These actigrams indicate that the rhythmic mole rats have a predictable period of activity during the light period whereas locomotor activity in the arrhythmic animals is irregular.

tomys hottentotus *Fukomys anselli* *Fukomys damare*

c

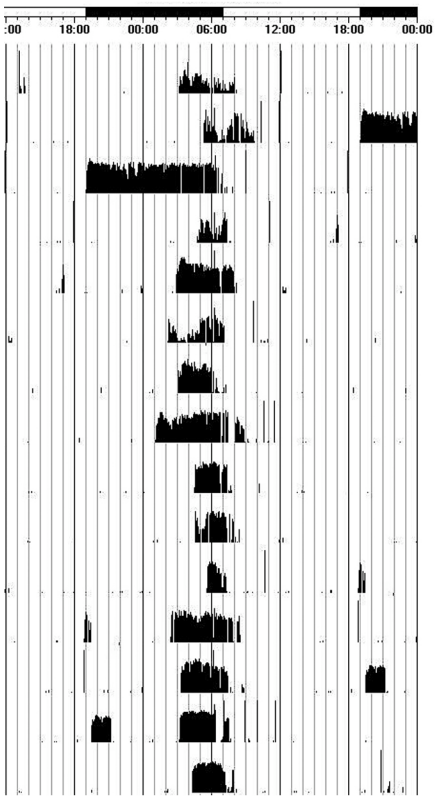

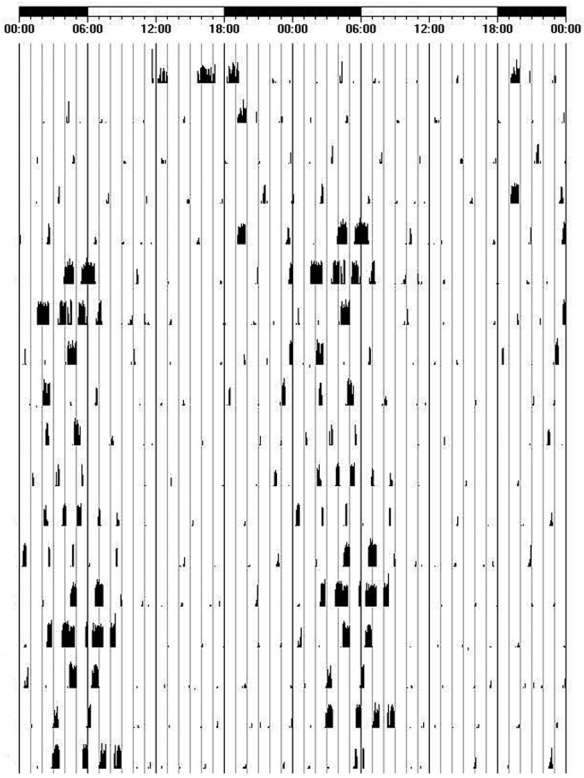

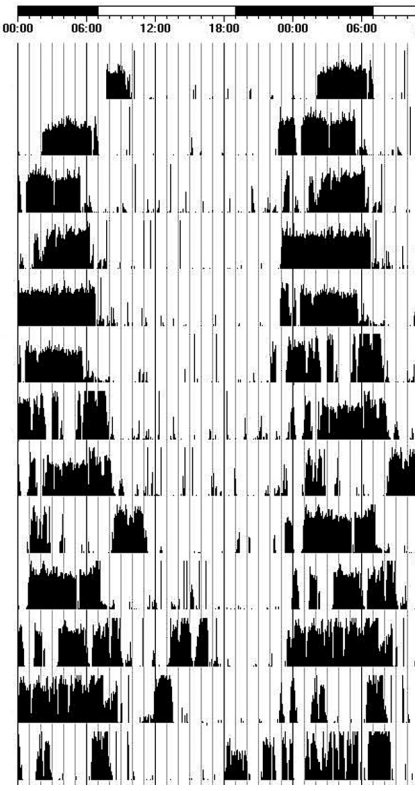

nic

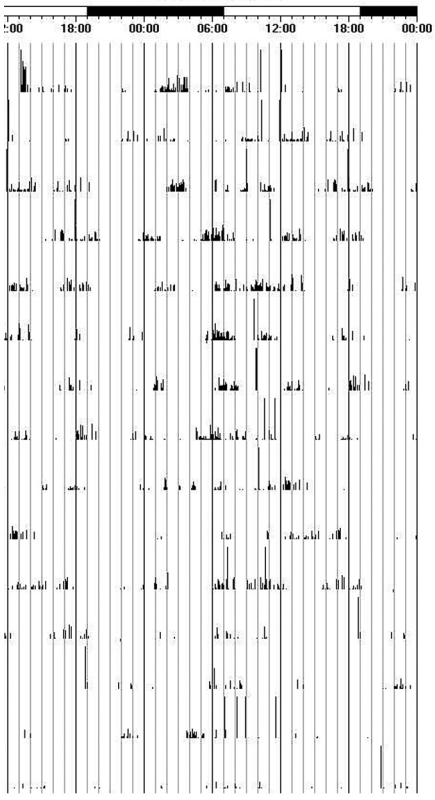

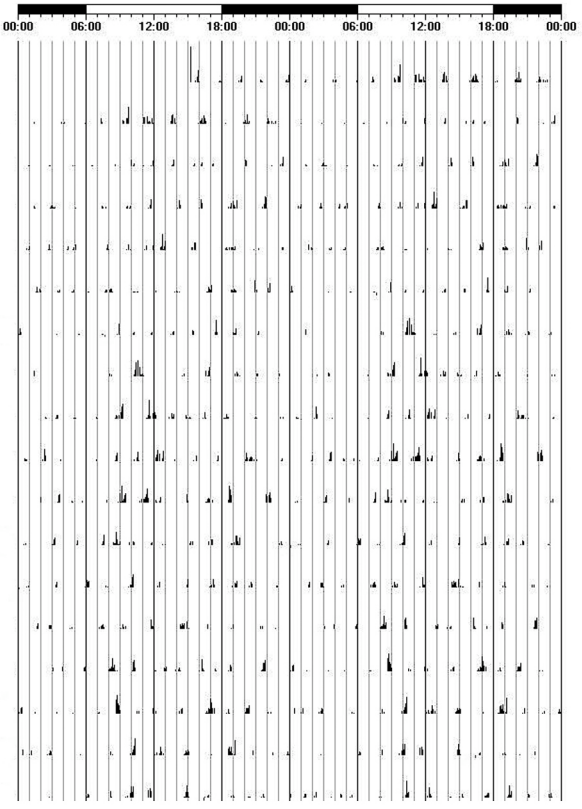

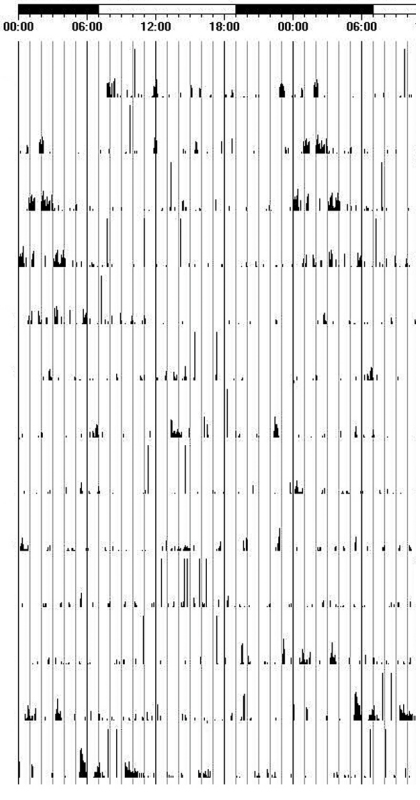

Figure 5.2: Photomicrographs showing the orexin-A immunoreactive neurons within the hypothalamus of rhythmic and arrhythmic chronotypes of *C. hottentotus pretoriae* (A, B), *F. anselli* (C, D) and *F. damarensis* (E, F). Scale = 1 mm and applies to all.

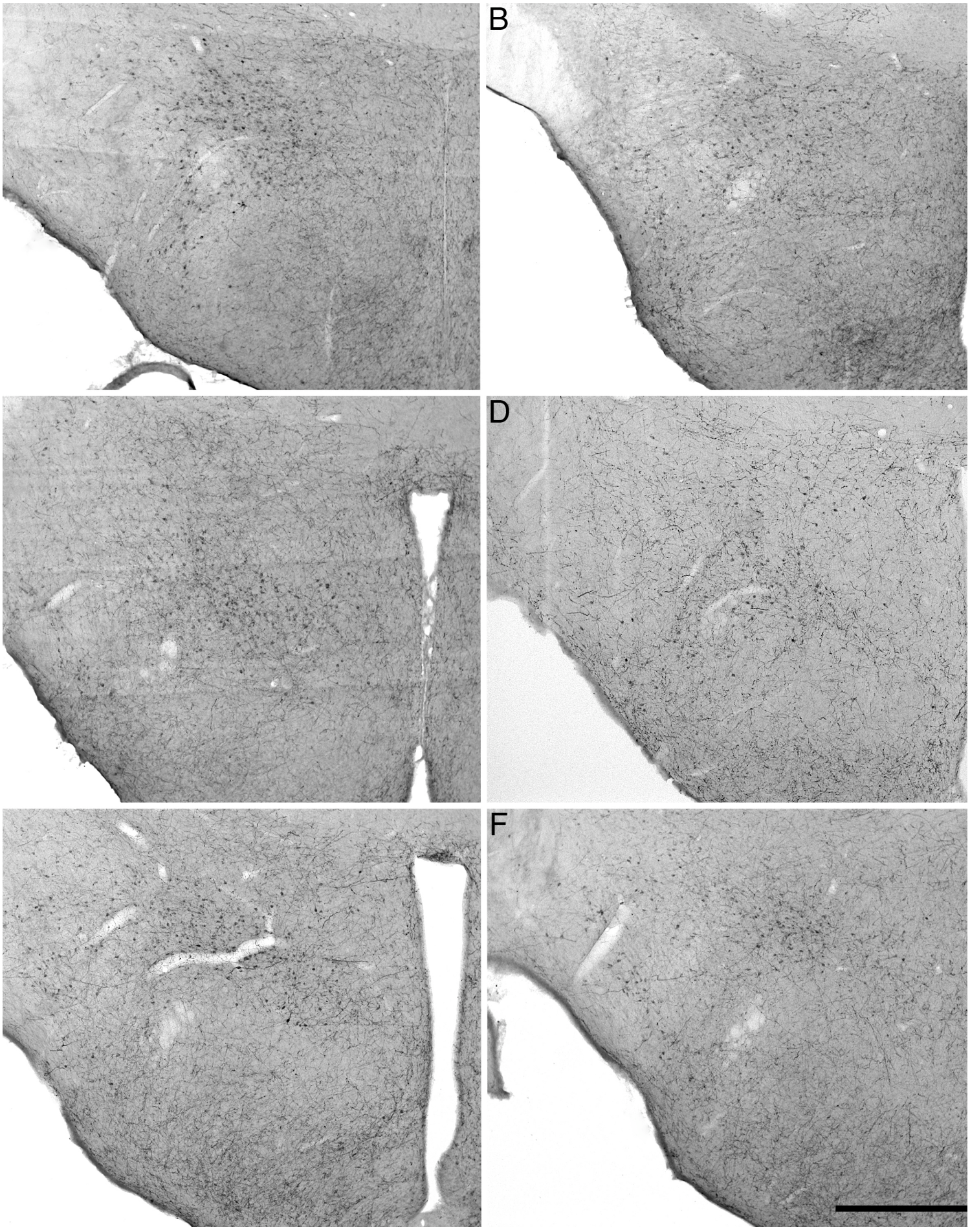
B
D
F

Figure 5.3: High power photomicrographs showing the morphology of orexin-A immunoreactive neurons within the hypothalamus of rhythmic and arrhythmic chronotypes of *C. hottentotus pretoriae* (A, B), *F. anselli* (C, D) and *F. damarensis* (E, F). Scale = 100 μm and applies to all.

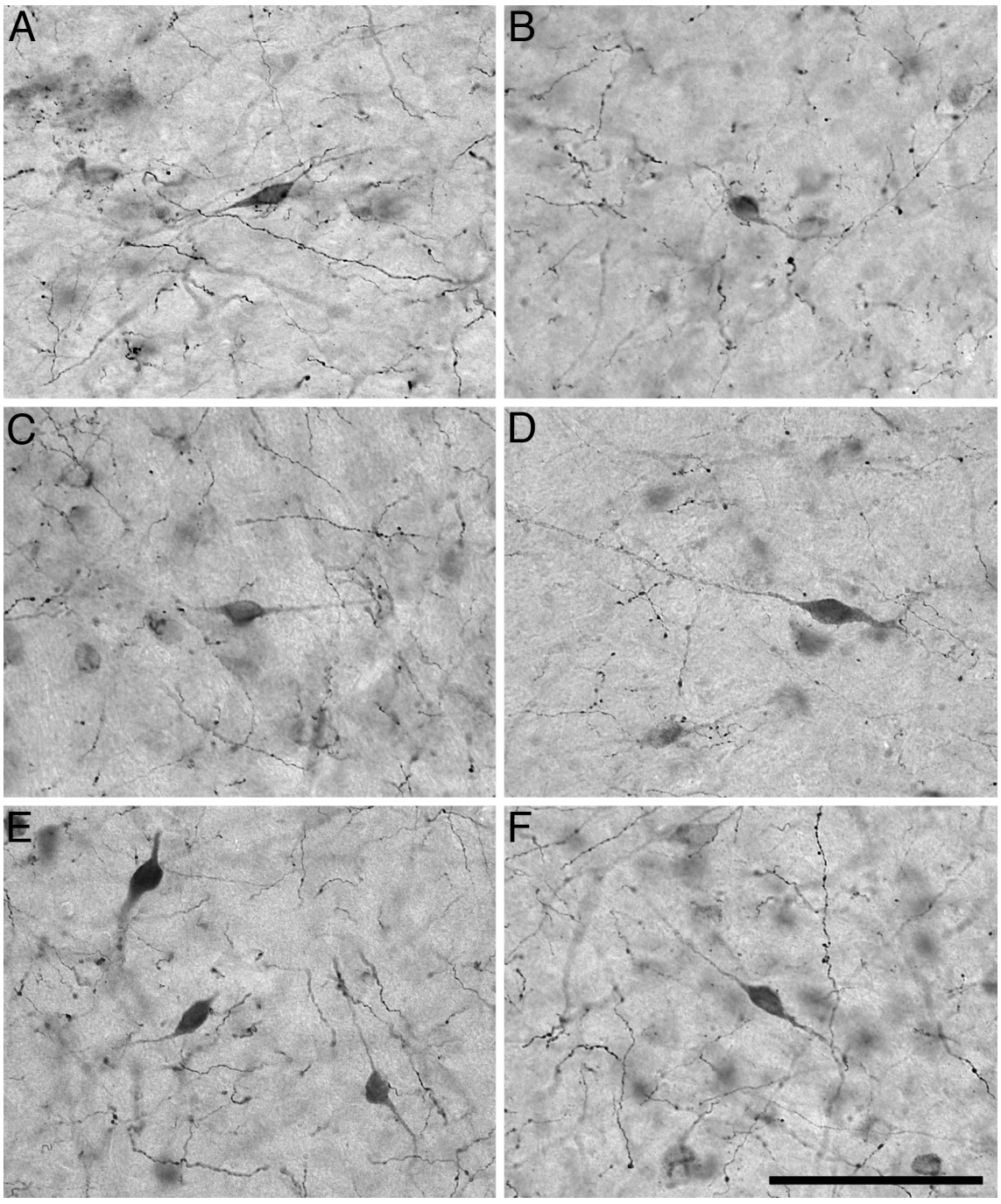
A
B
C
D
E
F

Figure 5.4: Graphs showing the various parameters of stereological data for arrhythmic and arrhythmic individuals (grey bars) of *C. hottentotus pretoriae*, *F. anselli* and *F. damarensis* and the respective weighted means (black bars). The graphs indicate average estimated values for somal number, volume, area and length.

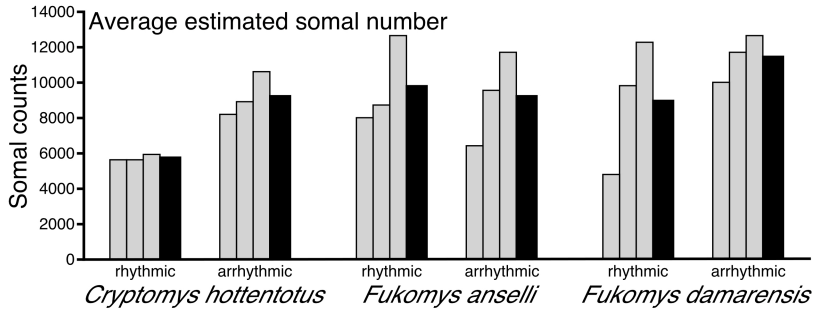
Average estimated somal number
Somal counts
14000
12000
10000
8000
6000
4000
2000
0
rhythmic
arrhythmic
rhythmic
arrhythmic
rhythmic
arrhythmic
Cryptomys hottentotus
Fukomys anselli
Fukomys damarensis

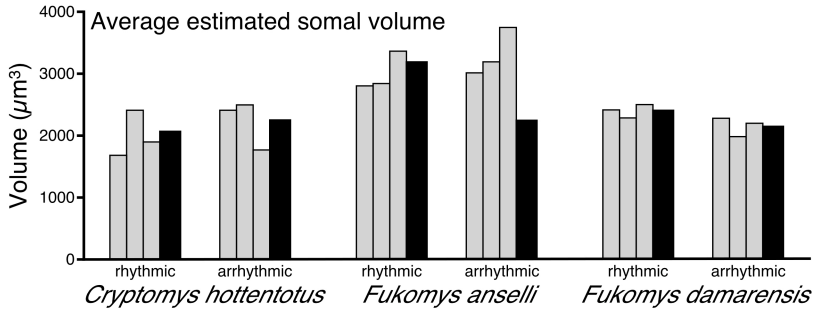
Average estimated somal volume
Volume (μm3)
4000
3000
2000
1000
0
rhythmic
arrhythmic
rhythmic
arrhythmic
rhythmic
arrhythmic
Cryptomys hottentotus
Fukomys anselli
Fukomys damarensis

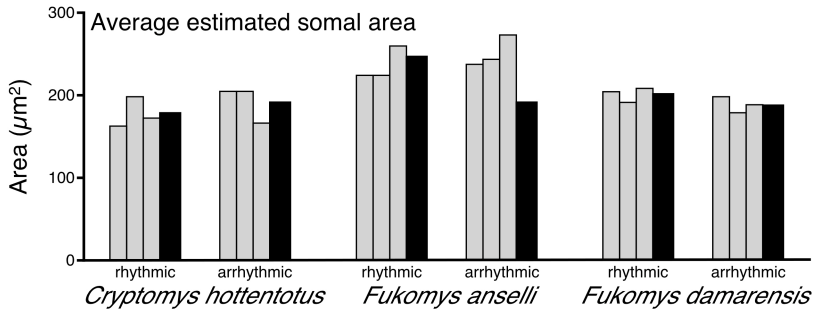
Average estimated somal area
Area (μm2)
300
200
100
0
rhythmic
arrhythmic
rhythmic
arrhythmic
rhythmic
arrhythmic
Cryptomys hottentotus
Fukomys anselli
Fukomys damarensis

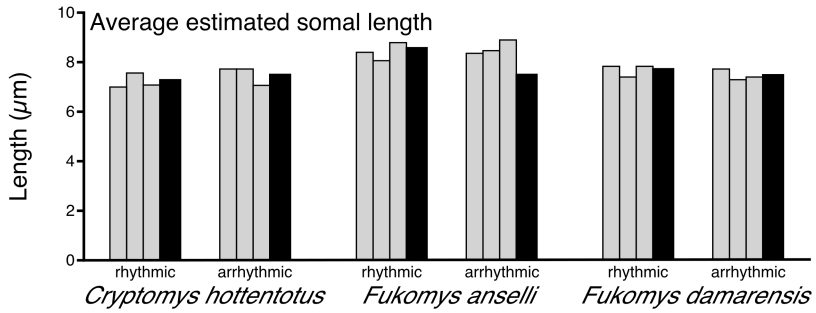
Average estimated somal length
Length (μm)
10
8
6
4
2
0
rhythmic
arrhythmic
rhythmic
arrhythmic
rhythmic
arrhythmic
Cryptomys hottentotus
Fukomys anselli
Fukomys damarensis

Table 5.1: Table presenting data for rhythmic and arrhythmic individuals of *C. hottentotus pretoriae*, *F. anselli* and *F. damarensis* and the respective weighted means for: M_b, M_{br}, EQ, estimated cell counts, average estimated volume, average estimated cell area, and average estimated cell length.

Animal ID	Sex	Circadian Chronotype	Body mass (g)	Brain mass (g)	EQ	Estimated Cell Counts	Average Estimated Cell Volume (μm^3)	Average Estimated Cell Area (μm^2)	Average Estimated Cell Length (μm)
Cryptomys hottentotus pretoriae									
CHP2	F	R	174.5	1.6	0.6	4875	1701.4	163.2	6.9
CHP8	F	R	126.1	1.3	0.6	12344	2438.3	198.9	7.6
CHP12	M	R	97.9	1.4	0.8	9922	1936.5	174.4	7.2
Mean/ Weighted mean R			**132.8**	**1.4**	**0.6**	**9047**	**2068.0**	**180.9**	**7.3**
CHP1	M	AR	110.4	1.4	0.7	11794	2441.3	203.9	7.8
CHP3	M	AR	157.8	1.4	0.5	12753	2520.2	204.1	7.7
CHP7	M	AR	100.7	1.7	0.9	10095	1797.2	167.8	7.1
Mean/ Weighted mean AR			**123.0**	**1.5**	**0.7**	**11547**	**2281.2**	**193.3**	**7.5**
Fukomys anselli									
FA2	M	R	95.9	1.2	0.7	5693	2837.0	225.3	7.9
FA3	M	R	86.3	1.1	0.6	5944	2875.9	223.6	8.1
FA7	M	R	89.6	1.2	0.7	5719	3407.7	259.6	8.8
Mean/ Weighted mean R			**90.6**	**1.2**	**0.7**	**5786**	**3228.6**	**247.7**	**8.6**
FA4	M	AR	69.3	1.2	0.8	8242	3036.8	238.6	8.4
FA5	M	AR	100.1	1.1	0.6	10686	3233.0	243.7	8.5
FA6	M	AR	66.0	1.2	0.9	8969	3792.3	271.9	9.0
Mean/ Weighted mean AR			**78.5**	**1.2**	**0.8**	**9299**	**3337.3**	**250.7**	**8.6**
Fukomys damarensis									
FD4	M	R	76.9	1.6	1.0	8803	2428.4	204.8	7.8
FD6	M	R	149.2	1.8	0.7	8024	2318.9	191.1	7.5
FD7	M	R	139.7	2.0	0.8	12723	2524.6	209.7	7.9
Mean/ Weighted mean R			**121.9**	**1.8**	**0.9**	**9850**	**2429.5**	**202.4**	**7.8**
FD1	M	AR	102.2	1.9	1.0	11704	2289.6	198.3	7.7
FD8	F	AR	104.4	1.9	1.0	9638	1988.0	180.3	7.4
FD13	M	AR	74.5	1.7	1.0	6482	2211.6	188.8	7.4
Mean/ Weighted mean AR			**93.7**	**1.8**	**1.0**	**9275**	**2163.2**	**189.3**	**7.5**

Table 5.2: Table showing results of statistical comparisons between various data sets. (*) denotes statistical significance (using post hoc Mann-Whitney U test with Bonferroni correction factor where $p<0.05$) and letters in subscript indicate the species or chronotype of mole rat where the higher mean was observed. CHP = *C. hottentotus pretoriae*, FA = *F. anselli*, FD = *F. damarensis*, and AR = arrhythmic.

	Between species						
	Body Mass	Brain Mass	EQ	Counts	Volume	Area	Length
CHP vs.. FA	$*_{CHP}$	$*_{CHP}$	-	-	$*_{FA}$	$*_{FA}$	$*_{FA}$
CHP vs.. FD	-	-	$*_{FD}$	-	-	-	-
FA vs.. FD	-	$*_{FD}$	$*_{FD}$	-	$*_{FA}$	$*_{FA}$	-
	Within Species						
CHP R vs.. NR	-	-	-	-	-	-	-
FA R vs.. NR	-	-	-	$*_{AR}$	-	-	-
FD R vs.. NR	-	-	-	-	-	-	-

Between Species Corrected for Body Mass				
	Counts	Volume	Area	Length
CHP vs.. FA	-	$*_{FA}$	$*_{FA}$	$*_{FA}$
CHP vs.. FD	-	-	-	-
FA vs.. FD	-	$*_{FA}$	$*_{FA}$	-
Within species Corrected for Body Mass				
CHP R vs. NR	-	-	-	-
FA R vs. NR	$*_{AR}$	-	-	-
FD R vs. NR	-	-	-	-

Between species corrected for Brain Mass				
	Counts	Volume	Area	Length
CHP vs. FA	-	$*_{FA}$	$*_{FA}$	$*_{FA}$
CHP vs. FD	-	$*_{CHP}$	$*_{CHP}$	$*_{CHP}$
FA vs. FD	-	$*_{FA}$	$*_{FA}$	$*_{FA}$
Within species corrected for Brain Mass				
CHP R vs. NR	-	-	-	-
FA R vs. NR	$*_{AR}$	-	-	-
FD R vs. NR	-	-	-	-

All R vs. NR Corrected for Body Mass					
	EQ	Counts	Volume	Area	Length
All R vs. NR	-	$*_{AR}$	-	-	-

All R vs. NR corrected for Brain Mass					
	EQ	Counts	Volume	Area	Length
All R vs. NR	-	-	-	-	-

5.4 Discussion

It is well known that orexins are involved in the maintenance of the waking state, and it has been demonstrated that increased orexinergic activity is associated with motor activities (Estabrooke et al., 2001; Mileykovskiy et al., 2005; Lee et al., 2005; Saper et al., 2005). It has been shown that the decreased number of hypothalamic orexin neurons in narcoleptic individuals produced excessive sleepiness (Siegel, 1999; Siegel, 2004; Baumann and Bassetti, 2005; Thannickal et al., 2009). In the previous chapter it was observed that the arrhythmic chronotype spent more time awake and less time in slow wave sleep (SWS) compared to the rhythmic chronotype. Therefore the initial aim of the current study was to determine whether rhythmic and arrhythmic chronotypes had different numbers of hypothalamic orexin immunopositive neurons with the hypothesis of elevated hypothalamic orexinergic neurons in the arrhythmic chronotypes as a result of the involvement of orexins in the sleep-wake cycle. The results of the current study indicated statistically significant differences between the circadian chronotypes of *F. anselli*, where the arrhythmic group had higher mean numbers of hypothalamic orexin neurons compared to the rhythmic group. These differences were observed when the raw data was compared and when the raw data was corrected for M_b and M_{br}. *C. hottentotus pretoriae* showed tendencies toward the hypothesis though the data was not significantly different. *F. damarensis* showed data that was opposite to the hypothesis though this data was not significantly different. A statistically significant difference was noted between all rhythmic and arrhythmic individuals of the current study when the counts of orexin neurons were corrected for M_b.

5.4.1 Orexins, sleep-wake cycle and circadian rhythmicity

The results of the present study indicated statistically significant differences between circadian chronotypes of *F. anselli* for the counts of hypothalamic Orx+ neurons when the raw data was compared. In this case the arrhythmic chronotype consistently displayed higher mean counts of hypothalamic Orx+ neurons than the rhythmic chronotype. A similar tendency, though not statistically significantly, was observed when the raw data was compared between the chronotypes of *C. hottentotus pretoriae*; however, a similar comparison between chronotypes of *F. damarensis* showed that the mean count of Orx+ neurons in the rhythmic group was higher than the rhythmic group, but statistical significance was not reached. The raw data analysis of two mole rat species supports the hypothesis of elevated Orx+ neurons in the hypothalamus. Given the previous suggestions for the role of orexins in the sleep-wake cycle (Siegel, 2004; Baumann and Bassetti, 2005), the results of the current study indicate that the arrhythmic chronotypes of *F. anselli* and *C. hottentotus pretoriae* would theoretically have an enhanced maintenance of waking and a reduced amount of time spent in SWS relative to the rhythmic chronotypes. The study of sleep in rhythmic and arrhythmic chronotypes of a species of African mole rat (see previous chapter) has shown that the arrhythmic group was statistically more awake and spent less time in SWS compared to the rhythmic group. This supports the proposed hypothesis of the current study.

It is known that the bifurcated ascending arousal system incorporates firstly, a pathway to the thalamus which excites thalamic relay neurons that transmit information to the cerebral cortex and secondly, a branch that bypasses the thalamus to activate neurons in the lateral hypothalamic area, basal forebrain and cerebral cortex (Saper,

1985; Hallanger et al., 1987; Saper et al., 2001, 2005; Jones, 2003). Orexinergic neurons, neuroanatomically restricted to the hypothalamus, have ascending projections to the cerebral cortex and descending projections to the cholinergic (basal forebrain, lateral dorsal tegmental nucleus, pedunculopontine nucleus) and monaminergic (locus coeruleus, ventral tegmentum area, raphe) nuclear groups of the arousal systems (Peyron et al., 1998; Chemelli et al., 1999; Baumann and Bassetti, 2005; Bhagwandin et al., 2011). The exact role of orexins in REM is unclear as some studies suggest increased orexinergic activity during REM (Kilduff and Peyron, 2000) while others report the contrary (Hungs and Mignot, 2001); however, a recent study has postulated that orexin neurons mediate the circadian timing of REM by suppressing REM during the active period (Kantor et al., 2009). In light of the results of the current study it would appear that the increased numbers of hypothalamic orexinergic neurons observed within arrhythmic chronotypes, through possible increased activity and the resulting effect on wakefulness and motor activities, may facilitate a higher level of vigilance allowing for extended foraging and feeding activity.

Baumann and Bassetti (2005) proposed that orexins are under control of the suprachiasmatic nucleus (SCN) and that orexins do not significantly affect circadian rhythmicity. Saper (2005) described a 3 stage circuitry integrator for circadian rhythms that involve a pathway from the SCN to the subparaventricular zone (SPZ) and finally to dorsomedial nucleus of the hypothalamus (DMH). The DMH communicates directly with the lateral hypothalamic area, the region with the highest population of orexinergic neurons, and the ventrolateral preoptic nucleus (VLPO), the area primarily concerned with the promotion of SWS. The rationale behind the 3 stage pathway lies in the

observation that in both diurnal and nocturnal animals, the SCN is primarily active during the light period and the VLPO during the dark period (Sherin et al., 1996; Gaus et al., 2002). Therefore, in animals that are nocturnal *vs* diurnal, there should be an intervening circuitry that allows the circadian cycle to be set at opposite phases (Saper, 2005). It is well known that mole rats have unusual patterns of circadian rhythmicity (Oosthuizen et al., 2003; Lovegrove and Muir, 1996; Lovegrove and Papenfus, 1995) and that mole rats have different neuropeptide populations in the SCN compared to other rodents (Negroni, 2003). Therefore, the increased counts of Orx+ neurons in the hypothalamus in the arrhythmic chronotypes of the current study may alter the circadian control of wakefulness in these individuals.

5.4.2 Orexins and appetite regulation

The results of the present study indicated statistically significant differences between circadian chronotypes of *F. anselli* when the raw data for counts of Orx+ neurons were corrected for M_b and M_{br}, where the arrhythmic groups showed higher mean counts than the rhythmic groups. This can be interpreted as the arrhythmic chronotype having a higher number of Orx+ neurons per gram of M_b or M_{br} compared to the rhythmic chronotype. Since the initial demonstration of orexin induced hyperphagia in rats (Sakurai et al., 1998), orexins have become synonymous with mechanisms of appetite regulation and increased food intake that is driven by orexin involvement in motivated behaviour (Rodgers et al., 2002). Cai et al. (2001) have reported activation of the lateral hypothalamic orexin neurons in response to low blood glucose levels and an empty stomach, signals that indicate replenishment, and concluded that this context-

dependency explains the effects associated with orexin activation – increased food intake with delayed onset of satiety and increased wakefulness with vigilance and behavioural activity. It is also known that orexins are involved in appetite regulation through activation of the leptin sensitive neurons of the arcuate nucleus and its subsequent feeding associated signalling to orexinergic neurons of the lateral hypothalamus (LH) and henceforth interaction between LH and the hypothalamic ventro-medial nucleus (VMH) (Stellar, 1954; Rodgers et al., 2002; Sakurai, 2003; Sakurai, 2005). Therefore it would seem fair to infer that the elevated counts of hypothalamic in the arrhythmic chronotype of *F. anselli* have greater drive for motivated behaviour and theoretically a higher food intake compared to the rhythmic chronotype.

Interestingly though, the results of the present study showed a statistically significant difference for the counts of Orx+ neurons that were corrected for M_b when all rhythmic individuals were compared to all arrhythmic individuals from all three species of mole rats examined. This indicated that the arrhythmic individuals have a higher number of Orx+ neurons per gram of M_b. Given the effect of orexins on motivated behaviour and food intake, this may be indicative of a higher body mass in the arrhythmic individuals compared to the arrhythmic individuals. This was not the case as it was observed in the present study that the mean body mass of the arrhythmic chronotype in each species investigated was lower than that of the rhythmic chronotype. A possible explanation for this could lie in the assessment of the impact of chronic administration of orexin-A on food intake on rats (Haynes et al., 1999; Yamanaka et al., 1999). Both these studies indicated an increased food intake during the light period and a compensatory reduction of food intake during the dark period, and both agree that chronic

administration of orexin-A does not alter 24 h food intake or body mass gain. In addition, Lubkin and Stricker-Krongrad (1998) postulated that orexins may increase overall metabolic rate to support increased motor activity; however, Nicolaidis (2006) suggests that overall metabolic rate be divided into resting metabolism and locomotion-related metabolism and based on resting metabolism, a hypometabolic but physically active animal has a higher (total) metabolism than a hypermetabolic animal that remains quiet. This supports the mole rats of the current study as it has been previously reported that subterranean mole rats have lower resting metabolic rates than surface dwelling mammals (Bennett and Faulkes, 2000). It has been reported that increased body temperature correlates with increased motor activity (Siegel, 2004) though this is difficult to explain in the mole rats of the current study, while they are reported to have a lower body temperature than surface dwelling mammals (Bennett and Faulkes, 2000) it is unknown whether body temperature differences exist between different circadian chronotypes. Furthermore, it has been suggested that sleep duration tracks the metabolism of nutrients in a meal and the size of a meal, with the effect that a higher nutritional content and larger meal size produces a longer sleep duration (Danguir and Nicolaidis, 1980). Despite this, brain metabolism is conserved and independent from that of the periphery, the ventromedial nucleus, dorsomedial nucleus and paraventricular nucleus, metabolic strategic areas, are capable of reflecting metabolic changes resulting from bodily depletion and repletion (Nicolaidis, 2006). Therefore, it may be possible that a higher peripheral metabolism may result in a lower body mass despite the elevated Orx+ neurons observed in the arrhythmic chronotype compared to the rhythmic chronotype.

Chapter 6 – The interrelations of the distribution and terminal networks of sleep associated nuclei in the brain of an African species of mole rat

6.1. Introduction

In order to further understand the sleep-wake cycle its neuroanatomical substrates need to be investigated. There are several neuronal groups known to participate in the control of the sleep-wake cycle and these have been grouped in two regions, the first incorporates nuclei in the basal forebrain and hypothalamus and the second comprises neuronal groups forming a cluster within the ponto-medullary junction of the brainstem (Siegel, 2004; Lyamin et al., 2008).

It is known that the cholinergic, catecholaminergic, serotonergic, orexinergic and histaminergic systems are involved with the control of sleep-wake states (Siegel, 2004; McGinty and Szymisiak, 2005; Lyamin et al., 2008). The neurons forming the cholinergic nuclei of the basal forebrain and hypothalamus have been identified as the main telencephalic arousal system, while the cholinergic neurons of the pons are active during wake and REM sleep (Siegel, 2000) and are responsible for the desynchronised EEG during waking and REM sleep by inhibiting discharge of thalamic mechanisms responsible for slow waves (McCormick, 1989; Steriade et al., 1990; Steriade et al., 1993). Noradrenergic neurons of the locus coeruleus complex, located in the dorsolateral pontine region, have been associated with the regulation of muscle tone and motor activity (Siegel et al., 1992; Wu et al., 1999). The serotonergic neurons forming the nuclei of the rostral serotonergic cluster (Bjarkam et al., 1997) send projections to the

telencephalon and may have a role in maintaining arousal and regulating muscle tone, as well as regulating some of the phasic events of REM sleep (Tork, 1990; Wu et al., 1999; Wu et al., 2004; John et al., 2004; Lyamin et al., 2008). Orexinergic neurons of the hypothalamus are located between the sleep-active neurons of the anterior hypothalamus and the wake-active neurons of the posterior hypothalamus (Gerashchenko and Shiromani, 2004). These orexinergic neurons are associated with motor activities and maintenance of waking through strong projections upon other arousal systems (Siegel, 2004; Gerashchenko and Shiromani, 2004). Histaminergic neurons located in the posterior hypothalamus are strongly associated with the modulation of wakefulness and their inactivity appears to be tightly linked to sleepiness (Saper et al., 2001; Siegel, 2004).

While all these neuronal types act through modulation or excitation, many aspects of the regulation of sleep-wake cycles involve inhibitory mechanisms (Siegel, 2004). _-aminobutyric acid (GABA) is the most common inhibitory neurotransmitter in the brain, and it has been reported that GABAergic neurons are maximally active during slow wave sleep (SWS) and minimally active during waking and REM sleep (Syzmusiak, 1995; Syzmusiak et al., 2001; Siegel, 2004). GABAergic neurons in the basal forebrain and anterior hypothalamus inhibit cholinergic neurons of the basal forebrain and histaminergic neurons of the posterior hypothalamus (Lyamin et al., 2008), while GABAergic neurons located in the tegmentum of the midbrain and dorsal pons are known to inhibit serotonergic and noradrenergic neurons (Nitz and Siegel, 1997a,b). The median preoptic nucleus (MnPN) contributes to the descending projections of the preoptic area (POA) and distributes terminals in the region of the perifornical lateral hypothalamic (pLH) orexinergic neurons (Gong et al., 2002), but the MnPN has a high

density of GABAergic neurons with the effect that stimulation of the MnPN produces inhibition of the pLH wake active neurons (McGinty et al., 2004). Therefore, GABAergic neurons are crucial in promoting sleep by inhibiting the cholinergic, catecholaminergic, serotonergic and histaminergic neuronal populations involved in wakefulness and arousal (Siegel, 2004).

In the present study brains of the giant Zambian mole rat (*Cryptomys mechowi*) were immunohistochemically examined for choline acetyltransferase (ChAT), tyrosine hydroxylase (TH), serotonin (5HT), orexin (Orx), histamine and the calcium binding proteins calbindin (CB), calretonin (CR) and parvalbumin (PV). The mole rats of the current study have a reduced visual system, live a subterranean lifestyle and have unusual patterns of circadian rhythmicity (Lovegrove and Papenfus, 1995; Lovegrove and Muir, 1996; Oelschlager et al., 2000; Cernuda-Cernuda et al., 2003; Negroni et al., 2003; Oosthuizen et al., 2003; Gutjahr et al., 2004; Nemec et al., 2004). Brains from circadian distinct rhythmic and arrhythmic individuals were examined (see Chapter 4). The unusual circadian patterns of individuals within this species provides an interesting model to examine whether neuronal organisation and terminal networks related to the sleep-wake cycle differs between circadian chronotypes.

6.2. Materials and Methods

In the current study the brains of six adult male giant Zambian mole rats (*Cryptomys mechowi*) (average body mass: 278 g; average brain mass: 2.2 g) were used. The animals were obtained directly after the termination of sleep recording (see chapter 4). This species of mole rat displays a seasonal breeding pattern. All animals were treated

and used according to the guidelines of the University of the Witwatersrand Animal Ethics Committee, which parallel those of the NIH for the care and use of animals in scientific experimentation.

The mole-rats were placed under deep barbiturate anaesthesia (Euthanaze, 200mg sodium pentobarbital/kg, i.p.), and then perfused intracardially upon cessation of respiration. The perfusion was initially done with a rinse of 0.9% saline solution at 4°C, followed by a solution of 4% paraformaldehyde in 0.1M phosphate buffer (PB, pH: 7.4) (approximately 1 l for each kilogram of body mass of each solution). Brains were then removed from the skull and post-fixed overnight (24 h) in 4% paraformaldehyde in 0.1M PB, and then allowed to equilibrate in 30% sucrose in 0.1 M PB. The brains were then frozen and sectioned into serial coronal sections of 50µm thickness. A one in ten series of stains was made for Nissl, myelin, choline-acetyltransferase (ChAT), tyrosine hydroxylase (TH), and serotonin (5HT), orexin (Orx), calbindin (CB), calretonin (CR), parvalbumin (PV) and histamine (Hst). Sections kept for the Nissl series were mounted on 0.5% gelatine coated glass slides, cleared in a solution of 1:1 chloroform and absolute alcohol, then stained with 1% cresyl violet to reveal cell bodies. Myelin sections were stored in 5% formalin for a period of two weeks and were then mounted on 1% gelatine coated glass slides and subsequently stained with a modified silver solution to reveal myelin sheaths (Gallyas, 1979).

For immunohistochemical staining the sections were first treated for 30 min with an endogenous peroxidase inhibitor (49.2% methanol: 49.2% of 0.1PB: 1.6% of 30% H_2O_2) followed by three 10 min rinses in 0.1M PB. This was followed by a 2 h pre-incubation, at room temperature, in a solution (blocking buffer) containing 3% normal

goat serum (NGS) for tyrosine hydroxylase, serotonin, orexin, calbindin, calretonin, parvalbumin and histamine but 3% normal rabbit serum (NRS) for ChAT sections, 2% bovine serum albumin (BSA, Sigma), and 0.25% Triton X-100 (Merck) in 0.1M PB. The sections were then placed in a primary antibody solution containing the appropriately diluted antibody in blocking buffer (as described above) for 48 h at 4°C under gentle agitation. To reveal cholinergic neurons we used anti-cholineacetyltransferase (AB144P, Chemicon, raised in goat) at a dilution of 1:3000. To reveal catecholaminergic neurons we used anti-tyrosine hydroxylase (TH) (AB151, Chemicon, raised in rabbit) at a dilution of 1:10000. To reveal serotonergic neurons we used anti-serotonin (AB938, Chemicon, raised in rabbit) at a dilution of 1:10000. To reveal orexinergic neurons we used anti-orexin-A (AB 3704, Chemicon, raised in rabbit) at a dilution of 1:3000. To reveal GABAergic calbindin neurons we used anti-calbindin (CB38a, Swant, raised in rabbit) at a dilution of 1:25000.To reveal GABAergic calretinin neurons we used anti-calretinin (7699/3H, Swant, raised in rabbit) at a dilution of 1:25000. To reveal GABAergic parvalbumin neurons we used anti-parvalbumin (PV28, Swant, raised in rabbit) at a dilution of 1:25000. To reveal histaminergic neurons we used anti-histamine (AB5508, Chemicon, raised in rabbit) at a dilution of 1:4000. This step was followed by three 10 min rinses in 0.1M PB, after which the sections were incubated in a secondary antibody for 2 h (room temperature, 22-24°C). The secondary antibody solution contained a 1:1000 dilution of biotinylated anti-rabbit IgG (BA-1000, Vector Labs) in 3% NGS (or anti-goat IgG, BA-5000 in 3% NRS for the ChAT sections), and 2% BSA in 0.1M PB. After three 10 min rinses in 0.1M PB, the sections were incubated for 1 h in AB solution (Vector Labs), and again rinsed. The sections were then treated in a solution of 0.05%

diaminobenzidine (DAB) in 0.1M PB for 5 min, following which 3µl of 30% H_2O_2 was added to each 1 ml of solution in which each section was immersed. Staining development was monitored visually and checked under a low power stereomicroscope until the background staining was at a level at which it could assist reconstruction without obscuring the immunopositive neuronal structures. Development was then arrested by placing the sections in 0.1M PB, and then rinsed twice more in the same solution. Sections were mounted on glass slides coated with 0.5% gelatine and left to dry overnight. They were then dehydrated in a graded series of alcohols, cleared in xylene, and coverslipped with Depex. Two controls were employed in the immunohistochemistry, including the omission of the primary antibody, and omission of the secondary antibody in selected sections from which no staining was evident.

The sections were viewed with a low power stereomicroscope, and the architectonic borders of the sections traced according to the Nissl and myelin stained sections using a camera lucida. The immuno-stained sections were then matched to the drawings and the immuno-positive neurons marked for ChAT, TH, 5HT, Orx and Hst and the terminal networks marked for 5HT, Orx and Hst. The immuno-positive GABA-ergic (parvalbumin, calbindin and calretonin) interneurons and the distribution of their terminal networks, due to their very high number, were only noted when found in close proximity to neuronal groups of the cholinergic, catecholaminergic, serotonergic, orexineric and histaminergic systems. The drawings were then scanned and redrawn using the Canvas 8 drawing program. The nomenclature used for the cholinergic, catecholaminergic, serotonergic and orexinergic systems was taken from Bhagwandin et al. (2008, 2011; see Chapters 2 and 3) as previously described for mole rats. The remaining descriptions of

cellular and terminal network locations were based on neuroanatomical landmarks determined with Nissl and myelin staining.

6.3 Results

In the present study a range of immunohistochemical stains were conducted on serially sectioned brains of rhythmic and arrhythmic chronotypes of the giant Zambian mole rats (*Cryptomys mechowi*). The aim was to outline as much as possible of the known nuclei and projections of the sleep-wake system in each chronotype and then compare between chronotypes. In the current study the cholinergic, catecholaminergic, serotonergic, orexinergic and histaminergic systems as well as the interneurons containing the calcium binding proteins calbindin, calretonin and parvalbumin, associated with the GABAergic interneurons of the basal forebrain, diencephalon and pons were visualised using immunohistochemical techniques. Our analysis of these systems indicated both global and specific similarity in terms of nuclear organisation, neuronal morphology and terminal networks in the vast majority of instances, thus the following description applies to both chronotypes unless otherwise specified. Furthermore, the cohort of nuclei described in the present study for both circadian chronotypes does not differ from observations previously provided for these systems in other mole rats (Da Silva et al., 2006; Bhagwandin et al., 2008, 2011) and other rodent species (Moon et al., 2007; Dwarika et al., 2008., Limacher et al., 2008). The two differences of significance found between the chronotypes in the current study were that the orexinergic terminal networks were more strongly expressed within the intergeniculate leaflet and the arcuate nucleus of the rhythmic chronotype.

6.3.1 Cholinergic nuclei

The cholinergic system of mammals is often divided into striatal, basal forebrain, diencephalic, pontomesencephalic and motor cranial nerve nuclei (Woolf, 1991; Manger et al., 2002a; Maseko et al., 2007). Both circadian chronotypes of mole rat investigated showed no specific differences to this general mammalian organisational plan. In the present study choline acetyltransferase immunopositive (ChAT+) neurons associated with the sleep-wake cycle were identified within the basal forebrain, hypothalamus and pontine region and included: (1) the medial septal nucleus, diagonal band of Broca, islands of Calleja and olfactory tubercle, and nucleus basalis of the basal forebrain (Figs. 6.1A-E, 6.2A, 6.3A, 6.4 and 6.5); (2) the dorsal, lateral and ventral hypothalamic nuclei of the hypothalamus (Figs. 6.1E-J); and (3) the parabigeminal (PBg), pedunculo-pontine tegmental (PPT) and laterodorsal tegemental (LDT) nuclei of the pontine region (Figs. 6.1N-R, 6.8A). The locations and morphology of the cholinergic nuclei and neurons were identical to those previously described in other mole rat species (Bhagwandin et al., 2008). Interestingly ChAT+ neurons, possibly representing GABAergic interneurons, were observed within the periaqueductal grey adjacent to the catecholaminergic A10dc nucleus and dorsal to the cerebral aqueduct; within the superior colliculus; and within the lateral superior olive (LSO). Similar ChAT+ immunoreactive neruons have been reported in other parts of the brain of other rodents and mammals (Bhagwandin et al., 2006; Gravett et al., 2009; Pieters et al., 2010).

6.3.2 Catecholaminergic nuclei

Tyrosine hydroxylase immunoreactive neurons (TH+) form a number of distinct regional clusters and the locations of TH+ nuclear complexes and nuclei of both chronotypes of mole rat investigated in the current study were identical to those seen in other mole rats (Bhagwandin et al., 2008). For simplicity, the nuclei are referred to using the nomenclature of Dahlstrom and Fuxe (1964) and Hokfelt et al. (1984). No catecholaminergic nuclei outside the bounds of the classically defined nuclei (Smeets and Gonzalez, 2000) were identified. In the present study, TH+ nuclear complexes and nuclei associated with the sleep-wake cycle were identified within the hypothalamus and pontine region. The hypothalamic nuclei comprised six clusters of TH+ neurons, forming distinct nuclei, namely: the anterior hypothalamic group, dorsal division (A15d); the anterior hypothalamic group, ventral division (A15v); the rostral periventricular cell group (A14); the zona incerta (A13); the tuberal cell group (A12); and the caudal diencephalic group (A11) (Figs. 6.1D-K, 6.3C, 6.6A). In the pons, TH+ neurons were observed within the locus coeruleus complex and were readily subdivided into three distinct nuclei, these being: the subcoeruleus compact portion (A7sc), subcoeruleus diffuse portion (A7d), locus coeruleus diffuse portion (A6d) (Figs. 6.1Q-S, 6.2E, 6.9A). The locations and morphology of TH+ neurons and nuclei were identical to those described in other mole rats (Bhagwandin et al., 2008).

6.3.3 Serotonergic nuclei

Serotonergic nuclei located within the brainstem can readily be divided into a rostral and a caudal cluster. The serotonergic (5HT+) nuclei identified in both circadian

chronotypes of mole rat in the current study were identical to those previously described in other mole rats and eutherian mammals studied to date (Maseko et al., 2007; Bhagwandin et al., 2008; Dell et al., 2010). In the present study, 5HT+ nuclear complexes and nuclei associated with the sleep-wake cycle were observed within the rostral cluster. These were identified as being: the caudal linear (CLi) nucleus; the supralemniscal (B9) nucleus; the median raphe (MnR) nucleus; and the dorsal raphe (DR) nuclear complex (Figs. 6.1M-S). The DR nuclear complex was comprised of six distinct nuclei: the dorsal raphe interfascicular (DRif) nucleus, dorsal raphe ventral (DRv) nucleus, dorsal raphe dorsal (DRd) nucleus, dorsal raphe lateral (DRl) nucleus, dorsal raphe peripheral (DRp) nucleus and the dorsal raphe caudal (DRc) nucleus (Figs. 6.1M-R, 6.3E, 6.4E, 6.7A). The morphology and locations of 5HT+ neurons and nuclei were identical to those reported in other mole rats (Bhagwandin et al., 2008).

6.3.4 Orexinergic nuclei

In both circadian chronotypes of mole rat examined, immunohisochemically identifiable, morphologically homogenous, orexinergic (Orx+) neurons were limited to the hypothalamus as previously reported in other mole rat species (Bhagwandin et al., 2011). In the present study, Orx+ neurons were observed in three clusters within the hypothalamus. These clusters were identified as being: main cluster (Mc) encompassing the orexinergic neurons of the lateral hypothalamic area (LHA) and the perifornical region (PFR); the zona incerta cluster (ZIc) formed from neurons extending from the main cluster into the hypothalamic region adjacent to the zona incerta; and the optic tract cluster (OTc) encompassing neurons found in the lateral ventral hypothalamic supraoptic

area (LVHA) (Figs. 6.1D-I, 6.2C, 6.4C). No Orx+ neurons could be identified in the anterior hypothalamic paraventricular subnucleus in either circadian chronotype of mole rat as sometimes observed in other rodents (Nixon and Smale, 2007). The morphology and locations of Orx+ neurons and nuclei were identical to those reported in other mole rat species (Bhagwandin et al., 2011).

6.3.5 Terminal Networks

The serotonergic (5HT+), orexinergic (Orx+) and histaminergic (Hst+) terminal networks are described in relation to the cholinergic, catecholaminergic, serotonergic, orexinergic and histaminergic nuclei. While it is clear that these systems project far more widely throughout the brain (e.g. Inagaki et al., 1988; Leger et al., 2001; Nixon and Smale, 2007) the description was limited to the nuclei involved in the sleep-wake cycle to allow us to determine how each of these systems may affect the activity of the other systems.

6.3.5.1 Serotonergic terminal networks

Within the basal forebrain there was only one region of high-density 5HT+ terminal networks, this being within the lateral septal nucleus. The terminal networks in this region of high-density formed cellular basket endings around specific neurons (Fig. 6.1A). Medium-density varicose 5HT+ terminal networks were observed within the cholinergic medial septal nucleus, the cholinergic diagonal band of Broca, the cholinergic islands of Calleja and olfactory tubercle and the cholinergic nucleus basalis (Figs. 6.1A-D, 6.2B). Throughout the hypothalamus a medium-density varicose 5HT+ terminal

network was observed, and this was also characteristic of all the sleep-wake associated nuclei (the cholinergic, catecholaminergic and orexinergic nuclei described above) (Figs. 6.1D-J, 6.2D). Within the midbrain a medium-density varicose 5HT+ terminal network was observed within the serotonergic caudal linear nucleus (CLi), the supralemniscal serotonergic nucleus (B9) and the serotonergic dorsal raphe nuclear complex. The same type of medium density varicose network was observed within the cholinergic (PBg, PPT, LDT), catecholaminergic (A6d) and serotonergic (DRc, MnR) of the pontine region, while a low-density network was observed in the other catecholaminergic nuclei (A7sc, A7d) (Figs. 6.1M-S, 6.2F).

6.3.5.2 Orexinergic terminal networks

A medium-density varicose Orx+ terminal network was observed within the cholinergic nuclei of the basal forebrain, including the diagonal band of Broca, the islands of Calleja and olfactory tubercle and the nucleus basalis (Figs. 6.1B-D, 6.3B), but only a low-density varicose Orx+ terminal network was observed within the medial septal nucleus. Within the hypothalamus a high-density varicose Orx+ terminal network was observed within the catecholaminergic anterior hypothalamic group, dorsal division (A15d) (Figs. 6.1 D and E, 6.3D). A second region of high-density Orx+ terminals was observed within the hypothalamic arcuate nucleus in the rhythmic chronotype, but only a medium-density Orx+ terminal network was noted for the homologous region in the arrhythmic chronotype (Figs. 6.1E, 6.10 A and B). This was the first difference noted between chronotypes. For the remaining regions of the hypothalamus, including those areas in which the cholinergic and remaining catecholaminergic nuclei (A15v, A14, A13,

A12, A12) were found a medium-density varicose Orx+ network was observed (Figs. 6.1D-I). The second difference of note was found in the density of the Orx+ terminal network to the intergeniculate leaflet, which was of a high-density in the rhythmic chronotype, but of low density in the arrhythmic chronotype (Figs. 6.1H-J, 6.10 C and D).

Within the midbrain a medium-density varicose Orx+ terminal network was observed within the serotonergic nuclei (CLi, B9 and the dorsal raphe nuclear complex). A high-density varicose Orx+ terminal network was observed within the pontine cholinergic pedunculopontine (PPT) nucleus, the catecholaminergic subcoeruleus compact portion (A7sc) and locus coeruleus diffuse portion (A6d) and the serotonergic dorsal raphe caudal nucleus (DRc). A medium-density varicose Orx+ terminal network was observed within the cholinergic laterodorsal tegmental (LDT) nucleus and the serotonergic median raphe nucleus (MnR) and a low density varicose Orx+ terminal network was observed within the cholinergic parabigeminal nucleus (PBg) and the catecholaminergic subcoeruleus diffuse portion (A7d) nuclei (Figs. 6.1M-S, 6.3 F and H).

6.3.5.3 Histaminergic terminal networks

In both circadian chronotypes of mole rat a medium-density varicose Hst+ terminal network was observed within the cholinergic nucleus basalis, but only a low-density varicose terminal network was observed in the remaining cholinergic sleep-wake associated nuclei of the basal forebrain (Figs. 6.1A-D, 6.4B). A medium-density varicose Hst+ terminal network was observed within the cholinergic hypothalamic nuclei, the catecholaminergic hypothalamic nuclei, and the orexinergic hypothalamic nuclei (Figs.

6.1D-I, 6.4D). In the midbrain, a medium-density varicose terminal network was observed within the serotonergic caudal linear nucleus (CLi) and the serotonergic dorsal raphe complex, but only a low-density terminal network was observed within the supralemniscal serotonergic nucleus (B9) (Figs 6.1M-S, 6.4F). Within the pontine region a medium-density varicose Hst+ terminal network was observed within the cholinergic PBg and LDT nuclei, the catecholaminergic A6d nucleus and the serotonergic DRc and MnR nuclei (Figs. 6.1P-R). A low-density varicose terminal network was observed in the cholinergic PPT nucleus and the catecholaminergic A7sc and A7d nuclei.

6.3.6 GABAergic interneurons

The calcium binding proteins calbindin (CB), calretinin (CR) and parvalbumin (PV) label specific subsets of GABAergic interneurons which are known to play a major role in the transition of one state to another (Siegel, 2004). In the following sections, the density of these immunopositive (CB+, CR+ and PV+) interneurons and their respective terminal networks are described in relation to the identified sleep-wake associated nuclei of the cholinergic, catecholaminergic, serotonergic and orexinergic systems located within the basal forebrain, hypothalamus, midbrain and pons. The current analysis of the distribution and terminal network densities of these GABAergic interneuron types indicated overall similarity in both circadian chronotypes, thus the following description applies to both unless otherwise specified.

6.3.6.1 Relations of GABAergic interneurons to cholinergic nuclei

A medium density of CB+ interneurons was found to intermingle with the cholinergic medial septal neurons, islands of Calleja, olfactory tubercle and nucleus basalis and a medium density CB+ terminal network was observed within these cholinergic nuclei (Fig. 6.5B). A low-density of CB+ interneurons intermingled with the cholinergic neurons of the diagonal band of Broca and a medium density CB+ terminal network was observed in this region. A medium-density of CR+ interneurons intermingled with the neurons of the medial septal nucleus and nucleus basalis and a medium density CR+ terminal network was observed within these regions. A low-density CR+ interneurons was found to intermingle with the neurons of the diagonal band of Broca, the islands of Calleja and the olfactory tubercle and a low density CR+ terminal network was observed within these regions (Fig. 6.5C). A low-density of PV+ interneurons was observed to intermingle with neurons of the medial septal nucleus, diagonal band of Broca and nucleus basalis and a low density PV+ terminal network was observed within these regions.

A medium to high density of CB+ and CR+ interneurons with a medium to high density CB+ and CR+ terminal network were found intermingled with neurons of the dorsal, lateral and ventral hypothalamic groups. No PV+ interneurons or terminal networks were observed either intermingled with or adjacent to the cholinergic nuclei of the hypothalamus. A low-density of CB+ interneurons intermingled with the neurons of the PPT, PBg and LDT and a medium to high density CB+ terminal network was observed in these nuclei (Fig. 6.8B). A low to medium-density of CR+ interneurons intermingled with the neurons of the LDT, a low-density of CR+ neurons intermingled

with the PPT and a low density of CR+ interneurons intermingled with the PBg (Fig. 6.8C). Medium to high density, medium and low-density CR+ terminal networks were observed within the LDT, PBg and PPT respectively. Only a very few PV+ interneurons, with very low density PV+ terminal networks were observed within the PPT, PBg and LDT (Fig. 6.8D).

6.3.6.2 Relations of GABAergic interneurons to catecholaminergic nuclei

A medium to high-density of CB+ and CR+ interneurons, with a medium to high density CB+ and CR+ terminal networks were found intermingled with hypothalamic catecholaminergic neurons (A15d, A15v, A14, A13, A12 and A11 groups). No PV+ interneurons or terminal networks were observed within the hypothalamic catecholaminergic nuclei (Figs. 6.6B-D). A medium-density of CB+ interneurons was only intermingled with the neurons of the A6d catecholaminergic nucleus (Fig. 6.9B). A medium to high density CB+ terminal network was observed within the A6d, whereas a medium density was observed in the A7d and A7sc. A low-density of CR+ interneurons were intermingled with neurons of the A6d and a medium density CR+ terminal network was observed in this region. A low-density of CR+ interneurons were intermingled with neurons of both divisions of the A7 and a low to medium CR+ terminal network was observed in these regions (Fig. 6.9C). A low-density of PV+ interneurons with low density PV+ terminal networks were found intermingled with the catecholaminergic neurons throughout locus coeruleus (A6d, A7sc, A7d) (Fig. 6.9D).

6.3.6.3 Relations of GABAergic interneurons to serotonergic nuclei

A high density of CB+ interneurons were observed intermingled with the neurons of the caudal linear (CLi) nucleus and a high density CB+ terminal network was observed within this region. A medium to high-density of CB+ interneurons was observed intermingling with the neurons of the dorsal raphe (DR) complex and the median raphe (MnR) nucleus and a medium to high-density CB+ terminal network was observed within these nuclei (Fig. 6.7B). A medium-density of CB+ interneurons were found within the supralemniscal nucleus (B9) along with a medium density CB+ terminal network. A medium-density of CR+ interneurons and medium density CR+ terminal networks were found intermingled with neurons of the DRl, DRp, DRc, and CLi nuclei (Fig. 6.7C), but only a low-density of CR+ interneurons and terminal networks were observed intermingled with neurons of the DRif, DRv, DRd, B9, and MnR nuclei (Fig. 6.7C). A few isolated PV+ interneurons and low-density PV+ terminal networks were identified within the dorsal raphe (DR) complex, CLi, B9 and MnR nuclei (Fig. 6.7D).

6.3.6.4 Relations of GABAergic interneurons to orexinergic nuclei

A medium to high-density of CB+ and CR+ interneurons with a medium to high-density CB+ and CR+ terminal network was found intermingled with orexinergic neurons throughout the hypothalamus. No PV+ interneurons or terminal networks were observed within the hypothalamus.

Figure 6.1: Drawings of serial coronal sections A to S through the right half of the brain of a Zambian mole rat (*Cryptomys mechowi*) with a rhythmic chronotype from the basal forebrain through to the pontomedullary junction. The drawings depict the architecture based on nissl and myelin sections; immunopositive neurons of the cholinergic, catecholaminergic (those that were immunoreactive for tyrosine hydroxylase), serotonergic and orexinergic systems (each black dot represents a single neuron); and the distribution of serotonergic, orexinergic and histaminergic terminal network densities (an absence of shading represents low density, grey shaded areas represent medium density and black shaded areas represent high density). See list for abbreviations.

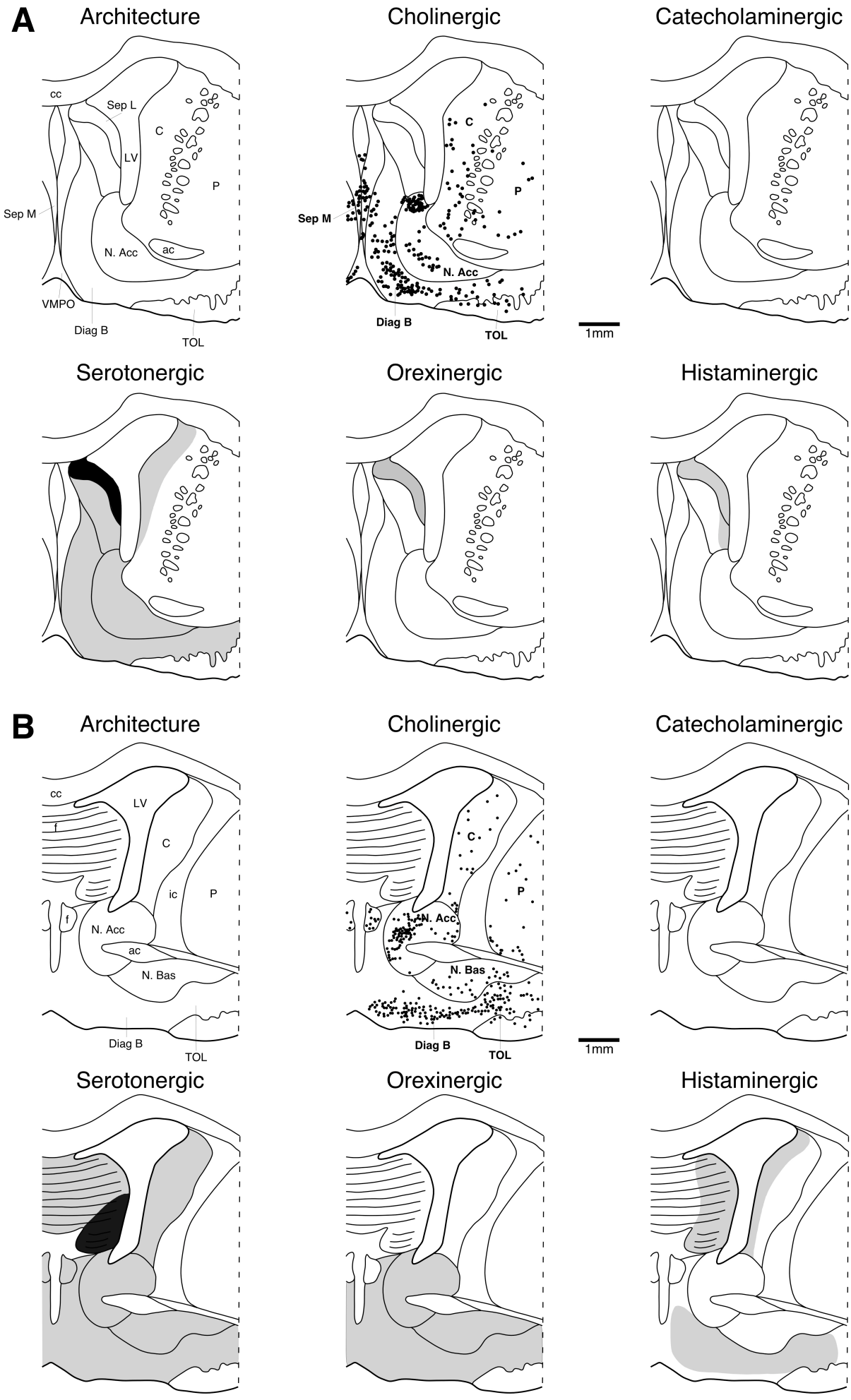
A
Architecture
Cholinergic
Catecholaminergic
cc
Sep L
C
LV
P
Sep M
N. Acc
ac
VMPO
Diag B
TOL
Sep M
C
P
N. Acc
Diag B
TOL
1mm
Serotonergic
Orexinergic
Histaminergic
B
Architecture
Cholinergic
Catecholaminergic
cc
LV
f
C
ic
P
f
N. Acc
ac
N. Bas
Diag B
TOL
C
P
N. Acc
N. Bas
Diag B
TOL
1mm
Serotonergic
Orexinergic
Histaminergic

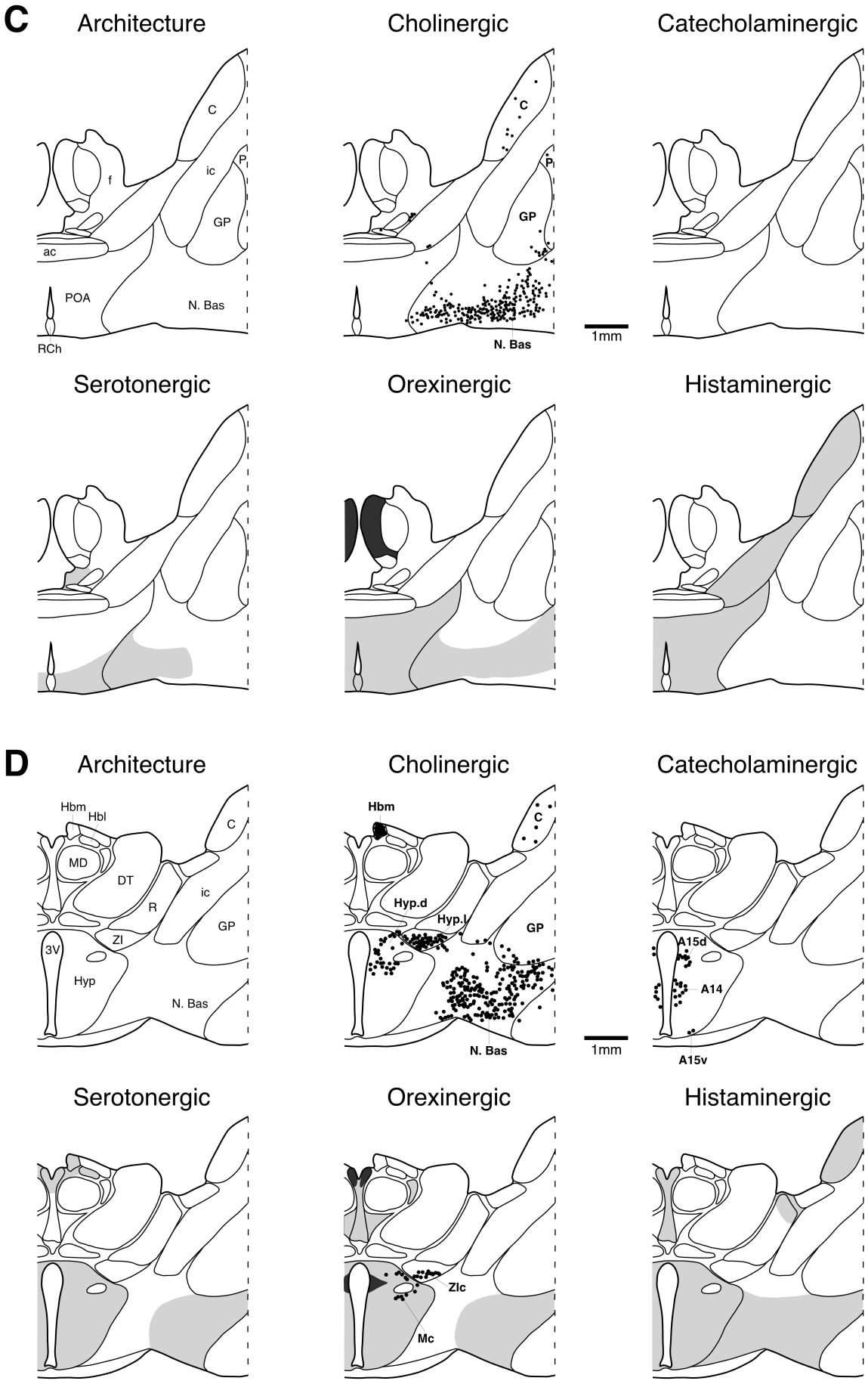
C
Architecture
Cholinergic
Catecholaminergic
C
P
ic
f
GP
ac
POA
N. Bas
RCh
1mm
Serotonergic
Orexinergic
Histaminergic
D
Architecture
Cholinergic
Catecholaminergic
Hbm
Hbl
C
MD
DT
ic
R
GP
ZI
3V
Hyp
N. Bas
Hyp.d
Hyp.l
A15d
A14
A15v
Serotonergic
Orexinergic
Histaminergic
Zlc
Mc

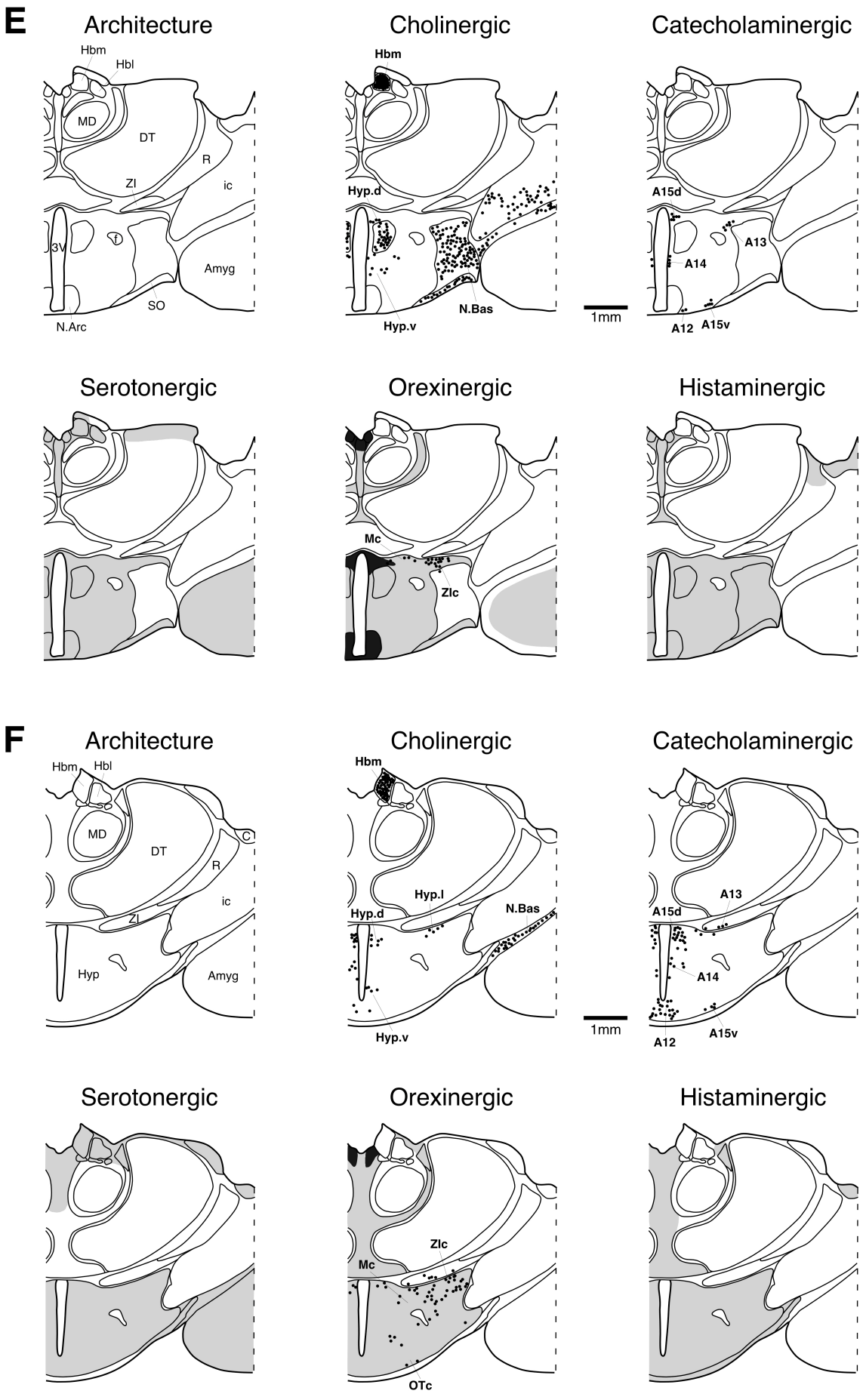
E
Architecture
Cholinergic
Catecholaminergic
Hbm
Hbl
MD
DT
R
ZI
ic
3V
f
Amyg
SO
N.Arc
Hbm
Hyp.d
N.Bas
Hyp.v
1mm
A15d
A13
A14
A12
A15v
Serotonergic
Orexinergic
Histaminergic
Mc
Zlc
F
Architecture
Cholinergic
Catecholaminergic
Hbm
Hbl
MD
DT
C
R
ic
ZI
Hyp
Amyg
Hbm
Hyp.l
Hyp.d
N.Bas
Hyp.v
1mm
A13
A15d
A14
A12
A15v
Serotonergic
Orexinergic
Histaminergic
Zlc
Mc
OTc

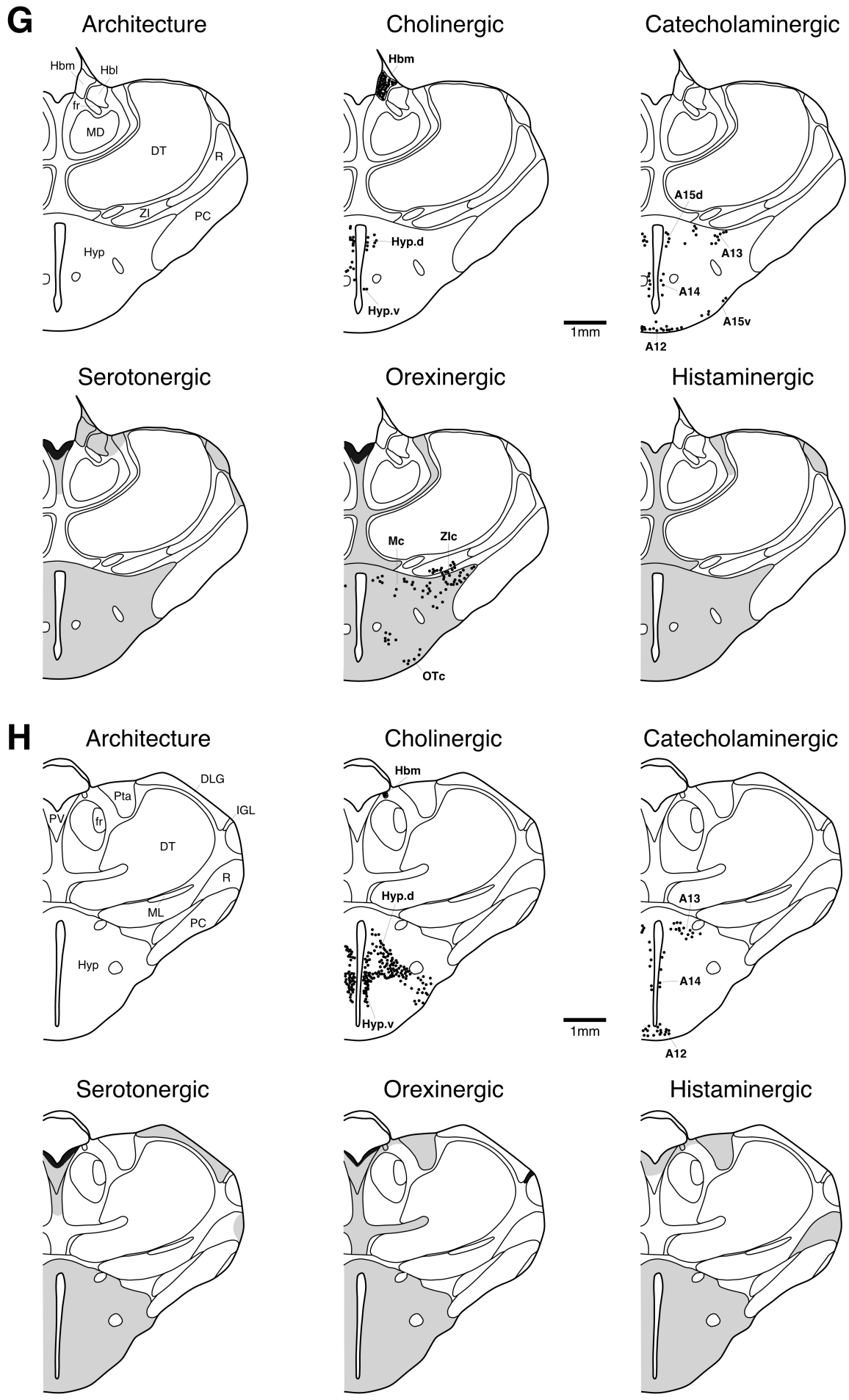
G
Architecture
Cholinergic
Catecholaminergic
Hbm
Hbl
fr
MD
DT
R
ZI
PC
Hyp
Hbm
Hyp.d
Hyp.v
A15d
A13
A14
A15v
A12
1mm
Serotonergic
Orexinergic
Histaminergic
Mc
Zlc
OTc
H
Architecture
Cholinergic
Catecholaminergic
DLG
Pta
IGL
PV
fr
DT
R
ML
PC
Hyp
Hbm
Hyp.d
Hyp.v
A13
A14
A12
1mm
Serotonergic
Orexinergic
Histaminergic

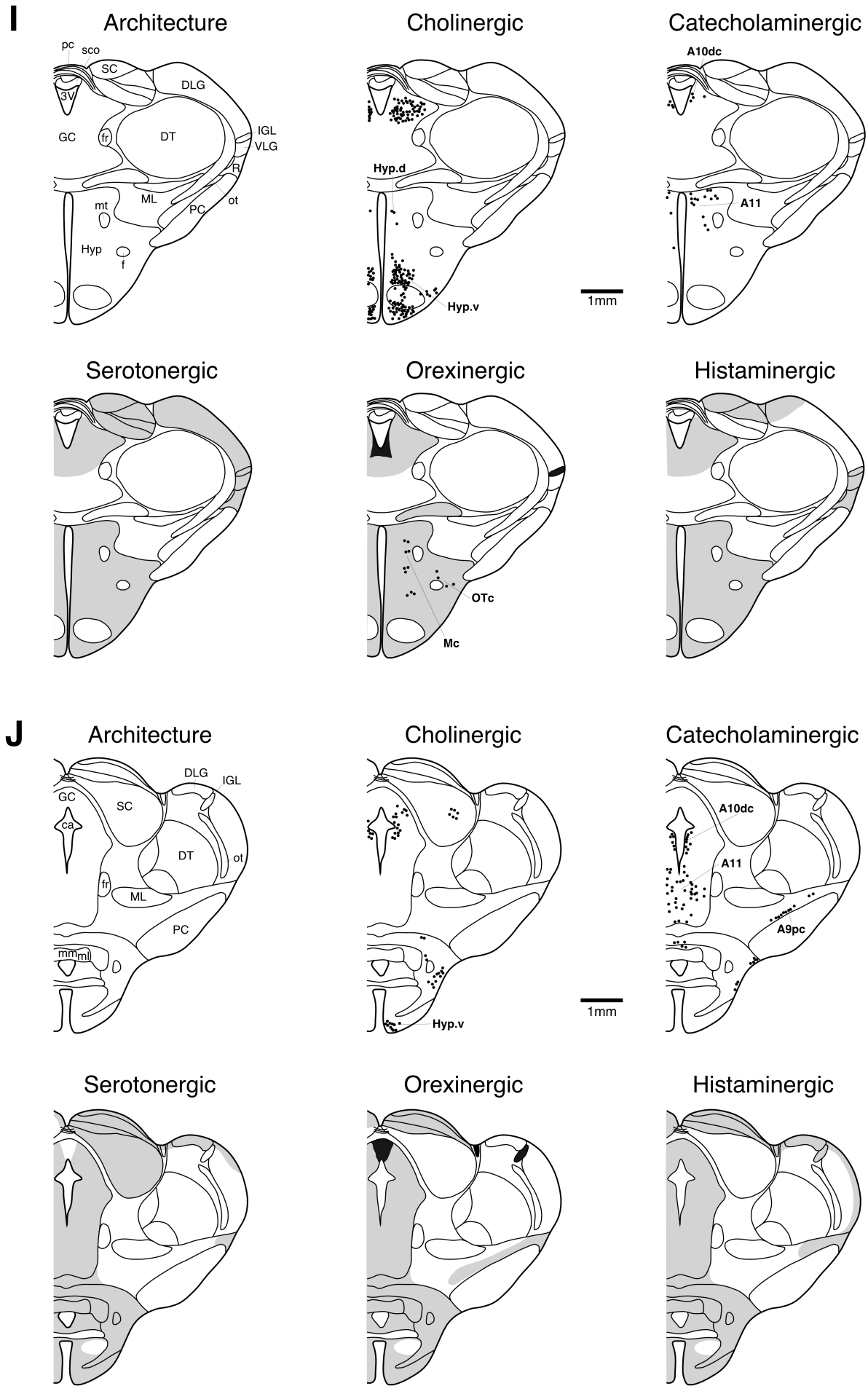
I
Architecture
Cholinergic
Catecholaminergic
pc
sco
SC
DLG
3V
GC
fr
DT
IGL
VLG
R
ot
ML
PC
mt
Hyp
f
Hyp.d
Hyp.v
1mm
A10dc
A11
Serotonergic
Orexinergic
Histaminergic
OTc
Mc
J
Architecture
Cholinergic
Catecholaminergic
DLG
IGL
GC
SC
ca
DT
ot
fr
ML
PC
mm
ml
Hyp.v
1mm
A10dc
A11
A9pc
Serotonergic
Orexinergic
Histaminergic

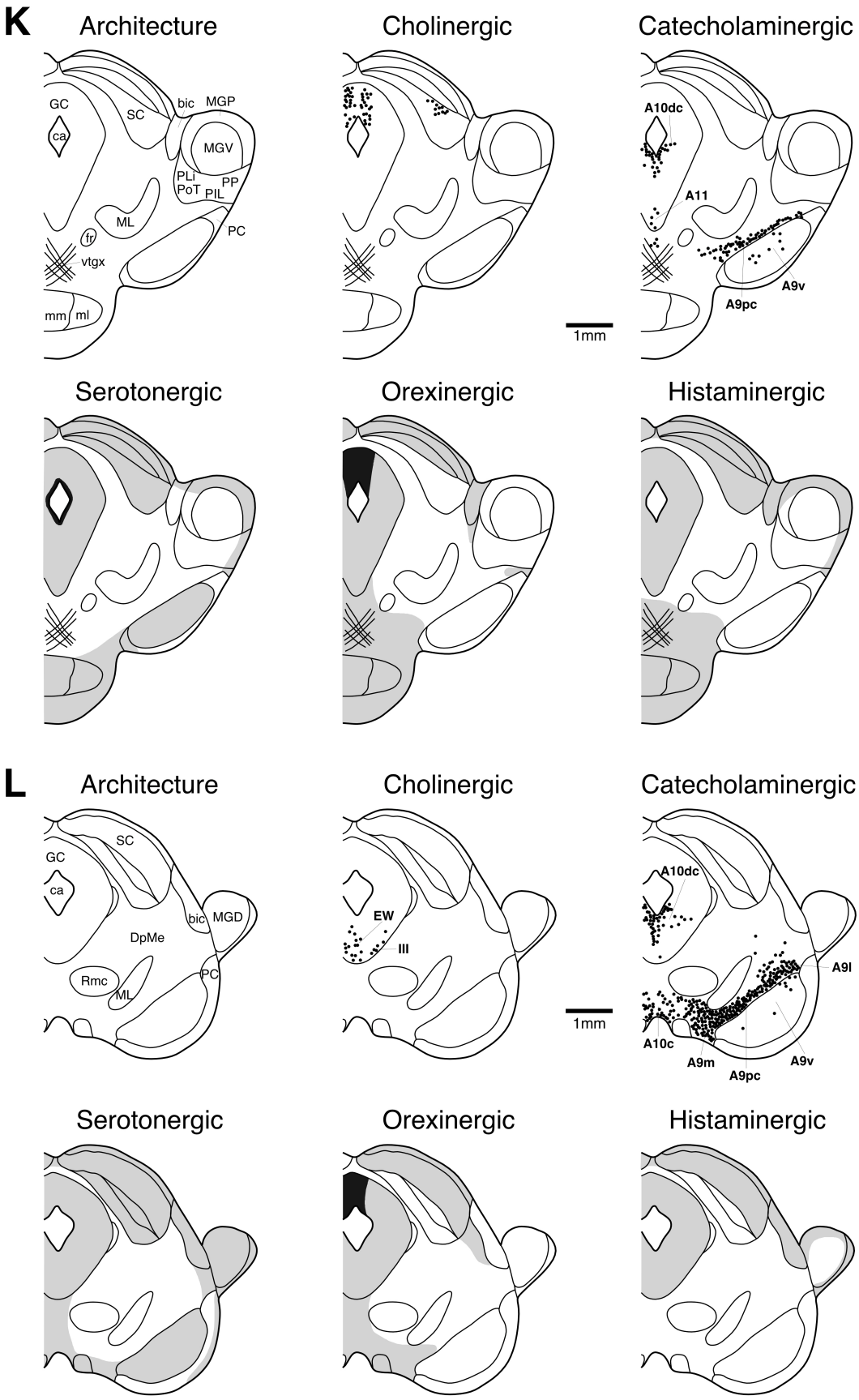
K
Architecture
Cholinergic
Catecholaminergic
GC
SC
bic
MGP
ca
MGV
PLi
PoT
PIL
PP
ML
fr
PC
vtgx
mm
ml
A10dc
A11
A9v
A9pc
1mm
Serotonergic
Orexinergic
Histaminergic
L
Architecture
Cholinergic
Catecholaminergic
SC
GC
ca
bic
MGD
DpMe
Rmc
ML
PC
EW
III
A10dc
A9l
A10c
A9m
A9v
A9pc
1mm
Serotonergic
Orexinergic
Histaminergic

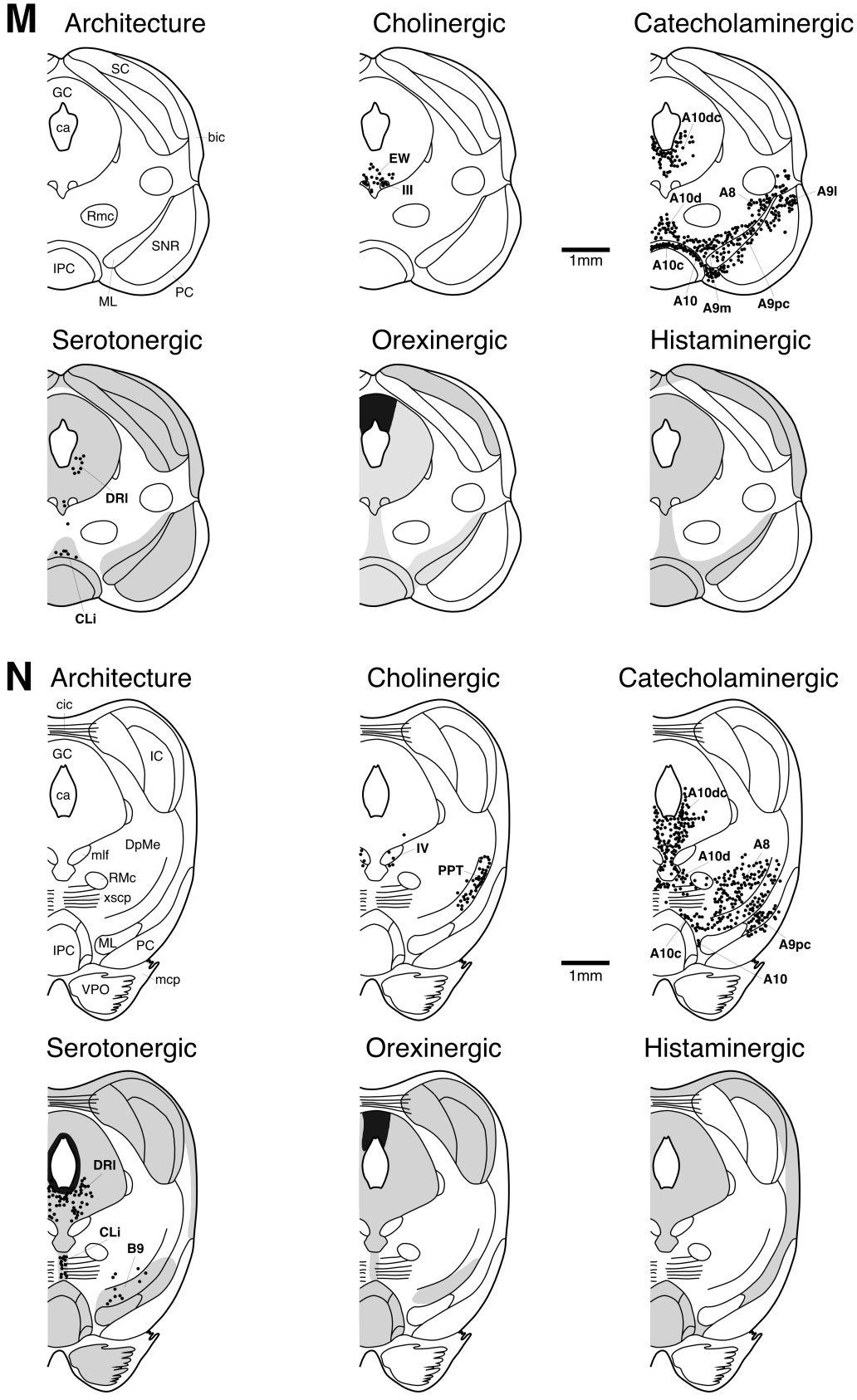
M
Architecture
Cholinergic
Catecholaminergic
SC
GC
ca
bic
Rmc
SNR
IPC
ML
PC
EW
III
1mm
A10dc
A10d
A8
A9l
A10c
A10
A9m
A9pc
Serotonergic
Orexinergic
Histaminergic
DRl
CLi
N
Architecture
Cholinergic
Catecholaminergic
cic
GC
IC
ca
DpMe
mlf
RMc
xscp
IPC
ML
PC
VPO
mcp
IV
PPT
1mm
A10dc
A10d
A8
A9pc
A10c
A10
Serotonergic
Orexinergic
Histaminergic
DRl
CLi
B9

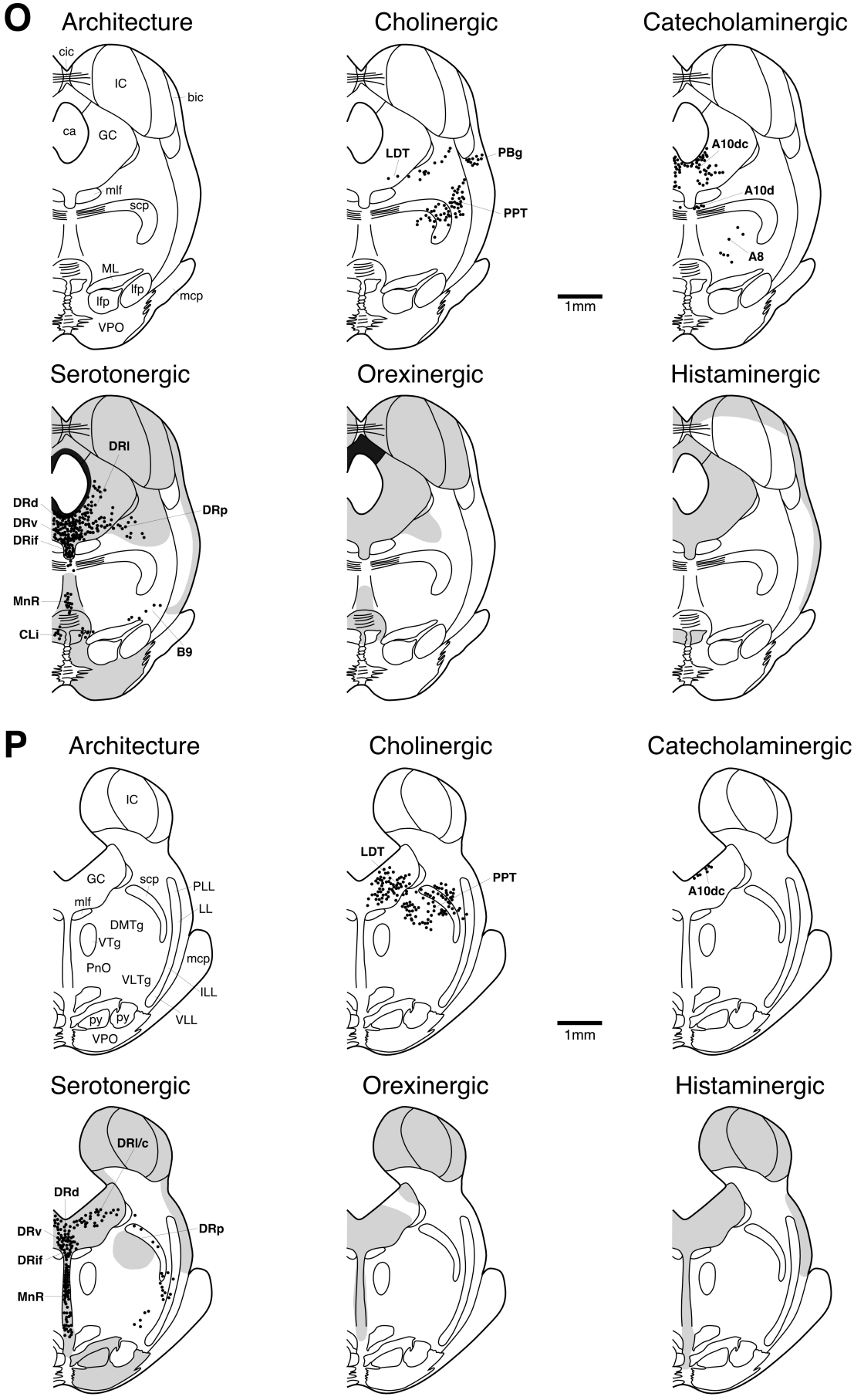
O
Architecture
Cholinergic
Catecholaminergic
cic
IC
bic
ca
GC
mlf
scp
ML
lfp
lfp
mcp
VPO
LDT
PBg
PPT
1mm
A10dc
A10d
A8
Serotonergic
Orexinergic
Histaminergic
DRl
DRd
DRv
DRif
DRp
MnR
CLi
B9
P
Architecture
Cholinergic
Catecholaminergic
IC
GC
scp
PLL
mlf
LL
DMTg
VTg
PnO
mcp
VLTg
lLL
py
py
VLL
VPO
LDT
PPT
A10dc
1mm
Serotonergic
Orexinergic
Histaminergic
DRl/c
DRd
DRv
DRif
MnR
DRp

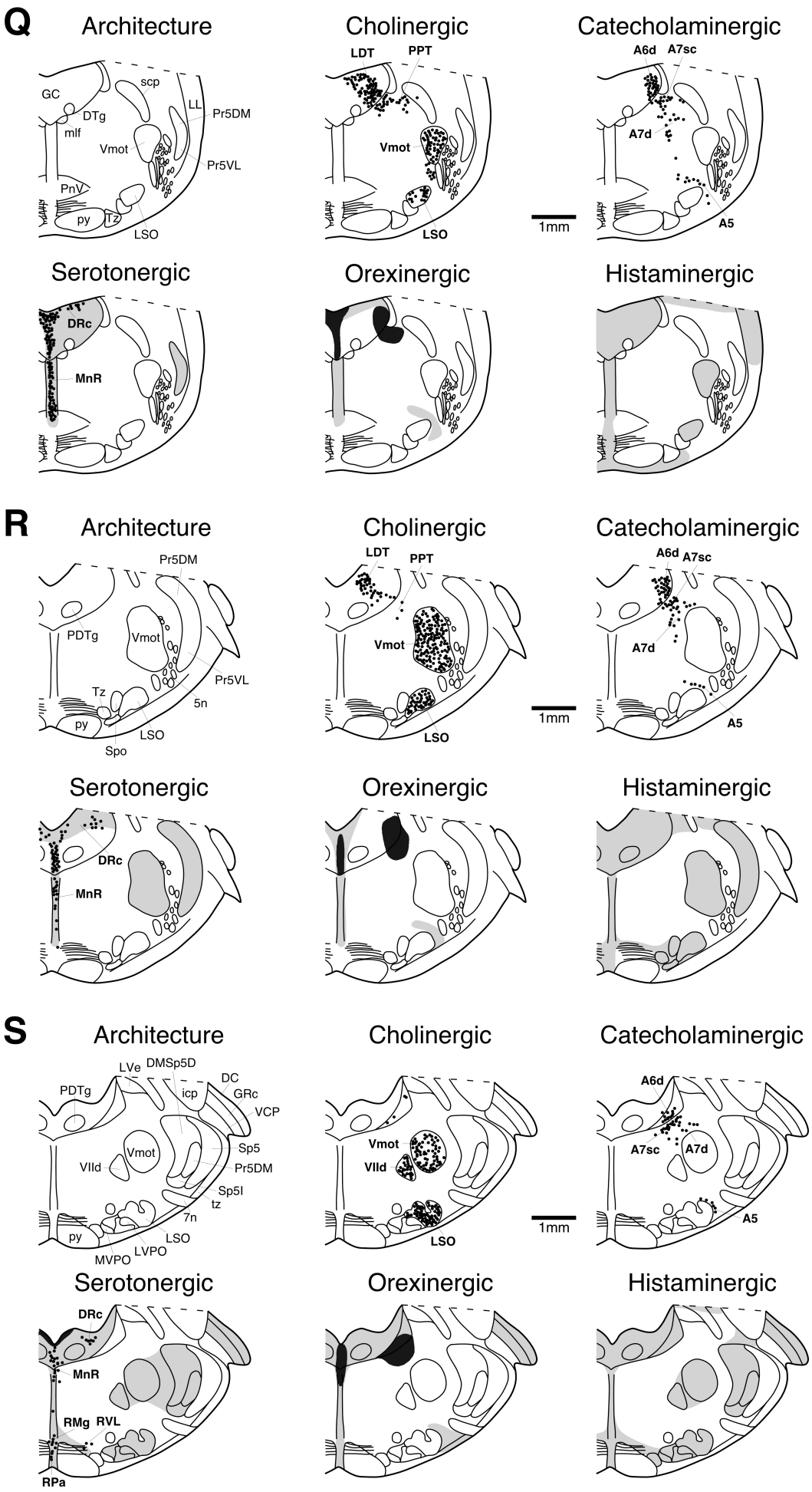
Q
Architecture
Cholinergic
Catecholaminergic
GC
scp
LL
Pr5DM
DTg
mlf
Vmot
Pr5VL
PnV
py
Tz
LSO
LDT
PPT
Vmot
LSO
1mm
A6d
A7sc
A7d
A5
Serotonergic
Orexinergic
Histaminergic
DRc
MnR
R
Architecture
Cholinergic
Catecholaminergic
Pr5DM
PDTg
Vmot
Pr5VL
Tz
5n
py
LSO
Spo
LDT
PPT
Vmot
LSO
1mm
A6d
A7sc
A7d
A5
Serotonergic
Orexinergic
Histaminergic
DRc
MnR
S
Architecture
Cholinergic
Catecholaminergic
LVe
DMSp5D
DC
PDTg
icp
GRc
VCP
Vmot
Sp5
VIId
Pr5DM
Sp5I
tz
7n
py
LSO
MVPO
LVPO
Vmot
VIId
LSO
1mm
A6d
A7sc
A7d
A5
Serotonergic
Orexinergic
Histaminergic
DRc
MnR
RMg
RVL
RPa

Figure 6.2: High power photomicrographs showing immunopsitive neurons of the cholinergic (ChAT+), orexinergic (Orx+) and catecholaminergic (TH+) systems and the associated serotonergic (5HT+) terminal network in the brain of the Zambian mole rat (*Cryptomys mechowi*). (A) ChAT+ neurons within the diagonal band of Broca, (B) Medium density 5HT+ terminal network in the region of the diagonal band of Broca, (C) Orx+ neurons of the lateral hypothalamic area, (D) Medium density 5HT+ terminal network in the region of the lateral hypothalamic area, (E) TH+ neurons of the subcoeruleus compact portion (A7sc), (F) Medium density 5HT+ terminal network in the region of A7sc. In each photomicrograph dorsal is to the top and medial to the left. Scale = 100μm and applies to all.

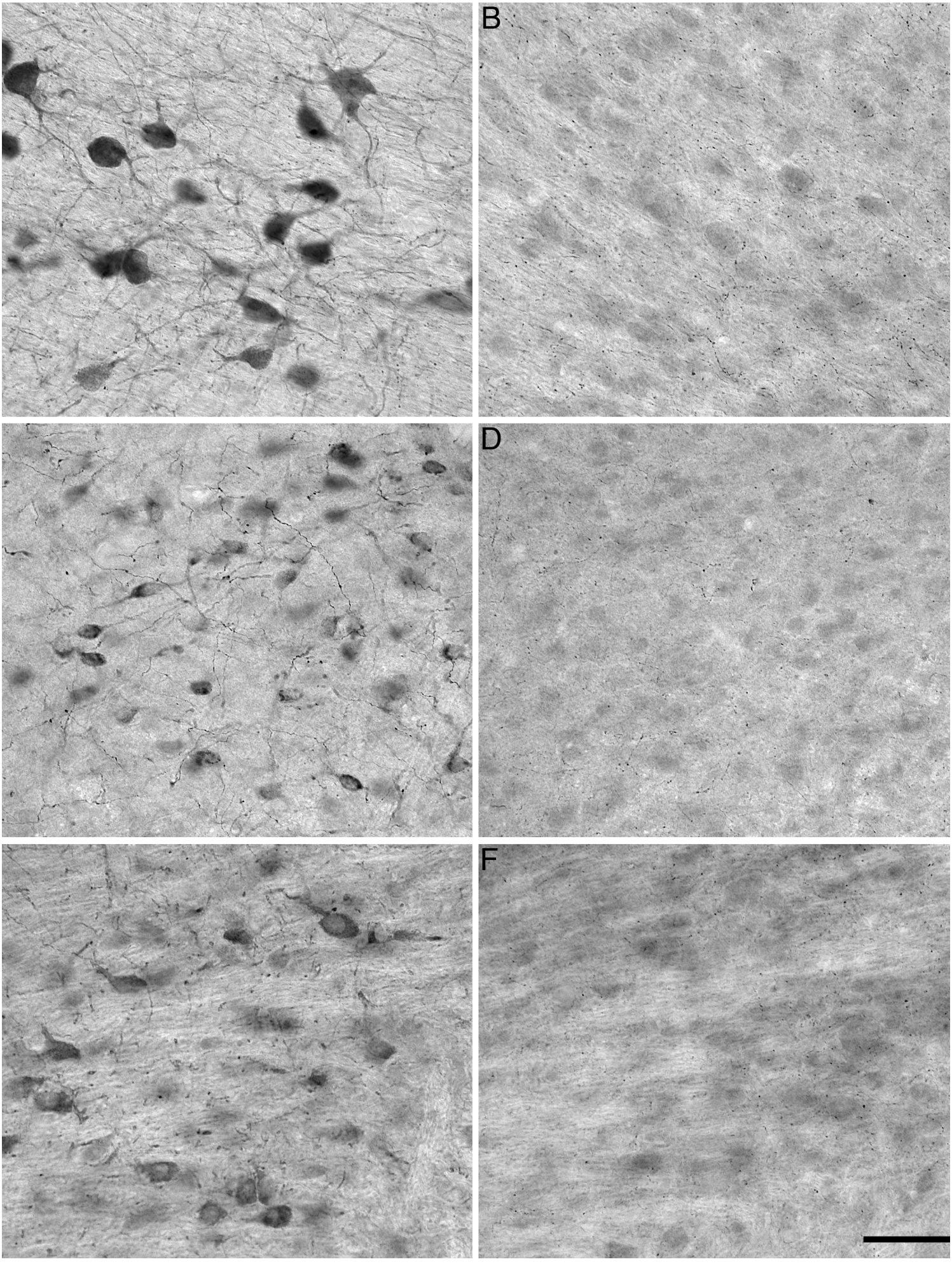
B
D
F

Figure 6.3: High power photomicrographs showing immunopsitive neurons of the cholinergic (ChAT+), catecholaminergic (TH+) and serotonergic (5HT+) systems and the associated immunopositive orexinergic (Orx+) terminal network the brain of a the Zambian mole rat (*Cryptomys mechowi*). (A) ChAT+ neurons of nucleus basalis, (B) Medium density Orx+ terminal network in the region of nucleus basalis, (C) TH+ neurons of the A15d, (D) Medium density Orx+ terminal network in the region of A15d, (E) 5HT+ neurons of the DRl, (F) Medium density Orx+ terminal network in the region of DRl, (G) TH+ neurons of the A6d, (H) High density Orx + terminal network in the region of A6d. In each photomicrograph dorsal is to the top and medial to the left. Scale = 100μm and applies to all.

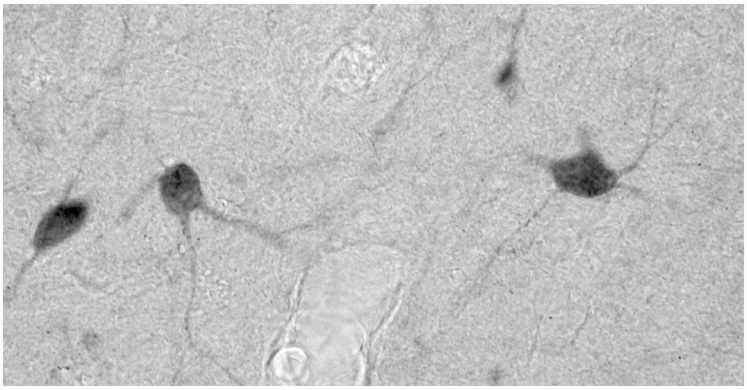
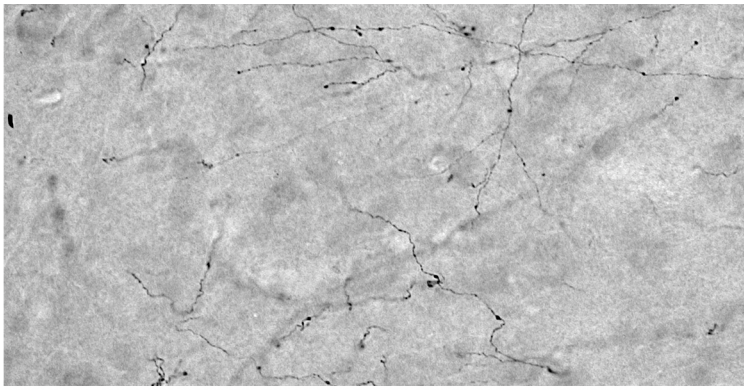
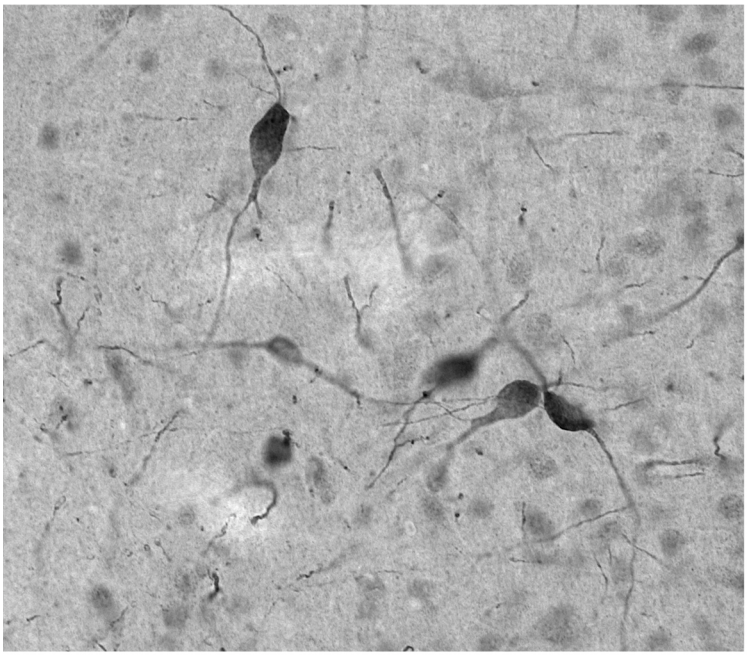
D
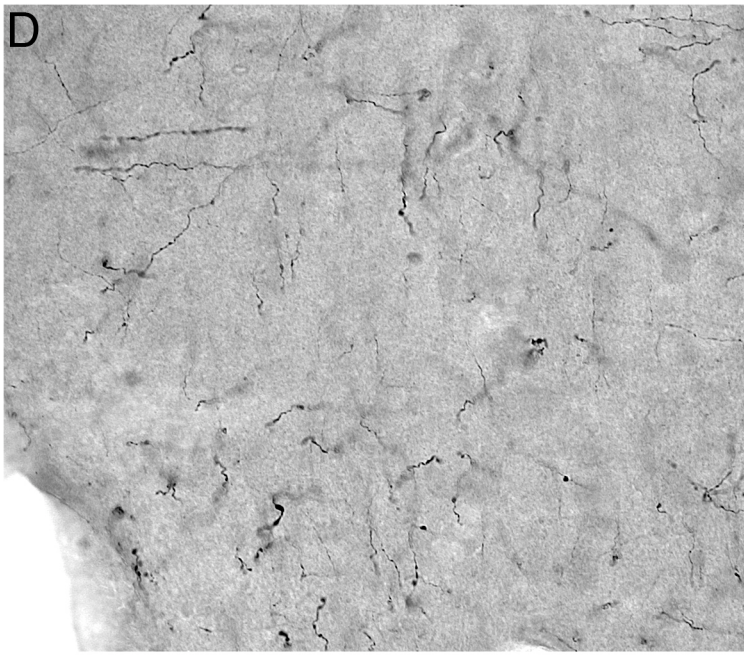
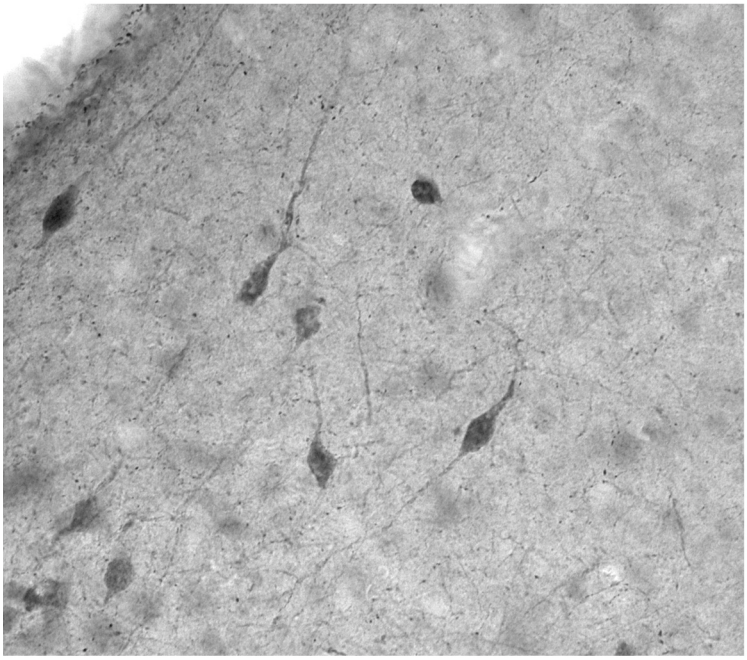
F
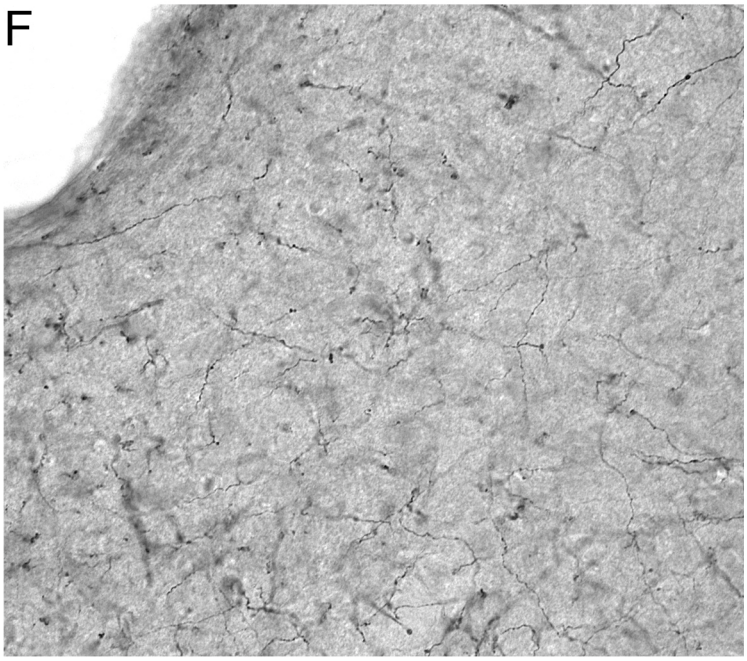
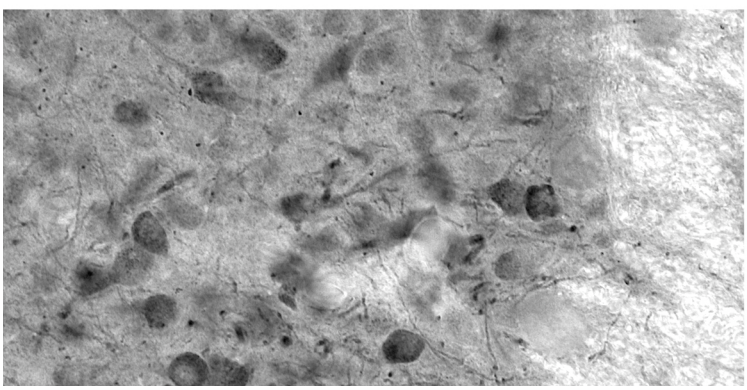
H
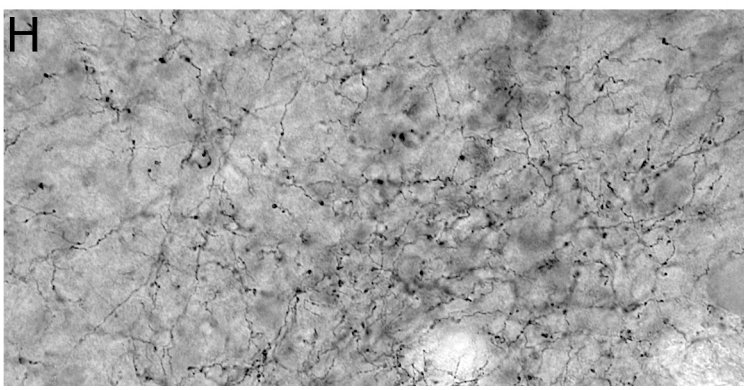

Figure 6.4: High power photomicrographs showing immunopsitive neurons of the cholinergic (ChAT+), orexinergic (Orx+) and serotonergic (5HT+) systems and the associated immunopositive histaminergic (Hst+) terminal network the brain of the Zambian mole rat (*Cryptomys mechowi*). (A) ChAT+ neurons of the medial septal nucleus, (B) Low density Hst+ terminal network in the region of the medial septal nucleus, (C) Orx+ neurons of the OTc, (D) Medium density Hst+ terminal network in the region of the OTc, (E) 5HT+ neurons of the DRd, (F) Medium density Hst+ terminal network in the region of the DRd. In each photomicrograph dorsal is to the top and medial to the left. Scale = 100μm and applies to all.

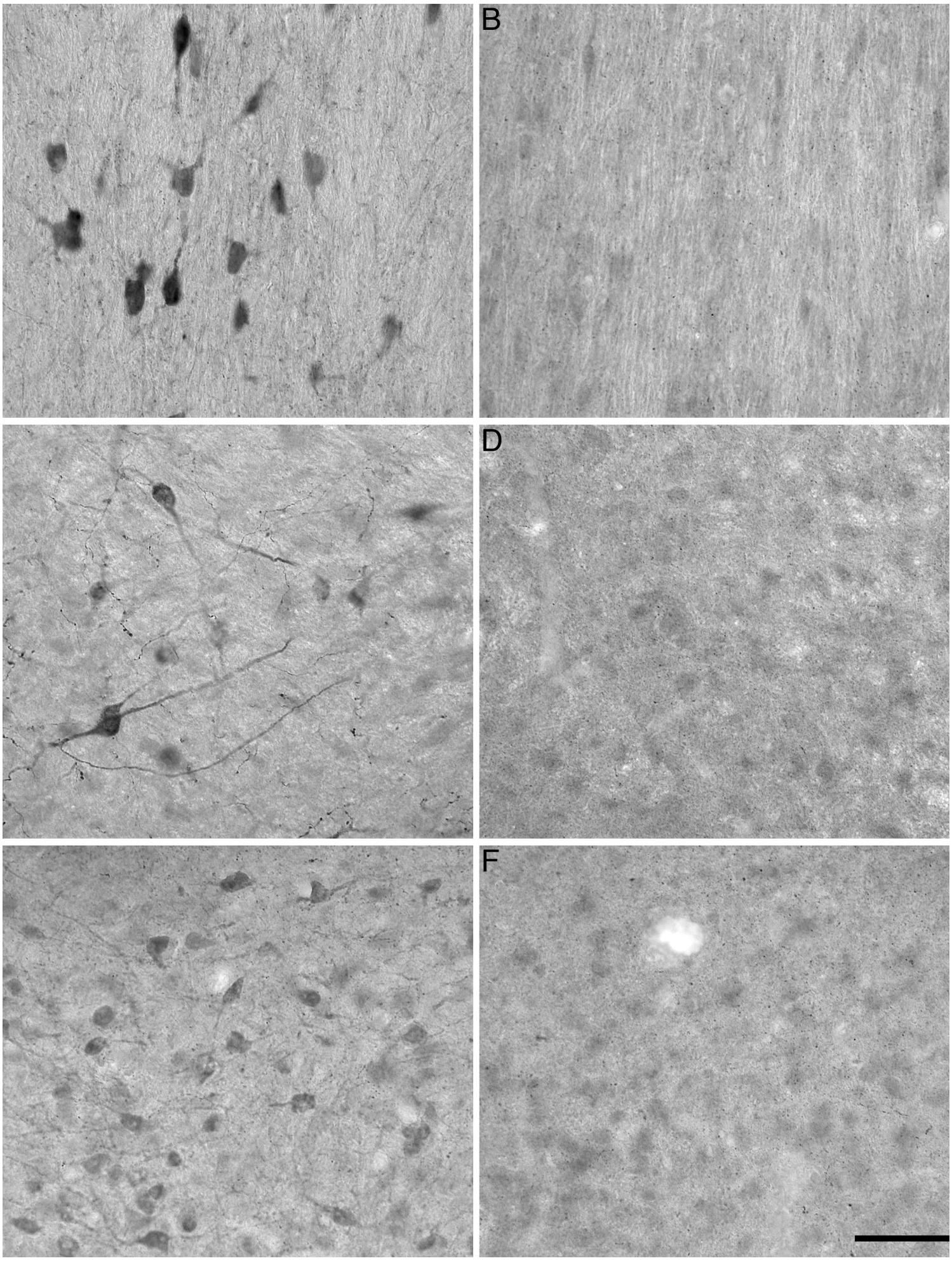
B
D
F

Figure 6.5: Photomicrographs showing immunopositive neurons of the cholinergic (ChAT+) system and calcium binding proteins calbindin (CB+), calretinin (CR+) and parvalbumin (PV+) in relation to the cholinergic neurons. (A) ChAT+ neurons of the olfactory tubercle, (B) medium density CB+ interneurons intermingled with cholinergic neurons of the olfactory tubercle, (C) low density CR+ interneurons intermingled with cholinergic neurons of the olfactory tubercle, (D) low density PV+ interneurons intermingled with the cholinergic neurons of the olfactory tubercle. In each photomicrograph dorsal is to the top and medial to the left. Scale = 500µm and applies to all.

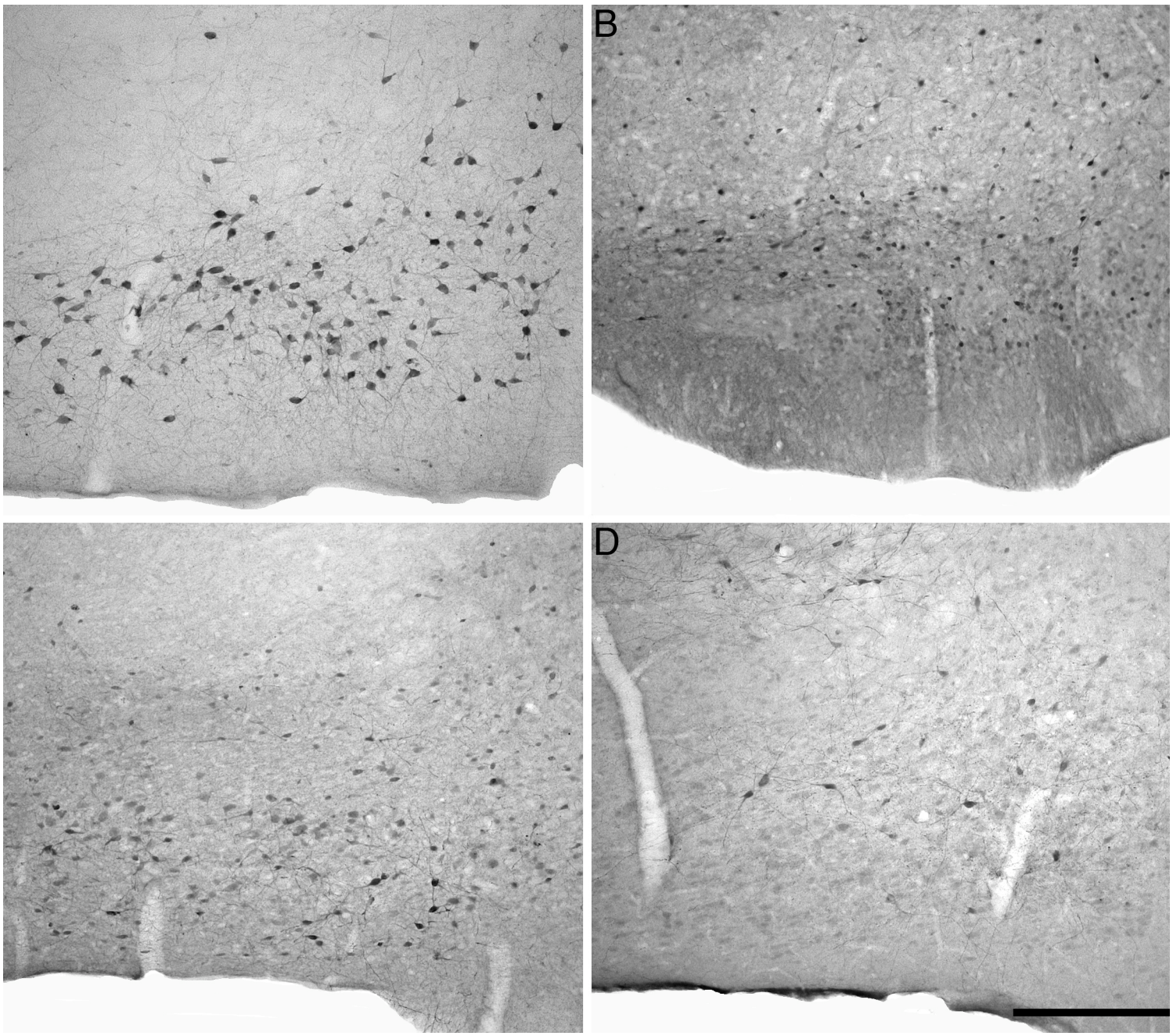
B
D

Figure 6.6: : Photomicrographs showing immunopositive neurons of the catecholaminergic (TH+) system and calcium binding proteins calbindin (CB+), calretinin (CR+) and parvalbumin (PV+) in relation to the TH+ neurons. (A) TH+ neurons of the A11, (B) medium density CB+ interneurons intermingled with A11, (C) medium density CR+ interneurons intermingled with A11, (D) absence of PV+ interneurons in the region of A11. In each photomicrograph dorsal is to the top and medial to the left. Scale = 500μm and applies to all.

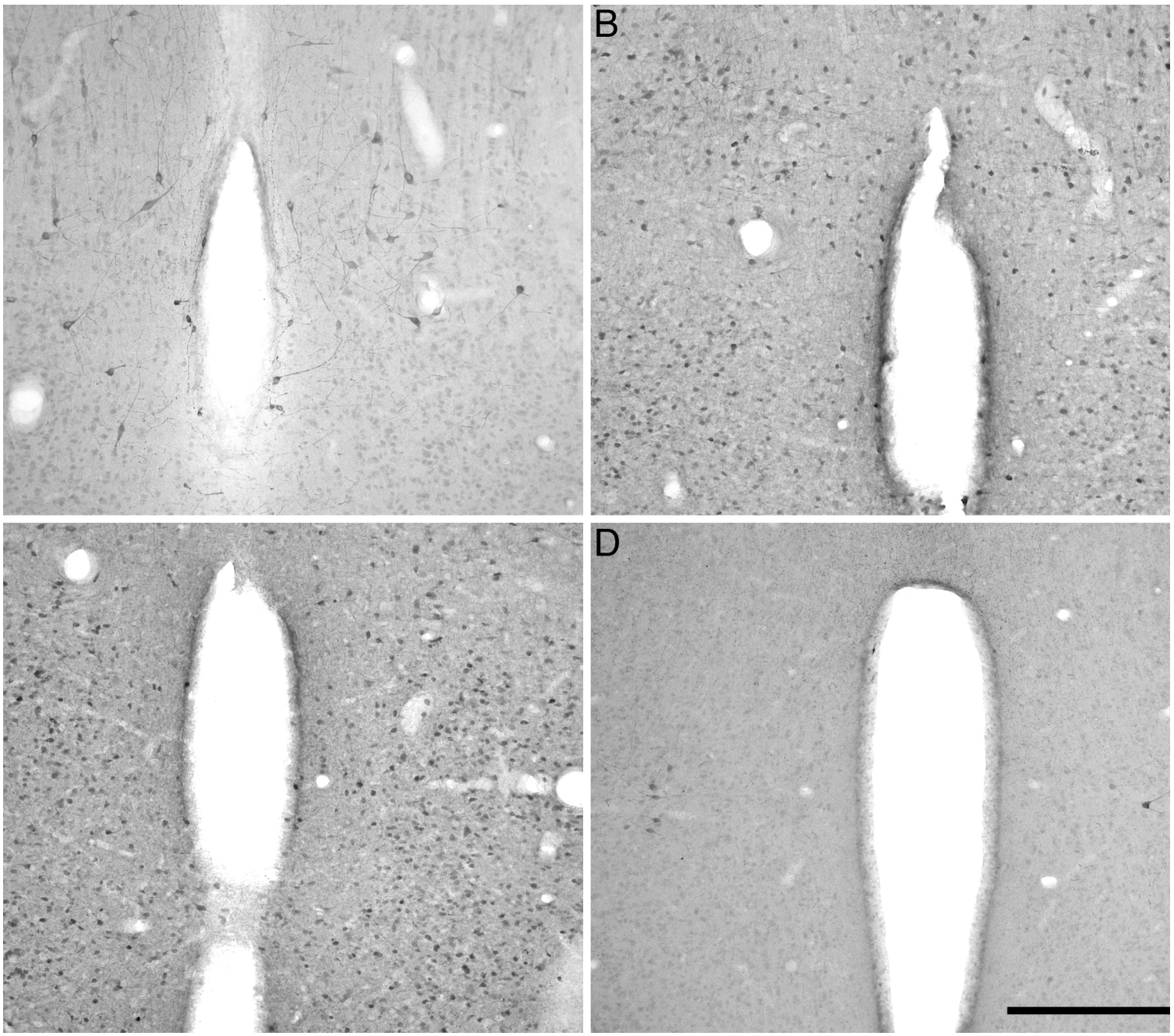
B
D

Figure 6.7: Photomicrographs showing immunopositive neurons of the serotinergic (5HT+) system and calcium binding proteins calbindin (CB+), calretinin (CR+) and parvalbumin (PV+) in relation to the 5HT+ neurons. (A) 5HT+ neurons of the DR nuclear complex, (B) medium density CB+ interneurons throughout the DR nuclear complex, (C) low density CR+ interneurons with the DRd, DRv and DRif nuclei, (D) absence of PV+ interneurons throughout the DR nuclear complex. In each photomicrograph dorsal is to the top and medial to the left. Scale = 500μm and applies to all.

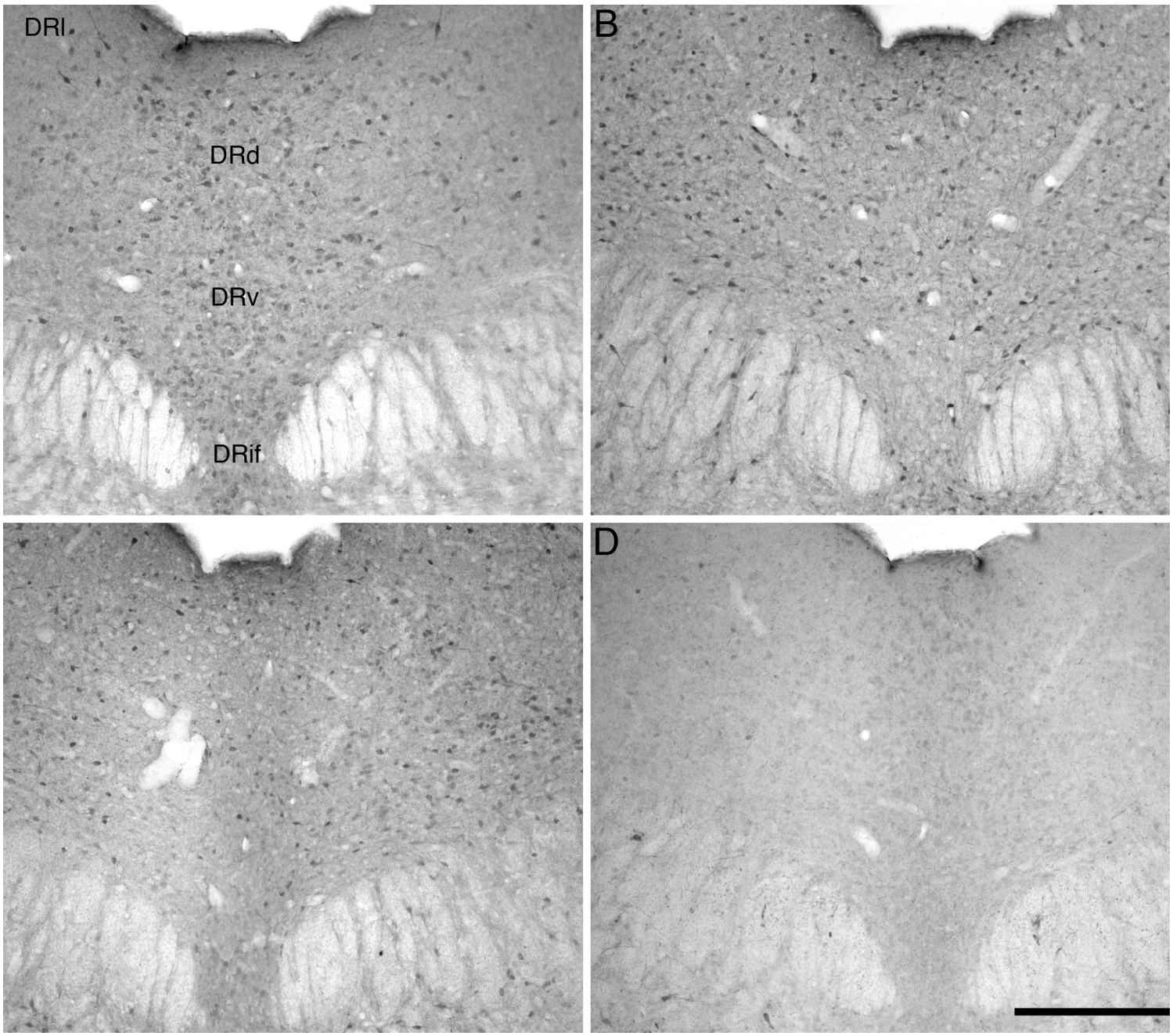
DRl
DRd
DRv
DRif
B
D

Figure 6.8: Photomicrographs showing immunopositive neurons of the cholinergic (ChAT+) system and calcium binding proteins calbindin (CB+), calretinin (CR+) and parvalbumin (PV+) in relation to the cholinergic neurons. (A) ChAT+ neurons of the pedunculopontine (PPT) and laterodorsal tegmental (LDT) nuclei, (B) low to high density CB+ interneurons intermingled with PPT and LDT, (C) low to medium density CR+ interneurons intermingled PPT and LDT, (D) absence of PV+ interneurons in the regions of PPT and LDT. In each photomicrograph dorsal is to the top and medial to the left. Scale = 500μm and applies to all.

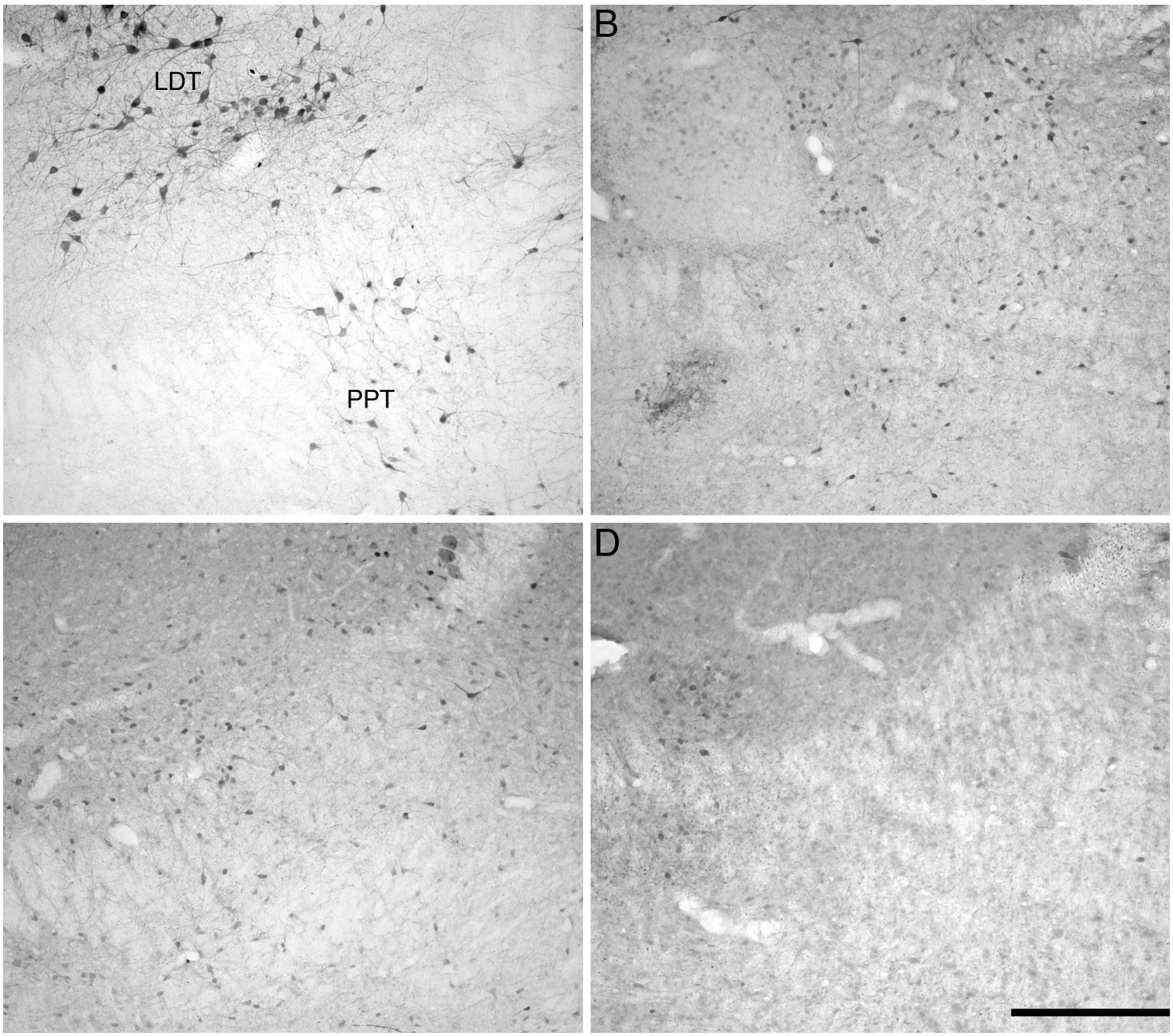
LDT
PPT
B
D

Figure 6.9: Photomicrographs showing immunopositive neurons of the catecholaminergic (TH+) system and calcium binding proteins calbindin (CB+), calretinin (CR+) and parvalbumin (PV+) in relation to the TH+ neurons. (A) TH+ neurons of part of the locus coeruleus complex (A6d and A7sc), (B) medium density CB+ interneurons intermingled with A6d only, (C) low density CR+ interneurons intermingled with A6d and A7sc, (D) absence of PV+ interneurons. In each photomicrograph dorsal is to the top and medial to the left. Scale = 500μm and applies to all.

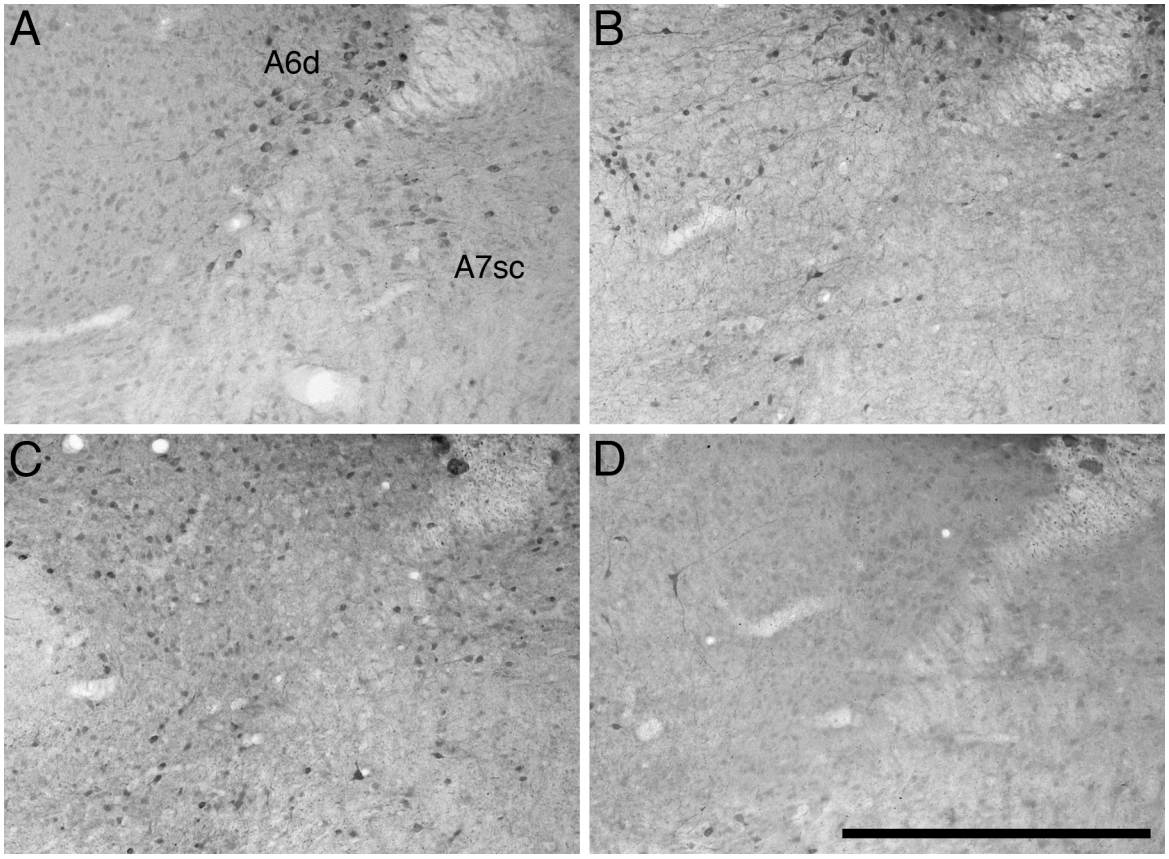
A
A6d
A7sc
B
C
D

Figure 6.10: Photomicrographs showing possible differences in orexinergic (Orx+) terminal network densities between rhythmic and arrhythmic chronotypes of the Zambian mole rat (*Cryptomys mechowi*) in the hypothalamic arcuate nucleus and the intergeniculate leaflet (IGL). (A) High density Orx+ terminal network in the region of the hypothalamic arcuate nucleus in the rhythmic chronotype, (B) Medium density Orx+ terminal network in the region of the hypothalamic arcuate nucleus in the arrhythmic chronotype, (C) High density Orx+ terminal network in the region of the IGL in the rhythmic chronotype, (D) Medium density Orx+ terminal network in the region of the IGL in the arrhythmic chronotype. In each photomicrograph dorsal is to the top and medial to the left. Scale = 500μm and applies to all.

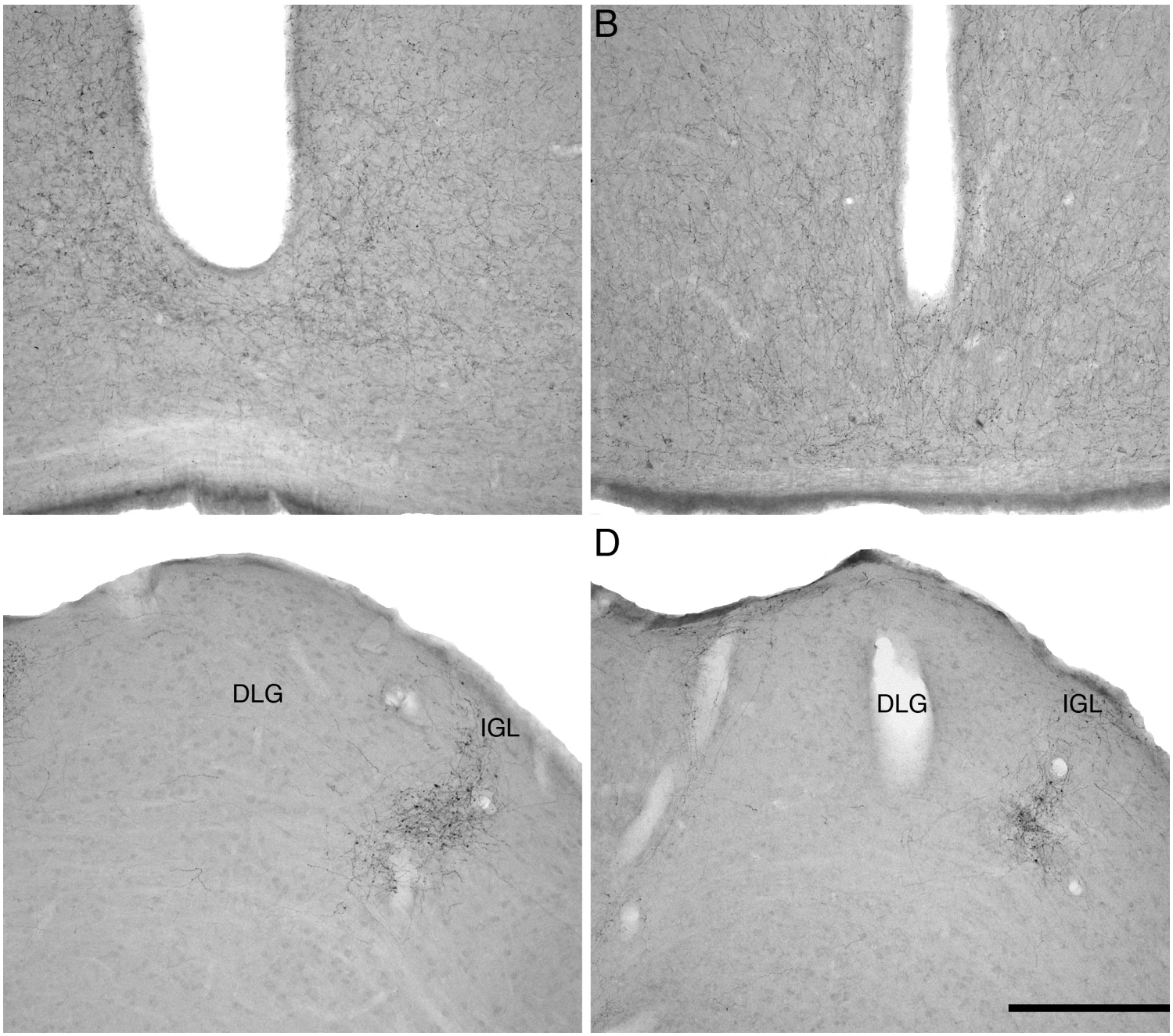
B
DLG
IGL
D
DLG
IGL

6.4 Discussion

The results of the present study indicated that in both circadian chronotypes of mole rat immunopositive neurons and nuclear complexes of the cholinergic, catecholaminergic, serotonergic and orexinergic systems were similar to those previously reported in other mole rats and rodents. It was also observed that the distribution of serotonergic, orexinergic and histaminergic terminal networks in both circadian chronotypes of mole rat were similar to those reported in other rodents and mammals. It is known that the calcium binding proteins calbindin (CB), calretinin (CR) and parvalbumin (PV) are subtypes of the GABAergic neuronal population. In the current study it was found that the immunopostive parvalbumin (PV+) interneurons did not associate with nuclei known to be involved in the sleep-wake cycle. Immunopostive calbindin (CB+) interneurons were ubiquitous in distribution and found in all nuclei involved with the sleep-wake cycle; however, the immunohistochemical revelation of the distribution of immunopostive calretinin (CR+) interneurons resulted in distinct variations within nuclear complexes involved in the sleep-waked cycle. These differences were observed in: (1) the cholinergic pedunculopontine (PPT) and laterodorsal tegmental (LDT) nucleus, where CR+ interneurons were observed in low and medium densities respectively; (2) the catecholaminergic locus coerulues complex where A6d had a medium-density of CR+ interneurons whereas the A7sc had a low-density of these interneurons; (3) the serotonergic dorsal raphe complex where a low-density of CR+ interneurons were observed within the midline components of this complex (DRd, DRv and DRif nuclei), whereas a medium-density of CR+ interneurons were observed in the lateral and peripheral (DRl, DRp and DRc nuclei) regions of this complex. Finally the

results of the present study indicated observable differences in the density of orexinergic (Orx+) terminal networks between rhythmic and arrhythmic chronotypes. These differences were observed in the hypothalamic arcuate nucleus and intergeniculate leaflet, both of which had a high-density Orx+ terminal network in the rhythmic chronotype as opposed to a medium-density Orx+ terminal network in the arrhythmic chronotype.

6.4.1 Comparison of cholinergic, catecholaminergic, serotonergic and orexinergic nuclei and serotonergic, orexinergic and histaminergic terminal networks to other rodents

The similarity of nuclei and nuclear complexes of the cholinergic, catecholaminergic serotonergic and orexinergic systems of the distinct circadian chronotypes of mole rat in the present study to previously published reports of other mole rats and rodents (see Bhagwandin et al., 2008, 2011 for detailed references) indicates a strong phylogenetic constraint at the systems level of nuclear organisation despite differences in lifestyle, phenotype and circadian rhythmicity. The results of the present study provide an extension of the hypothesis proposed by Manger (2005) that suggests the complement of homologous nuclei at the systems level of neuronal organisation will remain the same amongst species of a mammalian order irrespective of brain size, phenotype and life history. Similarly, the results of the present study indicate phylogenetic constraints acting on the distribution of serotonergic, orexinergic and histaminergic terminal networks when compared to other rodents and mammals as no

major differences were observed (Inagaki et al., 1988; Leger et al., 2001; Nixon and Smale, 2007).

6.4.2 GABAergic interneurons

The neuroanatomical relations of the GABAergic neuronal subtypes has not been comprehensively studied in relation to nuclei involved in the regulation of sleep-wake states. GABAergic neurons are known to play a central role in the sleep-wake cycle, such as, for example, directly or indirectly inhibiting cholinergic neurons of the basal forebrain and the histaminergic cells of the posterior hypothalamus causing deactivation of the cerebral cortex (Lyamin et al., 2008), and inhibiting serotonergic and noradrenergic neuronal populations of the brainstem (Nitz and Siegel, 1997a,b). These actions in combination with observed maximal GABAergic activity during slow wave sleep (SWS) and minimal activity during waking, make GABAergic neurons potent sleep-promoters (Szymusiak, 1995; Szymusiak et al., 2001; Siegel, 2004). The differential expression of three calcium binding proteins calbindin (CB), caretinin (CR) and parvalbumin (PV) defines three subtypes of GABAergic interneurons (Celio, 1986, 1990; Hendry et al., 1989; Jacobowitz and Winsky, 1991; Van Brederode et al., 1991; Biambridge et al., 1992; Rodgers, 1992; Kubota et al., 1994). It has been demonstrated that each subtype has a particular firing pattern: calbindin interneurons are associated with regular spiking characterised by a marked accommodation; calretinin interneurons are associated with bursts of spiking at irregular frequencies; and parvalbumin interneurons are associated with fast spiking displaying tonic discharges of fast action potentials with no accommodation (Cauli et al., 1997). Therefore in accordance with the results of the

present study it would seem fair to infer that the ubiquitous distribution of CB+ interneurons in relation to identified sleep-wake nuclei may possibly maintain a particular state as a result of their regular spiking action potentials. The differential and lower density distribution of CR+ neurons in relation to sleep-wake nuclei may play a role in state transitions as a result of their pattern of irregular spiking. It is interesting that within the midline nuclei of the serotonergic dorsal raphe complex, the cholinergic pedunculopontine and laterodorsal tegmental nuclei and the catecholaminergic locus coeruleus that the density of CR+ neurons was quite low. This may indicate that these nuclei interact with different GABAergic pathways as has been previously demonstrated with the inhibition of perifornical lateral hypothalamic orexinergic neurons by the GABAergic rich median preoptic nucleus (Gong et al., 2002; McGinty et al., 2004).

The open question that is the current study raises is the understanding of which of the calcium binding subtypes of GABAergic neurons are involved during the particular states, or state transitions, of the sleep-wake cycle. It has been shown that GABAergic neurons within the basal forebrain and anterior hypothalamus are maximally active during SWS, have a reduced level of activity during REM sleep and display minimal activity during waking (Syzmusiak, 1995; Syzmusiak et al., 2001; Siegel, 2004). Similar activity has been noted with some of the GABAergic neurons found in the tegmentum of the midbrain and the pons (Nitz and Siegel, 1997a,b). Furthermore, cessation of brainstem serotonergic and noradrenergic nuclear activity by the application of GABA triggers REM (Nitz and Siegel, 1996; Nitz and Siegel, 1997a,b). It is known that GABAergic neurons have short-range and long-range projections (Ascoli et al., 2008). Therefore it is likely that the observed CB+ and CR+ interneurons found adjacent to- and

intermingled with- identified sleep-wake nuclei, through local activity and their specific action potential firing patterns, may induce inhibition of wake active nuclei during sleep and inhibit sleep active neurons during waking. This hypothesis is, however, very speculative and a great deal more work is necessary to clarify this situation.

6.4.3 Rhythmic *vs* arrhythmic differences

The results of the present study indicated a high-density orexinergic (Orx+) terminal network in the hypothalamic arcuate nucleus of the rhythmic chronotype but a medium-density Orx+ terminal network within the same nucleus of the arrhythmic chronotype. The strong reciprocal connections between leptin-sensitive neurons of the arcuate nucleus and orexinergic neurons of the lateral hypothalamus provide an argument for orexinergic involvement in signalling pathways associated with feeding (Broberger et al., 1998; Elias et al., 1998; Horvath et al., 1999; Guan et al., 2001). The observed decrease in Orx+ terminal network density could indicate a decrease in orexinergic involvement in the signalling pathway associated with feeding possibly resulting in decreased food intake. Therefore it would seem fair to infer that the decrease in orexinergic density within the arrhythmic chronotype of the current species of mole rat may facilitate enhanced arousal and vigilance behaviour rather than feeding behaviour.

The results of the present study also indicated a less dense orexinergic terminal network within the intergeniculate leaflet (IGL) of the arrhythmic chronotype of mole rat. It is known that the afferent projections of certain types of retinal ganglion cells are bifurcated and terminate in both the surprachaismatic nucleus (SCN) and the IGL (Pickard, 1985). Despite the reduced eye size and regressed visual system of mole rats the

responses of the circadian rhythm to light remains intact as mole rats are able to entrain their circadian activity rhythms to the light-dark cycle (Oosthuizen et al., 2010). The IGL, part of the non-image forming visual system, projects to the SCN (Mrosovsky, 1995) and neuropeptide-Y cells of the IGL exhibit orexinergic fibre appositions and as a result orexins pose as a potential source of activity state feedback to the IGL (Nixon and Smale, 2005). Therefore the reduction in the density of the orexinergic terminal network observed within the IGL of the arrhythmic chronotype may compromise activity state feedback to the circadian system which may result in differences in patterns of daily activity resulting in the two types of chronotypes within the same species of mole rat.

Chapter 7 - Conclusion

7.1 Concluding Remarks

The oscillatory discharge of neuronal populations within the basal forebrain, hypothalamus and ponto-medullary junction results in the physiological phenomenon that is commonly referred to as the sleep-wake cycle (Siegel, 1990; Lyamin et al., 2008), and this cycle has been investigated behaviourally and physiologically in many mammalian species (McNamara et al., 2008). The present series of studies was aimed at investigating the somnogenic system in representatives of an unusual family of rodents – the Bathyergid mole rats, which are known for their subterranean lifestyle, regressed visual system (Cooper et al., 1993; Hart et al., 2004; Nemec et al., 2004; McMullen et al., 2010) and unusual patterns of circadian rhythmicity (Lovegrove and Papenfus, 1995; Lovegrove and Muir, 1996). Locomotor activity studies have demonstrated the coexistence of distinct circadian chronotypes (i.e. rhythmic and arrhythmic) within a species of mole rat (Oosthuizen et al., 2003), therefore these unusual rodents provide a good model to test the interplay of sleep physiology, circadian rhythmicity and the anatomy of the somnogenic system.

This series of studies started with the neuroanatomical examination of the cholinergic, catecholaminergic and serotonergic systems in the brains of the Highveld mole rat (*Cryptomys hottentotus*) and the Cape-dune mole rat (*Bathyergus suillus*) – systems that are involved in promoting arousal and maintaining wakefulness (McGinty and Szymusiak, 2005). The results of this study indicated that the location and morphology of the neurons of these systems in the mole rats were similar to those

previously reported in other rodents and mammals despite noteworthy differences in lifestyle, phenotype and circadian rhythmicity. These results are congruent with the hypothesis that the systems level of neuronal organisation remains similar amongst the species of an order irrespective of lifestyle, phenotype or phylogenetic relationships (Manger, 2005); however, it was observed that the mole rats investigated in this study showed a weakly represented cholinergic parabigeminal nucleus, in terms of number of neurons, compared to other rodents and mammals. This low neuronal number within the parabigeminal nucleus of these mole rats is consistent with the reduced visual system of these rodents as previously suggested (Da Silva et al., 2006).

In 1998, two research groups simultaneously discovered that the activity of two peptides contributed significantly to the maintenance of wakefulness and motivated behaviour. These peptides are commonly referred to as orexin-A and orexin-B (also known as hypocretin-1 and hypocretin-2 respectively) (De Lecea et al., 1998; Sakurai et al., 1998). That orexins promote wakefulness motivated the investigation of the distribution of orexinergic neurons and terminal networks in the brains of two species of African mole rat (Highveld mole rat - *Cryptomys hottentotus*; and Cape-dune mole rat - *Bathyergus suillus*). The results of this study indicated that in both species of mole rats orexinergic neurons were limited to the hypothalamus and formed three distinct clusters, a large homogenous cluster spanning the lateral and perifornical regions, a cluster extending into the region of the zona incerta and a final cluster in the ventral hypothalamus adjacent to the optic tracts. These results share many similarities to other rodents studied to date, but no orexinergic neurons could be identified within the anterior hypothalamic paraventricular subnucleus in either species as was previously reported in

Murid rodents (Nixon and Smale, 2007). This is not the first time such a Murid *vs* non-Murid difference has been observed for such systems in rodents (Bhagwandin et al., 2006). Orexinergic terminal networks were more strongly expressed in the Cape-dune mole rat compared to the Highveld mole rat; however, the distribution of terminal networks in both species, for the most part, was congruent with those reported in other rodents. Interestingly, despite the reduced superior colliculus noted for mole rats, a medium-density orexinergic terminal network was observed in this region, whereas the homologous region in other rodents have a low-density orexinergic terminal network. Furthermore, only the Cape-dune mole rat exhibited a high-density orexinergic terminal network within area postrema (AP), whereas the same region in all other rodents studied to date have reported a low to medium-density orexinergic terminal network. What these differences in terminal network density actually mean in a functional sense is currently unclear.

From the results obtained in the studies reported in chapters 2 and 3 it was evident that despite the subterranean lifestyle and regressed visual capabilities characteristic of mole rats the neuroanatomy of the cholinergic, catecholaminergic, serotonergic and orexinergic arousal systems remained remarkably similar to other rodents. Interest subsequently developed as to whether notable differences existed in the sleep patterns of mole rats compared to other rodents and whether sleep patterns were significantly different in the distinct circadian chronotypes of a species of mole rat. In chapter 4, sleep was physiologically and behaviourally recorded in distinct circadian chronotypes of the giant Zambian mole rat (*Cryptomys mechowi*). Both circadian chronotypes of mole rat in this study showed physiological criteria characteristic of waking, slow wave sleep (SWS)

and rapid eye movement (REM) sleep. The results indicated that the arrhythmic individuals spent more time in the state of wake, with a longer average duration of a waking episode, and less time in SWS, with a shorter average duration of a SWS episode, though with a greater slow wave sleep intensity. The increase in sleep intensity is congruent with Tobler's (1995) findings that show consistent increases in slow wave activity (SWA) during SWS, an accepted measure of sleep intensity, in sleep deprived mammals. Total time spent in sleep (TST) for both chronotypes of this rodent species was shorter than that seen in other rodents. This was a result of the species studied spending less time in SWS compared to other rodents, as the amount of time spent in REM sleep was within the range, though at the upper end of the range, reported previously for other rodents. An additional possible explanation for the discrepancy observed between the mole rats of the current study and other rodents could lie in the genetic variation of these rodents. Some of the classic sleep disorders have been associated with single gene mutations (Kimura and Winkelmann, 2007) and several studies have identified genomic regions that contain allelic variations affecting quantifiable sleep parameters commonly referred to as quantitative trait loci (QLT) (Tafti et al., 1997; Tafti, 2007). It was interesting that the average duration of a REM episode remained similar between chronotypes yet was slightly longer compared to other rodents. It has been shown that REM activity is maximal when body temperature is lowest (Dijk and Franken, 2005). Mole rats are known to have lower body temperatures compared to surface dwelling mammals (Bennett and Faulkes, 2000), therefore it could be possible that the extended duration of a REM episode compared to other rodents is regulated in relation to body temperature irrespective of chronotype. In addition, the observed

increase in slow wave activity (SWA) during SWS of the arrhythmic group was congruent with genetic manipulation and suprachiasmatic nuclear (SCN) ablation studies that postulate independence of circadian rhythmicity and sleep homeostasis (Dijk and Franken, 2005).

The statistically significant increase in the time spent in waking and the duration of an episode of waking in the arrhythmic group presents an interesting conundrum in the sense that there are several neural systems implicated in arousal behaviour and maintenance of wakefulness. The question of which neuromodulatory system to investigate was directed by evidence demonstrating decreased numbers of orexinergic neurons in narcoleptic individuals (Siegel, 1999). Conversely, increased activity of orexinergic neurons has been demonstrated during wakefulness and motivated behaviour (Estabrooke et al., 2001; Mileykovskiy et al., 2005; Lee et al., 2005). Therefore in chapter 5, orexinergic cell bodies within the brains of rhythmic and arrhythmic circadian chronotypes from three species of African mole rat (Highveld mole rat - *Cryptomys hottentotus pretoriae*, Ansel's mole rat – *Fukomys anselli* and the Damaraland mole rat – *Fukomys damarensis*) were identified using immunohistochemistry for orexin-A. Immunopositive orexinergic (Orx+) cell bodies were stereologically assessed and absolute numbers of orexinergic cell bodies were determined for the distinct circadian chronotypes of each species of mole rat examined. The aim of the study was to investigate whether the absolute numbers of identified orexinergic neurons differed between distinct circadian chronotypes with the hypothesis of elevated hypothalamic orexinergic neurons in the arrhythmic chronotypes compared to the rhythmic chronotypes. Statistically significant differences between the circadian

chronotypes of *F. anselli* were identified, where the arrhythmic group had higher mean numbers of hypothalamic orexin neurons compared to the rhythmic group. These differences were observed when the raw data was compared and when the raw data was corrected for body mass (M_b) and brain mass (M_{br}). *C. hottentotus pretoriae* showed similar tendencies though the data was not significantly different. Analysis of *F. damarensis* revealed data that was opposite to the trend identified in the other two species, though this data was not statistically significant. Given the previous suggestions for the role of orexins in the sleep-wake cycle (Siegel, 2004; Baumann and Bassetti, 2005), it would seem fair to infer that the elevated numbers of hypothalamic orexinergic neurons observed in the arrhythmic chronotypes of *F. anselli* and *C. hottentotus pretoriae*, through possible increased activity and the resulting effect on wakefulness and motor activities, may facilitate a higher level of vigilance allowing for extended foraging and feeding activity compared to the rhythmic chronotype. Additionally, comparisons of hypothalamic orexinergic counts between all rhythmic and arrhythmic individuals only showed a statistically significant difference when orexinergic counts were corrected for body mass (M_b) where the arrhythmic individuals had higher hypothalamic orexinergic counts. Since the discovery of orexins in 1998, these peptides have also become synonymous with appetite regulation and increased food intake that is driven by involvement in motivated behaviour. This in combination with increased orexinergic counts would theorectically indicate increased body mass in arrhythmic individuals; however, this was not the case as arrhythmic individuals had a lower mean body mass compared to the rhythmic individuals. A possible explanation could lie in the metabolism of arrhythmic individuals, as Nicolaidis (2006) suggests that based on resting metabolic

rate, a hypometabolic but physically active animal has a higher (total) metabolism than a hypermetabolic animal that remains quiet. This supports the mole rats of the current study as it has been previously reported that subterranean mole rats have lower resting metabolic rates than surface dwelling mammals (Bennett and Faulkes, 2000). Incidentally, brain metabolism is controlled independent of peripheral body metabolism, but metabolically strategic areas within the brain are capable of reflecting changes in peripheral body metabolism (Nicolaidis, 2006). Therefore, it may be possible that a higher peripheral metabolism may result in a lower body mass despite the elevated Orx+ neurons observed in the arrhythmic chronotype compared to the rhythmic chronotype.

In chapters 4 and 5 it was determined that the arrhytyhmic chronotype was physiologically more awake than its rhythmic counterpart and this finding was supported by the elevated hypothalamic orexinergic numbers in the arrhythmic chronotype; however, in order to further understand the sleep-wake cycle its neuranatomical substrates need to be investigated. Therefore interest arose as to whether potential differences existed in the nuclear complement and the distribution of terminal networks related to nuclei of the sleep-wake cycle between the distinct circadian chronotypes. Subsequently, brains of the giant Zambian mole rat (*Cryptomys mechowi*), from the individuals in which sleep was recorded, were immunohistochemically examined for choline acetyltransferase (ChAT), tyrosine hydroxylase (TH), serotonin (5HT), orexin (Orx), histamine and the calcium binding proteins calbindin (CB), calretinin (CR) and parvalbumin (PV). The cholinergic, catecholaminergic, serotonergic, orexinergic and histaminergic systems are frequently associated with arousal and maintenance of wakefulness and GABAergic neurons are known to promote sleep (Siegel, 2004). The

results of this study indicated similarity in nuclei and distribution of terminal networks of the cholinergic, catecholaminergic, serotonergic and orexinergic systems between the circadian chronotypes and all other rodents and mammals previously examined (Bhagwandin et al., 2008, 2011).The distribution of histaminergic terminal networks remained similar between circadian chronotypes and other rodents (Inagaki et al., 1988). These results indicate a strong phylogenetic constraint at the systems level of mammalian neuronal organisation. Despite this broad similarity, two differences were observed in the distribution of orexinergic terminal network within the hypothalamic arcuate nucleus and the intergeniculate of the thalamus where the arrhythmic chronotype displayed a reduced orexinergic terminal network in both regions. It could be possible that these differences may enhance vigilance and arousal behaviour relative to feeding behaviour and may also compromise activity state feedback to the circadian system that could alter the daily activity patterns in the arrhythmic chronotype, findings which are partly indicated and supported by the results in chapter 4. The GABAergic subtypes examined in this study have previously been separated based on their rates of depolarization. Fast spiking neurons with no accommodation have been associated with parvalbumin, regular spiking neurons with calbindin and irregular spiking neurons with calretinin (Celio, 1986, 1990; Hendry et al., 1989; Jacobowitz and Winsky, 1991; Van Brederode et al., 1991; Biambridge et al., 1992; Rodgers, 1992; Kubota et al., 1994). GABAergic neurons of the basal forebrain and anterior hypothalamus as well as the brainstem are known to inhibit local wake active neurons (Nitz and Siegel, 1997a,b; Lyamin et al., 2008). The results of this study showed no association of parvalbumin with sleep-wake related nuclei, a ubiquitous association of calbindin with sleep-wake nuclei and a ubiquitous, but less

numerous, calretinin association with sleep-wake nuclei. Given the spiking rates of calbindin and calretinin it seems likely that calbindin may be involved in the maintenance of a physiological state such as wake, SWS or REM, whereas calretinin may be involved in state transitions. Despite the observed differences of calbindin and calretinin within the cholinergic, catecholaminergic, serotonergic and orexinergic nuclei, it is also possible that these regions are also under the influence of distantly located GABAergic inerneuronal populations, similar to those previously reported in the anterior hypothalamus (Gong et al., 2002; McGinty et al., 2004). The study of the relationship of GABAergic neuronal subtypes and the sleep systems is an area that needs a great deal of future research, especially in a comparative neuroanatomical setting.

7.2 Future Directions

Despite the studies carried out here, many unanswered questions still remain and many were raised in the course of these studies. It would be useful to concurrently record body temperature, brain temperature, electroencephalogram (EEG), electromyogram (EMG), and behaviour in circadian chronotypes of mole rats. The peaks and troughs of body temperature and brain temperature associated with physiologically defined sleep and wake states may provide a more holistic picture of the baseline sleep-wake patterns in these unusual rodents. It would be interesting to determine from such a study whether body temperature differs between circadian chronotypes within a species of mole rat. It will also be of interest to determine the level of correlation between body temperature and brain temperature during physiologically defined sleep and wake states and note whether a trend such as increases in brain temperature when body temperature is at its

lowest range can be associated with the onset of REM sleep in distinct circadian chronotypes of mole rat. Additionally examination of the genetic composition, specifically the loci of chromosomes 5, 7, 12 and 17 which have been associated with the vigilance phenotype in mice (Tafti, 1997), may provide further details regarding the genetic control of sleep in circadian chronotypes of mole rat and may explain the difference in sleep architecture observed between mole rats and other rodents (see chapter 4).

To further understand the puzzling nature of increased numbers of orexinergic neurons that was associated with lower body mass in the arrhythmic chronotype compared to the rhythmic chronotype, a study concurrently measuring the locomotor and resting metabolic rates of the brain and peripheral body tissues may provide a more clear understanding of the role of orexin in the brain of distinct circadian chronotypes. Furthermore, single unit recordings from hypothalamic orexinergic meurons in the brains of distinct circadian chronotypes during normal behaviour, induced fasting behaviour and hyperphagic behaviour may shed light on the level of activity of, and possible role of, orexinergic neurons in motivated behaviour. Similar single unit recordings of hypothalamic orexinergic neurons in the brains of distinct circadian chronotypes of mole rat during waking, SWS and REM may shed light on the level of orexinergic activity during physiologically defined sleep and wake states. These single unit recordings may indicate whether orexins in the brains of circadian chronotypes are more closely associated with arousal and maintenance of wakefulness or regulation of appetite and increased food intake. It could also be possible that orexins play a role in both these processes, but additional understanding of metabolic rate in distinct circadian

chronotypes of mole rats could provide an answer to the finding of elevated numbers of orexinergic neurons in arrhythmic mole rats. Additional single unit recordings of calbindin, calretinin and parvalbumin GABAergic activity in relation to the activity of wake promoting neurons of the basal forebrain, hypothalamus and pontine region during sleep and wake states may provide a better understanding of the sleep-wake cycle in distinct circadian chronotypes of mole rat as well as shed more light on the mechanisms of action of the calcium binding GABAergic interneurons.

The African mole rats are clearly very unusual creatures in many respects. Given that the Bathyergidae are an evolutionary successful radiation of the rodents and that many of the unusual aspects of their anatomy and physiology have been determined, future studies of mole rats could serve to test hypotheses regarding sleep and circadian rhythm in very specific ways.

7.3 Limitations

One limitation that may arise from this thesis is the comparison between species across studies. Whilst neuroanatomically such comparisons are possible under the argument of phylogenetic constraint it is more difficult when drawing conclusions between neuroanatomy and physiology. Therefore it would be useful in other studies emerging from this thesis to increase the sample size in for example a study such as that comparing neuronal numbers within species and between species.

8. References

Adkins, R.M., Walton, A.H., Honeycutt, R.L., 2003. Higher-level systematics of rodents and divergence time estimates based on two congruent nuclear genes. Molecular Phylogenetics and Evolution. 26, 409-420.

Alfodi, P., Tobler, I., Borbely, A.A., 1990. Sleep regulation in rats during early development. American Journal of Physiology - Regulatory, Integrative and Comparative Physiology 258, R634-R644.

Allison, T., Van Twyver, H., 1970. The evolution of sleep. Natural History 79, 56-65.

Ambrosini, M. V., Gambelunghe, C., Mariucci, G., Bruschelli, G., Adami, M., Guiditta, A., 1994. Sleep-wake variables and EEG power spectra in Mongolian gerbils and Wistar rats. Physiology and Behaviour 56, 963-968.

Armstrong, D.M., Saper, C.B., Levey, A.I., Wainer, H., Terry, R.D., 1983. Distribution of cholinergic neurons in rat brain: demonstrated by the immunocytochemical localization of choline acetyl transferase. Journal of Comparative Neurology 216, 53-68.

Ascoli, G.A., Alonso-Nanclares, L., Anderson, S.A., Barrionuevo, G., Benavides-Piccione, R., Burkhalter, A., Buzsáki, G., Cauli, B., DeFelipe, J., Fairén, A., Feldmeyer, D., Fishell, G., Fregnac, Y., Freund, T.F., Gardner, D., Gardner, E.P., Goldberg, J.H., Helmstaedter, M., Hestrin, S., Karube, F., Kisvárday, Z.F., Lambolez, B., Lewis, D.A., Marin, O., Markram, H., Muñoz, A., Packer, A., Petersen, C.C.H., Rockland, K.S., Rossier, J., Rudy, B., Somogyi, P., Staiger, J.F., Tamas, G., Thomson, A.M., Toledo-Rodriguez, M., Wang, Y., West, D.C., Yuste, R., 2008. Petilla terminology: nomenclature of features of GABAergic interneurons of the cerebral cortex. Nature Reviews Neuroscience 9, 557-568.

Ayala-Guerrero, F., Vargas-Reyna, L., Ramos, J. I., Mexicano, G., 1998. Sleep patterns of the volcano mouse (*Neotomodon alstoni alstoni*). Physiology and Behaviour 64, 557-580.

Baimbridge, K.G., Celio, M.R., Rogers, J.H., 1992. Calcium-binding proteins in the nervous system. Trends in Neuroscience 15, 303–308.

Baldo B.A., Daniel R.A., Berridge C.W., Kelley A.E., 2003. Overlapping distributions of orexin/hypocretin- and dopamine-ß-hydroxylase immunoreactive fibers in rat brain. Regions mediating arousal, motivation, and stress. Journal of Comparative Neurology 464, 220–237.

Baumann, C.R., Bassetti, C.L., 2005. Hypocretins (orexins): clinical impact of the discovery of a neurotransmitter. Sleep Medicine Reviews 9, 253-268.

Bennett, N.C., Jarvis, J.U.M., 1988. The reproductive biology of the Cape mole-rat, *Georychus capensis* (Rodentia: Bathyergidae). Journal of Zoology London 214, 95-106.

Bennett, N.C., 1992. The social behaviour of a captive colony of thye common mole-rat *Cryptomys hottentotus* from South Africa. Zeitschrift Säugetierk 57, 294-309.

Bennett, N.C., Faulkes, C.G., 2000. African Mole-Rats: Ecology and Eusociality. Cambridge University Press, United Kingdom.

Berthoud, H.R., Patterson, L.M., Sutton, G.M., Morrison, C., Zheng, H., 2005. Orexin inputs to caudal raphe neurons involved in thermal, cardiovascular, and gastrointestinal regulation. Histochemical Cell Biology 123, 147-156.

Bhagwandin, A., Fuxe, K., Manger, P.R., 2006. Choline acetyltransferase immunoreactive cortical interneurons do not occur in all rodents: a study of the phylogenetic occurrence of this neural characteristic. Journal of Chemical Neuroanatomy 32, 208-216.

Bhagwandin, A., Fuxe, K., Bennett, N.C., Manger, P.R., 2008. Nuclear organization and morphology of cholinergic, putative catecholaminergic and serotonergic neurons in the brains of two species of African mole-rat. Journal of Chemical Neuroanatomy 35, 371-387.

Bhagwandin, A., Fuxe, K., Bennett, N.C., Manger, P.R., 2011. Distribution of orexinergic neurons and their terminal networks in the brains of two species of African mole rats. Journal of Chemical Neuroanatomy 41, 32-42.

Bjarkam, C.R., Sorensen, J.C., Geneser, F.A., 1997. Distribution and morphology of serotonin-immunoreactive neurons in the brainstem of the New Zealand white rabbit. Journal of Comparative Neurology 380, 507–519.

Björklund, A., Lindvall,O., 1984. Dopamine-containing systems in the CNS. In: Björklund, A., Hökfelt, T., Handbook of Chemical Neuroanatomy, vol. 2. Classical Neurotransmitters in the CNS, part 1. Elsevier, Amsterdam.

Blanga-Kanfi, S., Miranda, H., Penn, O., Pupko, T., DeBry, R.W., Huchon, D., 2009. Rodent phylogeny revisited: analysis of six nuclear genes from all major rodent clades. BMC Evolutionary Biology 9: 71.

Borbély, A.A., Neuhaus, U., 1979. Sleep-deprivation: effects on sleep and EEG in the rat. Journal of Comparative Physiology 133, 71-87.

Bourgin, P., Huitron-Resendiz, S., Spier, A.D., Fabre, V., Morte, B., Criado, J.R., Sutcliffe, J.G., Henriksen, S.J., de Lecea, L., 2000. Hypocretin-1 modulates rapid eye movement sleep through activation of locus coeruleus neurons. Journal of Neuroscience 20, 7760–7765.

Broberger, C., de Lecea, L., Sutcliffe, J.G., Hokfelt ,T., 1998. Hypocretin/orexin and melanin-concentrating hormone-expressing cells form distinct populations in the rodent lateral hypothalamus: relationship to the neuropeptide Y and agouti gene-related protein systems. Journal of Comparative Neurology 402, 460–74.

Burda, H., Kawalika, M., 1993. Evolution of eusociality in the Bathyergidae: the case of the giant mole-rat (*Cryptomys mechowi*). Naturwissenschaften 80, 235-237.

Bux, F., Bhagwandin, A., Fuxe, K., Manger, P.R., 2010. Organization of cholinergic, putative catecholaminergic and serotonergic nuclei in the diencephalon, midbrain and pons of sub-adult male giraffes. Journal of Chemical Neuroanatomy 39, 189-203.

Cai, X.J., Evans, M.L., Lister, C.A., Leslie, R.A., Arch, J.R.S., Wilson, S., Williams, G., 2001. Hypoglycaemia activates orexin neurons and selectively increases hypothalamic orexin-B levels. Responses inhibited by feeding and possibly mediated by the nucleus of the solitary tract. Diabetes 50, 105-112.

Campbell, S.S., and Tobler, I., 1984. Animal Sleep: A review of sleep duration across phylogeny. Neuroscience and Behavioural Reviews 8, 296-300.

Capellini, I., Barton, R.A., McNamara, P., Nunn, C.L., 2008. A phylogenetic analysis of the ecology and evolution of mammalian sleep. Evolution 62, 1764-1776.

Cauli, B., Audinat, E., Lambolez, B., Angulo, M.C., Ropert, N., Tsuzuki, K., Hestrin, S., Rossier, J., 1997. Molecular and physiological diversity of cortical nonpyramidal cells. Journal of Neuroscience 17, 3894-3906.

Celio, M.R., 1986. Parvalbumin in most gamma-aminobutyric acid containing neurons of the rat cerebral cortex. Science 231, 995–997.

Celio, M.R., 1990. Calbindin D-28k and parvalbumin in the rat nervous system. Neuroscience 35, 375– 475.

Cernuda-Cernuda, R., García-Fernández, J.M., Gordijn, M.C.M., Bovee-Geurts, P.H.M., DeGrip, W.J., 2003. The eye of the African mole-rat *Cryptomys anselli*: to see or not to see? European Journal of Neuroscience 17, 709-720.

Chemelli, R.M., Willie, J.T., Sinton, C.M., Elmquist, J.K., Scammell, T., Lee, C., Richardson, J.A., Williams, S.C., Xiong, Y., Kisanuki, Y., Fitch, T.E., Nakazato, M., Hammer, R.E., Saper, C.B., Yanagisawa, M., 1999. Narcolepsy in orexin knockout mice: molecular genetics of sleep regulation. Cell 98, 437-451.

Chen, C.T., Dun, S.L., Kwok, E.H., Dun, N.J., Chang, J.K., 1999. Orexin A-like immunoreactivity in the rat brain. Neuroscience Letters 260, 161-164.

Chepkasov, I. E., 1980. Daily rhythm of sleep and wakefulness in the Arctic ground squirrel (*Citellus parryi*) during the summer season. Zhurnal Evoliutsionnoi Biokimii Fiziologii 17, 77-80.

Chimimba, C.T., Bennett, N.C., 2005. Order Rodentia. In: Skinner, J.D., Chimimba, C.T., The mammals of the Southern African Subregion, 2005, Cambridge University Press.

Chou, T.C., Bjorkum, A.A., Gaus, S.E., Lu, J., Scammell, T.E., Saper, C.B., 2002. Afferents to the ventrolateral preoptic nucleus. Journal of Neuroscience 22, 977–990.

Chou, T.C., Rotman, S.R., Saper, C.B., 2004. Lateral hypothalamic acetylcholinesterase-immunoreactive neurons co-express either orexin or melanin concentrating hormone Neuroscience Letters 370, 123–126.

Cooper, H.M., Herbin, M., Nevo., 1993. Visual system of a naturally microphthalamic mammal: the blind mole rat, *Spalax ehrenbergi*. Journal of Comparative Neurology 328, 313-350.

Crutcher, K.A., Humbertson, A.O., 1978. The organization of monoamine neurons within the brainstem of the North American opossum (*Didelphis virginiana*). Journal of Comparative Neurology 179, 195-222.

Cutler, D.J., Morris, R., Sheridhar, V., Wattam, T.A.K., Kolmes, S., Patel, S., Atch, J.R.S., Wilson, S., Buckingham, R.E., Evans, M.L., Leslie, R.A., Williams, G., 1999. Differential distribution of orexin-A and orexin-B immunoreactivity in the rat brain and spinal cord. Peptides 20, 1455-1470.

Czeisler, C.A., Weitzman, E.D., Moore-Ede, E.D., Zimmerman, J.C., Knauer, R.S., 1980. Human sleep: Its duration and organisation dependant on its circadian phase. Science 210, 1264-1267.

Dahlström, A., Fuxe, K., 1964. Evidence for the existence of monoamine-containing neurons in the central nervous system. I. Demonstration of monoamine in the cell bodies of brainstem neurons. ACTA Physiologica Scandinavica 62, 1-52.

Danguir, J., Nicolaidis, S., 1980. Cortical activity and sleep in the rat lateral hypothalamic syndrome. Brain Research 185, 305-321.

Danguir, J., Nicolaidis, S., 1980. Intravenous infusion of nutrients and sleep in the rat: an ischymetric sleep regulation hypothesis. American Journal of Physiology 238, E307-E312.

Da Silva, J.N., Fuxe, K., Manger, P.R., 2006. Nuclear parcellation of certain immunohistochemically identifiable neuronal systems in the midbrain and pons of the Highveld mole-rat (*Cryptomys hottentotus*). Journal of Chemical Neuroanatomy 31, 37-50.

http:/www.datasci.com

Date, Y., Ueta, Y., Yamashita, H., Yamaguchi, H., Matsukura, S., Kangawa, K., Sakurai, T., Yanagisawa, M., Nakazato, M., 1999. Orexins, orexigenic hypothalamic peptides, interact with autonomic, neuroendocrine and neuroregulatory systems. Proceedings of the National Academy of Sciences, USA 96, 748-753.

Daszuta, A., Portalier, P., 1985. Distribution and quantification of 5-HT nerve cell bodies in the nucleus raphe dorsalis area of C57BL and BALBc mice. Relationship between anatomy and biochemistry. Brain Research 360, 58-64.

Deboer, T., Franken, P., Tobler, I., 1994. Sleep and cortical temperature in the Djungarian hamster under baseline conditions and after sleep deprivation. Journal of Comparative Physiology 174, 145-155.

De Graaf, G., 1971. Family Bathyergidae. In: Meester, J., Setzer, H.W., The Mammals of Africa: An Identification Manual. Smithsonian Institution Press, Washington DC.

De Graaf, G., 1981. The rodents of Southern Africa. Butterworth, Johannesburg.

Dell, L.A., Kruger, J.L., Bhagwandin, A., Jillani, N.E., Pettigrew, J.D., Manger, P.R., 2010. Nuclear organization of cholinergic, putative catecholaminergic and serotonergic systems in the brains of two megachiropteran species. Journal of Chemical Neuroanatomy 40, 177-195.

De Lecea, L., Kilduff, T., Peyron, C., Gao, X.B., Foye, P.E., Danielson, P.E., Fukuhara, C., Battenberg, E.L.F., Gautvik, V.T., Bartlett, F.S., Frankel, W.N., van den Pol, A.N., Bloom, F.E., Gautvik, K.M., Sutcliffe, J.G., 1998. The hypocretins: hypothalamus-specific peptides with neuroexcitatory activity. Proceedings of the National Academy of Sciences, USA 95, 322-327.

D'Este, L., Casini, A, Puglisi-Allegra, S., Cabib, S., Renda, T.G., 2007. Comparative immunohistochemical study of the dopaminergic systems in two inbred mouse strains (C57BL/6J and DBA/2J). Journal of Chemical Neuroanatomy 33, 67-74.

Dijk, D.J., Daan, S., 1989. Sleep EEG spectral analysis in a diurnal rodent: *Eutamias sibiricus*. Journal of Comparative Physiology 165, 205-215.

Dijk, D.J., Franken, P., 2005. Interaction of sleep homeostasis and circadian rhythmicity: Dependant or independat systems? In: Kryger, M.H., Roth, R., and Dement, W.C., Principles and Practices of Sleep Medicine, 4th edition. New York, Saunders.

Dwarika, S., Maseko, B.C., Ihunwo, A.O., Fuxe, K., Manger, P.R., 2008. Distribution and morphology of putative catecholaminergic and serotonergic neurons in the brain of the greater canerat, *Thryonomys swinderianus*. Journal of Chemical Neuroanatomy 35, 108-122.

Ebbesson, S.O., 1980. The parcellation theory and its relation to interspecific variability in brain organization, evolutionary and ontogenetic development, and neuronal plasticity. Cell Tissue Research 213, 179-212.

Edwards,.C.M., Abusnana, S., Sunter, D., Murphy, K.G., Ghatei, M.A., Bloom, S.R., 1999. The effect of the orexins on food intake: comparison with neuropeptide Y, melanin concentrating hormone and galanin. Journal of Endocrinology 160, R7–R12.

Elias, C.F., Saper, C.B., Maratos-Flier, E., Tritos, N.A., Lee, C., Kelly, J., Tatro, J.B., Hoffmann, G.E., Ollmann, M.M., Barsh, G.S., Sakurai, T., Yanagisawa, M., Elmquist, J.K., 1998. Chemically defined projections linking the mediobasal hypothalamus and the lateral hypothalamus. Journal of Comparative Neurology 402, 442-459.

Espana, R.A., Reis, K.M., Valentino, R.J., Berridge, C.W., 2005. Organization of hypocretin/orexin efferents to locus coeruleus and basal forebrain arousal-related structures. Journal of Comparative Neurology 481, 160-178.

Estabrooke, I., McCarthy, M.T., Ko, E., Chou, T.C., Chemelli, R.M., Yanagisawa, M., 2001. Fos expression in orexin neurons varies with behavioral state. Journal of Neuroscience 21, 1656-1662.

Estep, D., Canney, E. L., Cochran, C. C., Hunter, J. L., 1978. Components of activity and sleep in two species of chipmunks: *Tamias striatus* and *Eutomias dorsalis*. Bulletin of the Psychonomic Society 12, 341-343

Ettrup, K.S., Sørensen, J.S., Bjarkam, C.R., 2010. The anatomy of the Göttingen minipig hypothalamus. Journal of Chemical Neuroanatomy 39, 151-165.

Faulkes, C.G., Verheyen, E., Verheyen, W., Jarvis, J.U.M., Bennett, N.C., 2004. Phylogeographical patterns of genetic divergence and speciation in African mole-rats (Family: Bathyergidae). Molecular Ecology 13, 613-629.

Fite, K.V., Janusonis, S., 2001. Retinal projection to the dorsal raphe nucleus in the Chilean degus (*Octodon degus*). Brain Research 895, 139-145.

Folk, M.A., 1963. The daily distribution of sleep and wakefulness in the arctic ground squirrel. Journal of Mammalogy 44, 575-577.

Franken, P., Dijk, D.J., Tobler, I., Borbely, A.A., 1991. Sleep deprivation in the rat: effects of the electroencephalographic power spectra, vigilance states and cortical temperature. American Journal of Physiology 261, R198-R208.

Franken, P., Tobler, I., Borbély, A.A., 1992. Cortical temperature and EEG slow-wave activity in the rat: analysis of vigilance state related changes. Pflügers Arch (European Journal of Physiology) 420, 500-507.

Franken, P., Malafosse, A., Tafti, M., 1998. Genetic variation in the EEG during sleep in inbred mice. American Journal of Physiology 275, R1127-R1137.

Franken, P., Malafosse, A., Tafti, M., 1998. Genetic determinants of sleep regulation in inbred mice. Sleep 22, 155-169.

Fuxe, K., Hökfelt, T., Ungerstedt, U., 1969. Distribution of monoamines in the mammalian central nervous system by histochemical studies. In: Hooper, G., Metabolism of Amines in the Brain. Macmillan, London.

Fuxe, K., Hökfelt, T., Ungerstedt, U., 1970. Morphological and functional aspects of central monoamine neurons. International Review Neurobiology 13, 93–126.

Gallyas, F., 1979. Silver staining of myelin by means of physical development. Neurological Research 1, 203–209.

Gamundi, A., Gonzalez, J., Akaarir, M., Nicolau, M.C., Esteban, S., Coenen, A.M., Rial Planas, R.V., 2003. Dualism and uniformism in sleep. Medical Hypotheses 60, 116-118.

Gaus, S.E., Strecker, R.E., Tate, B.A., Parker, R.A., Saper, C.B., 2002. Ventrolateral preoptic nucleus contains sleep-active galaninergic neurons in multiple mammalian species. Neuroscience 115, 285-294.

Gerashchenko, D., Shiromani, P.J., 2004. Different neuronal phenotypes in the lateral hypothalamus and their role in sleep and wakefulness. Molecular Neurobiology 29, 41-59.

Ginovart, N., Marcel, D., Bezin, L., Garcia, C., Gagne, C., Pujol, J.F., Weissman, D., 1996. Tyrosine hydroxylase expression within Balb/C and C57Black/6 mouse locus coeruleus. I. Topological organization and phenotypic plasticity of the enzyme-containing cell population. Brain Research 721, 11-21.

Gravett, N., Bhagwandin, A., Fuxe, K., Manger, P.R., 2009. Nuclear organization and morphology of cholinergic, putative catecholaminergic and serotonergic neurons in the brain of the rock hyrax, *Procavia capensis*. Journal of Chemical Neuroanatomy 38, 57-74.

Gong, H., McGinty, D., Szymusiak, R., 2002. Projections from the median preoptic nucleus to hypocretin and forebrain cholinergic systems in rats. Sleep 25, A155.

Guan, J-L., Soatome, T., Wang, Q-P., Funahashi, H., Hori, T., Tanaka, S., Shioda, S., 2001. Orexinergic innervation of POMC-containing neurons in the rat arcuate nucleus. NeuroReport 12, 547-551.

Gutjahr, G.H., Janse van Rensburg, L., Malpaux, B., Richter, T.A., Bennett, N.C., 2004. The endogenous rhythm of plasma melatonin and its regulation by light in the highveld mole-rat (*Cryptomys hottentotus pretoriae*): a micropthalmic, seasonally breeding rodent. Journal of Pineal Research 37, 185-192.

Hagan, J.J., Leslie, R.A., Patel, S., Evans, M.L., Wattam, T.A., Holmes, S., 1999. Orexin A activates locus coeruleus cell firing and increases arousal in the rat. Proceedings of the National Academy of Sciences, USA 96, 10911–10916.

Hallanger, A.H., Levey, A. I., Lee, H. J., Rye, D. B., Wainer, B. H., 1987. The origins of cholinergic and other subcortical afferents to the thalamus in the rat. Journal of Comparative Neurology 262, 104–124.

Hammer, O., Harper, D.A.T., Ryan, P.D., 2001. PAST: Paleontological Statistics software package for education and data analysis. Palaeontologia Electronica 4, 9pp.

Hart, L., Bennett, N.C., Malpaux, B., Chimimba, C.T., Oosthuizen, M.K., 2004. The chronobiology of the Natal mole rat, *Cryptomys hottentotus natalensis*. Physiological Behaviour 82, 563-569.

Haynes, A.C., Jackson, B., Overend, P., Buckingham, R.E., Wilson, S., Tadayyon, M., Arch JR., 1999. Effects of single and chronic intracerebroventricular administration of the orexins on feeding in the rat. Peptides 20, 1099.

Henderson, Z., 1987. Overlap in the distribution of cholinergic and catecholaminergic neurons in the upper brainstem of the ferret. Journal of Comparative Neurology 265, 581-592.

Hendry, S.H.C., Jones, E.G., Emson, P.C., Lawson, D.E.M., Heizmann, C.W., Streit, P., 1989. Two classes of cortical GABA neurons defined by differential calcium binding protein immunoreactivities. Experimental Brain Research 76, 467– 472.

Hökfelt, T., Johansson, O., Fuxe, K., Goldstein, M., Park, D., 1976. Immunohistochemical studies on the localization and distribution of monoamine neuron systems in the rat brain. I. Tyrosine hydroxylase in the mes- and diencephalon. Medical Biology 54, 427-53.

Hökfelt, T., Martenson, R., Björklund, A., Kleinau, S., Goldstein, M., 1984. Distributional maps of tyrosine-hydroxylase-immunoreactive neurons in the rat brain. In: Björklund, A., Hökfelt, T., Handbook of Chemical Neuroanatomy, vol. 2. Classical Neurotransmitters in the CNS, part 1. Elsevier, Amsterdam.

Horvath, T.L., Diano, S., van den Pol, A.N., 1999. Synaptic interaction between hypocretin (orexin) and neuropeptide Y cells in the rodent and primate hypothalamus: a novel circuit implicated in metabolic and endocrine regulations. Journal of Neuroscience 19, 1072-1087.

Huber, R., Deboer, T., Tobler, I., 2000. Effects of sleep deprivation on sleep EEG in three mouse strains: empirical data and simulations. Brain Research 857, 8-19.

Hungs, M., Mignot, E., 2001. Hypocretin/orexin, sleep and narcolepsy. Bioessays 12, 397-408.

Hungs, M., Fan, J., Lin, L., Lin, X., Maki, R.A., Mignot, E., 2001. Identification and functional analysis of mutations in the hypocretin (orexin) genes of narcoleptic canines. Genome Research 11, 531-539.

Ichikawa, T., Ajiki, K., Matsuura, J., Misawa, H., 1997. Localization of two cholinergic markers, choline acetyltransferase and vesicular acetylcholine transporter in the central nervous system of the rat: in situ hybridization histochemistry and immunohistochemistry. Journal of Chem Neuroanatomy 13, 23-29.

Inagaki, N., Yamatodani, A., Ando-Yamamoto, M., Tohyama, M., Watanabe, T., Wada, H., 1988. Organisation of histaminergic fibres in the rat brain. Journal of Comparative Neurology 273, 283-300.

Ishimura, K., Takeuchi, Y., Fujiwara, K., Tominaga, M., Yoshioka, H., Sawada, T., 1988. Quantitative analysis of the distribution of serotonin-immunoreactive cell bodies in the mouse brain. Neuroscience Letters 91, 265-270.

Iqbal, J., Pompolo, S., Sakurai, T., Clarke, I.J., 2001. Evidence that orexin-containing neurones provide direct input to gonadotropin-releasing hormone neurones in the ovine hypothalamus. Journal of Neuroendocrinology 13, 1033-1041.

Jacobowitz, D.M., Winsky, L., 1991. Immunocytochemical localization of calretinin in the forebrain of the rat. Journal of Comparative Neurology 304, 198 –218.

Jansa, S.A., Weksler, M., 2004. Phylogeny of the murid rodents: relationships within and among major lineages as determined by IRBP gene sequences. Molecular Phylogenetics and Evolution 31, 256–276.

Janusonis, S., Fite, K.V., 2001. Diurnal variation of c-Fos expression in subdivisions of the dorsal raphe nucleus of the Mongolian gerbil (*Meriones unguiculatus*). Journal of Comparative Neurology 440, 31-42.

Janusonis, S., Fite, K.V., Foote, W., 1999. Topographic organization of serotonergic dorsal raphe neurons projecting to the superior colliculus in the Mongolian gerbil (*Meriones unguiculatus*). Journal of Comparative Neurology 413, 342-355.

Janusonis, S., Fite, K.V., Bengston, L., 2003. Subdivision of the dorsal raphe nucleus projecting to the lateral geniculate nucleus and primary visual cortex in the Mongolian gerbil. NeuroReport. 14, 459-462.

Jarvis, J.U.M., 1969. The breeding season and litter size of African mole-rats. Journal of Reprod. Fert. Suppl. 6, 237-248.

Jarvis, J.U.M., 1981. Eu-sociality in a mammal – cooperative breeding in naked mole-rat *Heterocephalus glaber* colonies. Science 212, 571-573.

John, J., Wu, M.F., Boehmer, L.N., Siegel, J.M., 2004. Cataplexy-active neurons in the hypothalamus: implications for the role of histamine in sleep and waking behaviour. Neuron 42, 619-634.

Johnson, J.I., 1990. Comparative development of somatic sensory cortex. In: Jones, E.G., Peters, A., Cerebral Cortex Volume 8B, Comparative Structure and Evolution of Cerebral Cortex, Part II. New York: Plenum Press.

Jones, B. E., 2003. Arousal systems. Frontiers in Bioscience 8, S438–S451.

Kantor, S., Mochizuki, T., Janisiewicz, A.M., Clark, E., Nishino, S., Scammell, T.E., 2009. Orexin neurons are necessary for the circadian control of REM sleep. Sleep 32, 1127-1134.

Karasawa, N., Takeuchi, T., Yamada, K., Iwasa, M., Isomura, G., 2003. Choline acetyltransferase positive neurons in the laboratory shrew (*Suncus murinus*) brain: coexistence of ChAT/5-HT (Raphe dorsalis) and ChAT/TH (Locus ceruleus). Acta Histochemica et Cytochemica 36, 399-407.

Kas, M.J., Edgar, D. M., 1998. Crepuscular rhythms of EEG sleep-wake in a hystricomorph rodent, *Octodon degus*. Journal of Biological Rhythms 13, 9-17.

Kastaniotis, C., Kaplan, P., 1976. Sleep and wakefulness in the Mongolian gerbil *Meriones unguiculalus.* Sleep Research 5, 96.

Kavanau, J.L., 2002. REM and NREM sleep as natural accompaniments of the evolution of warm-bloodedness. Neurosience Biobehaviour Review 26, 889-906.

Khorooshi, R.M., Klingenspor, M., 2005. Neuronal distribution of melanin-concentrating hormone, cocaine- and amphetamine regulated transcript and orexin-B in the brain of the Djungarian hamster (*Phodopus sungorus*). Journal of Chemical Neuroanatomy 29, 137-148.

Kilduff, T.S., Peyron, C., 2000. The hypocretin/orexin ligand-receptor system: implications for sleep and sleep disorders. Trends in Neuroscience. 23, 359-365.

Kilduff, T.S., Peyron, C., 2000. The hypocretin/orexin ligand-receptor system: implications for sleep and sleep disorders. Trends in Neuroscience 35, 359-365.

Kimura, H., McGeer, P.L., Peng, J.H., McGeer, E.G., 1981. The central cholinergic system studied by choline acetyltransferase immunohistochemistry in the cat. Journal of Comparative Neurology 200, 151-201.

Kimura, M., Winkelmann, J., 2007. Genetics of sleep and sleep disorders. Cellular and Molecular Life Sciences 64, 1216-1226.

Kirouac, G.J., Parsons, M.P., Li, S., 2005. Orexin (hypocretin) innervation of the paraventricular nucleus of the thalamus. Brain Research 1059, 179-188.

Kitahama, K., Geffard, M., Okamura, H., Nagatsu, I., Mons, N., Jouvet, M., 1990. Dopamine- and dopa-immunoreactive neurons in the cat forebrain with reference to tyrosine hydroxylase-immunohistochemistry. Brain Research 518, 83-94.

Kitahama, K., Sakamoto, N., Jouvet, A., Nagatsu, I., Pearson, J., 1996. Dopamine-beta-hydroxylase and tyrosine hydroxylase immunoreactive neurons in the human brainstem. Journal of Chemical Neuroanatomy 10, 137-146.

Kopp, C., Albrecht, U., Zheng, B., Tobler, I., 2002. Homeostatic sleep regulation is preserved in mPer1 and mPer2 mutant mice. European Journal of Neuroscience 16, 1099-1106.

Kotz, C.M., Teske, J.A., Levine, J.A., Wang, C., 2002. Feeding and activity induced by orexin-A in the lateral hypothalamus in rats. Regulatory Peptides 104, 27-32.

Kruger, J-L., Dell, L-A., Pettigrew, J.D., Manger, P.R., 2010. Cellular location and major terminal networks of the orexinergic system in the brains of five microchiropteran species. Journal of Chemical Neuroanatomy 40, 256-262.

Kubota, Y., Hattori, R., Yui, Y., 1994. Three distinct subpopulations of GABAergic neurons in rat frontal agranular cortex. Brain Research 649, 159 –173.

Kunii, K., Yamanaka, A., Nambu, T., Matsuzaki, I., Goto, K., Sakurai, T., 1999. Orexins/hypocretins regulate drinking behaviour. Brain Research 842, 256-261.

Lavoie, B., Parent, A., 1994. Pedunculopontine nucleus in the squirrel monkey: distribution of cholinergic and monoaminergic neurons in the mesopontine tegmentum with evidence for the presence of glutamate in cholinergic neurons. Journal of Comparative Neurology 344, 190-209.

Lee, M. G., Hassani, O. K., Jones, B. E., 2005. Discharge of identified orexin/hypocretin cell bodies across the wake-sleep cycle. Journal of Neuroscience 25, 6716–6720.

Léger, L., Charnay, Y., Burlet, S., Gay, N., Schaad, N., Bouras, C., Cespuglio, R., 1998. Comparative distribution of nitric oxide synthase- and serotonin-containing neurons in the raphe nuclei of four mammalian species. Histochemical Cell Biology 110, 517-525.

Leger, L., Charnay, Y., Hof, P.R., Bouras, C., Cespuglio, R., 2001. Anatomical distribution of serotonin-containing neurons and axons in the central nervous system of the cat. Journal of Comparative Neurology 433, 157-182.

Lichtensteiger, W., 1966. Uptake of norepinephrine in periglomerular cells of the olfactory bulb in the mouse. Nature 210, 955-956.

Lidbrink, P., Jonsson, G., Fuxe, K., 1974. Selective reserpine-resistant accumulation of catecholamines in central dopamine neurones after dopa administration. Brain Research 67, 439-456.

Lidov, H.G.W., Molliver, M.E., 1982. Immunohistochemical study of the development of serotonergic neurons in the rat CNS. Brain Research Bulletin 9, 559-604.

Limacher, A.M., Bhagwandin, A., Fuxe, K., Manger, P.R., 2008. Nuclear organization and morphology of cholinergic, putative catecholaminergic and serotonergic neurons in the brain of the Cape porcupine (*Hystrix afric*aeaustralis): Increased brain size does not lead to increased organizational complexity. Journal of Chemical Neuroanatomy 36, 33-52.

Lin, L., Faraco, J., Kadotani, H., Rogers, W., Lin, X., Qui, X., de Jong, P., Nishino, S., Mignot, E., 1999. The REM sleep disorder canine narcolepsy is caused by a mutation in the hypocretin (orexin) receptor gene. Cell 98, 365-376.

Lindowski, P., Kerkhofs, M., Hauspie, R., Mendlewicz, J., 1991. Genetic determinants of EEG sleep: A study in twins living apart. Electroencephalography and Clinical Neurophysiology 79, 114-118.

Lindvall, O., Björklund, A., 1974. The organization of the catecholamine neuron systems in the rat brain as revealed by the glyoxylic acid fluorescence method. ACTA Physiologica Scandinavica Supplement 412, 1-48.

Lovegrove, B.G., 1988. Colony size and structure, activity patterns and foraging behaviour of a colony of the social mole-rat *Cryptomys damarensis* (Bathyergidae). Journal of Zoology, London 216, 301-402.

Lovegrove, B.G., Papenfus, M.E., 1995. Circadian activity rhythms in the solitary Cape mole rat (*Georychus capensis*: Bathyergidae) with some evidence of splitting. Physiology and Behaviour 58, 679-685.

Lovegrove, B.G., Muir, A., 1996. Circadian body temperature rhythms of the solitary Cape mole rat, *Georychus capensis* (Bathyergidae). Physiology and Behaviour 60, 991-998.

Lubkin, M., Stricker-Krongrad, A., 1998. Independent feeding and metabolic actions of orexins in mice. Biochemical and Biophysical Research Communications 25, 241-245.

Lyamin, O.I., Manger, P.R., Ridgway, S.H., Mukhametov, L.M., Siegel, J.M., 2008. Cetacean sleep: an unusual form of mammalian sleep. Neuroscience and Biobehavioural Reviews 32: 1451-1484.

Mahoney, M.M., Ramanathan, C., Smale, L., 2007. Tyrosine hydroxylase positive neurons and their contacts with vasoactive intestinal polypeptide-containing fibres in the hypothalamus of the diurnal murid rodent, *Arvicanthis niloticus*. Journal of Chemical Neuroanatomy 33, 131-139.

Manger, P.R., Fahringer, H., Pettigrew, J.D., Siegel, J.M., 2002a. Distribution and morphology of cholinergic neurons in the brain of the monotremes as revealed by ChAT immunohistochemistry. Brain Behaviour and Evolution 60, 275-297.

Manger, P.R., Fahringer, H., Pettigrew, J.D., Siegel, J.M., 2002b. The distribution and morphological characterstics of catecholaminergic cells in the brain of monotremes as revealed by tyrosine hydroxylase immunhistochemistry. Brain Behaviour and Evolution 60: 298-314.

Manger, P.R., Fahringer, H., Pettigrew, J.D., Siegel, J.M., 2002c. Distribution and morphology of serotonergic neurons in the brain of the monotremes. Brain Behaviour and Evolution 60: 315-332.

Manger, P.R., Ridgway, S.H., Siegel, J.M., 2003. The locus coeruleus complex of the bottlenose dolphin (*Tursiops truncatus*) as revealed by tyrosine hydroxylase immunhistochemistry. Journal of Sleep Research 12, 149-155.

Manger, P.R., Fuxe, K., Ridgway, S.H., Siegel, J.M., 2004. The distribution and morphological characteristics of catecholaminergic cells in the diencephalon and midbrain of the bottlenose dolphin (*Tursiops truncatus*). Brain Behaviour and Evolution 42, 42-60.

Manger, P.R., 2005. Establishing order at the systems level in mammalian brain evolution. Brain Research Bulletin 66, 282-289.

Manger, P.R., 2006. An examination of cetacean brain structure with a novel hypothesis correlating thermogenesis to the evolution of a big brain. Biological Review 81, 293-338.

Manger, P.R., Cort, J., Ebrahim, N., Goodman, A., Henning, J., Karolia, M., Rodrigues, S., Strkalj, G., 2008. Is 21st century neuroscience too focussed on the rat/mouse model of brain function and dysfunction? In: Brain Mapping Research Trends, Nova Science Publishers Inc., New York.

Maseko, B.C., Manger, P.R., 2007. Distribution and morphology of cholinergic, catecholaminergic and serotonergic neurons in the brain of Schreiber's long-fingered bat, *Miniopterus schreibersii*. Journal of Chemical Neuroanatomy 34, 80-94.

Maseko, B.C., Bourne, J.A., Manger, P.R., 2007. Distribution and morphology of cholinergic, putative catecholaminergic and serotonergic neurons in the brain of the Egyptian Rousette flying fox, *Rousettus aegyptiacus*. Journal of Chemical Neuroanatomy 34, 108-127.

McCormick, D.A., 1989. Cholinergic and noradrenergic modulation of thalamocortical processing. Trends in Neuroscience 12, 215-221.

McGinty, D., Gong, H., Suntsova, N., Alam, Md.H., Methippara, M., Guzman-Marin, R., Szymusiak, R., 2004. Sleep promoting functions of the hypothalamic median preoptic nucleus: inhibition of arousal systems. Archives Italiannes de Biologie 142, 501-509.

McGinty, D., Syzmusiak, R., 2005. Sleep-promoting mechanisms in mammals. In: Kryger, M.H., Roth, R., and Dement, W.C., Principles and Practices of Sleep Medicine, 4th edition. New York, Saunders.

McGranaghan, P.A., Piggins, H.D., 2001. Orexin A-like immunoreactivity in the hypothalamus and thalamus of the Syrian hamster (*Mesocricetus auratus*) and Siberian hamster (*Phodopus sungorus*), with special reference to circadian structures. Brain Research 904, 234-244.

McMullen, C.A., Andrade, F.H., Crish, S.D., 2010. Underdeveloped extraocular muscles in the naked mole-rat (*Heterochephalus glaber*). The Anatomical Record 293, 918-923.

McNamara, P., Capellini, I., Harris, S., Nunn, C.L., Barton, R.A., Preston, B., 2008. The phylogeny of sleep database: A new resource for sleep scientists. Open Sleep Journal 1, 11-14.

McNamara, P., Barton, R.A., Nunn, C.L., 2010. Evolution of sleep: Phylogenetic and functional perspectives, 1st edition. New York, Cambridge University Press.

Meister, B., Hökfelt, T., Steinbusch, H.W., Skagerberg, G., Lindvall, O., Geffard, M., Joh, T.H., Cuello, A.C., Goldstein, M., 1988. Do tyrosine hydroxylase-immunoreactive neurons in the ventrolateral arcuate nucleus produce dopamine or only L-dopa? Journal of Chemical Neuroanatomy 1, 59-64.

Meredith, G.E., Blank, B., Groenewegen, H.J., 1989. The distribution and compartmental organization of the cholinergic neurons in nucleus accumbens of the rat. Neuroscience 31, 327- 345.

Mesulam, M.M., Geula, C., Bothwell, M.A., Hersch, L.B., 1989. Human reticular formation: cholinergic neurons of the pedunculopontine tegmental nuclei and some cytochemical comparisons of forebrain cholinergic neurons. Journal of Comparative Neurology 281, 611-633.

Mileykovskiy, B. Y., Kiyashchenko, L. I., Siegel, J. M., 2005. Behavioral correlates of activity in identified hypocretin/orexin neurons. Neuron 46, 696-698.

Mintz, E.M., van Den Pol, A.N., Casano, A.A., Albers, H.E., 2001. Distribution of hypocretin (orexin) immunoreactivity in the central nervous system of Syrian hamsters (*Mesocricetus auratus*). Journal of Chemical Neuroanatomy. 21, 225–238.

Mislberger, R.E., Bergmann, B.M., Waldenar, W., Rechtschaffen, A., 1983. Recovery sleep following sleep deprivation in intact and suprachiasmatic nuclei-lesioned rats. Sleep 6, 217-233.

Mizukawa, K., McGeer, P.L., Tago, H., Peng, J.H., McGeer, E.G., Kimura, H., 1986. The cholinergic system of the human hindbrain studied by choline acetyltransferase immunohistochemistry and acetylcholinesterase histochemistry. Brain Research 379, 39-55.

Mondal, M.S., Nakazato, M., Date, Y., Murakami, N., Hanada, R., Sakata, T., Matsukura, S., 1999. Characterization of orexin-A and orexin-B in the microdissected rat brain nuclei and their contents in two obese rat models. Neuroscience Letters 273, 45-48.

Moon, D.J., Maseko, B.C., Ihunwo, A., Fuxe, K., Manger, P.R., 2007. Distribution and morphology of catecholaminergic and serotonergic neurons in the brain of the highveld gerbil, *Tatera brantsii*. Journal of Chemical Neuroanatomy 34, 134-144.

Moore, R.Y., Abrahamson, E.A., Van Den Pol, A., 2001. The hypocretin neuron system: an arousal system in the human brain. Archives Italiennes de Biologie 139, 195-205.

Mrosovsky, N., 1995. A non photic gateway to the circadian clock of hamsters. Ciba Foundation Symposium 183, 154-167; discussion 167-174.

Mufson, E.J., Cunningham, M.G., 1988. Observations on choline acetyltransferase containing structures in the CD-1 mouse brain. Neuroscience Letters 84, 7-12.

Mukhametov, L.M., Supin, A.Y., Polyakova, I.G., 1977. Interhemispheric asymmetry of the electroencephalographic sleep patterns in dolphins. Brain Research 134, 581-584.

Mukhametov, L.M., 1984. Sleep in marine mammals. Experimental Brain Research 8, 227-238.

Mukhametov, L.M., Supin, A.Y., Lyamin, O.I., 1988. Interhemispheric asymmetry of the EEG during sleep in marine mammals. In: Oniani T., Neurobiology of sleep-wakefulness cycle, Tbilisi: Metsniereba; 147-159.

Mukhametov, L.M., 1988. The absence of paradoxical sleep in dolphins. In: Koella, W.P., Obal, F., Schulz, H., Visser, P., Sleep ’86, New York: Gustav Fischer.

Mukhametov, L.M., 1995. Paradoxical sleep peculiarities in aquatic mammals. Sleep Research 24A, 202.

Mulders, W.H.A.M., Roberston, D., 2005. Catecholaminergic innervation of guinea pig superior olivary complex. Journal of Chemical Neuroanatomy 30, 230-242.

Murray, H.M., Dominguez, W.F., Martinez, J.E., 1982. Catecholaminergic neurons in the brain stem of tree shrew (*Tupaia*). Brain Research Bulletin 9, 205-215.

Nambu, T., Sakurai, T., Mizukami, K., Hosoya, Y., Yanagisawa, M., Goto, K., 1999. Distribution of orexin neurons in the adult rat brain. Brain Research 827, 243-260.

Negroni, J., Bennett, N.C., Cooper, H.M., 2003. Organization of the circadian system in the subterranean mole rat, *Cryptomys hottentotus* (Bathyergidae). Brain Research 967, 48-62.

Nemec, P., Burda, H., Peichl, L., 2004. Subcortical visual system of the African mole-rat *Cryptomys anselli*: to see or not to see? European Journal of Neuroscience 20, 757-768.

Nicolaidis, S., 2006. Metabolic mechanism of wakefulness (and hunger) and sleep (and satiety): role of adenosine triphosphate and hypocretin and other peptides. Metabolism: Clinical and Experimental 55, S24-S29.

Nicolau, M.C., Akaarir, M., Gamundi, A., Gonzalez, J., Rial, R.V., 2000. Why we sleep: the evolutionary pathway to the mammalian sleep. Progress in Neurobiology 62, 379-406.

Nitz, D., Siegel, J.M., 1996. GABA release in the posterior hypothalamus across sleep-wake cycle. American Journal of Physiology 271, R1707-R1712.

Nitz, D., Siegel, J.M., 1997a. GABA release in the locus coeruleus as a function of sleep/wake state. Neuroscience 78, 795-801.

Nitz, D., Siegel, J.M., 1997b. GABA release in the dorsal raphe nucleus: role in the control of REM sleep. American Journal of Physiology 273, R451-R455.

Nixon, J.P., Smale, L., 2005. Orexin fibres form appositions with Fos expressing neuropeptide-Y cells in the grass rat intergeniculate leaflet. Brain Research 1053, 33-37.

Nixon, J.P., Smale, L., 2007. A comparative analysis of the distribution of immunoreactive orexin-A and -B in the brains of nocturnal and diurnal rodents. Behaviour Brain and Function 13, 28.

Novak, C.M., Albers, H.E., 2002. Localization of hypocretin-like immunoreactivity in the brain of the diurnal rodent, *Arvicanthis niloticus*. Journal of Chemical Neuroanatomy 23, 49-58.

Oelschläger, H.H.A., Nakamura, M., Herzog, M., Burda, H., 2000. Visual system labeled by c-Fos immunohistochemistry after light exposure in the 'blind' subterranean Zambian mole-rat (*Cryptomys anselli*). Brain Behaviour and Evolution 55, 209-220.

Oh, J.D., Woolf, N.J., Roghani, A., Edwards, R.H., Butcher, L.L., 1992. Cholinergic neurons in the rat central nervous system demonstrated by in situ hybridization of choline acetyltransferase mRNA. Neuroscience 47, 807–822.

Olson, L., Fuxe, K., 1972. Further mapping out of the central noradrenaline neurons systems: projections of the "subcoeruleus" area. Brain Research 43, 289-295.

Oosthuizen, M.K., Cooper, H.M., Bennett, N.C., 2003. Circadian rhythms of locomotor activity in solitary and social species of African mole rats (Family:Bathyergidae). Journal of Biological Rhythms 18, 481-490.

Oosthuizen, M.K., Bennett, N.C., Cooper, H.M., 2010. Photic induction of Fos in the suprachiasmatic nucleus of African mole-rats: responses to increasing irradiance. Chronobiology International 27, 1532-1545.

Peyron, C., Tighe, D.K., van den Pol, A.N., de Lecea, L., Heller, H.C., Sutcliffe, J.G., Kilduff, T.S., 1998. Neurons containing hypocretin (orexin) project to multiple neuronal systems. Journal of Neuroscience 18, 9996-10015.

Peyron, C., Faraco, J., Rogers, W., Ripley, B., Overeem, S., Charnay, Y., Nevsimalova, S., Aldrich, M., Reynolds, D., Albin, R., Li, R., Hungs, M., Pedrazzoli, M., Padigaru, M., Kucherlapati, M., Fan, J., Maki, R., Lammers, G.J., Bouras, C., Kucherlapati, R., Nishino, S., Mignot, E., 2000. A mutation in a case of early onset narcolepsy and a generalized absence of hypocretin peptides in human narcoleptic brains. Nature Medicine 6, 991-997.

Pickard, G.E., 1985. Bifurcating axons of retinal ganglion cells terminate in the hypothalamic suprachiasmatic nucleus and intergeniculate leaflet of the thalamus. Neuroscience Letters 55, 211-217.

Pieters, R.P., Gravett, N., Fuxe, K., Manger, P.R., 2010. Nuclear organization of cholinergic, putative catecholaminergic and serotonergic nuclei in the brain of the eastern rock elephant shrew, *Elephantulus myurus*. Journal of Chemical Neuroanatomy 39, 175-188.

Piper, D.C., Upton, N., Smith, M.I., Hunter, A.J., 2000. The novel brain neuropeptide, orexin-A, modulates the sleep-wake cycle of rats. European Journal of Neuroscience 12, 726–730.

Pu, S., Jain, M.R., Kalra, P.S., Kalra, S.P., 1998. Orexins, a novel family of hypothalamic neuropeptides, modulate pituitary luteinizing hormone secretion in an ovarian steroid dependent manner. Regulatory Peptides 78, 133–136.

Raghanti, M,A., Stimpson, C.D., Marcinkiewicz, J.L., Erwin, J.M., Hof, P.R., Sherwood, C.C., 2008. Cholinergic innervation of the frontal cortex: differences among humans, chimpanzees, and macaque monkeys. Journal of Comparative Neurology 506, 409-424.

Raghanti, M.A., Stimpson, C.D., Marcinkiewicz, J.L., Erwin, J.M., Hof, P.R., Sherwood, C.C., 2008. Differences in cortical serotonergic innervation among humans, chimpanzees, and macaque monkeys: a comparative study. Cerebral Cortex 18, 584-597.

Rattenborg, N.C., Amlaner, C.J., Lima, S.L., 2000. Behavioural, neurophysiological and evolutionary perspectives on unihemispheric sleep. Neuroscience Biobehavioural Reviews 24, 817-842.

Richardson, G. S., Moore-Ede, M. C., Czeisler, C. A., Dement, W. C. 1985. Circadian rhythms of sleep and wakefulness in mice: Analysis using long-term automated recording of sleep. American Journal of Physiology: Regulatory, Integrative and Comparative Physiology 248, R320-R330.

Risold, P.Y., Griffond, B., Kilduff, T.S., Sutcliffe, J.G., Fellmann, D., 1999. Preprohypocretin (orexin) and prolactin-like immunoreactivity are coexpressed by neurons of the rat lateral hypothalamic area. Neuroscience Letters 259, 153–156.

Roberts, A., 1951. The Mammals of South Africa. Trustees of the 'Mammals of South Africa' book fund. Central News Agency, Cape Town.

Rogers, J.H., 1992. Immunohistochemical markers in rat cortex: colocalization of calretinin and calbindin-D28k with neuropeptides and GABA. Brain Research 587, 147–157.

Rodgers, R.J., Ishii, Y., Halford, J.C.G., Blundell, J.E., 2002. Orexins and appetite regulation. Neuropeptides 36, 303-325.

Ruggerio, D.A., Baker, H., Joh, T.H., Reis, D.J., 1984. Distribution of catecholamine neurons in the hypothalamus and preoptic region of mouse. Journal of Comparative Neurology 223, 556-582.

Ruggiero, D.A., Anwar, M., Gootman, P.M., 1992. Presumptive adrenergic neurons containing phenylethanolamine N-methyltransferase immunoreactivity in the medulla oblongata of neonatal swine. Brain Research 583, 105-119.

Sakurai, T., Amemiya, A., Ishii, M., Matsuzaki, I., Chemelli, R.M., Tanaka, H., Williams, S.C., Richardson, J.A., Kozlowski, G.P., Wilson, S., Arch, J.R.S., Buckingham, R.E., Haynes, A.C., Carr, S.A., Annan, R.S., McNulty, D.E., Liu, W.S., Terrett, J.A., Elshourbagy, N.A., Bergsma, D.J., Yanagisawa, M., 1998. Orexins and orexin receptors: a family of hypothalamic neuropeptides and G protein-coupled receptors that regulate feeding behavior. Cell 92, 573-585.

Sakurai, T., 2003. Orexin: A link between energy homeostasis and adaptive behavior. Current Opinion in Clinical Nutrition and Metabolic Care 6, 353-360.

Sakurai, T., 2005. Roles of orexin/hypocretin in regulation of sleep/wakefulness and energy homeostasis. Sleep Medicine Reviews 9, 231- 241.

Sakurai, T., Nagata, R., Yamanaka, A., Kawamura, H., Tsujino, N., Muraki, Y., Kageyama, H., Kunita, S., Takahashi, S., Goto, K., Koyama, Y., Shioda, S., Yanagisawa, M., 2005. Input of orexin/hypocretin neurons revealed by a genetically encoded tracer in mice. Neuron 46, 297-308.

Saper, C. B., 1985. Organization of cerebral cortical afferent systems in the rat. II. Hypothalamocortical projections. Journal of Comparative Neurology 237, 21.

Saper, C.B., Chou, T.C., Seammell, T.E., 2001. The sleep switch: hypothalamic control of sleep and wakefulness. Trends in Neuroscience 24, 726-731.

Saper, C. B., Chou, T. C., Scammell, T. E., 2001. The sleep switch: hypothalamic control of sleep and wakefulness. Trends in Neuroscience 24, 726–731.

Saper, C.B., Scammeli, T.E., Lu, J., 2005. Hypothalamic regulation of sleep and circadian rhythms. Nature 437, 1257-1263.

Satoh, K., Fibiger, H. C., 1985. Distribution of central cholinergic neurons in the baboon (*Papio papio*). I. General morphology. Journal of Comparative Neurology 236, 197-214.

Satoh, K., Armstrong, D.M. and Fibiger, H.C., 1983. A comparison of the distribution of central cholinergic neurons as demonstrated by acetylcholinesterase pharmacohistochemistry and choline acetyltransferase immunohistochemistry. Brain Research Bulletin 11, 693-720.

Satoh, J., Irino, M., Martin, P.M., Mailman, R.B., Suzuki, K., 1991. Neurochemical and immunocytochemical studies of catecholamine system in the brindled mouse. Journal of Neuropathology and Experimental Neurology 50, 793-808.

Serafetinides, E.A., Shurley, J.T., Brooks, R.E., 1972. Electroencephalogram of the pilot whale, *Globicephala scammoni*, in wakefulness and sleep: lateralisation aspects. International Journal of Psychobiology 2, 129-135.

Sherin, J.E., Shiromani, P.J., McCarley, R.W., Saper, C.B., 1996. Activation of ventrolateral preoptic neurons during sleep. Science 271, 216-219.

Shiromani, P.J., Armstrong, D.M., Berkowitz, A., Jeste, D.V., Gillin, J.C., 1988. Distribution of choline acetyltransferase immunoreactive somata in the feline brainstem: implications for REM sleep generation. Sleep. 11, 1-16.

Shiromani, P.J., Xu, M., Winston, E.M., Shiromani, S.N., Gerashchenko, D., Weaver, D.R., 2004. Sleep rhythmicity and homeostasis in mice with targeted disruption of mPeriod genes. American Journal of Physiology: Regulatory, Integrative and Comparative Physiology, 287, R47-R57.

Shurley, J.T., Serafetinides, E.A., Brooks, R.E., Elsner, R., Kenney, D.W., 1969. Sleep in cetaceans: I. The pilot whale, *Globicephala scammoni*. Psychophysiology 6: 230.

Siegel, J.M., 1990. Mechanisms of sleep control. Journal of Clininical Neurophsiology 7, 49-65.

Siegel, J.M., Nienhuis, R., Fahringer, H.M., Chiu, C., Dement, W.C., Mignot, E., Lufkin, R., 1992. Activity of medial mesopontine units during cataplexy and sleep-waking states in the narcoleptic dog. Journal of Neuroscience 12, 1640-1646.

Siegel, J.M., 1995. Phylogeny and the function of REM sleep. Behavioural Brain Research 69, 29-34.

Siegel, J.M., Manger, P.R., Nienhuis, R., Fahringer, H.M., Pettigrew, J.D., 1996. The echidna *Tachyglossus aculeatus* combines REM and non-REM aspects in a single sleep state: implications for the evolution of sleep. Journal of Neuroscience 16, 3500-3506.

Siegel, J.M., Manger, P.R., Nienhuis, R., Fahringer, H.M., Pettigrew, J.D., 1998. Monotremes and the evolution of rapid eye movement sleep. Philosophical Transactions of the Royal Society London B: Biological Sciences 353, 1147-1157.

Siegel, J,M., 1999. Narcolepsy: a key role for hypocretins (orexins). Cell 98, 409-412.

Siegel, J.M., Manger, P.R., Nienhuis, R., Fahringer, H.M., Pettigrew, J.D., 1999. Sleep in the platypus. Neuroscience 91, 391-400.

Siegel, J.M., 2000. Brainstem mechanisms generating REM sleep. In: Kryger, M.H., Roth, R., and Dement, W.C., Principles and Practices of Sleep Mechanisms, WB Saunders, Philadelphia.

Siegel, J.M., 2003. Why we sleep. Scientific American, 92-97.

Siegel, J.M., 2004. Sleep phylogeny: Clues to the evolution and function of sleep, In: Luppi, P.H., Sleep: Circuits and functions, CRC Press, Boca Raton.

Siegel, J.M., 2004. Hypocretin (Orexin): Role in normal behaviour and neuropathology. Annual Review of Psychology 55, 125-148.

Siegel, J.M., 2004. The neurotransmitters of sleep. Journal of Clinical Psychiatry 65, 4-7.

Siegel, J.M., 2008. Do all animals sleep? Trends in Neuroscience 31, 208-213.

Siegel, J.M., 2009. Sleep viewed as a state of adaptive inactivity. Nature Reviews Neuroscience 10, 747-753.

Smeets, W.J.A.J., González, A., 2000. Catecholamine systems in the brain of vertebrates: new perspectives through a comparative approach. Brain Research Review 33, 308-379.

Staedt, J., Stoppe, G., 2001. Evolution and function of sleep. Fortschritte der Neurologie-Psychiatrie 69, 51-57.

Steinbusch, H.W.M., 1981. Distribution of serotonin-immunoreactivity in the central nervous system of the rat – cell bodies and terminals. Neuroscience. 6, 557-618.

Stellar, E., 1954. The physiology of motivation. Psychological Record 61, 5-22.

Steriade, M., Pare, D., Datta, S., Oakson, G., Curro Dossi, R., 1990. Different cellular types in mesopontine cholinergic nuclei related to ponto-geniculo-occipital waves. Journal of Neuroscience 10, 2560-2579.

Steriade, M., McCormick, D.A., Sejnowski, T.J., 1993. Thalamocortical oscillations in the sleeping and aroused brain. Science 262, 679-685.

Susic, V., Masirevic, G., 1986. Sleep patterns in the Mongolian gerbil (*Meriones unguilculatus*). Physiology and Behaviour 37, 257-261.

Szymusiak, R., 1995. Magnocellular nuclei of the basal forebrain: substrates of sleep and arousal regulation. Sleep 18, 478-500.

Syzmusiak, R., Steininger, T., Alam, N., McGinty, D., 2001. Preoptic area sleep-regulating mechanisms. Archives Italiennes de Biologie 139, 77-92.

Tafti, M., Franken, P., Kitahama, K., Malafosse, A., Jouvet, M., Valtax, J,-L., 1997. Localisation of candidate genomic regions influencing paradoxical sleep in mice. NeuroReport 8, 3755-3758.

Tafti, M., 2007. Quantitative genetics of sleep in inbred mice. Dialogues in Clinical Neuroscience 9, 273-278.

Taheri, S., Lin, L., Austin, D., Young, T., Mignot, E., 2004. Short sleep duration is associated with reduced leptin, elevated ghrelin, and increased body mass index. PLoS Medicine 1, e62.

Tago, H., McGeer, P.L., McGeer, E.G., Akiyama, H., Hersch, L.B., 1989. Distribution of choline acetyltransferase immunopositive structures in the rat brainstem. Brain Research 495, 271-297.

Tang, X., Sanford, L. D., 2002. Telemetric recording of sleep and home cage activity in mice. Sleep 25, 691-699.

Takahashi, N., Okumura, T., Yamada, H., Kohgo, Y., 1999. Stimulation of gastric acid secretion by centrally administered orexin-A in conscious rats. Biochemical and Biophysical Research Communications 254, 623–627.

Taylor, L., Vana, A., Givon, L., 2000. The evolution of sleep: a reconsideration of the development of quiet sleep/active sleep cycles. Medical Hypotheses 54, 761-766.

Thannickal, T.C., Moore, R.Y., Nienhuis, R., Ramanathan, L., Gulyani, S., Aldrich, M., Cornford, M., Siegel, J.M., 2000. Reduced number of hypocretin neurons in human narcolepsy. Neuron 27, 469–474.

Thannickal., T.C., Lai, Y.Y., Siegel, J.M., 2007. Hypocretin (orexin) cell loss in Parkinson's disease. Brain 130, 1586-1595.

Thannickal, T.C., Nienhuis. R., Siegel, J.M., 2009. Localized loss of hypocretin (orexin) cells in narcolepsy without cataplexy. Sleep 32, 993-998.

Tinner, B., Fuxe, K., Köller, C., Hersh, L., Andersson, K., Jansson, A., Goldstein, M., Agnati, L.F., 1989. Evidence for the existence of a population of arcuate neurons costoring cholineacetyltransferase and tyrosine hydroxylase immunoreactivities in the male rat. Neuroscience Letters 99, 44-49.

Tobler, I., Jaggi, K., 1987. Sleep and EEG in the Syrian hamster (*Mesocrictus auratus*) under baseline conditions and following sleep deprivation. Journal of Comparative Physiology 161, 449-459.

Tobler, I., Franken, P., Jaggi, K., 1993. Vigilance states, EEG and cortical temperature in the guinea pig. American Journal of Physiology 264, R1125-R1132.

Tobler, I., Franken, P., 1994. Sleep homeostasis in the guinea pig: similar response to sleep deprivation in the light and dark period. Neuroscience Letters 164, 105-108.

Tobler, I., 1995. Is sleep fundamentally different between mammalian species? Behaviour Brain Research 69, 35-41.

Tobler, I., Deboer, T., 2001. Sleep in the blind mole rat *Spalax ehrenbergi*. Sleep 24, 147-154.

Törk, I., 1990. Anatomy of the serotonergic system. Annals of the New York Academy of Sciences 600, 9–35.

Tucci, V., Nolan, P.M., 2010. Toward and understanding of the function of sleep: New insights from mouse genetics. In: McNamara, P., Barton, R.A., Nunn, C.L., Evolution of sleep: Phylogenetic and functional perspectives, 1st edition. New York, Cambridge University Press.

Valtex, J.L., Bugat, R., 1974. Facteurs genetiques dans le deteminisme du cycle veile-sommeil chez la souris. Brain Research 69, 315-330.

Van Brederode, J.F.M., Helliesen, M.K., Hendrickson, A.E., 1991. Distribution of the calcium-binding proteins parvalbumin and calbindin-D28k in the sensorimotor cortex of the rat. Neuroscience 44, 157–171.

van den Pol, A.N., 2000. Narcolepsy: a neurodegenerative disease of the hypocretin system? Neuron 27, 415–418.

Van der Horst, G., 1972. Saesonal effects of anatomy and histology on the reproductive tract of the male rodent mole. Zool. Afr. 7, 491-520.

VanItallie, T.B., 2006. Sleep and energy balance: interactive homeostatic systems. Metabolism: Clinical and Experimental 55, S30-S35.

Van Twyver, H., 1969. Sleep patterns in five rodent species. Physiology and Behaviour 4, 901-905.

Vidal, L., Blanchard, J., Morin, L.P., 2005. Hypothalamic and zona incerta neurons expressing hypocretin, but not melanin concentrating hormone, project to the hamster intergeniculate leaflet. Neuroscience 134, 1081-1090.

Vincent, S.R., 1988. Distributions of tyrosine hydroxylase-, dopamine-β-hydroxylase-, and phenylehtanolamine-N-methyltransferase-immunoreactive neurons in the brain of the hamster (*Mesocricetus auratus*). Journal of Comparative Neurology 268, 584-599.

Vincent, S.R., Reiner, P.B., 1987. The immunohistochemical localization of choline acetyltransferase in the cat brain. Brain Research Bulletin 18, 371-415.

Von Coelln, R., Thomas, B., Savitt, J.M., Lim, K.L., Sasaki, M., Hess, E.J., Dawson, V.L., Dawson, T.M., 2004. Loss of locus coeruleus neurons and reduced startle in parkin null mice. Proceedings of the National Academy of Sciences, USA 101, 10744–10749.

Waterhouse, B.D., Border, B.,Wahl, L., Mihailoff, G.A., 1993. Topographic organization of rat locus coeruleus and dorsal raphe nuclei: distribution of cells projecting to visual system structures. Journal of Comparative Neurology 336, 345–361.

Wisor, J.P., O'Hara, B.F., Terao, A., Selby, C.P., Kilduff, T.S., Sancar, A., et al., 2002. A role for cryptochromes in sleep regulation. BMC Neuroscience 3, 20.

Woolf, N.J., 1991. Cholinergic systems in mammalian brain and spinal cord. Progress in Neurobiology 37, 475–524.

Wu, MF., Gulyani, S.A., Yau, E., Mignot, E., Phan, B., Siegel, J.M., 1999. Locus coeruleus neurons: cessation of activity during cataplexy. Neuroscience 91, 1389-1399.

Wu, M.F., John, J., Boehmer, L.N., Yau, D., Nguyen, G.B., Siegel, J.M., 2004. Activity of dorsal raphe cells across the sleep-waking cycle and during cataplexy in narcoleptic dogs. Journal of Physiology 55, 202-215.

Yamamoto, Y., McKinley, M.J., Nakazato, M., Yamashita, H., Shirahata, A., Ueta,Y., 2006. Postnatal development of orexin-A and orexin-B like immunoreactivities in the Eastern grey kangaroo (*Macropus giganteus*) hypothalamus. Neuroscience Letters 392, 124-128.

Yamanaka, A., Sakurai, T., Katsumoto, T., Yanagisawa, M., Goto, K., 1999. Chronic intracerebroventricular administration of orexin-A to rats increases food intake in daytime, but has no effect on body weight. Brain Research 849, 248-252.

Yoshida, K., McCormack, S., Espana, R.A., Crocker, A., Scammell, T.E., 2006. Afferents to the orexin neurons of the rat brain. Journal of Comparative Neurology 494, 845-861.

Yoshimichi, G., Yoshimatsu, H., Masaki, T., Sakata, T., 2001. Orexin-A regulates body temperature in coordination with arousal status. Experimental Biology and Medicine 226, 468-476.

Zhang, J.H., Sampogna, S., Morales, F.R., Chase, M.H., 2001. Orexin (hypocretin)-like immunoreactivity in the cat hypothalamus: a light and electron microscopic study. Sleep 24, 67–76.

Zhang, J.H., Sampogna, S., Morales, F.R., Chase, M.H., 2002. Co-localization of hypocretin-1 and hypocretin-2 in the cat hypothalamus and brainstem. Peptides 23, 1479–1483.

Zhang, S., Zeitzer, J.M., Yoshida, Y., Wisor, J.P., Nishino, S., Edgar, D.M., Mignot, E., 2004. Lesions of the suprachiasmatic nucleus eliminate the daily rhythm of hypocretin-1 release. Sleep 27, 619- 627.

Zulley, J., Wever, R., Aschoff, J., 1981. The dependence of onset and duration of sleep on the circadian rhythm of rectal temperature. Pflügers Arch (European Journal of Physiology) 391, 314-318.

Appendix A: Published original research article that emerged from the thesis

Journal of Chemical Neuroanatomy 35 (2008) 371–387

Contents lists available at ScienceDirect

Journal of Chemical Neuroanatomy

journal homepage: www.elsevier.com/locate/jchemneu

Nuclear organization and morphology of cholinergic, putative catecholaminergic and serotonergic neurons in the brains of two species of African mole-rat

Adhil Bhagwandin [a], Kjell Fuxe [b], Nigel C. Bennett [c], Paul R. Manger [a,*]

[a] School of Anatomical Sciences, Faculty of Health Sciences, University of the Witwatersrand, 7 York Road, Parktown, Johannesburg, Gauteng 2193, South Africa
[b] Department of Neuroscience, Karolinska Institutet, Retzius väg 8, S-171 77 Stockholm, Sweden
[c] Mammal Research Institute, Department of Zoology and Entomology, University of Pretoria, Pretoria 0002, South Africa

ARTICLE INFO

Article history:
Received 15 January 2008
Received in revised form 29 February 2008
Accepted 29 February 2008
Available online 8 March 2008

Keywords:
Acetylcholinesterase
Tyrosine hydroxylase
Serotonin
Evolution
Mammal
Rodent
Neural systems

ABSTRACT

The distribution, morphology and nuclear subdivisions of the cholinergic, putative catecholaminergic and serotonergic systems within the brains of two species of African mole-rat (Cape dune mole-rat – *Bathyergus suillus*; highveld mole-rat – *Cryptomys hottentotus pretoriae*) were identified following immunohistochemistry for acetylcholinesterase, tyrosine hydroxylase and serotonin. The aim of the present study was to investigate possible differences in the complement of nuclear subdivisions of these systems by comparing those of the mole-rats to published studies of other rodents. The mole-rats used exhibit a major reduction of the visual system and live a subterranean lifestyle. These wild caught animals also have differing social systems, the Cape dune mole-rat is strictly solitary whereas the highveld mole-rat occurs in social familial units. While these differences, especially that of phenotype, may lead to the prediction of significant differences in the nuclear complement of these systems, we found that all nuclei identified in all three systems in the laboratory rat and other rodents had direct homologs in the brains of the mole-rats studied. There were no additional nuclei in the brains of the mole-rats that are not found in the laboratory rat or other rodents and vice versa. The mole-rats are phylogenetically distant from the laboratory rat, but are still part of the order Rodentia. We conclude that changes in the nuclear organization of the systems studied appear to demonstrate a form of constraint related to the phylogenetic level of the order.

* Corresponding author at: School of Anatomical Sciences, Faculty of Health Sciences, University of the Witwatersrand, 7 York Road, Parktown, Johannesburg, Gauteng 2193, South Africa. Tel.: +27 11 717 2497; fax: +27 11 717 2422.
E-mail address: Paul.Manger@wits.ac.za (P.R. Manger).

Abbreviations: III, oculomotor nucleus; IV, trochlear nucleus; Vmot, motor nucleus of trigeminal nerve; VI, abducens nucleus; VIId, facial nerve nucleus, dorsal; VIIv, facial nerve nucleus, ventral; Vmes, fifth mesencephalic nucleus; X, dorsal motor vagus nucleus; XII, hypoglossal nucleus; 3V, third ventricle; 4V, fourth ventricle; A1, caudal ventrolateral medullary tegmental nucleus; A2, caudal dorsomedial medullary nucleus; A4, dorsal medial division of locus coeruleus; A5, fifth arcuate nucleus; A6d, diffuse portion of locus coeruleus; A7d, nucleus subcoeruleus, diffuse portion; A7sc, nucleus subcoeruleus, compact portion; A8, retrorubral nucleus; A9l, substantia nigra, lateral; A9m, substantia nigra, medial; A9pc, substantia nigra, pars compacta; A9v, substantia nigra, ventral, pars reticulata; A10, ventral tegmental area; A10c, ventral tegmental area, central; A10d, ventral tegmental area, dorsal; A10dc, ventral tegmental area, dorsal caudal; A11, caudal diencephalic group; A12, tuberal cell group; A13, zona incerta; A14, rostral periventricular nucleus; A15d, anterior hypothalamic group, dorsal division; A15v, anterior hypothalamic group, ventral division; A16, catecholaminergic neurons of the olfactory bulb; ac, anterior commissure; Amyg, amygdala; AP, area postrema; B9, supralemniscal serotonergic nucleus; C, caudate nucleus; C1, rostral ventrolateral medullary tegmental group; C2, rostral dorsomedial medullary nucleus; C3, rostral dorsal midline medullary nucleus; ca, cerebral aqueduct; cc, corpus callosum; cl, claustrum; CLi, caudal linear nucleus; CN, cerebellar nuclei; CVL, caudal ventrolateral serotonergic group; Diag. B, diagonal band of Broca; DR, dorsal raphe; DRc, dorsal raphe nucleus, caudal division; DRd, dorsal raphe nucleus, dorsal division; DRif, dorsal raphe nucleus, interfascicular division; DRl, dorsal raphe nucleus, lateral division; DRv, dorsal raphe nucleus, ventral division; DRp, dorsal raphe nucleus, peripheral division; DT, dorsal thalamus; EW, Edinger–Westphal nucleus; f, fornix; GC, central periaqueductal grey matter; GP, globus pallidus; Hbl, habenular nucleus, lateral; Hbm, habenular nucleus, medial; HIP, hippocampus; Hyp, hypothalamus; Hyp.d, dorsal hypothalamic cholinergic nucleus; Hyp.l, lateral hypothalamic cholinergic nucleus; Hyp.v, ventral hypothalamic cholinergic nucleus; IC, inferior colliculus; ic, internal capsule; io, inferior olive; IP, interpeduncular nucleus; Is.Call/TOL, islands of Calleja and olfactory tubercule; LDT, laterodorsal tegmental nucleus; LV, lateral ventricle; MnR, median raphe nucleus; mtf, cholinergic medullary tegmental field; N.Acc, nucleus accumbens; N.Amb, nucleus ambiguus; N.Bas, nucleus basalis; NEO, neocortex; OB, olfactory bulb; pVII, preganglionic motor neurons of the superior salivatory nucleus or facial nerve; pIX, preganglionic motor neurons of the inferior salivatory nucleus; P, putamen nucleus; PBg, parabigeminal nucleus; PC, cerebral peduncle; Pg, pineal gland; PIR, piriform cortex; PPT, pedunculopontine tegmental nucleus; py, pyramidal tract; R, thalamic reticular nucleus; RMg, raphe magnus nucleus; ROb, raphe obscurus nucleus; RPa, raphe pallidus nucleus; RVL, rostral ventrolateral serotonergic group; SC, superior colliculus; scp, superior cerebellar peduncle; Sep, septum; Sep.M, medial septal nucleus; TOL, olfactory tubercle; vh, ventral horn; VPO, ventral pons.

0891-0618/$ – see front matter © 2008 Elsevier B.V. All rights reserved.
doi:10.1016/j.jchemneu.2008.02.005

1. Introduction

Nearly half of all known mammalian species, over 2300, belong within the order Rodentia (Jansa and Weksler, 2004). Of these, the laboratory rat and mouse are the most commonly used animal models in modern neuroscience (Manger et al., in press); however, the extent to which the brains of these two species are representative of rodents, mammals, or indeed humans remains unclear. While there are many similarities, the differences are also quite significant, and knowledge of these similarities and differences in the structure of the brain within rodents is essential in aiding interpretation of the often-extrapolated findings based on studies of neural systems of laboratory rat and mouse to humans and other mammals. The question that might be posed here is: are the laboratory rodents always the best model animal to use when attempting to understand aspects of human brain function or dysfunction?

A recent study detailing the occurrence of cholinergic neurons in the cerebral cortex of various species of rodent revealed that these neurons were present in the cortex of members of the subfamily Muridae, but absent in the cortex of other species of rodent including the highveld mole-rat (Bhagwandin et al., 2006). However, a number of studies of two immunohistochemically identifiable neural systems (the catecholaminergic and serotonergic systems) within the subcortical regions of the brain of various rodents, such as the laboratory rat (Dahlström and Fuxe, 1964; Fuxe et al., 1969, 1970; Lindvall and Björklund, 1974; Björklund and Lindvall, 1984; Steinbusch, 1981; Hökfelt et al., 1976, 1984; Törk, 1990), laboratory mouse (Ruggerio et al., 1984; Daszuta and Portalier, 1985; Ishimura et al., 1988; Léger et al., 1998; Satoh et al., 1991; D'Este et al., 2007), highveld mole-rat (Da Silva et al., 2006), grass rat (Mahoney et al., 2007), guinea pig (Mulders and Roberston, 2005), hamster (Vincent, 1988), Mongolian gerbil (Janusonis et al., 1999, 2003; Janusonis and Fite, 2001), Chilean degus (Fite and Janusonis, 2001), highveld gerbil (Moon et al., 2007) and greater canerat (Dwarika et al., 2008), have all demonstrated that the nuclear organization of these systems are the same despite differences in phenotype, life history and many millions of years since the occurrence of the most recent common ancestor.

It has been hypothesised that irrespective of brain size, phenotype or life history, those species of the same mammalian order will exhibit the same complement of homologous nuclei, at the systems level of organization, for the imunohistochemically identifiable neuronal systems (Manger, 2005). Recent studies in rodents have shown that despite major increases in brain size (Dwarika et al., 2008), large phylogenetic distances (Da Silva et al., 2006; Moon et al., 2007; Dwarika et al., 2008), and substantive differences in phenotype (Da Silva et al., 2006; Moon et al., 2007; Dwarika et al., 2008), the nuclear organization of the catecholaminergic and serotonergic systems was identical. The cholinergic system has yet to be examined fully in this comparative sense, apart from the cortical cholinergic neurons (Bhagwandin et al., 2006); however, it may be predicted that all rodent species will show the same complement of homologous nuclei for the cholinergic system, as seen thus far for the catecholaminergic and serotonergic systems.

The current study extends the earlier work of Da Silva et al. (2006) by using two species of mole-rat, the highveld mole-rat (*Cryptomys hottentotus pretoriae*) and the Cape dune mole-rat (*Bathyergus suillus*) (Fig. 1), and examining the entire brain of each using immunohistochemistry for choline acetyltransferase, tyrosine hydroxylase and serotonin. This allows us to describe the nuclear organization and neuronal morphology of the cholinergic, putative catecholaminergic and serotonergic systems. Both species studied have a greatly reduced visual system (Oelschläger et al., 2000; Cernuda-Cernuda et al., 2003; Nemec et al., 2004), are subterranean and rarely exposed to light, and appear to have a free-running circadian activity oscillator (Lovegrove and Papenfus, 1995; Lovegrove and Muir, 1996; Negroni et al., 2003; Oosthuizen et al., 2003; Gutjahr et al., 2004). These unusual phenotypic and physiological features, combined with the phylogenetic distance of both species to the laboratory rat (Adkins et al., 2003; Faulkes et al., 2004), will provide a strong phenotypic and phylogenetic test of the hypothesis proposed by Manger (2005). If the prediction of Manger (2005) is supported, the nuclear organization of the systems under study will be identical to that seen in the laboratory rat; however, the phenotypic differences may be reflected in changes such as a reduction in total neuronal numbers within specific nuclei as demonstrated previously for the highveld mole-rat (Da Silva et al., 2006).

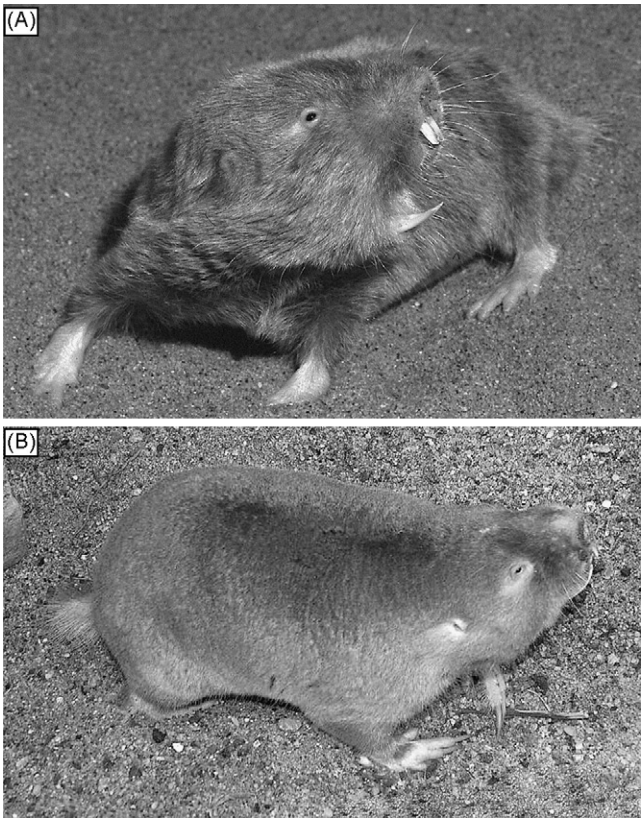

Fig. 1. Photographs of the two mole-rat species investigated. (A) Highveld mole-rat (***Cryptomys hottentotus***). (B) Cape dune mole-rat (***Bathyergus suilius***). Note the unusual phenotype associated with a subterranean lifestyle and the greatly reduced, though still present, eyes.

2. Materials and methods

The brains of six adult male highveld mole-rats (*C. hottentotus pretoriae*) (Fig. 1A) and six adult male Cape dune mole-rats (*B. suillus*) (Fig. 1B) were used in the current study. All animals were treated and used according to the guidelines of the University of the Witwatersrand Animal Ethics Committee, which parallel those of the NIH for the care and use of animals in scientific experimentation. The highveld mole-rats were captured within the north-eastern portion of Gauteng Province, South Africa, while the Cape dune mole-rats were caught in the metropolitan region of Cape Town, South Africa, both under the permission of the relevant Nature Conservation Directorates. The mole-rats were placed under deep barbiturate anaesthesia (Euthanaze, 200 mg sodium pentobarbital/kg, i.p.), and then perfused intracardially upon cessation of respiration. The perfusion was initially done with a rinse of 0.9% saline solution at 4 °C, followed by a solution of 4% paraformaldehyde

in 0.1 M phosphate buffer (PB) (approximately 1 l for each kilogram of body mass of each solution). Brains were then removed from the skull and post-fixed overnight in 4% paraformaldehyde in 0.1 M PB, and then allowed to equilibrate in 30% sucrose in 0.1 M PB. The brains were then frozen and sectioned into serial coronal and sagittal sections of 50 μm thickness. A one in five series of stains was made for Nissl, myelin, choline-acetyltransferase (ChAT), tyrosine hydroxylase (TH), and serotonin (5HT). Sections kept for the Nissl series were mounted on 0.5% gelatine coated glass slides, cleared in a solution of 1:1 chloroform and absolute alcohol, then stained with 1% cresyl violet to reveal cell bodies. Myelin sections were stored in 5% formalin for a period of two weeks and were then mounted on 1% gelatine coated glass slides and subsequently stained with silver solution to reveal myelin sheaths (Gallyas, 1979).

For immunohistochemical staining the sections were first treated for 30 min with an endogenous peroxidase inhibitor (49.2% methanol:49.2% of 0.1 M PB:1.6% of 30% H_2O_2) followed by three 10 min rinses in 0.1 M PB. This was followed by a 2 h pre-incubation, at room temperature, in a solution (blocking buffer) containing 3% normal goat serum (NGS) for serotonin and TH but 3% normal rabbit serum (NRS) for ChAT sections, 2% bovine serum albumin (BSA, Sigma), and 0.25% Triton X-100 (Merck) in 0.1 M PB. The sections were then placed in a primary antibody solution containing the appropriately diluted antibody in blocking buffer (as described above) for 48 h at 4 °C under constant gentle shaking. To reveal cholinergic neurons we used anti-cholineacetyltransferase (AB144P, Chemicon, raised in goat) at a dilution of 1:1500. To reveal putative catecholaminergic neurons we used anti-tyrosine hydroxylase (TH) (AB151, Chemicon, raised in rabbit) at a dilution of 1:6000. To reveal serotonergic neurons we used anti-serotonin (AB938, Chemicon, raised in rabbit) at a dilution of 1:7500. This step was followed by three 10 min rinses in 0.1 M PB, after which the sections were incubated in a secondary antibody for 2 h. The secondary antibody solution contained a 1:500 dilution of biotinylated anti-rabbit IgG (BA-1000, Vector Labs) in 3% NGS (or anti-goat IgG, BA-5000 in 3% NRS for the ChAT sections), and 2% BSA in 0.1 M PB. After three 10 min rinses in 0.1 M PB, the sections were incubated for 1 h in AB solution (Vector Labs), and again rinsed. The sections were then treated in a solution of 0.05% diaminobenzidine (DAB) in 0.1 M PB for 5 min, following which 3 μl of 30% H_2O_2 was added to each 1 ml of solution in which each section was immersed. Staining development was monitored visually and checked under a low power stereomicroscope. This was allowed to continue until the background staining was at a level at which it could assist reconstruction without obscuring the immunopositive neurons. Development was then arrested by placing the sections in 0.1 M PB, and then rinsed twice more in the same solution. Sections were mounted on glass slides coated with 0.5% gelatine and left to dry overnight. They were then dehydrated in a graded series of alcohols, cleared in xylene, and coverslipped with Depex. Two controls were employed in the immunohistochemistry, including the omission of the primary antibody, and omission of the secondary antibody in selected sections from which no staining was evident.

The sections were observed with a low power stereomicroscope, and the architectonic borders of the sections traced according to the Nissl and myelin stained sections using a camera lucida. The immuno-stained sections were then matched to the drawings and the immuno-positive neurons marked. The drawings were then scanned and redrawn using the Canvas 8 drawing program. The nomenclature used for the cholinergic system was adopted from Woolf (1991), Manger et al. (2002a), Maseko and Manger (2007), and Maseko et al. (2007), the putative catecholaminergic system from Dahlström and Fuxe (1964), Hökfelt et al. (1984), Smeets and González (2000), Manger et al. (2002b), Maseko and Manger (2007), Maseko et al. (2007), Moon et al. (2007), and Dwarika et al. (2008) and for the serotonergic system from Törk (1990), Bjarkam et al. (1997), Manger et al. (2002c), Maseko and Manger (2007), Maseko et al. (2007), Moon et al. (2007), and Dwarika et al. (2008). While we use the standard nomenclature for the catecholaminergic system in this paper, we realise that the neuronal groups we revealed with tyrosine hydroxylase immunohistochemistry may not correspond directly with these nuclei as has been described in previous studies by Dahlström and Fuxe (1964), Hökfelt et al. (1976), Meister et al. (1988), Kitahama et al. (1990, 1996), and Ruggiero et al. (1992). However, given the striking similarity of the results of the tyrosine hydroxylase immunohistochemistry to that seen in other mammals we feel this terminology is appropriate. Clearly further studies in the mole-rat species used with a wider range of antibodies, such as those to phenylethanolamine-*N*-methyltransferase (PNMT), dopamine-β-hydroxylase (DBH) and aromatic L-amino acid decarboxylase (AADC) would be required to fully determine the implied homologies ascribed in this study. We address this potential problem with the caveat of putative catecholaminergic neurons where appropriate in the text.

3. Results

In the current study the cholinergic, putative catecholaminergic, and serotonergic systems of two species of mole-rat were visualised using immunohistochemical techniques. The two species of mole-rat used, the highveld mole-rat (*C. hottentotus pretoriae*) and the Cape dune mole-rat (*B. suillus*) (Fig. 1), while being closely related (Bennett and Faulkes, 2000), differ substantially in both body and brain mass, where the Cape dune mole-rats had an average body mass of 965 g and an average brain mass of 3.4 g, while the highveld mole-rats had an average body mass of 86.5 g and an average brain mass of 1.5 g. Our analysis of these systems indicated extreme similarity in terms of both nuclear organization and neuronal morphology, thus the following description applies to both species unless otherwise specified. Moreover, the cohort of nuclei described in the present study for the two species of mole-rat does not differ from observations previously provided for these systems in other rodent species (e.g. Da Silva et al., 2006; Moon et al., 2007; Dwarika et al., 2008).

3.1. Cholinergic neurons

The cholinergic system of mammals is most often divided into striatal, basal forebrain, diencephalic, and pontomesencephalic groups, as well as the motor cranial nerve nuclei (Woolf, 1991; Manger et al., 2002a; Maseko et al., 2007). Each of these groups contains a cluster of distinct nuclei that are found throughout the brain from the level of the anterior horn of the lateral ventricle through to the spino-medullary junction. The mole-rats investigated showed no specific differences to this general mammalian organizational plan.

3.1.1. Striatal cholinergic interneurons

3.1.1.1.Nucleus accumbens. A cluster of choline acetyltransferase immunopositive (ChAT+) neurons located ventral to the dorsal striatopallidal complex (caudate, putamen, globus pallidus, see below) was designated as the nucleus accumbens. The anterior border of this nucleus was coincident with the anterior border of the lateral ventricle and the posterior border was located at the level of the anterior commissure (Figs. 2D–F and 3C–E). The location of the nucleus accumbens in the mole-rat species studied is typical of all mammals (Woolf, 1991; Manger et al., 2002a; Maseko et al., 2007). There was a moderate density of ChAT+ neurons throughout this nucleus and the cell bodies were ovoid in shape. These neurons evinced a varying mixture of bipolar and tripolar types and showed no specific dendritic orientation (Fig. 4A).

3.1.1.2.Dorsal striatopallidal complex—caudate/putamen and globus pallidus. This nuclear complex was located between the level of the anterior border of the lateral ventricle (anteriorly) and at the level of the habenular nuclei (posteriorly) within the cerebral hemisphere (Figs. 2D–I and 3C–H). It is not until the level of the globus pallidus that the caudate and putamen form distinct nuclei that are clearly split by the internal capsule. A moderate density of ChAT+ interneurons were observed throughout the caudate and putamen. Within the ventral portion of the globus pallidus, at its borders with the putamen and nucleus basalis (see below), a small number of ChAT+ neurons were observed. The ChAT+ neurons were ovoid in shape, mostly bipolar, but with some multipolar forms, and showed no specific dendritic orientation (Fig. 4A).

3.1.1.3.Islands of Calleja and olfactory tubercle. These nuclei were found in the ventral most portion of the anterior part of the telencephalon deep to the nucleus accumbens from the level of the anterior pole of the lateral ventricle to the level of the globus pallidus (Figs. 2D–F and 3C–E). A moderate density of ChAT+ neurons was observed throughout the olfactory tubercle with some clustering of neurons in the ventral most portions representing the islands of Calleja. The cell bodies were ovoid in

shape, a varying mixture of bi- and multipolar types and exhibited a weak mediolateral dendritic orientation.

3.1.2. Cholinergic nuclei of the basal forebrain

3.1.2.1.Medial septal nucleus. This nucleus was located in the rostral half of the medial wall of the cerebral hemispheres within the septal nuclear complex below the rostrum of the corpus callosum in a position dorsal to the diagonal band of Broca (see below) (Figs. 2E & 3E and F). A moderate to high density of ChAT+ neurons was found throughout this nucleus. The ChAT+ neurons were ovoid in shape, a varying mixture of bi- and multipolar types, and had a rough dorsoventral orientation of the dendrites.

3.1.2.2.Diagonal band of Broca. The diagonal band of Broca was located in the ventromedial corner of the cerebral hemispheres in a position anterior to the hypothalamus (Figs. 2D and E & 3D–F). A moderate to high density of ChAT+ neurons was found throughout this nucleus. The neuronal cells of this nucleus were slightly larger than those of adjacent cholinergic groups but they maintained an ovoid shape and were a mixture of bi- and multipolar types (Fig. 4A). The dendrites were oriented parallel to the ventromedial edge of the cerebral hemisphere. It was possible to divide this nucleus into both horizontal and vertical limbs, but this was not deemed necessary since it would not add any value to the description.

3.1.2.3.Nucleus basalis. ChAT+ neurons located ventral to the anterior pole of globus pallidus at the level of the anterior commissure as well as in a position ventral to globus pallidus and caudal to the olfactory tubercle were assigned to the nucleus basalis (Figs. 2F–I and 3F–H). A varying density, from low to high, of ChAT+ neurons was seen throughout this region. At the caudal region of this nucleus the neurons appear to be continuous with

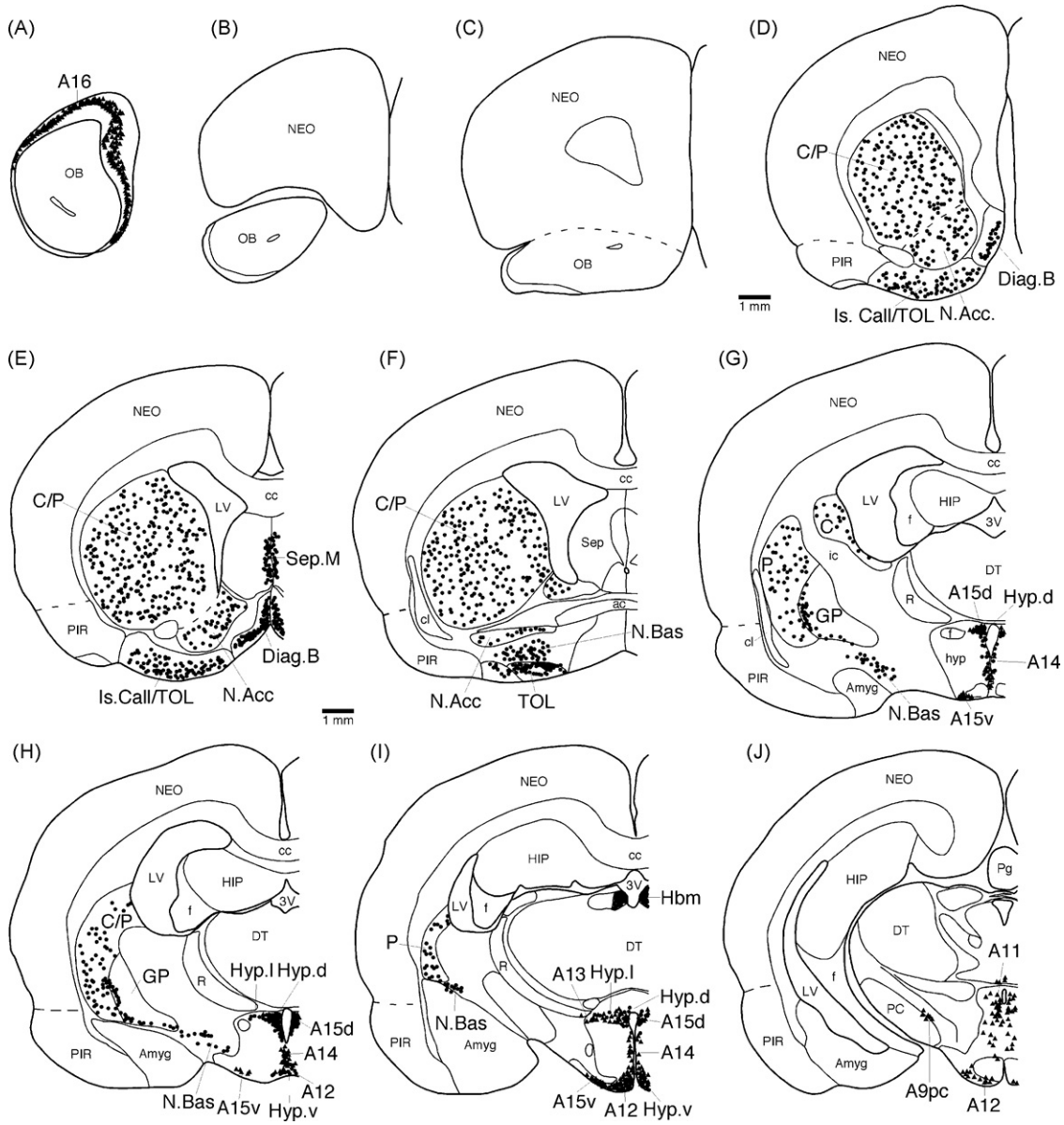

Fig. 2. Serial drawings of coronal sections through one half of the Cape dune mole-rat brain, from the olfactory bulbs through to the medulla. The outlines of the architectonic regions were drawn using nissl and myelin stains and immunoreactive cells marked on the drawings. Solid black circles depict cholinergic neurons, solid triangles depict catecholaminergic neurons (those immunoreactive for tyrosine hydroxylase) and open squares depict serotonergic neurons. Each circle, triangle or square represents an individual neuron. The figures are approximately 1500 μm apart. See list for abbreviations.

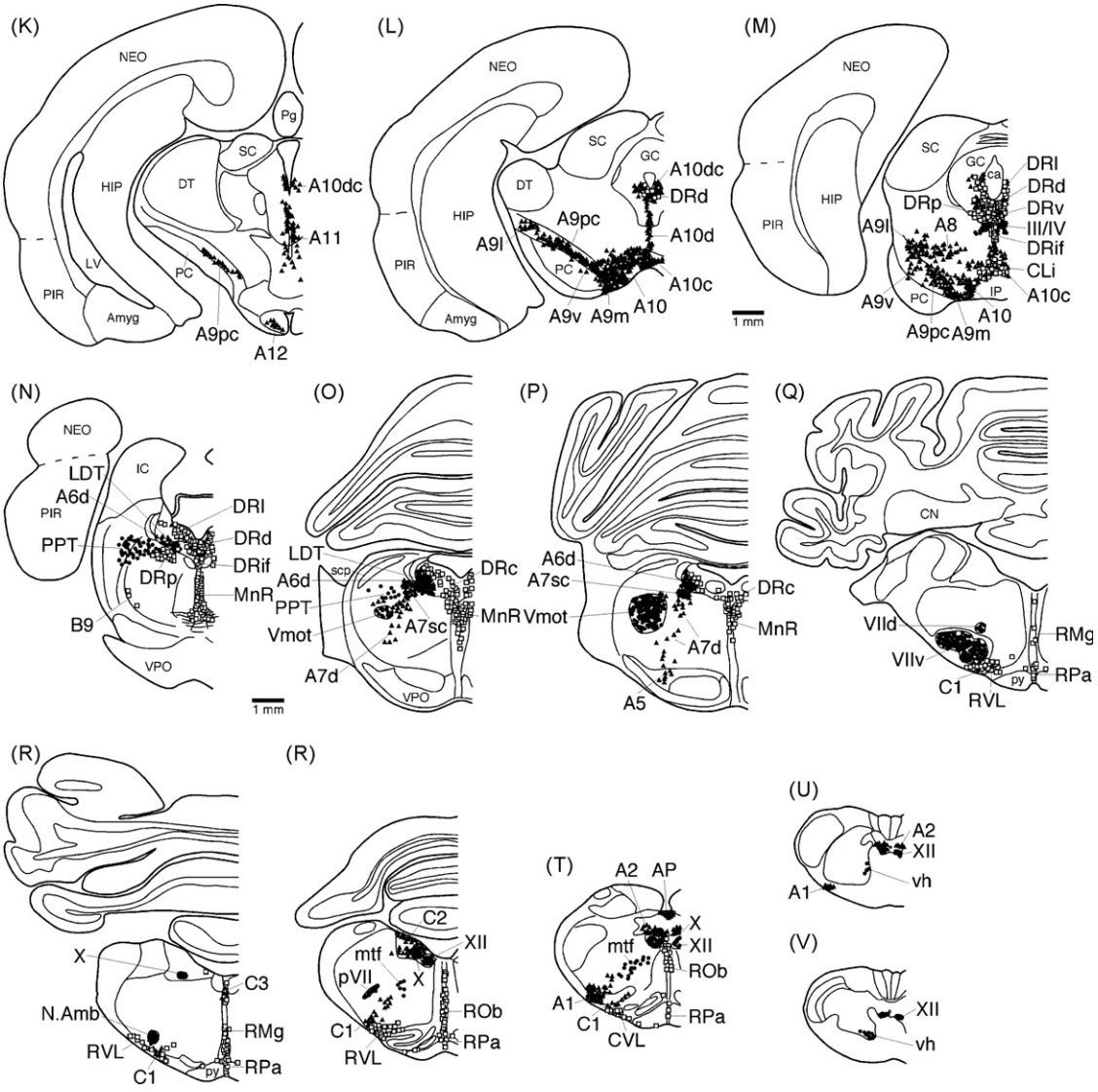

Fig. 2. (*Continued*).

those of the ventral portion of the globus pallidus (see above). These ChAT+ neurons were a mixture of ovoid and fusiform shapes, showed a varying combination of bi- and multipolar types, and evinced no specific dendritic orientation.

3.1.3. Diencephalic cholinergic nuclei

3.1.3.1Medial habenular nucleus. The medial habenular nucleus, which contained a dense aggregation of ChAT+ neurons, formed part of the epithalamus and was located in the dorsomedial aspect of the diencephalon adjacent to the third ventricle (Figs. 2I & 3H and I). The ChAT+ neurons in this nucleus were round and small in shape, and due to the dense packing it was impossible to determine if there was any specific dendritic orientation (Fig. 4B). The axons emanating from these neurons formed the distinct fasciculus retroflexus that was visible with ChAT immunoreactivity along its entire trajectory to the interpeduncular nucleus.

3.1.3.2.Dorsal hypothalamic group. Located within the dorsomedial aspect of the hypothalamus between the third ventricle and the fornix, a cluster of ChAT+ neurons, intermingled with those of the A15D nucleus (see below) was designated as the dorsal hypothalamic cholinergic group (Figs. 2G–I and 3I–K). The ChAT+ neurons were sparsely populated within this nucleus and they were also not intensely ChAT immunoreactive (in comparison to other immunoreactive neurons). These ChAT+ neurons were round to fusiform in shape and showed no specific dendritic orientation.

3.1.3.3.Lateral hypothalamic group. This nucleus was located within the dorsolateral portion of the hypothalamus, lateral to the fornix, and contained palely stained ChAT+ neurons, in a low to moderate density (Figs. 2H and I & 3J and K). The neurons forming this nucleus were intermingled with those of A13 nucleus (see below). The cell bodies of the ChAT+ neurons were ovoid in shape, bipolar in type and exhibited no specific dendritic orientation.

3.1.3.4.Ventral hypothalamic group. The ChAT+ neurons representing this nucleus were located in the ventral portion of the hypothalamus and were intermingled with neurons of the A12 and A15v nuclei (see below), respectively (Figs. 2H and I & 3J). At the midline a moderate density of ChAT+ neurons were found, but the density decreased steadily with distance from the midline. The neuronal bodies were round, bipolar in type, and exhibited a rough mediolateral dendritic orientation.

3.1.4. Pontomesencephalic cholinergic nuclei

3.1.4.1.Parabigeminal nucleus. Located at the very lateral aspect of the pontine tegmentum, ventral to the inferior colliculus, was a small cluster of ChAT+ neurons that were assigned to the parabigeminal nucleus (Fig. 3N). As previously reported (Da Silva et al., 2006) there were less than10 neurons in this nucleus in the highveld mole-rat, but up to approximately 50 neurons could be observed in this nucleus in the larger-brained Cape dune mole-rat. The neurons were palely stained as reported previously for rodents (Woolf, 1991) and specifically the highveld mole-rat (Da Silva et al., 2006), were found in a very low density, appeared ovoid in shape, were bipolar and showed no specific dendritic orientation.

3.1.4.2.Pedunculo-pontine tegmental (PPT) nucleus. The ChAT+ neurons comprising the PPT nucleus were located within the dorsal aspect of the pontine tegementum immediately inferior to the superior cerebellar peduncle, from the level of the oculomotor nucleus to the trigeminal motor nucleus, a position that is typical of all mammals (Figs. 2N and O & 3M–O) (Woolf, 1991; Manger et al., 2002a; Maseko et al., 2007). A moderate to high density of intensely reactive ChAT+ neurons were found throughout the region. The cell bodies of the ChAT+ neurons were of a mixture of varying shapes, and the neurons themselves expressed a mixture of bi- and multipolar types, with no specific dendritic orientation irrespective of polarity (Fig. 4C).

3.1.4.3.Laterodorsal tegemental (LDT) nucleus. A cluster of ChAT+ neurons located within the ventrolateral portion of the peri-aqueductal and periventricular grey matter, immediately caudal to the oculomotor nucleus were classified as belonging to the LDT nucleus (Figs. 2N and O & 3N and O). These neurons were seen to intermingle with the caudal-most neurons of the diffuse division of the locus coeruleus (A6d) neurons (see below). A moderate to high density of ChAT+ neurons were found throughout this region. The cell bodies were a mixture of ovoid and other shapes, mostly multipolar in type, with a predominant dorsomedial to ventro-lateral dendritic orientation (Fig. 4C).

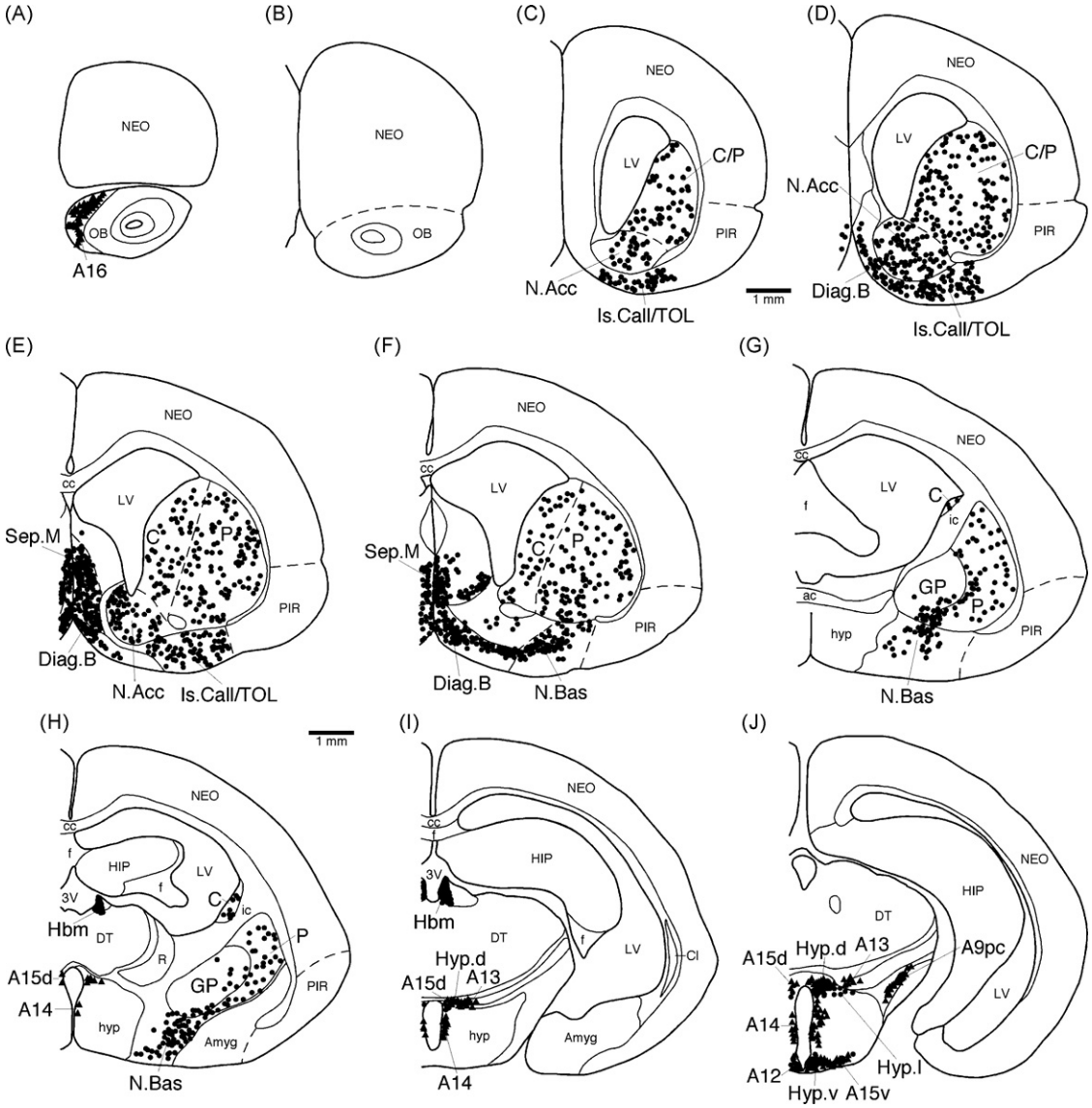

Fig. 3. Serial drawings of coronal sections through one half of the highveld mole-rat brain, from the olfactory bulbs through to the medulla. Conventions as in Fig. 2. The figures are approximately 750 μm apart. See list for abbreviations.

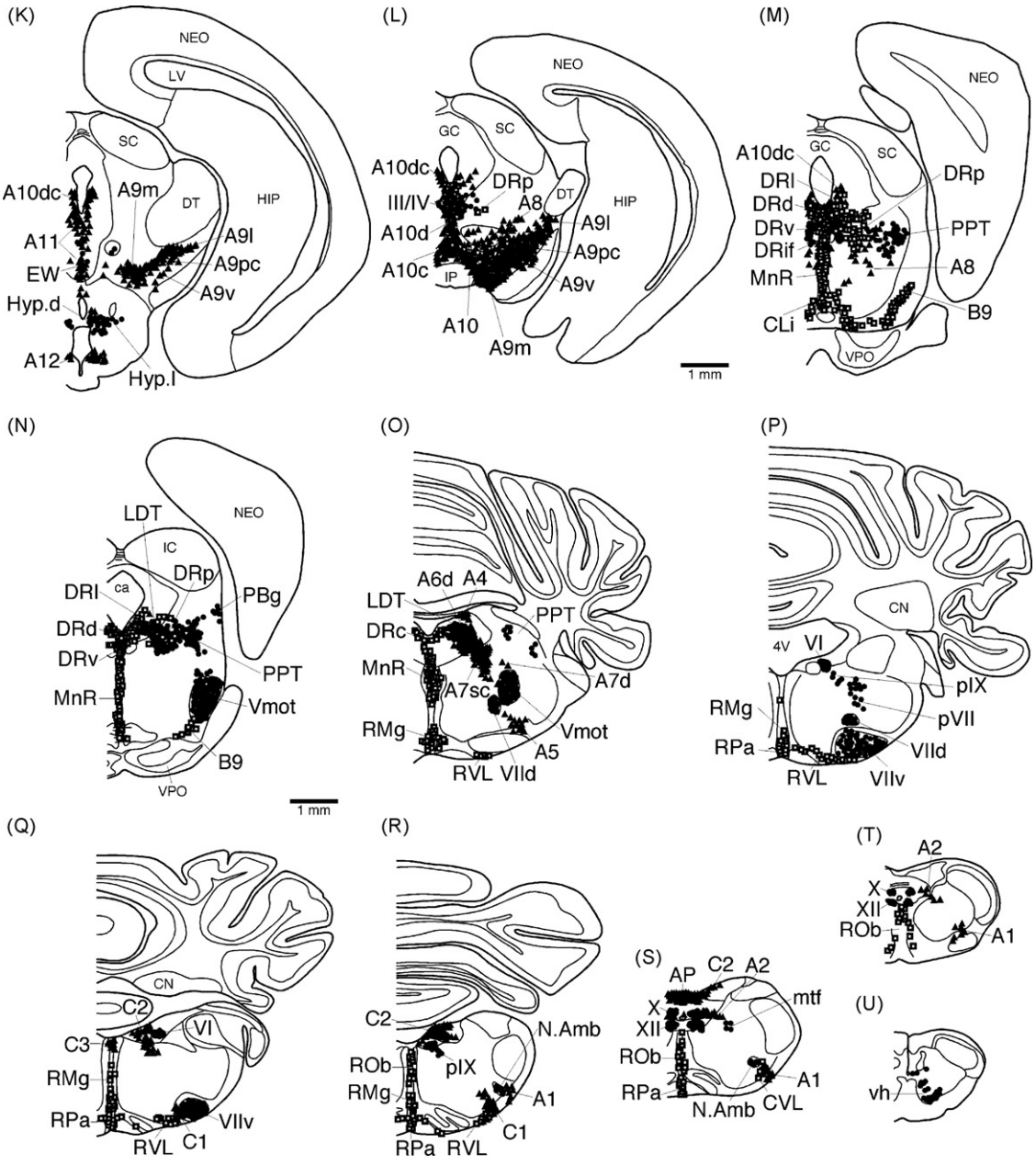

Fig. 3. (*Continued*).

3.1.5. Cholinergic cranial nerve motor nuclei

These nuclei were found in positions typical of all mammals and all contained large multipolar motor neurons (Woolf, 1991; Manger et al., 2002a; Maseko et al., 2007). The ChAT+ nuclei identified in both mole-rat species include: a fused oculomotor (III) and trochlear (IV) nucleus (Fig. 4D), motor division of the trigeminal (Vmot), adbucens (VI), dorsal and ventral subdivisions of the facial (VIId and VIIv), nucleus ambiguus, dorsal motor vagus (X), hypoglossal (XII), Edinger–Westphal (EW), medullary tegemental field (mtf) and the preganglionic motor neurons of the salivatory (pVII) and the glossopharyngeal (pIX) nerves (Figs. 2M–V and 3L–U). The few, small, round, palely stained ChAT+ neurons of the Edinger–Westphal nucleus, a primarily visual structure, were located in the midline between the fused oculomotor and trochlear nuclei and this nucleus was generally very reduced in size compared to other mammals. ChAT+ neurons found belonging to the pVII and pIX nerves were located in a region dorsal to the dorsal division of the facial nucleus and ventral to the abducens and dorsal motor vagus nuclei in the medullary tegmentum and evince a similar morphology to all other motor neurons. Caudal to these, cholinergic neurons of a similar morphology were assigned to the medullary tegmental field.

3.2. Putative catecholaminergic nuclei

Tyrosine hydroxylase immunoreactive neurons (TH+), classified in this study as putative catecholaminergic neurons (see above), formed a number of identifiable nuclear complexes and nuclei that were found throughout the brains of the mole-rats studied extending from the olfactory bulbs to the spinomedullary junction. The locations of these nuclear complexes and nuclei were identical to those seen in other rodents and other mammals, and divisible into distinct regional clusters including the olfactory bulb, diencephalic, midbrain, pontine and medullary nuclei. For

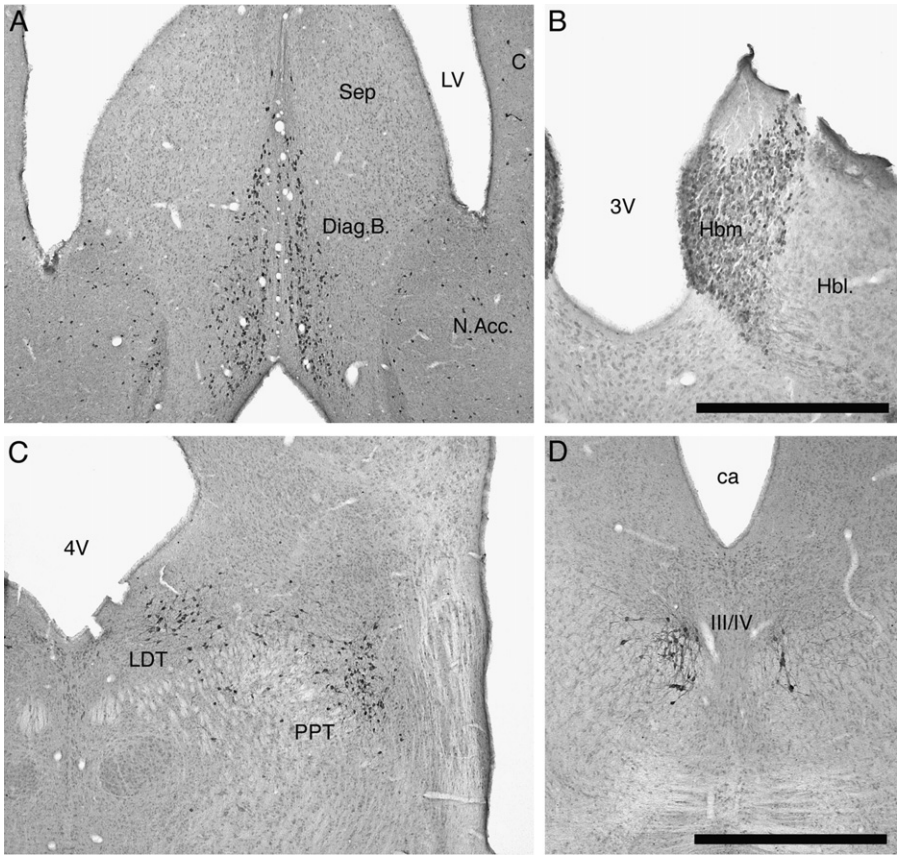

Fig. 4. Photomicrographs showing neuronal groups that are immunoreactive for choline acetyltrasnferase in the brain of the highveld mole-rat. (A) Basal forebrain showing the diagonal band of Broca (Diag.B.) located below the septal region (Sep) and medial to the nucleus accumbens (N.Acc.), lateral ventricle (LV) and head of the caudate nucleus (C). (B) The densely populated medial habenular nucleus (Hbm) located between the third ventricle (3V) and the lateral habenular nucleus (Hbl) in the dorsal diencephalon. (C) The laterodorsal tegemental (LDT) and pedunculopontine tegmental (PPT) nuclei in the dorsal pontine region ventral to the fourth ventricle (4V). (D) The merged oculomotor (III) and trochlear (IV) nuclei located in the midbrain. ca: cerebral aqueduct. Scale bar in B = 500 μm. Scale bar in D = 1 mm and applies to A, C and D.

simplicity, the nuclei are referred to using the nomenclature of Dahlström and Fuxe (1964) and Hökfelt et al. (1984). No putative catecholaminergic nuclei outside the bounds of the classically defined nuclei (e.g. Smeets and González, 2000) were found.

3.2.1. Olfactory bulb (A16)

A high density of TH+ neurons, probably representing periglomerular dopaminergic interneurons were found within the stratum granulosum of the olfactory bulb (Figs. 2A and 3A). The cell bodies were ovoid to triangular in shape, small in size, multipolar and were found surrounding the glomeruli, especially so the deeper aspect. A dense dendritic network emanating from these neurons was seen to surround the glomeruli.

3.2.2. Diencephalic nuclei

Six clusters of TH+ neurons, forming distinct nuclei, were observed within the hypothalamus, these being: the anterior hypothalamic group, dorsal division (A15d); the anterior hypothalamic group, ventral division (A15v); the rostral periventricular cell group (A14); the zona incerta (A13); the tuberal cell group (A12); and the caudal diencephalic group (A11) (Figs. 2G–K and 3H–K). Within the dorsal anterior portion of the hypothalamus, between the third ventricle and the fornix intermingled with cholinergic neurons of the dorsal hypothalamic group (see above), a moderate density of TH+ neurons representing the A15d nucleus was found. These neurons were ovoid in shape, bipolar and showed a mostly mediolateral dendritic orientation. The A15v nucleus was located in the ventrolateral portion of the hypothalamus close to the floor of the brain. A low to moderate density of TH+ neurons was found in this region and the cell bodies of these were ovoid in shape, bipolar, with a dendritic orientation running parallel to the floor of the hypothalamus (Fig. 5D). TH+ neurons assigned to the A14 nucleus were found in bilateral low to moderately densely packed columns adjacent to the lateral edges of the third ventricle. The cell bodies were ovoid in shape, predominantly bipolar but there were some multipolar neurons, and exhibited a dendritic orientation, for the most part, parallel to the lateral wall of the third ventricle (Fig. 5C). Within the dorsolateral aspect of the hypothalamus, lateral to the fornix and intermingling with the zona incerta of the ventral thalamus and the cholinergic neurons of the lateral hypothalamic group (see above) was a small number of TH+ neurons that were assigned to the A13 nucleus. These neurons appeared to form a lateral continuation of the A15d neurons and showed a similar ovoid, bipolar morphology with a mediolateral dendritic orientation. TH+ neurons assigned to the A12 nucleus were found in the ventral medial portion of the hypothalamus, surrounding and below the floor of the third ventricle in the vicinity of the arcuate nucleus. These neurons were ovoid, bipolar and showed a dendritic orientation either parallel to the floor of the hypothalamus or the wall of the third ventricle (Fig. 5D). Within the hypothalamic grey matter adjacent to the posterior pole of the third ventricle, a moderate density of TH+ neurons were located and these formed the A11 nucleus. For the most part, these neurons were ovoid and bipolar with a dorsoventral dendritic orientation (Fig. 5A and B).

3.2.3. Midbrain nuclei

3.2.3.1.Ventral tegmental area nuclei (VTA, A10 complex). In the medial portion of the tegmentum of the midbrain at the level of the oculomotor nucleus, a nuclear complex containing four nuclei (A10: ventral tegmental area; A10c: ventral tegmental area central; A10d: ventral tegmental area dorsal; A10dc: ventral tegmental area dorsal caudal) was found. These nuclei extended from within the periaqueductal grey matter around the base of the aqueduct, into the tegmentum below the periaqueductal grey matter around the midline, through to and around the interpeduncular nucleus (Figs. 2K–M and 3K–M). A high density of TH+ neurons, found dorsal and dorsolateral to the interpeduncular nucleus, between this nucleus and the root of the oculomotor nerve (IIIn), was assigned to the A10 nucleus. These neurons were ovoid in shape, bipolar in type and the dendrites were oriented parallel to the edge of the interpeduncular nucleus (Figs. 5E and 6). Immediately dorsal to the interpeduncular nucleus intermingled with neurons of the CLi (see below), in a location just anterior to the decussation of the superior cerebellar peduncle, was a dense cluster of ovoid, bipolar TH+ neurons forming the A10c nucleus (Figs. 5E and 6). The dendrites of these neurons were oriented parallel to the dorsal margin of the interpeduncular nucleus. Immediately dorsal to A10c, between it and the oculomotor nucleus, was a dense bilateral parasagittal cluster of ovoid, bipolar TH+ neurons, with a dorsoventral dendritic orientation, that formed the A10d subdivision (Figs. 5B and E & 6). The TH+ neurons assigned to the A10dc nuclear complex were found within the

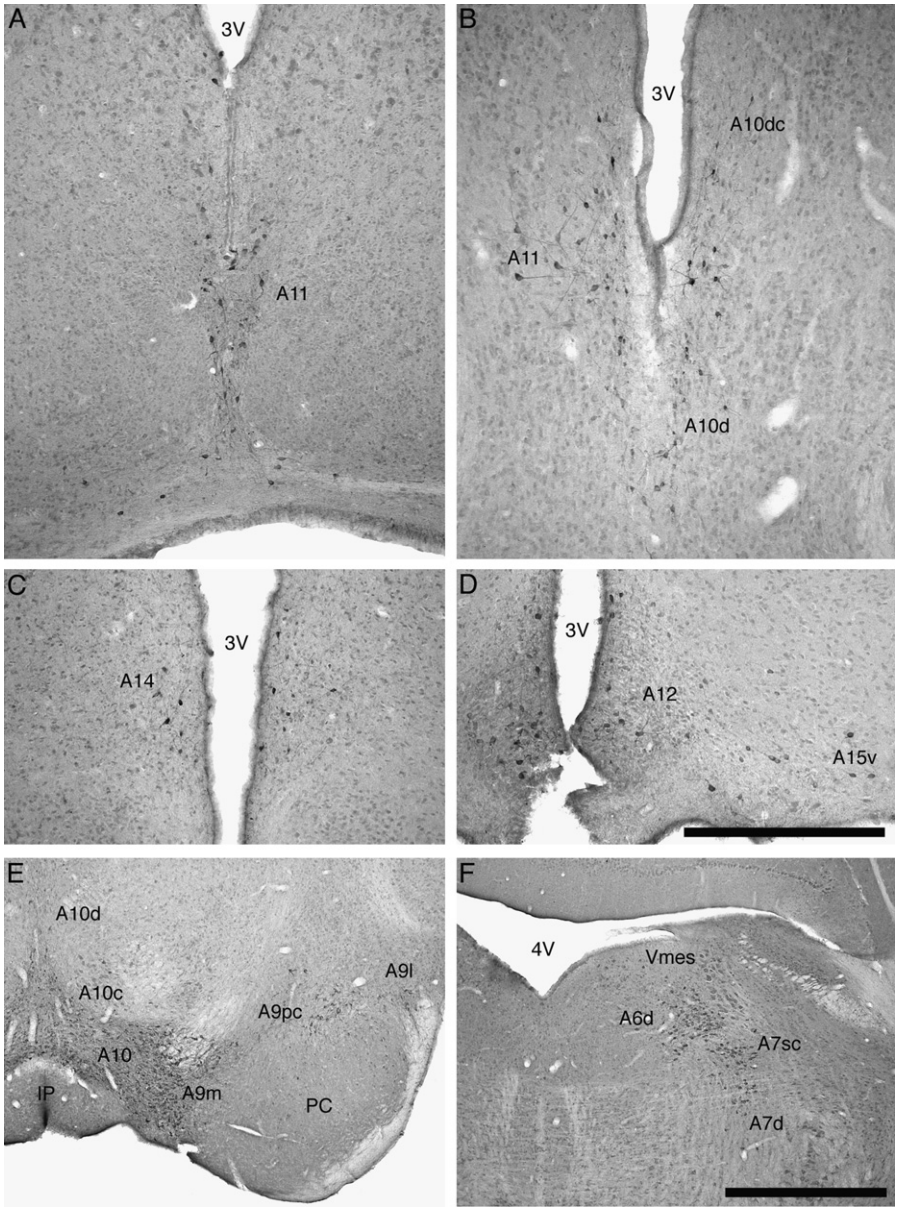

Fig. 5. Photomicrographs showing neuronal groups that are immunopositive for tyrosine hydroxylase in the diencephalon, midbrain and pons of the mole-rat brain. Images A, C and D are from the brain of the Cape dune mole-rat, and B, E and F are from the highveld mole-rat. (A) The caudal diencephalic group (A11) in the Cape dune mole-rat. (B) A11, ventral tegmental area, dorsal caudal nucleus (A10dc) and ventral tegmental area, dorsal nucleus (A10d) in the highveld mole-rat. (C) The rostral periventricular nucleus (A14) in the Cape dune mole-rat. (D) The ventral division of the anterior hypothalamic group (A15v) and the tuberal cell group (A12) in the Cape dune mole-rat. Scale bar in D = 500 μm and applies to A–D. (E) Some nuclei of the ventral tegmental area (A10, A10c, A10d) and substantia nigra (A9m, A9pc and A9l) in the highveld mole-rat. (F) Some nuclei of the locus coeruleus complex (A6d, A7sc and A7d) in the highveld mole-rat. Scale bar in F = 1 mm and applies to E and F. 3V: third ventricle; 4V: fourth ventricle; PC: cerebral peduncle; IP: interpeduncular nucleus; Vmes: fifth mesencephalic nucleus.

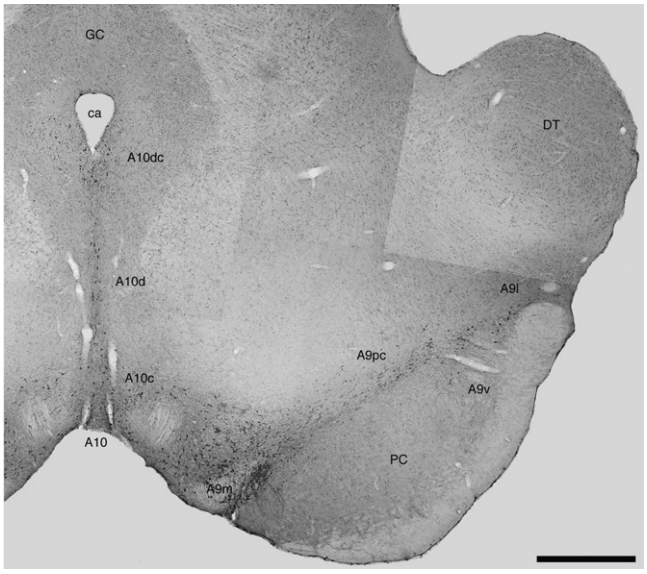

Fig. 6. Photomontage of the nuclear organization of the ventral tegmental area (A10, A10c, A10d and A10dc) and the substantia nigra (A9m, A9pc, A9l and A9v) in the Cape dune mole-rat as revealed using tyrosine hydroxylase immunohistochemistry. Scale bar = 1 mm. ca: cerebral aqueduct; PC: cerebral peduncle; DT: dorsal thalamus; GC: periaqueductal grey matter.

periaqueductal grey matter adjacent to and surrounding the ventral half of the cerebral aqueduct. A moderate density of small neurons was seen in this region and the cell bodies were ovoid in shape, a mixture of bi- and multipolar types with a dendritic orientation running parallel to the edge of the cerebral aqueduct (Figs. 5B and 6). The number of neurons in the A10dc nucleus appear to be far more numerous and widespread in the Cape dune mole-rat when compared with the highveld mole-rat (Fig. 7).

3.2.3.2.Substantia nigra (A9). The substantia nigra nuclear complex was located in the ventral and lateral portions of the midbrain tegmentum, lying just dorsal to the cerebral peduncles. Evidence for four distinct nuclei namely, the substantia nigra, pars compacta (A9pc), substantia nigra, ventral or pars reticulata (A9v), substantia nigra, pars lateralis (A9l) and substantia nigra, pars medialis (A9m), were found within the A9 complex (Figs. 2J–M and 3J–L). A9pc was seen to be a dense band of TH+ neurons that ran from medial to lateral immediately dorsal to the cerebral peduncle. The neurons were ovoid in shape, bipolar in type and showed a dendritic orientation parallel to the mediolateral orientation of the band (Figs. 5E and 6). Within the dorsal portion of the cerebral peduncle ventral to A9pc, occasional TH+ neurons that were ovoid in shape, bipolar in type, with no specific dendritic orientation, were assigned to the A9v nucleus (Fig. 6). Not many neurons were evident in this nucleus in either species. At the lateral edge of A9pc, a loose aggregation of ovoid, bipolar TH+ neurons formed the A9l nucleus (Figs. 5E and 6). Within this nucleus the neurons were moderate in density and showed no specific dendritic orientation. Medial to A9pc and lateral to the root of the oculomotor nerve (IIIn), a dense cluster of ovoid, bipolar TH+ neurons with no specific dendritic orientation, formed the A9m subdivision (Figs. 5E and 6).

3.2.3.3.Retrorubal nucleus (A8). Scattered throughout the midbrain tegmentum, in a position caudal to the magnocellular division of the red nucleus and dorsal to the A9 complex, was a sparsely packed but relatively numerous, cluster of TH+ neurons that formed the A8 nucleus (Figs. 2M & 3L and M). The cells of this region were ovoid in shape, a mixture of bipolar and multipolar types and showed no specific dendritic orientation.

3.2.3.4.The locus coeruleus (LC) nuclear complex. Within the pontine region a large number of TH+ neurons forming the locus coeruleus complex were readily identified in both species. In each mole-rat investigated the locus coeruleus complex could be readily subdivided into five nuclei, these being: the subcoeruleus compact portion (A7sc), subcoeruleus diffuse portion (A7d), locus coeruleus diffuse portion (A6d), fifth arcuate nucleus (A5), and the dorsal medial division of locus coeruleus (A4) (Figs. 2N–P and 3O). Within the dorsal portion of the pontine tegmentum adjacent to the ventrolateral region of the periaqueductal grey matter, a tightly packed cluster of TH+ neurons represented the A7 compact portion of the LC. This division is the same as what was previously described as the subcoeruleus (Dahlström and Fuxe, 1964; Olson and Fuxe, 1972). The cells were ovoid in shape, bipolar in type and showed no specific orientation of the dendrites (Fig. 5F). Ventral and lateral to the A7sc, a diffusely organised aggregation of TH+ neurons formed the A7d nuclear complex. These neurons are located both medially and laterally around the trigeminal motor nucleus (Vmot). They are more numerous in the cape dune mole-rat but this appears to be related to the larger brain size rather than a specific increase in number that may be interpreted as an adaptive increase in neuronal number. The TH+ neurons of this region were ovoid in

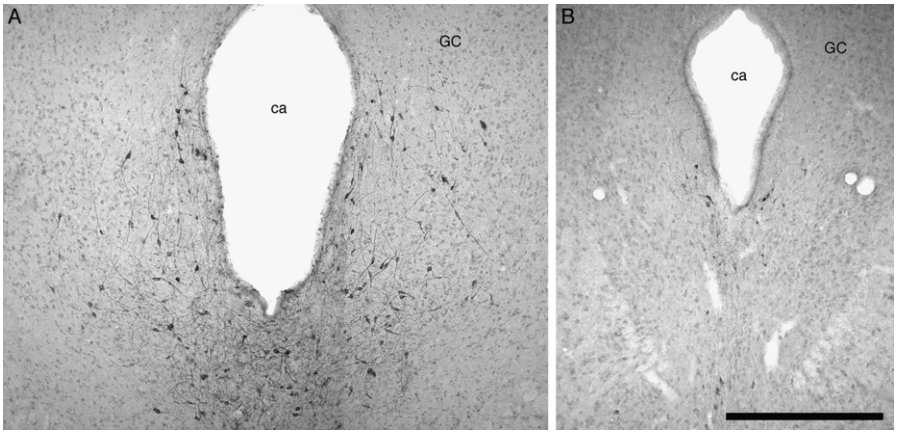

Fig. 7. Photomicrographs of the dorsal caudal nucleus of the ventral tegmental area (A10dc) in the (A) Cape dune mole-rat and (B) highveld mole-rat. Note the significant expression of this nucleus in the Cape dune mole-rat compared with the highveld mole-rat that has an A10dc nucleus similar to that seen in other rodents. It is unclear why this nucleus should be so well expressed in the Cape dune mole-rat in comparison to other rodents. Scale bar in B = 500 μm and applies to both A and B. ca: cerebral aqueduct; GC: periaqueductal grey matter.

shape, bipolar in appearance and showed no specific dendritic orientation (Fig. 5F). Within the ventrolateral portion of the periventricular grey matter a loose to moderate density of TH+ neurons were assigned to the A6d nucleus. The neurons of this group were not found adjacent to the wall of the fourth ventricle as seen in the laboratory rat (Dahlström and Fuxe, 1964) but were located in the ventrolateral half of the periventricular grey matter as seen in other rodent species (Moon et al., 2007; Dwarika et al., 2008). The neuronal morphology was again similar to that of other nuclei in this complex; however there was a predominant dendritic orientation in the dorsomedial to ventrolateral plane, although many other dendrites were oriented in various other directions (Fig. 5F).

In the ventrolateral pontine tegmentum lateral to the superior olivary nucleus and lateral to Vmot and A7d, a small cluster of TH+ neurons formed the A5 nucleus. These neurons showed irregular somal shapes, were mostly multipolar and formed a rough mesh-like dendritic network around the ascending fascicles located within the ventrolateral pontine tegmentum. Immediately adjacent to the wall of the fourth ventricle, in the dorsolateral portion of the periaqueductal grey matter, a very few TH+ neurons represent the A4 nucleus, which showed a similar morphology to the neurons of the A6d nucleus.

3.2.3.5.Medullary nuclei. Within the medulla of both species we found evidence for six putative catecholaminergic nuclei these being: rostral ventrolateral tegmental group (C1), rostral dorsomedial group (C2), rostral dorsal midline group (C3), caudal ventrolateral tegmental group (A1), caudal dorsomedial group (A2) and area postrema (AP) (Figs. 2Q–U and 3Q–T). The TH+ neurons forming the C1 nucleus were found in the ventrolateral medulla from the level of the facial nerve nucleus to the mid-level of nucleus ambiguus. The neurons were found at a low density throughout the region and the neuronal morphology was similar to those found in the A5 group. Continuing in the ventrolateral medulla, a column of TH+ neurons located laterally to the posterior most part of the C1 nucleus and extending to the spinomedullary junction, was designated as forming the A1 nucleus. The somata were irregular in shape, multipolar and formed a mesh-like dendritic network around the ascending fascicles. The A1 column was distinguished from the ventrolateral C1 column by occupying a position lateral to the lateral reticular nucleus and nucleus ambiguus, whereas C1 was located medial to these structures.

In the dorsal part of the medulla, in the region of the anterior part of the dorsal and medial border of the nucleus tractus solitarius, a distinct cluster of numerous TH+ neurons was designated as the C2 nucleus. Within this nucleus there was a clear region close to the floor of the fourth ventricle termed the dorsal strip and a continuation of this cluster into the region of the tractus solitarius termed the rostral subdivision of the C2 nucleus. Within the dorsal strip of C2 the neurons were ovoid in shape, bipolar in appearance and showed a dendritic orientation parallel to the floor of the fourth ventricle. In the rostral region the cells were ovoid in shape, a varying mixture of bi- and multipolar types and there was no specific orientation of the dendrites. Within the dorsal medial medullary tegmentum at the midline, dorsal to the raphe obscurus and close to the floor of the fourth ventricle, a small number of TH+ neurons representing the C3 nucleus were found. These neurons were ovoid in shape, bipolar in appearance and showed a dorsoventral dendritic orientation. Between the caudal portions of the dorsal motor vagus and hypoglossal cranial nerve nuclei, a small number of TH+ neurons represented the A2 nucleus. The cells bodies were ovoid in shape, with the neurons being mostly bipolar, but there were a few multipolar neurons in this cluster. These neurons showed a mediolateral orientation of the dendrites. Some of these A2 neurons were located a small distance into the dorsal caudal medullary tegmentum. Straddling the midline, dorsal to the central canal and the dorsal motor vagus nucleus, and between the most caudal region of the bilateral C2 nucleus, was a single large cluster of intensely stained TH+ neurons, the area postrema. These small round TH+ neurons were very densely packed within this region and no particular dendritic orientation could be identified.

3.3. Serotonergic nuclei

The serotonergic (5HT+) nuclei identified in the current study of the mole-rats were the same as those previously identified in all rodents and other eutherian mammals studied to date (Maseko et al., 2007). The serotonergic nuclei were all located within the brainstem and can be divided into a rostral and a caudal cluster. Both of these clusters contained a number of distinct nuclei that are found throughout the brainstem from the level of the decussation of the superior cerebellar peduncle through to the spinomedullary junction.

3.3.1. Rostral cluster

3.3.1.1.Caudal linear nucleus (CLi). This nucleus was the most rostral of the serotonergic nuclei found in the brains of both species of mole-rat studied. The 5HT+ neurons formed a cluster around the midline immediately dorsal to the interpeduncular nucleus in a location just anterior to the decussation of the superior cerebellar peduncle (Figs. 2M and 3M). A moderate density of 5HT+ neurons was seen throughout this region and the cell bodies were ovoid in shape, bipolar and show a dorsoventral orientation of the dendrites in the more dorsal parts of the nucleus but a mediolateral orientation in the remainder of the nucleus.

3.3.1.2.Supralemniscal (B9) nucleus. The neurons forming this nucleus appeared to be a lateral extension of the neuronal cluster comprising the most ventral portion of CLi (see above). The 5HT+ B9 neurons were found immediately caudal to the A9pc (see above) above the cerebral peduncle and extended as an arc of neurons into the lateral and ventrolateral portion of the midbrain tegmentum (Figs. 2N & 3M and N). The 5HT+ neurons exhibited a low to moderate density throughout this nucleus and the cell bodies were ovoid in shape, bipolar in type and exhibit a rough mediolateral dendritic orientation parallel to the upper border of the cerebral peduncle.

3.3.1.3.Median raphe (MnR). The median raphe nucleus was characterised by two distinct, densely packed 5HT+ neuronal columns on either side of the midline in a para-raphe position (Figs. 2N–P and 3M–O). The rostral border of this nucleus was coincident with the level of the decussation of the superior cerebellar peduncle and the caudal border of this nucleus was found at the level of the trigeminal motor nucleus (Vmot, see above). The 5HT+ neurons in this nucleus exhibited cell bodies that were ovoid in shape, bipolar, and had a mostly dorsoventral dendritic orientation (Fig. 8C and D).

3.3.1.4.Dorsal raphe (DR) nuclear complex. Within the 5HT+ neuronal region designated as the dorsal raphe nuclear complex there were six distinct nuclei, these being: the dorsal raphe interfascicular (DRif) nucleus, dorsal raphe ventral (DRv) nucleus, dorsal raphe dorsal (DRd) nucleus, dorsal raphe lateral (DRl) nucleus, dorsal raphe peripheral (DRp) nucleus and the dorsal raphe caudal (DRc) nucleus (Figs. 2L–P and 3L–O). These six nuclei were found, for the most part, within the periaqueductal and

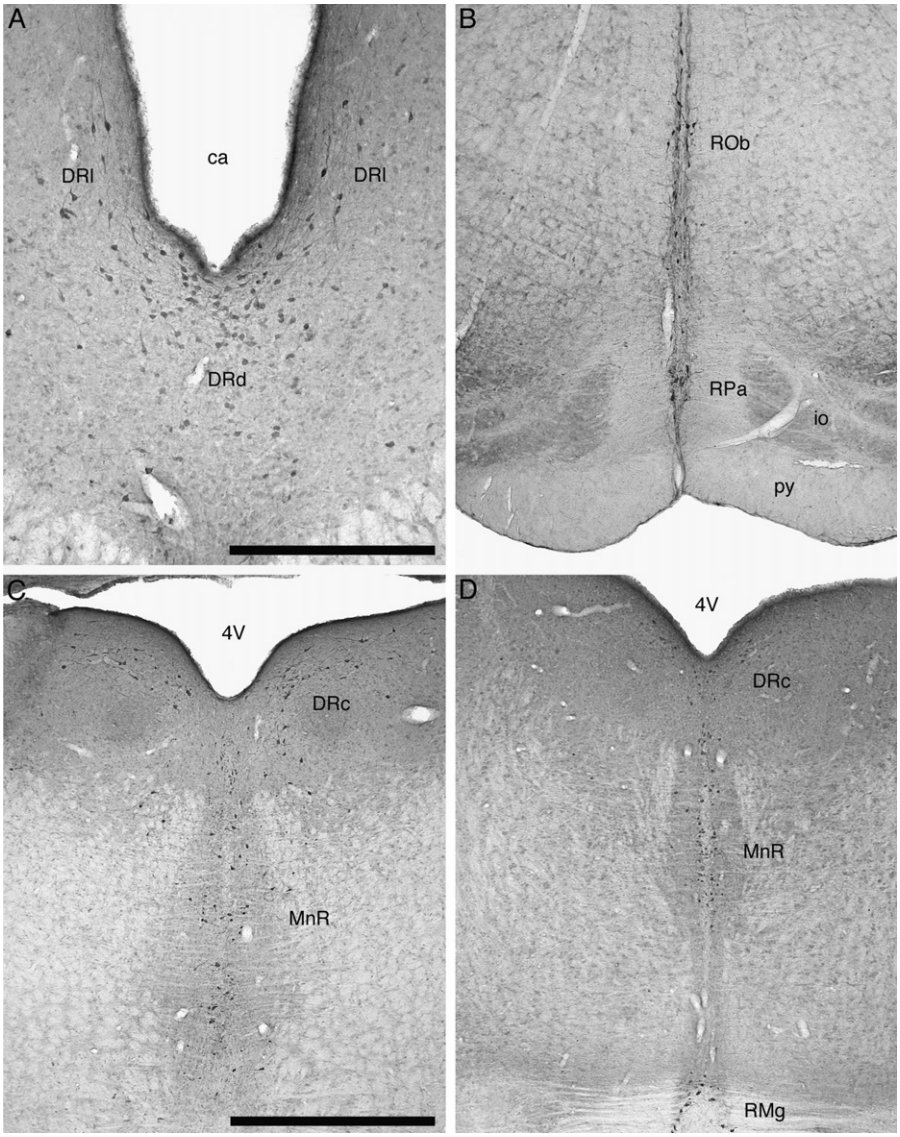

Fig. 8. Photomicrographs showing neuronal groups that are immunopositive for serotonin in the pons and medulla of the Cape dune mole-rat (A–C) and highveld mole-rat (D) brain. (A) The distinction between the morphology of the neurons comprising the lateral (DRl) and dorsal (DRd) nuclei of the dorsal raphe. (B) The raphe obscurus (ROb) and raphe pallidus (RPa) nuclei of the Cape dune mole-rat. (C) The caudal nucleus of the dorsal raphe (DRc) and median raphe nucleus (MnR) of the Cape dune mole-rat. (D) A similar image to C showing the caudal nucleus of the dorsal raphe (DRc), median raphe nucleus (MnR) and raphe magnus (RMg) of the highveld mole-rat. Scale bar in A = 500 μm. Scale bar in C = 1 mm and applies to B, C and D. 4V: fourth ventricle; ca: cerebral aqueduct; io: inferior olive; py: pyramidal tract.

periventricular grey matter from the level of the oculomotor nucleus to the trigeminal motor nucleus. The DRif was located between the two medial longitudinal fasciculi and exhibited a high density of 5HT+ neurons that were ovoid in shape, bipolar and had a dorsoventral dendritic orientation. The DRv was found immediately dorsal to the DRif between and just caudal to the oculomotor nuclei. The DRv exhibited a high density of 5HT+ neurons that had a similar neuronal morphology to the DRif but exhibited a range of dendritic orientations. Immediately dorsal to DRv and ventral to the inferior border of the cerebral aqueduct a cluster of 5HT+ neurons with a similar neuronal morphology to DRif and DRv, but with a mediolateral dendritic orientation, was designated as the DRd nucleus (Fig. 8A). 5HT+ neurons representing the DRp, were located in the ventrolateral portion of the periaqueductal grey matter lateral to the DRd and DRv. Some neurons were found in the adjacent tegmentum and are the only ones found outside the periaqueductal grey matter. There was a moderate density of these neurons within the periaqueductal grey matter and a lower density of more scattered neurons in the tegmental region. The 5HT+ neurons of the DRp were ovoid in shape and marginally larger than those of DRd, DRv and DRif. They were bipolar and showed no specific dendritic orientation. The 5HT+ neurons of the DRl were located dorsolateral to the DRd and adjacent to the ventrolateral edges of the cerebral aqueduct. The neurons of this nucleus were readily distinguishable from the remainder of the dorsal raphe nuclei since they were larger and showed a mixture of bipolar and multipolar neurons (Fig. 8A). These neurons showed dendrites orientated parallel to the wall of the aqueduct, and were found in a low to moderate density within the nucleus. The neurons of this serotonergic nucleus were intermingled with putative catecholaminergic neurons of the A10dc (see above). As we followed the DRl caudally, where the cerebral aqueduct opened into the fourth ventricle and the DRd, DRv and DRif dissappeared, the neurons of the DRl formed an arc across the midline of the dorsal portion of the periventricular grey matter. This caudal arc of the DRl was classified as the DRc nucleus

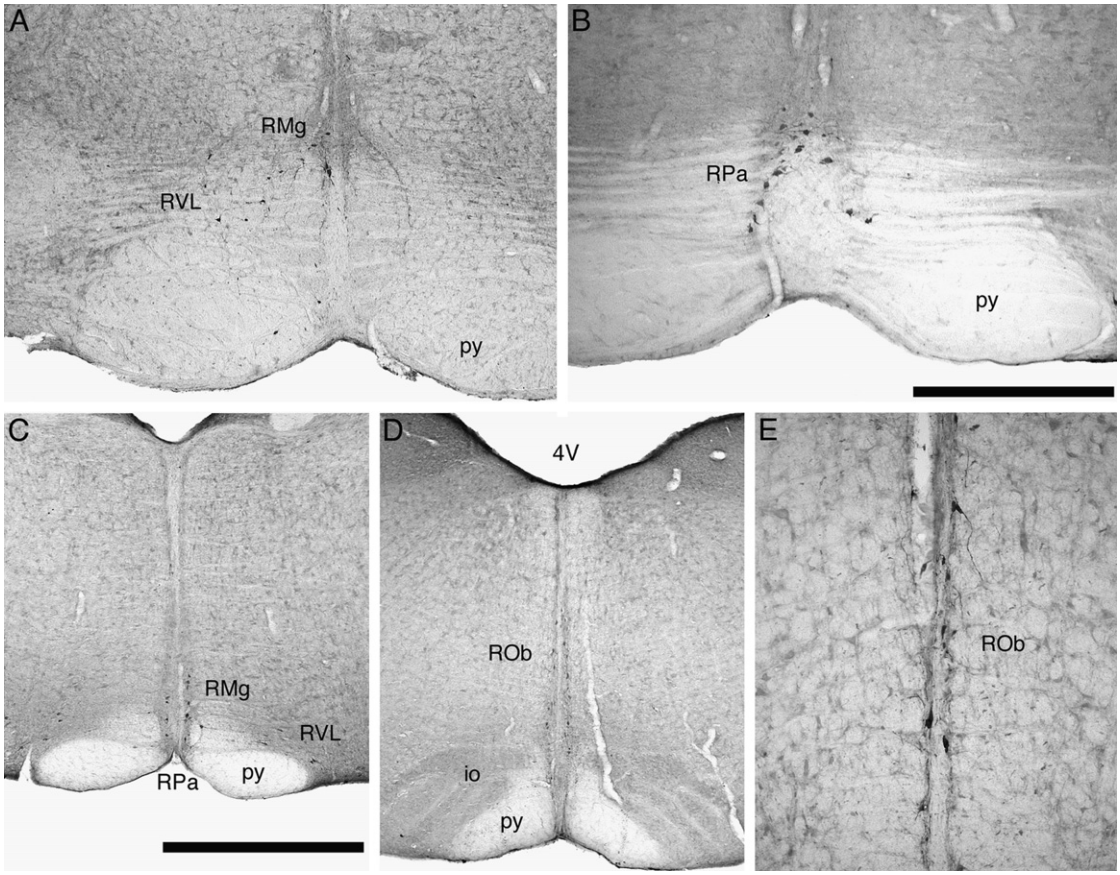

Fig. 9. Photomicrographs showing neuronal groups that are immunopositive for serotonin in the medulla of the Cape dune mole-rat (A and E) and highveld mole-rat (B–D) brain. (A) This photomicrograph depicts the lateral continuation of the raphe magnus nucleus (RMg) as it forms the most anterior portion of the rostral ventrolateral serotonergic group (RVL) in the Cape dune mole-rat. (B) The raphe pallidus (RPa) nucleus of the highveld mole-rat is intimately associated with the pyramidal tract (py). (C) The topography of the raphe magnus nucleus (RMg), raphe pallidus nucleus (RPa) and rostral ventrolateral serotonergic group (RVL) in the highveld mole-rat. (D) The pararaphe position of the raphe obscurus nucleus (ROb) of the highveld mole-rat. (E) A higher power view of the neuronal morphology of the raphe obscurus nucleus (ROb) in the Cape dune mole-rat. Scale bar in B = 500 μm and applies to B and E. Scale bar in C = 1 mm and applies to A, C and D. 4V: fourth ventricle; io: inferior olive; py: pyramidal tract.

(Fig. 8C and D). The neuronal morphology of the 5HT+ neurons in the DRc was identical to that of the DRl, but we classified this as an independent nucleus due to the lack of 5HT+ neurons in this region in the brain of monotremes (Manger et al., 2002c; Maseko et al., 2007).

3.3.2. Caudal cluster

3.3.2.1.Raphe magnus (RMg). This nucleus was seen to be two columns of loosely aggregated moderate to large 5HT+ neurons located either side of the midline from the level of the caudal pole of the trigeminal motor nucleus to the anterior pole of nucleus ambiguus (Figs. 2Q–R and 3O–R). The 5HT+ neurons within this nucleus were ovoid in shape, bipolar and exhibited a dorsoventral dendritic orientation (Figs. 8D and 9A and C).

3.3.2.2.Rostral and caudal ventrolateral nuclei (RVL and CVL). Within the left and right ventrolateral medullary tegmentum a distinct anteroposterior column of 5HT+ neurons extending from the level of the facial nucleus to the spinomedullary junction were observed (Figs. 2Q–T and 3O–S). These have previously been termed the rostral and caudal ventrolateral serotonergic columns (e.g. Maseko et al., 2007; Moon et al., 2007; Dwarika et al., 2008). The RVL began as a lateroventral continuation of 5HT+ neurons from the lower portion of the RMg extending over the pyramidal tracts and consolidating as a distinct column lateral to the inferior olives. This column was characterised by moderate density of 5HT+ neurons that exhibit a cellular morphology identical to those of the RMg except for a mediolateral dendritic orientation (Fig. 9A and C). The appearance of the inferior olive distinguishes left and right RVL and at the level of nucleus ambiguus the RVL becomes the CVL. The CVL continues in the caudal ventrolateral medullary tegmentum until the spinomedullary junction is reached. The neuronal morphology did not change. The number of neurons within this column steadily decreases from rostral to caudal. Although the RVL and CVL are continuous in the mole-rats studied, and indeed several other eutherian mammals previously studied (e.g. Maseko et al., 2007; Moon et al., 2007; Dwarika et al., 2008), we make the distinction of two components of these ventrolateral columns, as the caudal portions have not been reported in the opossum or the monotremes (Crutcher and Humbertson, 1978; Manger et al., 2002c).

3.3.2.3.Raphe pallidus (RPa). The 5HT+ neurons forming this nucleus were found in the ventral midline of the medulla associated with the pyramidal tracts (Figs. 2Q–T and 3P–S). These neurons were for the most part located between the two pyramidal tracts, but some neurons belonging to this nucleus (based on neuronal morphology) were identified dorsal to the pyramidal tract, between it and the inferior olive. The fusiform shaped 5HT+ neurons of the raphe pallidus were smaller than those of RMg, RVL and CVL, bipolar and exhibited a dendritic orientation parallel to the edges of the pyramidal tract (Figs. 8B & 9B and C).

3.3.2.4.Raphe obscurus (ROb). Two loosely arranged bilateral columns of 5HT+ neurons located either side of the midline from the level of nucleus ambiguus to the spinomedullary junction were classified as the raphe obscurus (Figs. 2S and T & 3R–T). These 5HT+ neurons were marginally smaller than those within the RMg but larger than those forming the RPa. The neurons were ovoid in shape, a mix of bi- and multipolar types and show a dorsoventral dendritic orientation irrespective of polarity (Figs. 8B & 9D and E). Occasional 5HT+ neurons associated with this nucleus were identified within a short distance (less than 200 μm) lateral to the central columns and were generally multipolar with some lateral dendritic orientation, but others showed a dorsoventral dendritic orientation.

4. Discussion

The central aim of the current study was to assess the nuclear organization of the cholinergic, putative catecholaminergic and serotonergic systems of two species of subterranean rodents that both have an extensively reduced visual system. The central finding was that there exists no difference in the nuclear complexity of these systems in both species of mole-rat studied compared with that of the laboratory rat. This lack of differences is in spite of several factors that may lead to the prediction of differences including the unusual phenotype and life history of the mole-rats and the time since the existence of the last common ancestor of these species and those of other rodents. All nuclei identified for the cholinergic, putative catecholaminergic and serotonergic systems appear to be homologous to those previously described for the laboratory rat (Dahlström and Fuxe, 1964; Fuxe et al., 1969, 1970; Lindvall and Björklund, 1974; Steinbusch, 1981; Björklund and Lindvall, 1984; Hökfelt et al., 1984; Meredith et al., 1989; Törk, 1990; Oh et al., 1992; Ichikawa et al., 1997) and other species of rodent (Ruggerio et al., 1984; Daszuta and Portalier, 1985; Ishimura et al., 1988; Mufson and Cunningham, 1988; Vincent, 1988; Léger et al., 1998; Satoh et al., 1991; Janusonis et al., 1999, 2003; Janusonis and Fite, 2001; Fite and Janusonis, 2001; Mulders and Roberston, 2005; Da Silva et al., 2006; D'Este et al., 2007; Mahoney et al., 2007; Moon et al., 2007; Dwarika et al., 2008). Moreover, there were not any nuclei that have been reported in laboratory rat that were not present in both the highveld and Cape dune mole-rats, or *vice versa*. This finding indicates the potential for the existence of a phylogenetic constraint in the evolution of the nuclear parcellation (*sensu* Ebbesson, 1980) of these systems acting at the level of the order (see tabulated data in Maseko et al., 2007). These findings support an earlier proposal indicating this to be the case for the nuclear organization of systems within the central nervous system (Manger, 2005).

4.1. Cholinergic system

Prior descriptions of the nuclear organization of the cholinergic system in rodents are limited to the laboratory rat (Meredith et al., 1989; Oh et al., 1992; Ichikawa et al., 1997) and the CD-1 strain of laboratory mouse (Mufson and Cunningham, 1988). The current study extends the basis for comparison in providing a full mapping study of the nuclear organization of this system in two species of mole-rat. The cholinergic nuclei of the dorsal striatopallidal complex and the basal forebrain of the mole-rats studied are similar to that seen in the rat (Oh et al., 1992) and mouse (Mufson and Cunningham, 1988). This result is perhaps not surprising, as all other mammals previously studied appear to demonstrate the same nuclear organization within these regions of the cholinergic system (Woolf, 1991; Manger et al., 2002a; Maseko and Manger, 2007; Maseko et al., 2007). Within the diencephalon of the mole-rats studied, four cholinergic nuclei were found, the lateral, ventral and dorsal hypothalamic cholinergic nuclei, as well as the medial habenular nucleus of the epithalamus. These three hypothalamic groups have been reported for rats, laboratory shrews, cats, primates, microbat and the megabat (Satoh et al., 1983; Tago et al., 1989; Vincent and Reiner, 1987; Tinner et al., 1989; Karasawa et al., 2003; Maseko and Manger, 2007; Maseko et al., 2007); however no hypothalamic cholinergic neuronal groups have been reported for the monotremes (Manger et al., 2002a). Within the pontine region of the mole-rats, the laterodorsal tegmental (LDT), pedunculopontine (PPT) and parabigeminal (PBg) cholinergic nuclei were observed. The LDT and PPT have been identified in all mammals studied to date (Woolf, 1991; Maseko et al., 2007); however the PBg has only been reported in rats, CD-1 mouse, highveld mole-rat, cat, ferret, tree shrew, megabat and primates (Kimura et al., 1981; Mufson and Cunningham, 1988; Murray et al., 1982; Vincent and Reiner, 1987; Henderson, 1987; Mesulam et al., 1989; Da Silva et al., 2006; Maseko et al., 2007). The parabigeminal nucleus in the mole-rats was weakly represented, in terms of number of neurons as observed previously in the mole-rat (Da Silva et al., 2006), and in terms of the strength of the immunoreactivity of the neurons, as described previously for the rat and mouse (Mufson and Cunningham, 1988; Woolf, 1991; Oh et al., 1992). This low neuronal number within the parabigeminal nucleus of the mole-rats appears to be consistent with the reduced visual system of these rodents as previously suggested (Da Silva et al., 2006). The parabigeminal nucleus has not been observed in the monotremes (Manger et al., 2002a), laboratory shrew (Karasawa et al., 2003) or the microbat (Maseko and Manger, 2007). A basic similarity in location and identity of the cranial nerve nuclei were found in both species of mole-rat as with all other mammals studied to date (Woolf, 1991; Maseko et al., 2007). Both species of mole-rat showed a small number of ChAT immunoreactive neurons in the Edinger–Westphal nucleus; however, this nucleus appeared to have fewer neurons than that seen in rat, cat, ferret, megabat and primates (Kimura et al., 1981; Armstrong et al., 1983; Satoh et al., 1983; Mizukawa et al., 1986; Henderson, 1987; Vincent and Reiner, 1987; Mesulam et al., 1989; Lavoie and Parent, 1994; Maseko et al., 2007). We also found ChAT immunoreactive neurons that represent the preganglionic motor neurons of the superior and inferior salivatory nuclei in both species of mole-rat, as reported for the rat, cat, ferret, megabat, and primates (Armstrong et al., 1983; Mesulam et al., 1989; Satoh and Fibiger, 1985; Mizukawa et al., 1986; Henderson, 1987; Shiromani et al., 1988; Maseko et al., 2007).

4.2. Putative catecholaminergic system

Putative catecholaminergic nuclei were found throughout the brain of both species of mole-rats, extending from the olfactory bulbs to the spinomedullary junction. Within the stratum granulosum of the olfactory bulbs, periglomerular TH+ neurons appear to be homologous to the dopaminergic neurons previously reported in other rodent and other mammalian species (Lichtensteiger, 1966; Lidbrink et al., 1974; Lindvall and Björklund, 1974; Hökfelt et al., 1976; Björklund and Lindvall, 1984; Smeets and González, 2000; Maseko et al., 2007; Moon et al., 2007; Dwarika et al., 2008). All nuclei previously reported for the putative catecholaminergic system within the diencephalon, midbrain, pons and medulla in the laboratory rat (Dahlström and Fuxe, 1964; Fuxe et al., 1969; Lindvall and Björklund, 1974; Björklund and Lindvall, 1984; Hökfelt et al., 1976, 1984), hamster (Vincent, 1988), grass rat (Mahoney et al., 2007), guinea pig (Mulders and Roberston, 2005), laboratory mouse (Ruggerio et al., 1984; Satoh

et al., 1991; D'Este et al., 2007), highveld mole-rat (Da Silva et al., 2006), highveld gerbil (Moon et al., 2007) and greater canerat (Dwarika et al., 2008) were found in both species of mole-rat examined in this study.

Despite the lack of difference in nuclear organization there were two differences of note. The first difference is that the number and density of tyrosine hydroxylase immunoreactive neurons in the dorsal caudal nucleus of the ventral tegmental complex (A10dc) of the cape dune mole-rat appeared to be far greater than that seen in the highveld mole-rat, or indeed any other rodent species previously examined (see references given above and Fig. 7). It is difficult to interpret what this difference might actually mean in terms of function, as even in the laboratory rat the connections and detailed neurochemistry of these neurons are unknown.

The second difference centres on the location and packing density of the diffuse nucleus of the locus coeruleus (A6d). In the laboratory rat the A6d nucleus, sometimes referred to just as the locus coeruleus, is found within the pontine periventricular grey matter but in a medial location adjacent to the ventricular wall. The catecholaminergic neurons within this region are densely packed and appear to be continuous dorso-caudally with the A4 nucleus (Dahlström and Fuxe, 1964; Fuxe et al., 1969; Lindvall and Björklund, 1974; Björklund and Lindvall, 1984; Hökfelt et al., 1976, 1984). This location, packing density and continuity with the A4 nucleus is different to that reported here for both species of mole-rat, and in comparison to that reported for other rodent species such as the laboratory mouse (Ginovart et al., 1996; Von Coelln et al., 2004), hamster (Vincent, 1988), guinea pig (Mulders and Roberston, 2005), highveld gerbil (Moon et al., 2007) and greater canerat (Dwarika et al., 2008). In these other rodents species studied, the locus coeruleus nucleus is located in the ventrolateral corner of the pontine periventricular grey matter and no neurons are found near the ventricular wall. In these other rodent species, only the neurons of the A4 nucleus are found adjacent to the ventricular wall and the packing density of the A6d neurons are much lower than that of the laboratory rat. It is unclear what the factors underlying the rat *vs*. other rodents difference may be; however, it is possible that this is a feature of the genus *Rattus*, or it may be the result of selected inbreeding of laboratory strains. Further studies of wild caught *Rattus* species may confirm or eliminate at least one of these possibilities (as previously demonstrated for the cortical cholinergic system, Bhagwandin et al., 2006).

4.3. Serotonergic system

The nuclei observed with immunohistochemistry for serotonin in the present study are identical in both species of mole-rat examined and to those previously described for the laboratory rat (Dahlström and Fuxe, 1964; Fuxe et al., 1969; Steinbusch, 1981; Lidov and Molliver, 1982; Waterhouse et al., 1993), mouse (Daszuta and Portalier, 1985), the Mongolian gerbil (Janusonis et al., 1999, 2003; Janusonis and Fite, 2001) greater canerat (Dwarika et al., 2008), highveld gerbil (Moon et al., 2007), and the portion of the brain studied in the Chilean degus (Fite and Janusonis, 2001). The nuclear organization of the serotonergic system across all eutherian mammals studied to date is identical (Bjarkam et al., 1997; Maseko et al., 2007); in nonplacental mammals, however, other patterns are seen. There are serotonergic neurons in the hypothalamus of monotremes (Manger et al., 2002c), there is a lack of serotonergic neurons in the region of the CVL column in the monotremes and the opossum (Manger et al., 2002c; Crutcher and Humbertson, 1978), and there is a lack of a caudal division of the dorsal raphe in the monotremes (Manger et al., 2002c).

4.4. Evolutionary considerations

The current investigation of three immunohistochemically identifiable neuronal systems in the brain of two species of wild caught mole-rat, demonstrates that despite major differences in phenotype (regressed visual system; Oelschläger et al., 2000; Cernuda-Cernuda et al., 2003; Nemec et al., 2004), life-history (unusual circadian rhythms, subterranean lifestyle, range of social systems; Lovegrove and Papenfus, 1995; Lovegrove and Muir, 1996; Negroni et al., 2003; Oosthuizen et al., 2003; Gutjahr et al., 2004) and time since evolutionary divergence (Adkins et al., 2003; Faulkes et al., 2004), no change in the complexity of the nuclear organization of the neural systems has occurred. It appears likely that a constraint, acting at the phylogenetic level of the order is limiting parcellation (*sensu* Ebbesson, 1980) of these systems, such that all species belonging to the same mammalian order demonstrate the same complement of homologous nuclei of these systems (Manger, 2005; Maseko et al., 2007). The complexity of nuclear organization, in terms of the number of nuclei, appears to be able to change between, but not within, orders (see tables provided in Maseko et al., 2007). The current study is aligned with previous studies in rodents that have shown that neither the time since evolutionary divergence (Da Silva et al., 2006; Dwarika et al., 2008), changes in phenotype (Moon et al., 2007), nor an increase in brain size (Dwarika et al., 2008) initiate any major differences in the nuclear complexity of the systems under study within the same mammalian order. Thus, it is possible to reasonably conclude at the moment that for the order Rodentia, varying phenotype, varying life history, evolutionary divergence and brain size do not lead to changes in nuclear complexity of the cholinergic, putative catecholaminergic and serotonergic systems. Further studies examining species that show greater changes in brain size, both large and small, and changes in relative brain size are required to fully test the proposed phylogenetic constraint that appears to be emerging as an explanation surrounding the observations made to date on various rodent, and other, species.

Acknowledgements

This study was supported by a grant from the South African National Research Foundation (Gun: 2054204) to PRM, and a Swedish Research Partnership Programme Bilateral Agreement between the Swedish International Development Cooperation Agency and the South African National Research Foundation to KF and PRM.

References

Adkins, R.M., Walton, A.H., Honeycutt, R.L., 2003. Higher-level systematics of rodents and divergence time estimates based on two congruent nuclear genes. Mol. Phylogenet. Evol. 26, 409–420.

Armstrong, D.M., Saper, C.B., Levey, A.I., Wainer, H., Terry, R.D., 1983. Distribution of cholinergic neurons in rat brain: demonstrated by the immunocytochemical localization of choline acetyl transferase. J. Comp. Neurol. 216, 53–68.

Bennett, N.C., Faulkes, C.G., 2000. African Mole-Rats: Ecology and Eusociality. Cambridge University Press, Cambridge.

Bhagwandin, A., Fuxe, K., Manger, P.R., 2006. Choline acetyltransferase immunoreactive cortical interneurons do not occur in all rodents: a study of the phylogenetic occurrence of this neural characteristic. J. Chem. Neuroanat. 32, 208–216.

Bjarkam, C.R., Sorensen, J.C., Geneser, F.A., 1997. Distribution and morphology of serotonin-immunoreactive neurons in the brainstem of the New Zealand white rabbit. J. Comp. Neurol. 380, 507–519.

Björklund, A., Lindvall, O., 1984. Dopamine-containing systems in the CNS. In: Björklund, A., Hökfelt, T. (Eds.), Handbook of Chemical Neuroanatomy, vol. 2: Classical Neurotransmitters in the CNS. Part 1. Elsevier, Amsterdam, pp. 55–122.

Cernuda-Cernuda, R., García-Fernández, J.M., Gordijn, M.C.M., Bovee-Geurts, P.H.M., DeGrip, W.J., 2003. The eye of the African mole-rat *Cryptomys anselli*: to see or not to see? Eur. J. Neurosci. 17, 709–720.

Crutcher, K.A., Humbertson, A.O., 1978. The organization of monoamine neurons within the brainstem of the North American opossum (*Didelphis virginiana*). J. Comp. Neurol. 179, 195–222.

Dahlström, A., Fuxe, K., 1964. Evidence for the existence of monoamine-containing neurons in the central nervous system. I. Demonstration of monoamine in the cell bodies of brainstem neurons. Acta Physiol. Scand. 62, 1–52.

Da Silva, J.N., Fuxe, K., Manger, P.R., 2006. Nuclear parcellation of certain immunohistochemically identifiable neuronal systems in the midbrain and pons of the Highveld mole-rat (*Cryptomys hottentotus*). J. Chem. Neuroanat. 31, 37–50.

Daszuta, A., Portalier, P., 1985. Distribution and quantification of 5-HT nerve cell bodies in the nucleus raphe dorsalis area of C57BL and BALBc mice. Relationship between anatomy and biochemistry. Brain Res. 360, 58–64.

D'Este, L., Casini, A., Puglisi-Allegra, S., Cabib, S., Renda, T.G., 2007. Comparative immunohistochemical study of the dopaminergic systems in two inbred mouse strains (C57BL/6J and DBA/2J). J. Chem. Neuroanat. 33, 67–74.

Dwarika, S., Maseko, B.C., Ihunwo, A.O., Fuxe, K., Manger, P.R., 2008. Distribution and morphology of putative catecholaminergic and serotonergic neurons in the brain of the greater canerat, *Thryonomys swinderianus*. J. Chem. Neuroanat. 35, 108–122.

Ebbesson, S.O., 1980. The parcellation theory and its relation to interspecific variability in brain organization, evolutionary and ontogenetic development, and neuronal plasticity. Cell Tissue Res. 213, 179–212.

Faulkes, C.G., Verheyen, E., Verheyen, W., Jarvis, J.U.M., Bennett, N.C., 2004. Phylogeographical patterns of genetic divergence and speciation in African mole-rats (Family: Bathyergidae). Mol. Ecol. 13, 613–629.

Fite, K.V., Janusonis, S., 2001. Retinal projection to the dorsal raphe nucleus in the Chilean degus (*Octodon degus*). Brain Res. 895, 139–145.

Fuxe, K., Hökfelt, T., Ungerstedt, U., 1969. Distribution of monoamines in the mammalian central nervous system by histochemical studies. In: Hooper, G. (Ed.), Metabolism of Amines in the Brain. Macmillan, London, pp. 10–22.

Fuxe, K., Hökfelt, T., Ungerstedt, U., 1970. Morphological and functional aspects of central monoamine neurons. Int. Rev. Neurobiol. 13, 93–126.

Gallyas, F., 1979. Silver staining of myelin by means of physical development. Neurolog. Res. 1, 203–209.

Ginovart, N., Marcel, D., Bezin, L., Garcia, C., Gagne, C., Pujol, J.F., Weissman, D., 1996. Tyrosine hydroxylase expression within Balb/C and C57Black/6 mouse locus coeruleus. I. Topological organization and phenotypic plasticity of the enzyme-containing cell population. Brain Res. 721, 11–21.

Gutjahr, G.H., Janse van Rensburg, L., Malpaux, B., Richter, T.A., Bennett, N.C., 2004. The endogenous rhythm of plasma melatonin and its regulation by light in the highveld mole-rat (*Cryptomys hottentotus pretoriae*): a micropthalmic, seasonally breeding rodent. J. Pineal Res. 37, 185–192.

Henderson, Z., 1987. Overlap in the distribution of cholinergic and catecholaminergic neurons in the upper brainstem of the ferret. J. Comp. Neurol. 265, 581–592.

Hökfelt, T., Johansson, O., Fuxe, K., Goldstein, M., Park, D., 1976. Immunohistochemical studies on the localization and distribution of monoamine neuron systems in the rat brain. I. Tyrosine hydroxylase in the mes- and diencephalons. Med. Biol. 54, 427–453.

Hökfelt, T., Martenson, R., Björklund, A., Kleinau, S., Goldstein, M., 1984. Distributional maps of tyrosine-hydroxylase-immunoreactive neurons in the rat brain. In: Björklund, A., Hökfelt, T. (Eds.), Handbook of Chemical Neuroanatomy, vol. 2: Classical Neurotransmitters in the CNS. Part 1. Elsevier, Amsterdam, pp. 277–379.

Ichikawa, T., Ajiki, K., Matsuura, J., Misawa, H., 1997. Localization of two cholinergic markers, choline acetyltransferase and vesicular acetylcholine transporter in the central nervous system of the rat: in situ hybridization histochemistry and immunohistochemistry. J. Chem. Neuroanat. 13, 23–29.

Ishimura, K., Takeuchi, Y., Fujiwara, K., Tominaga, M., Yoshioka, H., Sawada, T., 1988. Quantitative analysis of the distribution of serotonin-immunoreactive cell bodies in the mouse brain. Neurosci. Lett. 91, 265–270.

Jansa, S.A., Weksler, M., 2004. Phylogeny of the muroid rodents: relationships within and among major lineages as determined by IRBP gene sequences. Mol. Phylogenet. Evol. 31, 256–276.

Janusonis, S., Fite, K.V., 2001. Diurnal variation of c-Fos expression in subdivisions of the dorsal raphe nucleus of the Mongolian gerbil (*Meriones unguiculatus*). J. Comp. Neurol. 440, 31–42.

Janusonis, S., Fite, K.V., Foote, W., 1999. Topographic organization of serotonergic dorsal raphe neurons projecting to the superior colliculus in the Mongolian gerbil (*Meriones unguiculatus*). J. Comp. Neurol. 413, 342–355.

Janusonis, S., Fite, K.V., Bengston, L., 2003. Subdivision of the dorsal raphe nucleus projecting to the lateral geniculate nucleus and primary visual cortex in the Mongolian gerbil. NeuroReport 14, 459–462.

Karasawa, N., Takeuchi, T., Yamada, K., Iwasa, M., Isomura, G., 2003. Choline acetyltransferase positive neurons in the laboratory shrew (*Suncus murinus*) brain: coexistence of ChAT/5-HT (Raphe dorsalis) and ChAT/TH (Locus ceruleus). Acta Histochem. Cytochem. 36 (4), 399–407.

Kimura, H., McGeer, P.L., Peng, J.H., McGeer, E.G., 1981. The central cholinergic system studied by choline acetyltransferase immunohistochemistry in the cat. J. Comp. Neurol. 200, 151–201.

Kitahama, K., Geffard, M., Okamura, H., Nagatsu, I., Mons, N., Jouvet, M., 1990. Dopamine- and dopa-immunoreactive neurons in the cat forebrain with reference to tyrosine hydroxylase-immunohistochemistry. Brain Res. 518, 83–94.

Kitahama, K., Sakamoto, N., Jouvet, A., Nagatsu, I., Pearson, J., 1996. Dopamine-beta-hydroxylase and tyrosine hydroxylase immunoreactive neurons in the human brainstem. J. Chem. Neuroanat. 10, 137–146.

Lavoie, B., Parent, A., 1994. Pedunculopontine nucleus in the squirrel monkey: distribution of cholinergic and monoaminergic neurons in the mesopontine tegmentum with evidence for the presence of glutamate in cholinergic neurons. J. Comp. Neurol. 344, 190–209.

Léger, L., Charnay, Y., Burlet, S., Gay, N., Schaad, N., Bouras, C., Cespuglio, R., 1998. Comparative distribution of nitric oxide synthase- and serotonin-containing neurons in the raphe nuclei of four mammalian species. Histochem. Cell Biol. 110, 517–525.

Lichtensteiger, W., 1966. Uptake of norepinephrine in periglomerular cells of the olfactory bulb in the mouse. Nature 210, 955–956.

Lidbrink, P., Jonsson, G., Fuxe, K., 1974. Selective reserpine-resistant accumulation of catecholamines in central dopamine neurones after dopa administration. Brain Res. 67, 439–456.

Lidov, H.G.W., Molliver, M.E., 1982. Immunohistochemical study of the development of serotonergic neurons in the rat CNS. Brain Res. Bull. 9, 559–604.

Lindvall, O., Björklund, A., 1974. The organization of the catecholamine neuron systems in the rat brain as revealed by the glyoxylic acid fluorescence method. Acta Physiol. Scand. Suppl. 412, 1–48.

Lovegrove, B.G., Papenfus, M.E., 1995. Circadian activity rhythms in the solitary Cape mole-rat (*Georhycus capensis*: Bathyergidae) with some evidence of splitting. Physiol. Behav. 58, 679–685.

Lovegrove, B.G., Muir, A., 1996. Circadian body temperature rhythms of the solitary Cape mole rat *Georychus capensis* (Bathyergidae). Physiol. Behav. 60, 991–998.

Mahoney, M.M., Ramanathan, C., Smale, L., 2007. Tyrosine hydroxylase positive neurons and their contacts with vasoactive intestinal polypeptide-containing fibres in the hypothalamus of the diurnal murid rodent, *Arvicanthis niloticus*. J. Chem. Neuroanat. 33, 131–139.

Manger, P.R., 2005. Establishing order at the systems level in mammalian brain evolution. Brain Res. Bull. 66, 282–289.

Manger, P.R., Fahringer, H.M., Pettigrew, J.D., Siegel, J.M., 2002a. Distribution and morphology of cholinergic neurons in the brain of the monotremes as revealed by ChAT immunohistochemistry. Brain Behav. Evol. 60, 275–297.

Manger, P.R., Fahringer, H.M., Pettigrew, J.D., Siegel, J.M., 2002b. Distribution and morphology of catecholaminergic neurons in the brain of monotremes as revealed by tyrosine hydroxylase immunohistochemistry. Brain Behav. Evol. 60, 298–314.

Manger, P.R., Fahringer, H.M., Pettigrew, J.D., Siegel, J.M., 2002c. Distribution and morphology of serotonergic neurons in the brain of the monotremes. Brain Behav. Evol. 60, 315–332.

Manger, P.R., Cort, J., Ebrahim, N., Goodman, A., Henning, J., Karolia, M., Rodrigues, S., Strkalj, G., in press. Is 21st century neuroscience too focussed on the rat/mouse model of brain function and dysfunction? In: Brain Mapping Research Trends. Nova Science Publishers Inc., New York.

Maseko, B.C., Manger, P.R., 2007. Distribution and morphology of cholinergic, catecholaminergic and serotonergic neurons in the brain of Schreiber's long-fingered bat, *Miniopterus schreibersii*. J. Chem. Neuroanat. 34, 80–94.

Maseko, B.C., Bourne, J.A., Manger, P.R., 2007. Distribution and morphology of cholinergic, putative catecholaminergic and serotonergic neurons in the brain of the Egyptian Rousette flying fox, *Rousettus aegyptiacus*. J. Chem. Neuroanat. 34, 108–127.

Meister, B., Hökfelt, T., Steinbusch, H.W., Skagerberg, G., Lindvall, O., Geffard, M., Joh, T.H., Cuello, A.C., Goldstein, M., 1988. Do tyrosine hydroxylase-immunoreactive neurons in the ventrolateral arcuate nucleus produce dopamine or only L-dopa? J. Chem. Neuroanat. 1, 59–64.

Meredith, G.E., Blank, B., Groenewegen, H.J., 1989. The distribution and compartmental organization of the cholinergic neurons in nucleus accumbens of the rat. Neuroscience 31, 327–345.

Mesulam, M.M., Geula, C., Bothwell, M.A., Hersch, L.B., 1989. Human reticular formation: cholinergic neurons of the pedunculopontine tegmental nuclei and some cytochemical comparisons of forebrain cholinergic neurons. J. Comp. Neurol. 281, 611–633.

Mizukawa, K., McGeer, P.L., Tago, H., Peng, J.H., McGeer, E.G., Kimura, H., 1986. The cholinergic system of the human hindbrain studied by choline acetyltransferase immunohistochemistry and acetylcholinesterase histochemistry. Brain Res. 379, 39–55.

Moon, D.J., Maseko, B.C., Ihunwo, A., Fuxe, K., Manger, P.R., 2007. Distribution and morphology of catecholaminergic and serotonergic neurons in the brain of the highveld gerbil, *Tatera brantsii*. J. Chem. Neuroanat. 34, 134–144.

Mufson, E.J., Cunningham, M.G., 1988. Observations on choline acetyltransferase containing structures in the CD-1 mouse brain. Neurosci. Lett. 84, 7–12.

Mulders, W.H.A.M., Roberston, D., 2005. Catecholaminergic innervation of guinea pig superior olivary complex. J. Chem. Neuroanat. 30, 230–242.

Murray, H.M., Dominguez, W.F., Martinez, J.E., 1982. Catecholaminergic neurons in the brain stem of tree shrew (*Tupaia*). Brain Res. Bull. 9, 205–215.

Negroni, J., Bennett, N.C., Cooper, H.M., 2003. Organization of the circadian system in the subterranean mole rat, *Cryptomys hottentotus* (Bathyergidae). Brain Res. 967, 48–62.

Nemec, P., Burda, H., Peichl, L., 2004. Subcortical visual system of the African mole-rat *Cryptomys anselli*: to see or not to see? Eur. J. Neurosci. 20, 757–768.

Oelschläger, H.H.A., Nakamura, M., Herzog, M., Burda, H., 2000. Visual system labeled by c-Fos immunohistochemistry after light exposure in the 'blind'

subterranean Zambian mole-rat (*Cryptomys anselli*). Brain Behav. Evol. 55, 209–220.
Oh, J.D., Woolf, N.J., Roghani, A., Edwards, R.H., Butcher, L.L., 1992. Cholinergic neurons in the rat central nervous system demonstrated by in situ hybridization of choline acetyltransferase mRNA. Neuroscience 47, 807–822.
Olson, L., Fuxe, K., 1972. Further mapping out of the central noradrenaline neurons systems: projections of the "subcoeruleus" area. Brain Res. 43, 289–295.
Oosthuizen, M.K., Cooper, H.M., Bennett, N.C., 2003. Circadian rhythms of locomotor activity in solitary and social species of African mole-rats (Family: Bathyergidae). J. Biol. Rhythms 18, 481–490.
Ruggerio, D.A., Baker, H., Joh, T.H., Reis, D.J., 1984. Distribution of catecholamine neurons in the hypothalamus and preoptic region of mouse. J. Comp. Neurol. 223, 556–582.
Ruggiero, D.A., Anwar, M., Gootman, P.M., 1992. Presumptive adrenergic neurons containing phenylethanolamine *N*-methyltransferase immunoreactivity in the medulla oblongata of neonatal swine. Brain Res. 583, 105–119.
Satoh, K., Fibiger, H.C., 1985. Distribution of central cholinergic neurons in the baboon (*Papio papio*). I. General morphology. J. Comp. Neurol. 236, 197–214.
Satoh, K., Armstrong, D.M., Fibiger, H.C., 1983. A comparison of the distribution of central cholinergic neurons as demonstrated by acetylcholinesterase pharmacohistochemistry and choline acetyltransferase immunohistochemistry. Brain Res. Bull. 11, 693–720.
Satoh, J., Irino, M., Martin, P.M., Mailman, R.B., Suzuki, K., 1991. Neurochemical and immunocytochemical studies of catecholamine system in the brindled mouse. J. Neuropathol. Exp. Neurol. 50, 793–808.
Shiromani, P.J., Armstrong, D.M., Berkowitz, A., Jeste, D.V., Gillin, J.C., 1988. Distribution of choline acetyltransferase immunoreactive somata in the feline brainstem: implications for REM sleep generation. Sleep 11, 1–16.
Smeets, W.J.A.J., González, A., 2000. Catecholamine systems in the brain of vertebrates: new perspectives through a comparative approach. Brain Res. Rev. 33, 308–379.
Steinbusch, H.W.M., 1981. Distribution of serotonin-immunoreactivity in the central nervous system of the rat—cell bodies and terminals. Neuroscience 6, 557–618.
Tago, H., McGeer, P.L., McGeer, E.G., Akiyama, H., Hersch, L.B., 1989. Distribution of choline acetyltransferase immunopositive structures in the rat brainstem. Brain Res. 495, 271–297.
Tinner, B., Fuxe, K., Köller, C., Hersh, L., Andersson, K., Jansson, A., Goldstein, M., Agnati, L.F., 1989. Evidence for the existence of a population of arcuate neurons costoring cholineacetyltransferase and tyrosine hydroxylase immunoreactivities in the male rat. Neurosci Lett. 99, 44–49.
Törk, I., 1990. Anatomy of the serotonergic system. Ann. NY Acad. Sci. 600, 9–35.
Vincent, S.R., 1988. Distributions of tyrosine hydroxylase-, dopamine-β-hydroxylase-, and phenylehtanolamine-*N*-methyltransferase-immunoreactive neurons in the brain of the hamster (*Mesocricetus auratus*). J. Comp. Neurol. 268, 584–599.
Vincent, S.R., Reiner, P.B., 1987. The immunohistochemical localization of choline acetyltransferase in the cat brain. Brain Res. Bull. 18, 371–415.
Von Coelln, R., Thomas, B., Savitt, J.M., Lim, K.L., Sasaki, M., Hess, E.J., Dawson, V.L., Dawson, T.M., 2004. Loss of locus coeruleus neurons and reduced startle in parkin null mice. Proc. Natl. Acad. Sci. U.S.A. 101, 10744–10749.
Waterhouse, B.D., Border, B., Wahl, L., Mihailoff, G.A., 1993. Topographic organization of rat locus coeruleus and dorsal raphe nuclei: distribution of cells projecting to visual system structures. J. Comp. Neurol. 336, 345–361.
Woolf, N.J., 1991. Cholinergic systems in mammalian brain and spinal cord. Prog. Neurobiol. 37, 475–524.

Appendix B: Published original research article that emerged from the thesis

Journal of Chemical Neuroanatomy 41 (2011) 32–42

Contents lists available at ScienceDirect

Journal of Chemical Neuroanatomy

journal homepage: www.elsevier.com/locate/jchemneu

Distribution of orexinergic neurons and their terminal networks in the brains of two species of African mole rats

Adhil Bhagwandin [a], Kjell Fuxe [b], Nigel C. Bennett [c], Paul R. Manger [a,*]

[a] School of Anatomical Sciences, Faculty of Health Sciences, University of the Witwatersrand, 7 York Road, Parktown 2193, Johannesburg, South Africa
[b] Department of Neuroscience, Karolinska Institutet, Retzius väg 8, S-171 77 Stockholm, Sweden
[c] Mammal Research Institute, Department of Zoology and Entomology, University of Pretoria, Pretoria 0002, South Africa

ARTICLE INFO

Article history:
Received 9 October 2010
Received in revised form 1 November 2010
Accepted 3 November 2010
Available online 17 November 2010

Keywords:
Bathyergus
Cryptomys
Orexin
Hypocretin
Rodent
Comparative neuroanatomy

ABSTRACT

The distribution of orexinergic cell bodies and terminal networks within the brains of two species of African mole rat (Cape-dune mole rat – *Bathyergus suillus* and highveld mole rat – *Cryptomys hottentotus*) were identified using immunohistochemistry for orexin-A. The aim of the study was to investigate possible differences in the nuclear complement and terminal distribution of this system by comparing those of the mole rats to published studies of other rodents and mammals. The wild-caught mole rats used in this study live a subterranean lifestyle and are well known for their regressed visual system, which may lead to the prediction of differences in the distribution of the cell bodies and the terminal networks; however, we found that both species of mole rat displayed orexinergic nuclei limited to the hypothalamus in regions similar to those previously reported for other rodent and mammalian species. No immunoreactive neurons could be identified, in either species of mole rat within the anterior hypothalamic paraventricular nucleus, as has been reported for Murid rodents. The terminal networks, while remaining similar between the species, are more strongly expressed in the Cape-dune mole rat than in the highveld mole rat.

1. Introduction

Orexin (also known as hypocretin) is a neuropeptide that has been reported to play a role in the regulation of feeding, drinking, body temperature, general activity (Lubkin and Stricker-Krongrad, 1998; Edwards et al., 1999; Hagan et al., 1999; Kunii et al., 1999; Mondal et al., 1999; Piper et al., 2000; Estabrooke et al., 2001; Hungs et al., 2001; Yoshimichi et al., 2001; Kotz et al., 2002; Berthoud et al., 2005), energy homeostasis (Mintz et al., 2001), stimulation of gastric secretion in rats (Takahashi et al., 1999), increasing metabolic rate in rats (Lubkin and Stricker-Krongrad, 1998), altering luteinising hormone release in rats (Pu et al., 1998) and in the regulation of the sleep–wake cycle specifically associated with increased wakefulness and inhibition of REM sleep (Sakurai et al., 1998; Chemelli et al., 1999; Siegel, 1999; Bourgin et al., 2000; Kilduff and Peyron, 2000; Thannickal et al., 2000; van den Pol, 2000).

The distribution of orexin-immunopositive (Orx+) cell bodies and terminal networks within the brain have been reported in a range of mammals including: humans (*Homo sapiens*, Moore et al., 2001); domestic cat (*Felis catus*, Zhang et al., 2001, 2002); domestic sheep (*Ovis aries*, Iqbal et al., 2001); six species of rodent (laboratory rat, *Rattus norvegicus* – Broberger et al., 1998; Peyron et al., 1998; Chen et al., 1999; Cutler et al., 1999; Date et al., 1999; Hagan et al., 1999; Nambu et al., 1999; Risold et al., 1999; Baldo et al., 2003; Chou et al., 2004; Espana et al., 2005; Kirouac et al., 2005; Nixon and Smale, 2007; Nile grass rat, *Arvicanthus niloticus* – Novak and Albers, 2002; Nixon and Smale, 2007; golden or Syrian hamster, *Mesocricetus auratus* – McGranaghan and Piggins, 2001; Mintz et al., 2001; Vidal et al., 2005; Nixon and Smale, 2007; laboratory mouse, *Mus musculus*, C57B1 strain, Broberger et al., 1998; Siberian or Djungarian hamster, *Phodopus sungorus* – McGranaghan and Piggins, 2001; Khorooshi and Klingenspor, 2005; degu, *Octodon degus* – Nixon and Smale, 2007); five microchiropteran species (Kruger et al., 2010); and the Eastern grey kangaroo (*Macropus giganteus*, Yamamoto et al., 2006). The Orx+ neuronal cell bodies were invariably localized within the hypothalamus and while for most mammals they were represented as a rather homogenous loosely packed large cluster of neurons located in the perifornical and lateral hypothalamus (see above references), in certain rodents there may be up to four clusters, or nuclei, of orexinergic neurons – the two described above, plus one cluster located in the anterior hypothalamic paraventricular subnucleus and one in the lateral ventral hypothalamic supraoptic area (LVHA) (Nixon and Smale, 2007).

Orexin immunoreactive terminal networks have been found in differential relative densities throughout the varying brain regions

* Corresponding author. Tel.: +27 11 717 2497; fax: +27 11 717 2422.
E-mail address: Paul.Manger@wits.ac.za (P.R. Manger).

0891-0618/$ – see front matter © 2010 Elsevier B.V. All rights reserved.
doi:10.1016/j.jchemneu.2010.11.002

previously examined (see references cited above). A high relative density of Orx+ terminals has been consistently observed within the paraventricular nucleus of the epithalamus, the noradrenergic locus coeruleus complex and the serotonergic dorsal raphe nuclear complex. The majority of the nuclei of the hypothalamus as well as the septal region, cholinergic nuclei of the pons, the ventral tegmental area, the nuclei of the solitary tract, the remaining serotonergic nuclei and both limbs of the diagonal band of Broca were consistently described as having a medium relative density of Orx+ terminals. A low to absent density of Orx+ terminals has been recorded in regions such as the cerebral cortex, major nuclei of the dorsal thalamus and other regions of the central nervous system (see references above).

Recent studies have demonstrated that in rodents and other species, the complexity of the nuclear organization of the diffusely projecting cholinergic, catecholaminergic and serotonergic systems remains consistent within an order despite differences in brain size, phenotype, lifestyle or evolutionary distance (e.g. Manger, 2005; Maseko et al., 2007; Bhagwandin et al., 2008; Dwarika et al., 2008; Limacher et al., 2008; Gravett et al., 2009; Pieters et al., 2010; Bux et al., 2010). In terms of the orexinergic system this appears to hold true for most mammals; however, the observations of variance in the number of potential orexinergic nuclei in rodents (Nixon and Smale, 2007) may indicate greater organizational variance within an order for this diffusely projecting system than other systems previously studied.

In contrast to this order level consistency in nuclear organization, the pattern of terminal networks of these diffusely projecting neurotransmitter systems appears to be more variable within the order. For example, when the innervation patterns of the serotonergic (Raghanti et al., 2008a) and cholinergic (Raghanti et al., 2008b) terminal networks within the cerebral cortex of humans, chimpanzees and macaque monkeys were compared, there were no species differences in the primary motor cortex (Brodmann's area 4), but significant quantitative and qualitative differences were observed between macaques on the one hand and chimpanzees and humans on the other (which were similar) in two pre-motor cortical areas (Brodmann's areas 9 and 32). These studies are suggestive of family level consistencies and inter-family differences in the terminal networks of the diffusely projecting neural systems. Comparative studies of the orexinergic projections in rodents are also suggestive of certain qualitative differences in terminal network densities within and between families despite many overall similarities (McGranaghan and Piggins, 2001; Nixon and Smale, 2007).

In the current study, whole brains of two species of African mole rat, the highveld mole rat (*Cryptomys hottentotus*) and the Cape dune mole rat (*Bathyergus suillus*) were examined immunohistochemically for orexin-A. Both species studied have a greatly reduced visual system (Oelschlager et al., 2000; Cernuda-Cernuda et al., 2003; Nemec et al., 2004), are subterranean, and appear to have a free-running circadian activity oscillator (Lovegrove and Papenfus, 1995; Lovegrove and Muir, 1996; Negroni et al., 2003; Oosthuizen et al., 2003; Gutjahr et al., 2004). These atypical rodent features combined with the distant (but familial) relation to each other and to the non-familial laboratory rat (Adkins et al., 2003), provide an interesting model to examine changes in nuclear organization and terminal network patterns that may be related to phenotype, life history and behaviour.

2. Materials and methods

The brains of three adult highveld mole rats (*C. hottentotus*) (average body weight: 86.5 g; average brain weight: 1.5 g) and three adult Cape dune mole rats (*B. suillus*) (average body weight: 965 g; average brain weight: 3.4 g) were used in the current study. All animals were treated and used according to the guidelines of the University of the Witwatersrand Animal Ethics Committee, which parallel those of the NIH for the care and use of animals in scientific experimentation. The mole rats were placed under deep barbiturate anaesthesia (euthanaze, 200 mg sodium pentobarbital/kg, i.p.), and then perfused intracardially upon cessation of respiration. The perfusion was initially done with a rinse of 0.9% saline solution at 4 °C, followed by a solution of 4% paraformaldehyde in 0.1 M phosphate buffer (PB) (approximately 1l/kg of each solution). Brains were then removed from the skull and post-fixed overnight in 4% paraformaldehyde in 0.1 M PB, and then allowed to equilibrate in 30% sucrose in PB. The brains were then frozen and sectioned into serial coronal and sagittal sections of 50 μm thickness. A one in three series of stains was made for Nissl, myelin and orexin A. Sections kept for the Nissl series were mounted on 0.5% gelatine coated glass slides, cleared in a solution of 1:1 chloroform and absolute alcohol, then stained with 1% cresyl violet. Myelin sections were stored in 5% formalin at 4 °C for a period of two weeks and were then mounted on 1% gelatine coated glass slides and subsequently stained with a modified silver stain (Gallyas, 1979).

For immunohistochemical staining the sections were first treated for 30 min with an endogenous peroxidase inhibitor (49.2% methanol:49.2% of 0.1 PB:1.6% of 30% H_2O_2) followed by three 10 min rinses in 0.1 M PB. This was followed by a 2 h pre-incubation, at room temperature, in a solution (blocking buffer) containing 3% normal goat serum (NGS, Chemicon), 2% bovine serum albumin (BSA, Sigma), and 0.25% Triton X-100 (Merck) in 0.1 M PB. The sections were then placed in a primary antibody solution containing the appropriately diluted antibody in blocking buffer, for 48 h at 4 °C. To reveal orexinergic neurons we used the anti-orexin A antibody (AB 3704, Millipore, raised in rabbit) at a dilution of 1:1500. This step was followed by three 10 min rinses in 0.1 M PB, after which the sections were incubated in a secondary antibody for 2 h. The secondary antibody solution contained a 1:1000 dilution of biotinylated anti-rabbit IgG (BA-1000, Vector Labs) in 3% NGS, and 2% BSA in 0.1 M PB. After three 10 min rinses in 0.1 M PB, the sections were incubated for 1 h in AB solution (Vector Labs), and again rinsed. The sections were then treated in a solution of 0.05% diaminobenzidine in 0.1 M PB for 5 min, following which 3 μl of 30% H_2O_2 was added to the 1 ml of solution in which each section was immersed. Staining development was monitored visually and checked under a low power stereomicroscope until the background staining was at a level at which it could assist reconstruction without obscuring the immunopositive neuronal structures. Development was arrested by placing the sections in 0.1 M PB, and then rinsed twice more in the same solution. Sections were mounted on glass slides coated with 0.5% gelatine and left to dry overnight. They were then dehydrated in a graded series of alcohols, cleared in xylene, and coverslipped with Depex. Two controls were employed in the immunohistochemistry, including the omission of the primary antibody and the omission of the secondary antibody in selected sections. The sections were observed with a low power stereomicroscope, and the architectonic borders of the sections traced according to the Nissl stained sections using a camera lucida. The immunostained sections were then matched to the drawings and the immunopositive neurons marked, in addition the density of axon terminal staining was graded from low to high for each immunostained section and medium and high marked on the drawings. The drawings were then scanned and redrawn using the Canvas 8 drawing program. The location of Orx+ neuronal structures and the corresponding orexinergic terminal network distribution were described in relation to the general neuroanatomy of the brain and the cholinergic, catecholaminergic and serotonergic systems described previously for these two species of mole rat (Bhagwandin et al., 2008).

Abbreviations

III	oculomotor nucleus
IV	trochlear nucleus
Vmot	motor division of trigeminal nucleus
VI	abducens nucleus
VIId	facial nerve nucleus, dorsal division
VIIv	facial nerve nucleus, ventral division
X	dorsal motor vagus nucleus
XII	hypoglossal nucleus
3V	third ventricle
A1	caudal ventrolateral medullary tegmental nucleus
A2	caudal dorsomedial medullary nucleus
A4	dorsal medial division of locus coeruleus
A5	fifth arcuate nucleus
A6d	diffuse portion of locus coeruleus
A7d	nucleus subcoeruleus, diffuse portion
A7sc	nucleus subcoeruleus, compact portion
A8	retrorubral nucleus
A9l	substantia nigra, lateral
A9m	substantia nigra, medial

A9pc	substantia nigra, pars compacta
A9v	substantia nigra, ventral or pars reticulata
A10	ventral tegmental area
A10c	ventral tegmental area, central
A10d	ventral tegmental area, dorsal
A10dc	ventral tegmental area, dorsal caudal
A11	caudal diencephalic group
A12	tuberal cell group
A13	zona incerta
A14	rostral periventricular nucleus
A15d	anterior hypothalamic group, dorsal division
A15v	anterior hypothalamic group, ventral division
ac	anterior commissure
amyg	amygdala
AP	area postrema
B9	supralemniscal serotonergic nucleus
C	caudate nucleus
C1	rostral ventrolateral medullary tegmental group
C2	rostral dorsomedial medullary nucleus
C3	rostral dorsal midline medullary nucleus
ca	cerebral aqueduct
cc	corpus callosum
cc	central canal
Cing ctx	cingulate cortex
cl	claustrum
CLi	caudal linear nucleus
CN	cerebellar nuclei
CVL	caudal ventrolateral serotonergic group
Diag.B	diagonal band of Broca
DR	dorsal raphe
DRc	dorsal raphe nucleus, caudal division
DRd	dorsal raphe nucleus, dorsal division
DRif	dorsal raphe nucleus, interfascicular division
DRl	dorsal raphe nucleus, lateral division
DRp	dorsal raphe nucleus, peripheral division
DRv	dorsal raphe nucleus, ventral division
DT	dorsal thalamus
EW	Edinger–Westphal nucleus
f	fornix
GC	periaqueductal grey matter
GP	globus pallidus
Hbm	medial habenular nucleus
Hbl	lateral hebenular nucleus
hyp	hypothalamus
hyp. d	hypothalamus, dorsal division
hyp. l	hypothalamus, lateral division
hyp. v	hypothalamus, ventral division
HIP	hippocampus
ic	internal capsule
IC	inferior colliculus
IP	interpeduncular nucleus
Is.Call.	islands of Calleja
LHA	lateral hypothalamic area
LVHA	lateral ventral hypothalamic area
LDT	laterodorsal tegmental nucleus
LV	lateral ventricle
mtf	medullary tegmental field
MnR	median raphe nucleus
N.Acc	nucleus accumbens
N.Amb	nucleus ambiguus
N.Bas	nucleus basalis
NEO	neocortex
P	putamen
PFR	perifornical area
Pg	pineal gland
pVII	preganglionic motor neurons of the superior salivatory nucleus or facial nerve
pIX	preganglionic motor neurons of the inferior salivatory nucleus
PBg	parabigeminal nucleus
PC	cerebral peduncle
PIR	piriform cortex
PPT	pedunculopontine nucleus
PV	thalamic paraventricular nuclei
py	pyramidal tract
R	reticular nucleus of dorsal thalamus
RMg	raphe magnus nucleus
ROb	raphe obscurus nucleus
RPa	raphe pallidus nucleus
RVL	rostral ventrolateral serotonergic group
SC	superior colliculus
scp	superior cerebellar peduncle
Sep.M	medial septal nucleus
TOL	olfactory tubercle
vh	ventral horn
VPO	ventral pontine nucleus

3. Results

In both species of mole rat examined, immunohistochemically identifiable, morphologically homogenous, orexinergic (Orx+) cell bodies were limited to the hypothalamus, as previously reported in all other mammals studied to date. The terminal networks, while remaining similar in distribution between both species, are more strongly expressed in the Cape dune mole rat than in the highveld mole rat. The following descriptions of the Orx+ cell bodies and terminal networks, for both species of mole rat (unless otherwise specified), are provided in relation to the general anatomy of the brain, or to the neuronal groups of the cholinergic, catecholaminergic and serotonergic systems (as described for these particular species in Bhagwandin et al., 2008) where overlap occurs.

3.1. Orexinergic cell body distribution

Both species of mole rat expressed Orx+ neurons only within the hypothalamus and were observed as sharing a common neuronal locality within the lateral hypothalamic area (LHA), perifornical region (PFR) and the lateral ventral hypothalamic supraoptic area (LVHA) (Figs. 1G–I and 2I–J). Within the LHA of both species a moderate density of Orx+ cells bodies were found to intermingle with the lateral hypothalamic cholinergic nucleus and the dopaminergic neurons of the A13 (zona incerta) nucleus. The Orx+ neurons of the PFR were observed to show a moderate density and did not overlap with any previously described cholinergic or dopaminergic neurons. In both species, the LVHA Orx+ neurons were found in the same region as the dopaminergic A15v (ventral division of the anterior hypothalamic group) nucleus, in the lateral and ventral portions of the hypothalamus, immediately dorsal to the greatly reduced optic tract (Fig. 3). No Orx+ neurons could be identified in the anterior hypothalamic paraventricular subnucleus in either mole rat species. Thus, there appears to be three distinct clusters of Orx+ neurons in the hypothalamus of the mole rats

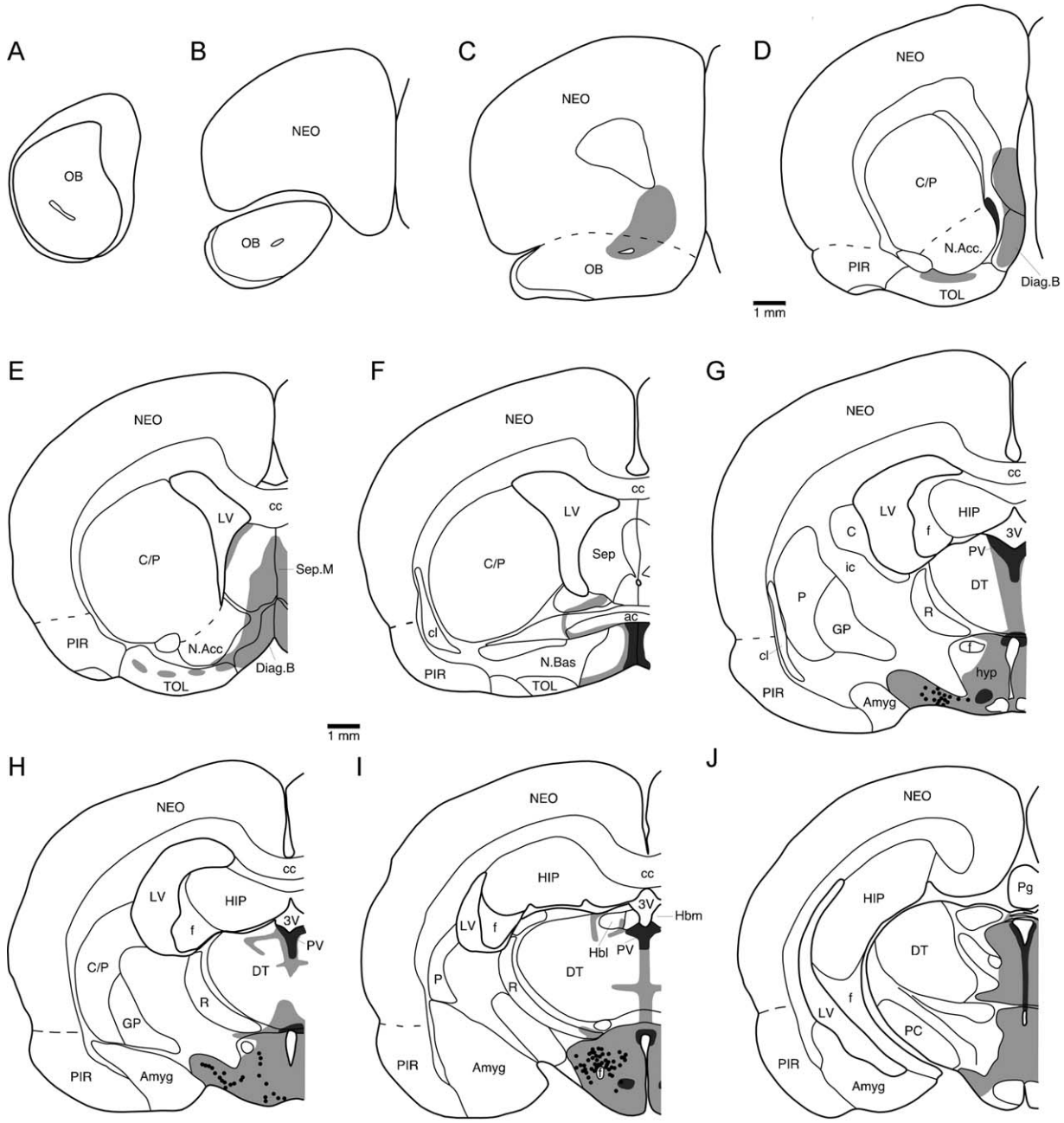

Fig. 1. Drawings of sections through one half of the brain of the Cape-dune mole rat (*Bathyergus suillus*) depicting the distribution of orexinergic terminal network densities (an absence of shading represents low density, grey shaded areas represent medium density and black shaded areas represent high density) and Orx immunoreactive neurons (each black dot represents a single neuron) relative to the nuclear organization of the cholinergic system, catecholiminergic system and serotonergic system [previously described in Bhagwandin et al. (2008) for this species]. Absence of shading indicates either a minor terminal network or no terminal network (see text for details). See list for abbreviations.

studied, a large homogenous cluster spanning the lateral and perifornical regions, a distinct cluster extending into the region of the zona incerta, and a final cluster in the ventral lateral hypothalamus adjacent to the optic tracts. Both mole rats exhibited neuronal cell bodies that were morphologically homogenous in all three clusters, and that were ovoid in shape, and a varying mixture of bi- and multi-polar types that showed no specific dendritic orientation (Fig. 3).

3.2. Orexinergic terminal networks

3.2.1. Telencephalon

Throughout the telencephalon of both species there was only one region of high-density Orx+ terminal networks, this being within the very anterior portion of the septal nuclear complex of the highveld mole rat (Fig. 2D). In both species a medium relative density of Orx+ terminals was observed within the shell of the nucleus accumbens, the entire septal nuclear complex (overlapping with the cholinergic medial septal nucleus), the cholinergic diagonal band of Broca, and in small portions of the nucleus basalis and the olfactory tubercule (Figs. 1C–F and 2C–F). All remaining regions of the telencephalon (cerebral cortex, the dorsal striatopallidal complex, hippocampal complex, amygdalar complex) were observed to have a low-density terminal network in both species of mole rat.

3.2.2. Diencephalon

A medium density Orx+ terminal network characterized the entire hypothalamus in both species examined; however, high terminal network densities were noted in a region adjacent to the

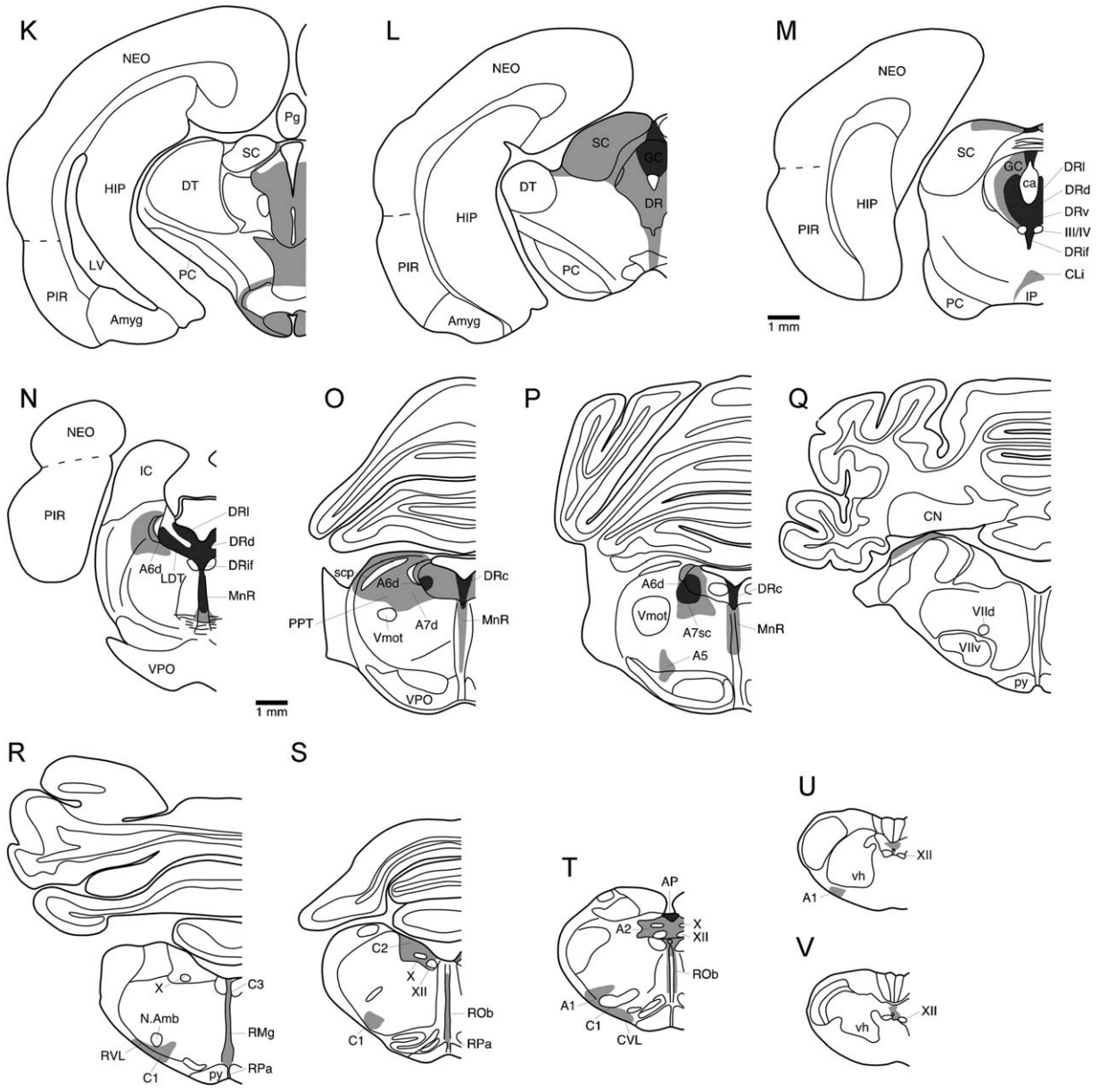

Fig. 1 (*Continued*).

dorsal aspect of the third ventricle within the hypothalamus of both species of mole rat in the region where the dopaminergic neurons of the A15d (dorsal division of the anterior hypothalamic group) nucleus were located (Figs. 1H–J and 2H, I). A second region of high-density Orx+ terminals was found in the premammillary nuclei of both species; however, the mammillary nuclei themselves only exhibited a low density of Orx+ terminals. A low-density terminal network was observed through both the dorsal and ventral thalamus, except for the intralaminar central median nucleus of the dorsal thalamus where a medium-density network of Orx+ terminals was observed. In contrast to this, the epithalamus evinced a high-density terminal network in the dorsal aspects of the paraventricular nuclei and a medium density terminal network in the ventral midline part of the paraventricular thalamic nuclei and in the regions surrounding the habenular nuclei, especially the lateral habenular nucleus and dorsal most portions of the fasciculus retroflexus (Figs. 1H, I, 2H, I and 5).

3.2.3. Midbrain (mesencephalon)

Within the midbrain of both species a high-density Orx+ terminal network was observed throughout the serotonergic dorsal raphe nuclear complex and the serotonergic median raphe nucleus (Figs. 1M, N, 2M–O and 6A). A second region of high-density Orx+ terminals was observed in the dorsomedial periaqueductal grey matter (DMPAG) in both species. The remainder of the periaqueductal grey matter was observed to contain a medium density Orx+ terminal network, which was also observed within the superior colliculus, parts of the ventral tegmental nuclear complex, specifically the A10dc, A10c and A10d nuclei, and in the serotonergic caudal linear nucleus (CLi) and supralemniscal serotonergic group (B9). The medium-density Orx+ terminal network within the midbrain of the highveld mole rat was more extensive than that seen in the Cape dune mole rat and was observed in the A10 nucleus, the inferior colliculus, upper midbrain tegmentum and interpeduncular nucleus, whereas in the Cape dune mole rat these regions only contained a low-density

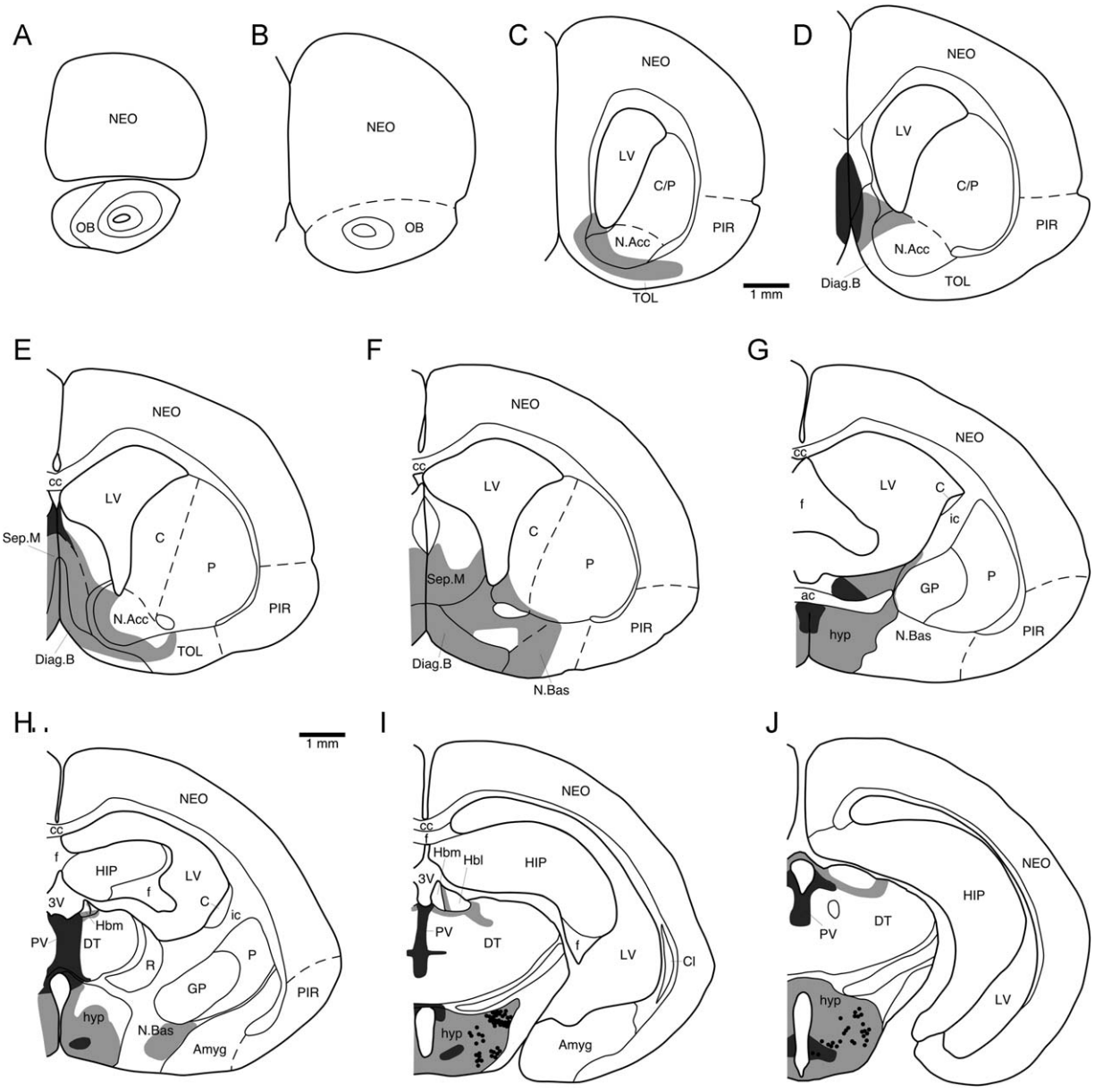

Fig. 2. Drawings of sections through one half of the brain of the highveld mole rat (*Cryptomys hottentotus*) depicting the distribution of orexinergic terminal network densities (an absence of shading represents low density, grey shaded areas represent medium density and black shaded areas represent high density) and Orx immunoreactive neurons (each black dot represents a single neuron) relative to the nuclear organization of the cholinergic system, catecholaminergic system and serotonergic system [previously described in Bhagwandin et al. (2008) for this species]. Absence of shading indicates either a minor terminal network or no terminal network (see text for details). See list for abbreviations.

Orx+ terminal network, or in the case of the superior colliculus and interpeduncular nucleus appeared to be limited to a specific portion of these nuclei (Figs. 1J–N and 2K–N). All other regions of the midbrain evinced a low-density Orx+ terminal network in both species of mole rat.

3.2.4. Pontine region (metencephalon)

Within the pons of both species, high-density Orx+ terminal networks were observed in the cholinergic laterodorsal tegmental nucleus (LDT), the noradrenergic diffuse nucleus of the locus coeruleus (A6d) and compact nucleus of the subcoeruleus (A7sc), and the serotonergic caudal nucleus of the dorsal raphe complex (DRc) (Figs. 1N–P, 2N, O, 4A and 6A). In the dorsal pontine tegmentum of both species, a medium-density Orx+ terminal network was seen to overlap with the regions where the neurons of the cholinergic pedunculopontine tegmental nucleus (PPT) and noradrenergic diffuse nucleus of the subcoeruleus (A7d) were found. Other medium density Orx+ terminal networks were observed to overlap with the distribution of the noradrenergic neurons of the fifth arcuate nucleus (A5) and the pontine portion of the serotonergic median raphe nucleus (MnR) (Fig. 6B). All other portions of the pontine region were observed to contain a relatively low-density Orx+ terminal network.

3.2.5. Medulla oblongata (myelencephalon) and cerebellum

Within the medulla there was only one region that contained a high-density Orx+ terminal network and this was the area postrema (AP) of the Cape dune mole rat (Fig. 1T). Interestingly, in the highveld mole rat there was only a low-density Orx+ terminal network in this structure. Medium-density Orx+ terminal networks were observed in all the regions where serotonergic neurons were located, which include the raphe magnus nucleus

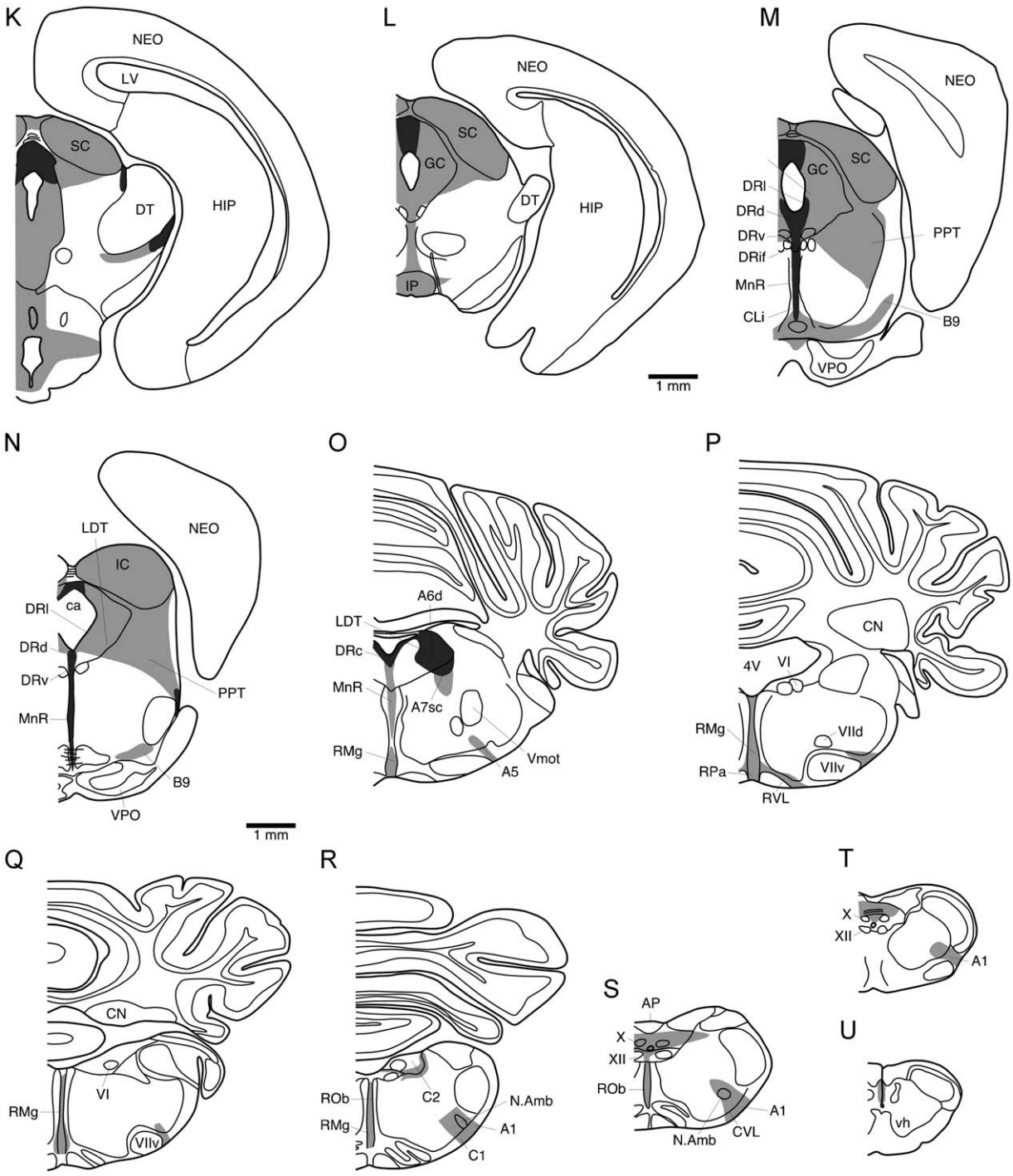

Fig. 2 (*Continued*).

(RMg) and its continuation in the rostral and caudal ventrolateral serotonergic columns (RVL and CVL), the raphe pallidus nucleus (RPa) and the raphe obscurus nucleus (ROb) (Fig. 6C). The remaining regions of the medulla that showed medium-density Orx+ terminal networks were coincident with the catecholaminergic nuclei previously reported, including the rostral ventrolateral medullary tegmental group (C1) (Fig. 4C), rostral dorsomedial medullary nucleus (C2), caudal ventrolateral medullary tegmental group (A1) and the caudal dorsomedial medullary nucleus (A2). The extent of this medium-density network around the C2 and A2 nuclei was quite expansive and appeared to include the majority of the nuclei of the solitary tract. A global low-density Orx+ terminal network was observed throughout the remaining regions of the medulla oblongata. No specific species differences were observed in the medulla. A low-density Orx+ terminal network was observed throughout all regions of the cerebellum, both cortical and nuclear, for both species.

4. Discussion

In the current study, it was observed that both species of mole rat displayed three clusters of orexinergic immunoreactive neurons within the hypothalamus, thereby maintaining significant congruency with previous studies in other mammals (see references listed in Section 1). In addition, it was noted that no immunoreactive orexinergic (Orx+) cell bodies, in either species of

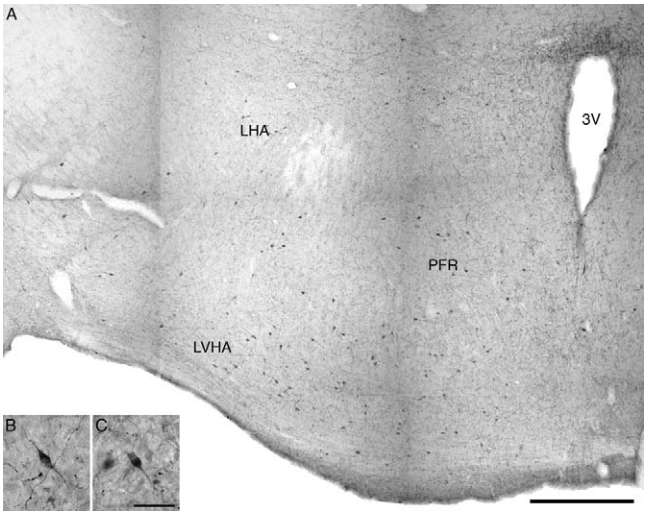

Fig. 3. (A) Photomicrographic montage showing the Orx immunoreactive neurons within the hypothalamus of *Bathyergus suillus*. Scale = 500 μm. (B and C) High power photomicrographs showing the morphology of Orx immunoreactive neurons within the hypothalamus of *Bathyergus suillus*. Scale = 50 μm.

mole rat, could be identified within the anterior hypothalamic paraventricular organ as was previously reported in some Murid rodents (Nixon and Smale, 2007). In both species of mole rat the orexinergic terminal network distribution, for the most part, maintained similarity to that observed in other mammals; however, a few differences were identified between both species of mole rat and collectively in all other mammals studied to date.

4.1. Comparison to other rodents and other mammals

4.1.1. Distribution of orexinergic cell bodies

The distribution of Orx+ cell bodies, in both species of mole rat, was both similar and different to those previously reported in other rodents. Both species of mole rat expressed Orx+ neurons within the perifornical region (PFR) and the lateral hypothalamic area (LHA), comprising the main cluster of orexinergic neurons, which is a common feature of the orexinergic system shared by all rodents studied to date; however, neither species of mole rat, as with the Syrian hamster and degu, displayed Orx+ neurons within the anterior hypothalamic paraventricular subnucleus as seen in the Long-Evans rat and grass rat (Nixon and Smale, 2007; but see Novak and Albers, 2002 who do not report these neurons in the Nile grass rat but they used an orexin B antibody). In this case we appear to have a difference in the nuclear organization of the orexinergic system within the rodents, with the two Murid rodents studied (Long-Evans rat and Nile grass rat, both closely related) showing a difference to the closely related Syrian hamster (a member of the Cricetidae) and the more distantly related Ctenohystrica (*Octodon* and the bathyergid mole rats) (Nixon and Smale, 2007; Blanga-Kanfi et al., 2009). This is not the first time such Murid *vs.* non-Murid differences have been observed for such systems in the rodents (Bhagwandin et al., 2006). In the mole rats, as with all other rodents, two additional, but smaller, clusters of orexinergic neurons were located, one in the dorsolateral region of the hypothalamus intermingling with the region of the zona incerta, and a second cluster in the ventrolateral region of the hypothalamus near the optic tract (that is immunoreactive for both orexin-A and orexin-B, Nixon and Smale, 2007), although the optic tract is greatly reduced in the mole rats. Thus, within the rodents, while many similarities in neural systems occur across all species, there are at least two differences reported to date (orexinergic

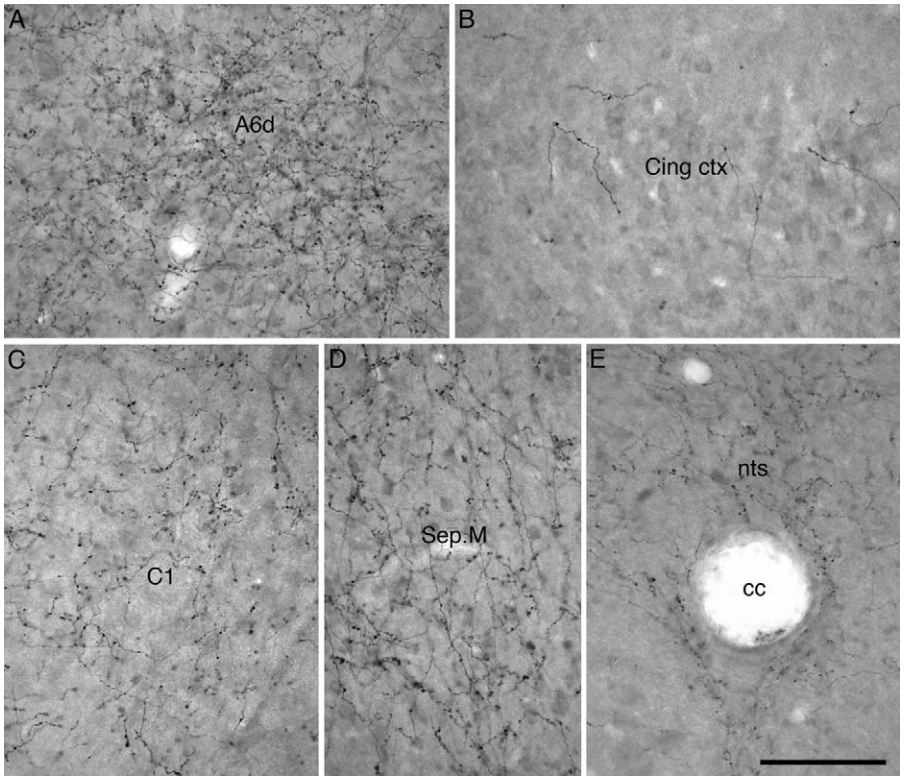

Fig. 4. High power photomicrographs showing varying orexinergic terminal network densities in the brains of *Cryptomys hottentotus* (A–D) and *Bathyergus suillus* (E). (A) High density terminal network within the A6d neuronal group. (B) Low density terminal network within the cingulate cortex. (C) Medium density terminal network in the region of the C1 nucleus. (D) Medium density terminal network within the cholinergic medial septal nucleus. (E) Medium density terminal networks surrounding the central canal. Scale = 100 μm and applies to all. See list for abbreviations.

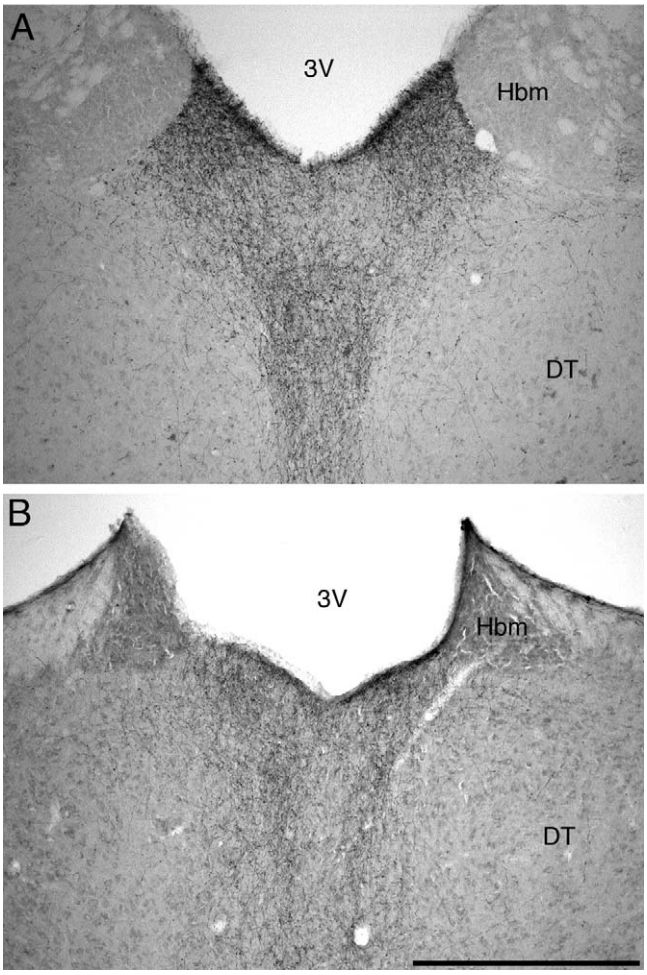

Fig. 5. Photomicrographs illustrating the difference in expression of high density orexinergic terminal networks within the paraventricular nucleus of: (A) *Bathyergus suillus*, (B) *Cryptomys hottentotus*. Scale = 500 μm and applies to both. See list for abbreviations.

anterior hypothalamic paraventricular neurons, Nixon and Smale, 2007; and cortical cholinergic neurons, Bhagwandin et al., 2006). These differences would be of interest to study further and delineate potential phylogenetic boundaries for these features and the possible behavioural correlates of these differences.

An important aspect of the parcellation of the orexinergic system needs to be highlighted at this point. In the current study we have lumped the orexinergic neurons of the PFR and LHA into a single cluster that we have termed the main cluster (in this study and in a previous study on microchiropterans, Kruger et al., 2010). This was done as there appears to be no anatomical distinction in the aggregation of the orexinergic neurons across this large cluster, being organized in what can be loosely termed a diffuse nucleus; however, a previous study of the connectivity of these regions of the main cluster (PFR and LHA) would suggest that these two regions likely represent distinct nuclei (Yoshida et al., 2006). Yoshida et al. (2006) showed that, while the PFR and LHA orexinergic neurons project to many of the same regions, the intensity of the projection differs substantially between several of these terminal territories. In addition, they showed that the medial, or PFR, portion of what we term the main orexinergic cluster innervates the anterior and ventromedial hypothalamus plus the suprachiasmatic nucleus, whereas the LHA orexinergic neurons do not. They also showed that the LHA orexinergic neurons innervate the dorsal raphe, whereas the PFR orexinergic neurons do not (Yoshida et al., 2006). These differences in projection fields appear to warrant a distinction of what we term the main orexinergic cluster into medial or PFR and LHA orexinergic nuclei. It would be of importance to study such differences across species to determine whether such differential projection territories exist in other mammals and warrant cross species parcellation of the orexinergic system in a similar manner.

In the mole rats and other rodents the location of the main cluster of orexinergic (Orx+) cell bodies (PFR and LHA), is similar to that seen in all other mammals studied to date (Iqbal et al., 2001; Moore et al., 2001; Zhang et al., 2001, 2002; Yamamoto et al., 2006; Kruger et al., 2010). Interestingly, all mammalian species appear to have orexinergic neurons overlapping with the medial most portion of the zona incerta. Of less similarity is the appearance of orexinergic neurons in the ventrolateral hypothalamus, near the optic tract, which while present in most mammals (and appears greatly expanded in the kangaroo, Yamamoto et al., 2006), are lacking in the microchiropterans (Kruger et al., 2010) and the two species of hamster studied to date (McGranaghan and Piggins, 2001; Mintz et al., 2001; Khorooshi and Klingenspor, 2005; Vidal et al., 2005; Nixon and Smale, 2007). Further contrasts in the location of orexinergic neurons amongst mammals include: (1) the presence of Orx+ neurons in the dorsomedial hypothalamic region in the sheep, minipig and kangaroo (Iqbal et al., 2001; Yamamoto et al., 2006; Ettrup et al., 2010); and (2) Orx+ neurons in the supraoptic and paraventricular magnocellular nucleus of the minipig (Ettrup et al., 2010). Thus, while for the most part the nuclear organization of the orexinergic system appears to quite conserved across mammalian species, there are definitely some

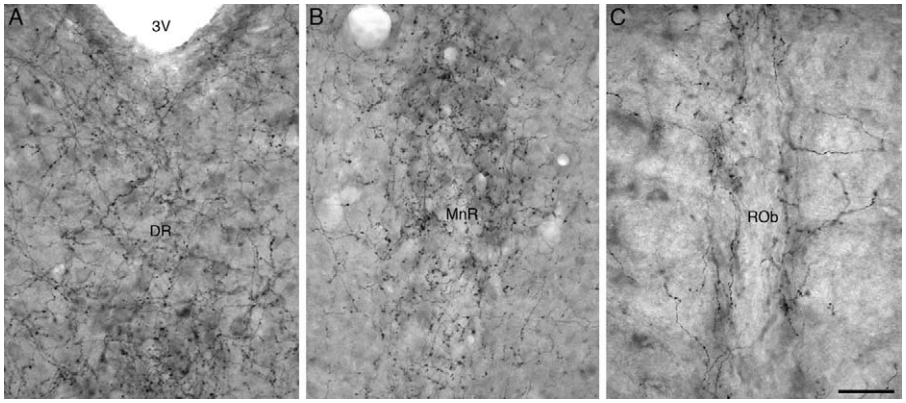

Fig. 6. High power photomicrograph showing varying terminal network densities within the brain of *Cryptomys hottentotus*. (A) high density orexinergic terminal networks within the serotonergic dorsal raphe nuclear complex (DR). (B) High density orexinergic terminal networks in the region of the serotonergic median raphe nucleus (MnR). (C) Medium density orexinergic terminal networks within the serotonergic raphe obscurus (ROb) nucleus, Scale = 50 μm and applies to all. See list for abbreviations.

points of departure that may be interesting in both a functional and phylogenetic aspect, and warrants the investigation of orexinergic cellular location in a broader range of mammalian species.

4.1.2. Distribution of orexinergic terminal networks

Previous studies of the terminal networks of the orexinergic neurons have demonstrated that in mammals the majority of the brain is either in receipt of very minor, or no, orexinergic innervation. In this sense the mole rats studied herein are no exception. These regions of minor to no orexinergic innervation include the cerebral neocortex, the dorsal striatopallidal complex, the dorsal thalamus, cerebellum and most of the brainstem.

Despite this, there are areas of the brain that consistently show medium to dense orexinergic innervation across many of the mammalian species studied to date. Within the telencephalon of the mole rats studied, medium to high-density orexinergic terminal networks were observed in the septal nuclei, the shell of the nucleus accumbens and the cholinergic basal forebrain. This telencephalic distribution is similar across all rodents and all mammals for which these projections have been described to date. Similarly, in the mole rats and all mammals studied, the paraventricular nuclei of the epithalamus exhibited a high-density orexinergic terminal network in the dorsal division. This specific network extended around the habenular nuclear complex in the mole rats, again being similar to that seen in other mammals. A medium density network was observed throughout the mole rat hypothalamus as seen in all other mammals. Interestingly, in several mammals studied, a clear medium-density orexinergic terminal network is observed in the intergeniculate leaflet, but this was not observed in the mole rats. This is likely due to the major reduction in size of the visual system in these species (Nemec et al., 2004). Previously, Vidal et al. (2005) demonstrated that the orexinergic projection to the intergeniculate leaflet arises from the orexinergic neurons located near the zona incerta. The mole rats possess these zona incerta orexinergic neurons, but not the projection to the intergeniculate leaflet. This indicates that these Orx+ zona incerta neurons mostly likely have projections to other structures in addition to the intergeniculate leaflet, and the existence of these additional, but currently unknown projections, are the possible reason for the maintenance of this cell group in the mole rats.

As in all species where the orexinergic terminal networks have been described, the mole rats studied herein have high to moderate density projections to all the serotonergic nuclei, the pontine cholinergic nuclei, and the locus coeruleus complex (Bhagwandin et al., 2008). In addition, both mole rats expressed a high to medium-density Orx+ terminal network within the periaqueductal grey matter and the ventral tegmental area (VTA), similar to that previously reported for other rodents and other mammals. Interestingly though, while a low to absent density of Orx+ terminal networks has been reported for the superior colliculus in other rodent species, a medium-density Orx+ terminal network was observed in this study despite the reduced size of the superior colliculus previously noted for mole rats (Nemec et al., 2004; Da Silva et al., 2006). Variations in terminal densities within the inferior colliculus (IC) and interperduncular (IP) nuclei, amongst rodent species, were similarly noted in both species of mole rat. The highveld mole rat expressed a medium-density Orx+ terminal network in both the IC and IP, similar to the hamster, grass rat, degu and Wistar rat; whereas the Cape dune mole rat demonstrated a low-density Orx+ terminal network within the IC and IP, consistent with the Long-Evans and Wistar rats; however, these terminal networks also appear to vary significantly across the IP and IC of other mammals studied to date.

Interestingly no other rodent species, except for the Cape dune mole rat of the current study, exhibited a high-density Orx+ terminal network within area postrema (AP) with medium-density Orx+ terminal networks reported within AP for the degu and Wistar rat, whereas the highveld mole rat demonstrates a low-density Orx+ terminal network for this homologous region. The catecholaminergic medullary nuclei (C1, C2, A1 and A2) expressed a medium-density Orx+ terminal network in both species of mole rat and this is congruent with previous rodent species however it must be noted that there is no clarity with regard to the distribution of Orx+ terminal networks within C2 amongst other rodent and mammalian species studied to date.

Ethical statement

The mole rats used in the present study were caught from wild populations in South Africa under permission and supervision from the appropriate wildlife directorates. All animals were treated and used according to the guidelines of the University of the Witwatersrand Animal Ethics Committee, which parallel those of the NIH for the care and use of animals in scientific experimentation.

References

Adkins, R.M., Walton, A.H., Honetcutt, R.L., 2003. Higher-level systematics of rodents and divergence time estimates based on two congruent nuclear genes. Mol. Phylogenet. Evol. 26, 409–420.

Baldo, B.A., Daniel, R.A., Berridge, C.W., Kelley, A.E., 2003. Overlapping distributions of orexin/hypocretin- and dopamine-β-hydroxylase immunoreactive fibers in rat brain. J. Comp. Neurol. 464, 220–237.

Berthoud, H.R., Patterson, L.M., Sutton, G.M., Morrison, C., Zheng, H., 2005. Orexin inputs to caudal raphe neurons involved in thermal, cardiovascular, and gastrointestinal regulation. Histochem. Cell Biol. 123, 147–156.

Bhagwandin, A., Fuxe, K., Manger, P.R., 2006. Choline acetyltransferase immunoreactive cortical interneurons do not occur in all rodents: a study of the phylogenetic occurrence of this neural characteristic. J. Chem. Neuroanat. 32, 208–216.

Bhagwandin, A., Fuxe, K., Bennett, N.C., Manger, P.R., 2008. Nuclear organization and morphology of cholinergic, putative catecholaminergic and serotonergic neurons in the brains of two species of African mole-rat. J. Chem. Neuroanat. 35, 371–387.

Blanga-Kanfi, S., Miranda, H., Penn, O., Pupko, T., DeBry, R.W., Huchon, D., 2009. Rodent phylogeny revisited: analysis of six nuclear genes from all major rodent clades. BMC Evol. Biol. 9, 71.

Bourgin, P., Huitron-Resendiz, S., Spier, A.D., Fabre, V., Morte, B., Criado, J.R., Sutcliffe, J.G., Henriksen, S.J., de Lecea, L., 2000. Hypocretin-1 modulates rapid eye movement sleep through activation of locus coeruleus neurons. J. Neurosci. 20, 7760–7765.

Broberger, C., de Lecea, L., Sutcliffe, J.G., Hokfelt, T., 1998. Hypocretin/orexin and melanin-concentrating hormone-expressing cells form distinct populations in the rodent lateral hypothalamus: relationship to the neuropeptide Y and agouti gene-related protein systems. J. Comp. Neurol. 402, 460–474.

Bux, F., Bhagwandin, A., Fuxe, K., Manger, P.R., 2010. Organization of cholinergic, putative catecholaminergic and serotonergic nuclei in the diencephalon, midbrain and pons of sub-adult male giraffes. J. Chem. Neuroanat. 39, 189–203.

Cernuda-Cernuda, R., Garcia-Fernandez, J.M., Gordijin, M.C.M., Bovee-Geurts, P.H.M., DeGrip, W.J., 2003. The eye of the African mole-rat *Cryptomys anselli*: to see or not to see? Eur. J. Neurosci. 17, 709–720.

Chen, C.T., Dun, S.L., Kwok, E.H., Dun, N.J., Chang, J.K., 1999. Orexin A-like immunoreactivity in the rat brain. Neurosci. Lett. 260, 161–164.

Chemelli, R.M., Willie, J.T., Sinton, C.M., Elmquist, J.K., Scammell, T., Lee, C., Richardson, J.A., Williams, S.C., Xiong, Y., Kisanuki, Y., Fitch, T.E., Nakazato, M., Hammer, R.E., Saper, C.B., Yanagisawa, M., 1999. Narcolepsy in orexin knockout mice: molecular genetics of sleep regulation. Cell 98, 437–451.

Chou, T.C., Rotman, S.R., Saper, C.B., 2004. Lateral hypothalamic acetylcholinesterase-immunoreactive neurons co-express either orexin or melanin concentrating hormone. Neurosci. Lett. 370, 123–126.

Cutler, D.J., Morris, R., Sheridhar, V., Wattam, T.A.K., Kolmes, S., Patel, S., Atch, J.R.S., Wilson, S., Buckingham, R.E., Evans, M.L., Leslie, R.A., Williams, G., 1999. Differential distribution of orexin-A and orexin-B immunoreactivity in the rat brain and spinal cord. Peptides 20, 1455–1470.

Date, Y., Ueta, Y., Yamashita, H., Yamaguchi, H., Matsukura, S., Kangawa, K., Sakurai, T., Yanagisawa, M., Nakazato, M., 1999. Orexins, orexigenic hypothalamic peptides, interact with autonomic, neuroendocrine and neuroregulatory systems. Proc. Natl. Acad. Sci. U.S.A. 96, 748–753.

Da Silva, J.N., Fuxe, K., Manger, P.R., 2006. Nuclear parcellation of certain immunohistochemically identifiable neuronal systems in the midbrain and pons of the Highveld mole-rat (*Cryptomys hottentotus*). J. Chem. Neuroanat. 31, 37–50.

Dwarika, S., Maseko, B.C., Ihunwo, A.O., Fuxe, K., Manger, P.R., 2008. Distribution and morphology of putative catecholaminergic and serotonergic neurons in the

brain of the greater canerat, *Thryonomys swinderianus*. J. Chem. Neuroanat. 35, 108–122.
Edwards, C.M.B., Abusnana, S., Sunter, D., Murphy, K.G., Ghatei, M.A., Bloom, S.R., 1999. The effect of the orexins on food intake: comparison with neuropeptide Y, melanin-concentrating hormone and galanin. J. Endocrinol. 160, R7–12.
Espana, R.A., Reis, K.M., Valentino, R.J., Berridge, C.W., 2005. Organization of hypocretin/orexin efferents to locus coeruleus and basal forebrain arousal-related structures. J. Comp. Neurol. 481, 160–178.
Estabrooke, I., McCarthy, M.T., Ko, E., Chou, T.C., Chemelli, R.M., Yanagisawa, M., 2001. Fos expression in orexin neurons varies with behavioral state. J. Neurosci. 21, 1656–1662.
Ettrup, K.S., Sørensen, J.S., Bjarkam, C.R., 2010. The anatomy of the Göttingen minipig hypothalamus. J. Chem. Neuroanat. 39, 151–165.
Gallyas, F., 1979. Silver staining of myelin by means of physical development. Neurolog. Res. 1, 203–209.
Gutjahr, G.H., van Rensburg, L.J., Malpaux, B., Richter, T.A., Bennett, N.C., 2004. The endogenous rhythm of plasma melatonin and its regulation by light in the highveld mole-rat (*Cryptomys hottentotus pretoriae*): a microphthalmic, seasonally breeding rodent. J. Pineal Res. 37, 185–192.
Gravett, N., Bhagwandin, A., Fuxe, K., Manger, P.R., 2009. Nuclear organization and morphology of cholinergic, putative catecholaminergic and serotonergic neurons in the brain of the rock hyrax, *Procavia capensis*. J. Chem. Neuroanat. 38, 57–74.
Hagan, J.J., Leslie, R.A., Patel, S., Evans, M.L., Wattam, T.A., Holmes, S., 1999. Orexin A activates locus coeruleus cell firing and increases arousal in the rat. Proc. Natl. Acad. Sci. U.S.A. 96, 10911–10916.
Hungs, M., Fan, J., Lin, L., Lin, X., Maki, R.A., Mignot, E., 2001. Identification and functional analysis of mutations in the hypocretin (orexin) genes of narcoleptic canines. Genome Res. 11, 531–539.
Iqbal, J., Pompolo, S., Sakurai, T., Clarke, I.J., 2001. Evidence that orexin-containing neurones provide direct input to gonadotropin-releasing hormone neurones in the ovine hypothalamus. J. Neuroendocrinol. 13, 1033–1041.
Khorooshi, R.M., Klingenspor, M., 2005. Neuronal distribution of melanin-concentrating hormone, cocaine- and amphetamineregulated transcript and orexin B in the brain of the Djungarian hamster (*Phodopus sungorus*). J. Chem. Neuroanat. 29, 137–148.
Kilduff, T.S., Peyron, C., 2000. The hypocretin/orexin ligand-receptor system: implications for sleep and sleep disorders. Trends Neurosci. 23, 359–365.
Kirouac, G.J., Parsons, M.P., Li, S., 2005. Orexin (hypocretin) innervation of the paraventricular nucleus of the thalamus. Brain Res. 1059, 179–188.
Kotz, C.M., Teske, J.A., Levine, J.A., Wang, C., 2002. Feeding and activity induced by orexin A in the lateral hypothalamus in rats. Reg. Peptides 104, 27–32.
Kunii, K., Yamanaka, A., Nambu, T., Matsuzaki, I., Goto, K., Sakurai, T., 1999. Orexins/hypocretins regulate drinking behaviour. Brain Res. 842, 256–261.
Kruger, J.-L., Dell, L.-A., Pettigrew, J.D., Manger, P.R., 2010. Cellular location and major terminal networks of the orexinergic system in the brains of five microchiropteran species. J. Chem. Neuroanat. 40, 256–262.
Limacher, A.M., Bhagwandin, A., Fuxe, K., Manger, P.R., 2008. Nuclear organization and morphology of cholinergic, putative catecholaminergic and serotonergic neurons in the brain of the Cape porcupine (*Hystrix afric*aeaustralis): increased brain size does not lead to increased organizational complexity. J. Chem. Neuroanat. 36, 33–52.
Lovegrove, B.G., Muir, A., 1996. Circadian body temperature rhythms of the solitary Cape mole rat (*Georychus capensis*: (Bathyergidae). Physiol. Behav. 60, 991–998.
Lovegrove, B.G., Papenfus, M.E., 1995. Circadian activity rhythms in the solitary Cape mole rat (*Georychus capensis*: Bathyergidae) with some evidence of splitting. Physiol. Behav. 58, 679–685.
Lubkin, M., Stricker-Krongrad, A., 1998. Independent feeding and metabolic actions of orexins in mice. Biochem. Biophys. Res. Commun. 25, 241–245.
Manger, P.R., 2005. Establishing order at the systems level in mammalian brain evolution. Brain Res. Bull. 66, 282–289.
Maseko, B.C., Bourne, J.A., Manger, P.R., 2007. Distribution and morphology of cholinergic, putative catecholaminergic and serotonergic neurons in the brain of the Egyptian Rousette flying fox, *Rousettus aegyptiacus*. J. Chem. Neuroanat. 34, 108–127.
McGranaghan, P.A., Piggins, H.D., 2001. Orexin A-like immunoreactivity in the hypothalamus and thalamus of the Syrian hamster (*Mesocricetus auratus*) and Siberian hamster (*Phodopus sungorus*), with special reference to circadian structures. Brain Res. 904, 234–244.
Mintz, E.M., van Den Pol, A.N., Casano, A.A., Albers, H.E., 2001. Distribution of hypocretin-(orexin) immunoreactivity in the central nervous system of Syrian hamsters (*Mesocricetus auratus*). J. Chem. Neuroanat. 21, 225–238.
Mondal, M.S., Nakazato, M., Date, Y., Murakami, N., Hanada, R., Sakata, T., Matsukura, S., 1999. Characterization of orexin-A and orexin-B in the microdissected rat brain nuclei and their contents in two obese rat models. Neurosci. Lett. 273, 45–48.
Moore, R.Y., Abrahamson, E.A., Van Den Pol, A., 2001. The hypocretin neuron system: an arousal system in the human brain. Arch. Ital. Biol. 139, 195–205.
Nambu, T., Sakurai, T., Mizukami, K., Hosoya, Y., Yanagisawa, M., Goto, K., 1999. Distribution of orexin neurons in the adult rat brain. Brain Res. 827, 243–260.
Negroni, J., Bennett, N.C., Cooper, H.M., 2003. Organization of the circadian system in the subterranean mole rat, *Cryptomys hottentotus* (Bathyergidae). Brain Res. 967, 48–62.
Nemec, P., Burda, H., Peichl, L., 2004. Subcortical visual systems of the African mole-rat *Cryptomys anselli*: to see or not to see? Eur. J. Neurosci. 20, 757–768.
Nixon, J.P., Smale, L., 2007. A comparative analysis of the distribution of immunoreactive orexin A and B in the brains of nocturnal and diurnal rodents. Behav. Brain Funct. 13, 28.
Novak, C.M., Albers, H.E., 2002. Localization of hypocretin-like immunoreactivity in the brain of the diurnal rodent, *Arvicanthis niloticus*. J. Chem. Neuroanat. 23, 49–58.
Oelschlager, H.H.A., Nakamura, M., Herzog, Burda, H., 2000. Visual system labelled by c-Fos immunohistochemistry after light exposure in the 'blind' subterranean Zambian mole-rat (*Cryptomys anselli*). Brain Behav. Evol. 55, 209–220.
Oosthuizen, M.K., Cooper, H.M., Bennett, N.C., 2003. Circadian rhythms of locomotor activity in solitary and social species of African mole rats (Family: Bathyergidae). J. Biol. Rhythms 18, 481–490.
Peyron, C., Tighe, D.K., van den Pol, A.N., de Lecea, L., Heller, H.C., Sutcliffe, J.G., Kilduff, T.S., 1998. Neurons containing hypocretin (orexin) project to multiple neuronal systems. J. Neurosci. 18, 9996–10015.
Pieters, R.P., Gravett, N., Fuxe, K., Manger, P.R., 2010. Nuclear organization of cholinergic, putative catecholaminergic and serotonergic nuclei in the brain of the eastern rock elephant shrew, *Elephantulus myurus*. J. Chem. Neuroanat. 39, 175–188.
Piper, D.C., Upton, N., Smith, M.I., Hunter, A.J., 2000. The novel brain neuropeptide, orexin-A, modulates the sleep-wake cycle of rats. Eur. J. Neurosci. 12, 726–730.
Pu, S., Jain, M.R., Kalra, P.S., Kalra, S.P., 1998. Orexins, a novel family of hypothalamic neuropeptides, modulate pituitary luteinizing hormone secretion in an ovarian steroid dependent manner. Reg. Peptides 78, 133–136.
Raghanti, M.A, Stimpson, C.D., Marcinkiewicz, J.L., Erwin, J.M., Hof, P.R., Sherwood, C.C., 2008a. Cholinergic innervation of the frontal cortex: differences among humans, chimpanzees, and macaque monkeys. J. Comp. Neurol. 506, 409–424.
Raghanti, M.A., Stimpson, C.D., Marcinkiewicz, J.L., Erwin, J.M., Hof, P.R., Sherwood, C.C., 2008b. Differences in cortical serotonergic innervation among humans, chimpanzees, and macaque monkeys: a comparative study. Cereb. Cortex 18, 584–597.
Risold, P.Y., Griffond, B., Kilduff, T.S., Sutcliffe, J.G., Fellmann, D., 1999. Preprohypocretin (orexin) and prolactin-like immunoreactivity are coexpressed by neurons of the rat lateral hypothalamic area. Neurosci. Lett. 259, 153–156.
Sakurai, T., Amemiya, A., Ishii, M., Matsuzaki, I., Chemelli, R.M., Tanaka, H., Williams, S.C., Richardson, J.A., Kozlowski, G.P., Wilson, S., Arch, J.R.S., Buckingham, R.E., Haynes, A.C., Carr, S.A., Annan, R.S., McNulty, D.E., Liu, W.S., Terrett, J.A., Elshourbagy, N.A., Bergsma, D.J., Yanagisawa, M., 1998. Orexins and orexin receptors: a family of hypothalamic neuropeptides and G protein-coupled receptors that regulate feeding behavior. Cell 92, 573–585.
Siegel, J.M., 1999. Narcolepsy: a key role for hypocretins (orexins). Cell 98, 409–412.
Takahashi, N., Okumura, T., Yamada, H., Kohgo, Y., 1999. Stimulation of gastric acid secretion by centrally administered orexin A in conscious rats. Biochem. Biophys. Res. Commun. 254, 623–627.
Thannickal, T.C., Moore, R.Y., Nienhuis, R., Ramanathan, L., Gulyani, S., Aldrich, M., Cornford, M., Siegel, J.M., 2000. Reduced number of hypocretin neurons in human narcolepsy. Neuron 27, 469–474.
Vidal, L., Blanchard, J., Morin, L.P., 2005. Hypothalamic and zona incerta neurons expressing hypocretin, but not melanin concentrating hormone, project to the hamster intergeniculate leaflet. Neuroscience 134, 1081–1090.
van den Pol, A.N., 2000. Narcolepsy: a neurodegenerative disease of the hypocretin system? Neuron 27, 415–418.
Yamamoto, Y., McKinley, M.J., Nakazato, M., Yamashita, H., Shirahata, A., Ueta, Y., 2006. Postnatal development of orexin-A and orexin-B like immunoreactivities in the Eastern grey kangaroo (*Macropus giganteus*) hypothalamus. Neurosci. Lett. 392, 124–128.
Yoshida, K., McCormack, S., Espana, R.A., Crocker, A., Scammell, T.E., 2006. Afferents to the orexin neurons of the rat brain. J. Comp. Neurol. 494, 845–861.
Yoshimichi, G., Yoshimatsu, H., Masaki, T., Sakata, T., 2001. Orexin-A regulates body temperature in coordination with arousal status. Exp. Biol. Med. 226, 468–476.
Zhang, J.H., Sampogna, S., Morales, F.R., Chase, M.H., 2001. Orexin (hypocretin)-like immunoreactivity in the cat hypothalamus: a light and electron microscopic study. Sleep 24, 67–76.
Zhang, J.H., Sampogna, S., Morales, F.R., Chase, M.H., 2002. Co-localization of hypocretin-1 and hypocretin-2 in the cat hypothalamus and brainstem. Peptides 23, 1479–1483.